DEVELOPING A FLUORESCENCE-BASED TOOL TO MEASURE NORADRENALINE TRANSPORTER FUNCTION IN CARDIOVASCULAR TISSUE

by

LILY LILI CAO

A thesis submitted to the

University of Birmingham

for the degree of

DOCTOR OF PHILOSOPHY

School of Biomedical Science

Institute of Clinical Science

College of Medical and Dental Sciences

University of Birmingham

February 2021

UNIVERSITY OF BIRMINGHAM

University of Birmingham Research Archive

e-theses repository

This unpublished thesis/dissertation is copyright of the author and/or third parties. The intellectual property rights of the author or third parties in respect of this work are as defined by The Copyright Designs and Patents Act 1988 or as modified by any successor legislation.

Any use made of information contained in this thesis/dissertation must be in accordance with that legislation and must be properly acknowledged. Further distribution or reproduction in any format is prohibited without the permission of the copyright holder.

ABSTRACT

Sympathetic noradrenergic transmission in both the heart and vasculature is modulated at central, ganglionic, and end-organ sites. It is ultimately within the neuroeffector junction where the dynamic interplay between noradrenaline (NAd) release and its subsequent reuptake by the noradrenaline transporter (NAT) that predominately determines the junctional availability of the neurotransmitter. However, despite the fact that NAT dysfunction is implicated in many cardiovascular diseases, the mechanisms that govern transporter modulation remain poorly defined due to the limited methodologies available. This study demonstrates the development and optimisation of a novel, fluorescence-based technique, NTUA (Neurotransmitter Transporter Uptake Assay), that permits dynamic measurements of NAT function at high spatiotemporal resolutions in whole organ preparations *ex vivo*. This technique was then used to explore putative NAT regulators. It was discovered that several known release-inhibiting modulators, such as the muscarinic acetylcholine receptor, α_2-adrenoceptor (α_2AR), and cannabinoid type I receptor (CB_1R), also suppress NAT function. Importantly, the neuromodulatory roles of α_2AR and CB_1R were also uncovered during bouts of sympathetic neuronal activity, which provides further insight into the complexity of net noradrenergic transmission. Moreover, the future potential for NTUA as an intravital stain to monitor disease progression *in vivo* was demonstrated by its use to simultaneously detect for changes in NAT function and sympathetic nerve density in a pre-clinical animal model of obstructive sleep apnoea, a disease with complex cardiovascular implications. These data, amongst others, show that NTUA will help future research into junctional NAd availability and hence the study of sympathetic transmission in the cardiovascular system.

DEDICATION

To my mum and dad.

ACKNOWLEDGEMENTS

First and foremost, I must express my sincerest gratitude to Dr Keith Brain for his tutelage, support, and continuous encouragement throughout this research project. His utmost enthusiasm for my work and phenomenal wealth of knowledge in and beyond Autonomic Neuroscience has been instrumental for my learning. Each meeting and conversation I have had with Keith has taught me something new, importantly the skill to think laterally, comprehensively, and objectively. Keith's approachable personality, sense of humour, and patience meant that I was never afraid to ask a question and we have had plenty of enjoyable chats, too. I would also like to thank my co-supervisors Professor Janice Marshall and Professor Larissa Fabritz for their valued help and advice; their expertise in cardiac and vascular physiology has been unmatched. I must also acknowledge Dr Andrew Holmes for his technical expertise and being the "go-to" person for many aspects of my project. His generosity and eagerness to assist on a daily basis has helped me tremendously and I cannot extend my thanks enough. Importantly, I am very grateful to the British Heart Foundation for the funding of this PhD opportunity, and for the additional support provided in light of the COVID-19 pandemic.

I am greatly indebted to my friends in the East Lower Ground office. They have made each and every day so enjoyable. Abdulaziz Alzahrani has been my cherished laboratory companion from day one as we embarked upon our PhD together, and his jokey personality has been the light to any conversation. I would like to thank Eyas Alhuthail for his friendship, support in and out of the laboratory, and for all the laughs we have had. Thank you to Hayyaf Aldossary for being so reliable and helpful whenever I needed an extra hand; your willingness (even at 7 am!) will always be remembered. And to former members of the ELG office - Dr Abimbola Aiku, Dr Suranjana Gupta, and Demitris

Nathanael, thank you for your continued friendship and support; I really have made friends for life. My thanks also go to the Birmingham Hypoxia and Arterial Chemoreceptor group for welcoming me to take part in collaborative work, and to the Translational Research on Heart Failure and Arrhythmias group for the instrumental training and guidance that I have received.

Outside of the laboratory I would like to thank my friends and family for their endless encouragement and support. In particular, thank you to Dr Amandeep Johal Kaur, who has been my 절친, personal cheerleader, and counsellor throughout, and to Sadie Sweetland, whom I have known for 15 years since that Textiles lesson in Year 7, for being there at only one call away (day or night) throughout this journey! I must also thank Dr Hannah Noordali, who has been my most trusted friend for any science-related questions and reminds me to have fun outside of the laboratory. And lastly, the greatest thanks to my mum, whose unconditional love and paramount support has been the constant pillar of strength for me.

PROJECT OUTCOMES

Abstracts

- **Pharmacology 2020**, (2021; virtual poster, P047). Cao, L.L., Marshall, J.M., Fabritz, L., Brain, K.L. Cannabinoid type I-receptor mediated inhibition of neuronal noradrenaline reuptake in the mouse heart. *Br J Pharmacol*, **178**: 381-486

- **31st International (and 1st Virtual) Symposium on the Autonomic Nervous System**, (2020; virtual poster, #21). Cao, L.L., Marshall, J.M., Fabritz, L., Brain, K.L. Norepinephrine transporter saturation at physiological sympathetic firing rates in the murine heart. *Clin Auton Res*, **30**: 453-498

- **11th Congress of the International Society for Autonomic Neuroscience**, University of California Los Angeles, USA (2019; oral communication, Neuron-Myocyte Interactions in Health and Disease session, ISAN19.047). Cao, L., Holmes, A., Marshall, J., Fabritz, L., Brain, K. A fluorescent method to monitor norepinephrine transporter rate in murine heart and blood vessels.

- **Midlands Cardiovascular Research Network 2nd Open Scientific Meeting,** (2018; poster presentation). Cao, L.L., Kabir, S.N., Wells, S.P., Holmes, A.P., Fabritz, L., Brain, K.L. A new fluorescence-based technique to label and monitor sympathetic nerve function in the murine heart and mesenteric artery.

Papers

- **Cao, L.L.,** Holmes, A.P., Marshall, J.M., Fabritz, L., Brain, K.L. (2020) Dynamic monitoring of single-terminal norepinephrine transporter rate in the rodent cardiovascular system: A novel fluorescence imaging method. *Auton Neurosci* **223**, 102611. doi: 10.1016/j.autneu.2019.102611. Appendix A.

- **Cao, L.L.,** Marshall, J.M., Fabritz, L., Brain, K.L. (2021) Resting cardiac sympathetic firing frequencies suppress terminal norepinephrine transporter uptake. *Auton Neurosci* **232**, 102794. doi: 10.1016/j.autneu.2021.102794. Appendix B.

- Alzahrani, A.A, **Cao, L.L.,** Aldossary, H.S., Nathanael, D., Fu, J., Ray, C.J., Brain, K.L., Kumar, P., Coney, A.M., Holmes, A.P. β-Adrenoceptor blockade prevents carotid body hyperactivity and elevated vascular sympathetic nerve density induced by chronic intermittent hypoxia. *Pflugers Arch*. **473**(1), 37-51. doi: 10.1007/s00424-020-02492-0. Appendix C.

Prizes

- 11th Congress of the International Society for Autonomic Neuroscience, University of California Los Angeles, USA. A fluorescent method to monitor norepinephrine transporter rate in the murine heart and blood vessels. For **2019 Geoffrey Burnstock Award** for Young Investigator Award: Best Oral Presentation.

TABLE OF CONTENTS

ABSTRACT ii

DEDICATION iii

ACKNOWLEDGEMENTS iv

PROJECT OUTCOMES vi

LIST OF FIGURES xv

LIST OF TABLES xviii

LIST OF APPENDICES xviii

ABBREVIATIONS xix

CHAPTER I. GENERAL INTRODUCTION 1

1.1. Overview 1

1.2. Autonomic nervous system 2

1.3. Cardiovascular system: basic anatomy and function 6
1.3.1. Heart 6
1.3.2. Resistance arteries 9

1.4. Sympathetic transmission and cardiovascular function 11
1.4.1. Basic anatomy of efferent SNS 11
1.4.2. Sympathetic innervation of cardiovascular tissue 12
1.4.2.1. General morphology 12
1.4.2.2. Heart 13
1.4.2.3. Resistance vessels 14
1.4.2.4. Methodologies to visualise innervation 14
1.4.3. Neuroeffector transmission in cardiovascular tissue 16
1.4.3.1. Autonomic chemical mediators 16
1.4.3.2. Primary chemical mediator: noradrenaline 18
1.4.3.3. Action potential-mediated exocytotic release 19
1.4.3.4. Neuromodulatory prejunctional receptors 21
1.4.3.5. Methods to measure for exocytotic release 22
1.4.3.6. Postjunctional action of NAd 24
1.4.3.7. Brief account of noradrenergic termination 26

1.5. Noradrenaline transporter 27
1.5.1. Neuronal uptake of biogenic amines 27
1.5.2. NAT (uptake$_1$) 28
1.5.3. NAT and cardiovascular disease 31
1.5.3.1. NAd and cardiovascular disease 31
1.5.3.2. Atrial fibrillation 32
1.5.3.3. Resistant hypertension 34
1.5.3.4. Chronic heart failure 36
1.5.3.5. Chronic intermittent hypoxia 38
1.5.4. Targeting NAT to treat cardiovascular disease? 39

1.6. Existing methodologies to measure NAT function 40
1.6.1. Radiolabelled NAT substrates 40
1.6.2. Rotating disk recordings 41
1.6.3. Quantitative fluorescence microscopy 42
1.6.3.1. ASP^+/APP^+ 42
1.6.3.2. False fluorescent neurotransmitters 43

1.6.3.3. GPCR activation-based NAd sensors ... 43
1.6.3.4. Neurotransmitter Transporter Uptake Assay ... 44

1.7. Cannabinoids ... 45
1.7.1. Cannabinoids and the cardiovascular system ... 46
1.7.2. Cannabinoid receptors ... 47
1.7.3. CB_1R at the sympathetic neuroeffector site ... 49
1.7.4. Endocannabinoids and its therapeutic potential ... 50

1.8. Objective and aims ... 52

CHAPTER II. MATERIAL AND METHODS ... 55

2.1. Ethical statement ... 55

2.2. Physiological saline solutions ... 55

2.3. Animals ... 55

2.4. Tissue isolation ... 56
2.4.1. Rodent heart isolation ... 56
2.4.1.1. Anaesthesia ... 56
2.4.1.2. Murine heart isolation ... 57
2.4.1.3. Rat heart isolation ... 57
2.4.2. Rodent mesenteric artery isolation ... 58

2.5. Measurement of single-terminal noradrenaline transporter rate ... 59
2.5.1. Neurotransmitter Transporter Uptake Assay (NTUA) ... 59
2.5.2. NTUA preparation ... 59
2.5.3. Tissue preparation for NTUA superfusion ... 60
2.5.3.1. Heart preparation ... 60
2.5.3.2. Mesenteric artery preparation ... 61
2.5.3.3. Implementation of the 'reduce' principle in animal research ... 61
2.5.4. Superfusion delivery system ... 62
2.5.5. Imaging and NTUA superfusion protocol ... 64
2.5.5.1. NTUA imaging with confocal microscopy ... 64
2.5.5.2. NTUA superfusion protocol ... 65
2.5.6. Image analysis of NTUA uptake rate ... 67
2.5.6.1. Quantification of single-terminal fluorescence intensity ... 67
2.5.6.2. Normalisation of single-terminal fluorescence intensity ... 67
2.5.6.3. Analysis of NTUA uptake rate ... 70
2.5.6.3.1. Straight-line analysis ... 70
2.5.6.3.2. Non-linear curve fit ... 70
2.5.7. Electrical field stimulation and NTUA uptake ... 73
2.5.8. Drug-induced effects of NTUA uptake ... 74
2.5.9. Langendorff delivery system ... 74
2.5.9.1. Aortic cannulation ... 74
2.5.9.2. Langendorff retrograde perfusion of NTUA ... 75
2.5.10. Multi-photon microscopy ... 76
2.5.11. Human tissue ... 77

2.6. Noradrenaline release ... 78
2.6.1. [^{3}H]-NAd overflow ... 78

2.7. The use of NTUA to quantify vascular sympathetic nerve density ... 79
2.7.1. Chronic intermittent hypoxia model ... 80
2.7.2. Image acquisition ... 80
2.7.3. Image analysis ... 81
2.7.3.1. Vascular fluorescent area ... 81

2.7.3.2. Surface density 82

2.8. Histochemistry 83
2.8.1. Chemofluorescence 83
2.8.2. Immunohistochemistry 84

2.9. Drugs 87

2.10. Statistical analyses 88

CHAPTER III. OPTIMISATION OF A FLUORESCENCE-BASED TOOL TO STUDY SINGLE-TERMINAL NORADRENALINE TRANSPORTER FUNCTION 91

3.1. Introduction 91
3.1.1. Overview 91
3.1.2. Objectives and aims 92

3.2. Results 93
3.2.1. NTUA labelling in rodent cardiovascular tissue 93
3.2.1.1. Confocal microscopy: NTUA labelling of neuronal structures 93
3.2.1.2. Multi-photon microscopy: NTUA labelling of neuronal structures 100
3.2.1.3. Glyoxylic acid-induced chemofluorescence of neuronal catecholamines 102
3.2.1.4. NTUA uptake is temperature sensitive 104
3.2.1.5. NTUA uptake is mediated by the noradrenaline transporter 106
3.2.1.5.1. Desipramine 106
3.2.1.5.2. Tyramine 111
3.2.1.6. Non-neuronal NTUA uptake into myocyte-like structures 113
3.2.1.7. Investigating different experimental conditions on NTUA uptake 118
3.2.1.7.1. Time course of NTUA uptake 118
3.2.1.7.2. NTUA fluorophore is photosensitive 118
3.2.1.7.3. Rodent sacrifice method affects NTUA uptake rate 121
3.2.2. Neuronal NTUA labelling in other rodent tissues 123
3.2.2.1. Vascular tissue 123
3.2.2.2. Carotid body 123
3.2.3. Negative NTUA labelling in human vessels 124

3.3. Discussion 127
3.3.1. Main findings 127
3.3.2. Radiotracers and NAT function 127
3.3.3. The use of fluorescence to monitor NAT function 128
3.3.4. NTUA: a fluorescence-based method to label sympathetic nerve terminals in rodent cardiovascular tissue 129
3.3.4.1. Morphology of sympathetic nerve terminals 129
3.3.4.2. Depth penetration of NTUA fluorescence 130
3.3.4.3. Advantage of NTUA over other techniques 131
3.3.4.4. Summary 132
3.3.5. Mechanisms of neuronal NTUA uptake (uptake$_1$) 133
3.3.5.1. Carrier-mediated transport 133
3.3.5.2. NTUA specificity for NAT 134
3.3.5.3. Nerve terminal localisation of NTUA 135
3.3.5.4. The use of NTUA to monitor NAT rate 136
3.3.5.5. NAT rate and anaesthetics 136
3.3.5.6. Summary 137
3.3.6. Mechanisms of non-neuronal NTUA uptake (uptake$_2$) 138
3.3.6.1. Heart 138
3.3.6.2. Physiological relevance of cardiac uptake$_2$ 139
3.3.6.3. Mesenteric artery 141
3.3.6.4. Summary 142

3.3.7. Neuronal NTUA labelling in other tissues 142
3.3.7.1. Other rat arterial vessels 142
3.3.7.2. Rat carotid body 144
3.3.7.3. Human mesenteric arteries 146
3.3.7.4. Summary 147
3.3.8. Limitations of NTUA 147
3.3.8.1. Photosensitivity 147
3.3.8.2. Fate of NTUA 148
3.3.8.3. Summary 149

3.4. Overall conclusion 149

CHAPTER IV. SINGLE-TERMINAL NORADRENALINE TRANSPORTER FUNCTION IN PHYSIOLOGY AND PATHOPHYSIOLOGY 152

4.1. Introduction 152
4.1.1. Overview 152
4.1.2. Objectives and aims 154

4.2. Results 155
4.2.1. Cardiac inter-chamber differences in NTUA uptake rate 155
4.2.2. NTUA uptake rate is faster in the rodent heart than artery 159
4.2.2.1. Mice 159
4.2.2.2. Rat 159
4.2.3. NTUA uptake rate is faster in mice than in the rat 162
4.2.3.1. Heart 162
4.2.3.2. Mesenteric artery 162
4.2.4. Muscarinic receptor-mediated inhibition of cardiac NTUA uptake 165
4.2.5. Electrical field stimulation rapidly reduces cardiac NTUA uptake 169
4.2.5.1. Frequency-dependent suppression of NTUA uptake 169
4.2.5.2. Local NAd release from the left atrium 172
4.2.5.3. Role of sympathetic prejunctional receptors on NTUA uptake during EFS 175
4.2.5.3.1. α_2-Adrenergic autoreceptor 175
4.2.5.3.2. Muscarinic heteroreceptor 175
4.2.5.4. Substrate competition: NAd and NTUA at NAT 178
4.2.5.4.1. NTUA competition with NAd during uptake 178
4.2.5.4.2. NTUA displacement by NAd during washout 180
4.2.5.5. Inhibition of exocytosis mechanism 182
4.2.6. Chronic intermittent hypoxia and NAT 184
4.2.6.1. CIH perturbs NTUA uptake in the heart 184
4.2.6.2. CIH does not affect NTUA uptake in the mesenteric arteries 185
4.2.6.3. β-adrenoceptor inhibition prevents CIH-induced vascular sympathetic hyperinnervation 185

4.3. Discussion 190
4.3.1. Main findings 190
4.3.2. NAT reuptake rate quantification method 190
4.3.2.1. Straight-line fit analysis 190
4.3.2.2. Non-linear curve fit analysis 191
4.3.2.3. Summary 192
4.3.3. NAT rate is faster in the heart than the vasculature 192
4.3.3.1. Heart 192
4.3.3.1.1. Inter-chamber differences 192
4.3.3.1.2. Physiological relevance of cardiac heterogeneity 194
4.3.3.1.3. Summary 196
4.3.3.2. Heart versus blood vessels 196
4.3.3.2.1. Cardiac dependence on NAT 196

4.3.3.2.2. Physiological relevance of tissue heterogeneity 197
4.3.3.3. Summary 198
4.3.4. NAT kinetics is faster in mice than the rat 199
4.3.4.1. Faster NAT function in mice 199
4.3.4.2. Interspecies variation in NAT amino acid sequence 199
4.3.4.3. Physiological relevance 200
4.3.4.4. Summary 201
4.3.5. Prejunctional mAChR-mediated inhibition of cardiac NAT rate 202
4.3.5.1. Mechanism of mAChR-mediated reduction in NAT function 202
4.3.5.2. mAChR subtype 205
4.3.5.3. Physiological relevance of sympathetic-parasympathetic interplay 205
4.3.5.4. Carbachol off-target effects 206
4.3.5.5. Summary 207
4.3.6. Suppression of NAT kinetics by sympathetic nerve activity 208
4.3.6.1. Shortcomings of previous studies 208
4.3.6.2. Sympathetic postganglionic nerve activity suppresses cardiac NAT kinetics ex vivo 210
4.3.6.3. Evoked [^{3}H]-NAd overflow experiments 212
4.3.6.4. α_2-adrenoceptor: a regulator of NAT kinetics? 214
4.3.6.5. Physiological relevance of α_2-adrenoceptor-mediated NAT inhibition 216
4.3.6.6. No mAChR-mediated effect on NAT during sympathetic nerve activity 219
4.3.6.7. Substrate competition at NAT 221
4.3.6.8. Clinical implications of activity-dependent NAT suppression 221
4.3.6.9. Attempt to inhibit NAd release during sympathetic nerve activity 223
4.3.6.10. Summary 224
4.3.7. NAT kinetics and sympathetic innervation in chronic intermittent hypoxia 225
4.3.7.1. Brief account of CIH-induced cardiovascular pathophysiology 225
4.3.7.2. CIH and NAT reuptake rate: heart 227
4.3.7.3. Propranolol prevents CIH-induced elevated vascular sympathetic nerve density 229
4.3.7.4. Summary 231
4.3.8. Limitations 231
4.3.8.1. Analysis methods of NAT reuptake rate 231
4.3.8.2. Sympathetic nerve activity and NAT function 232

4.4. Overall conclusion 233

CHAPTER V. (ENDO)CANNABINOIDS AND NORADRENALINE TRANSPORTER FUNCTION IN THE RODENT CARDIOVASCULAR SYSTEM 235

5.1. Introduction 235
5.1.1. Overview 235
5.1.2. Objectives and aims 236

5.2. Results: rodent heart 238
5.2.1. Mice 238
5.2.1.1. Localisation of CB_1R and TH in the murine heart 238
5.2.1.2. CB_1R-mediated reduction in murine cardiac NTUA uptake 241
5.2.1.2.1. WIN 55,212-2 241
5.2.1.2.2. ACEA 245
5.2.1.3. Sympathetic nerve activity reduces murine cardiac NTUA uptake via a CB_1R-dependent mechanism 248
5.2.2. Rat 251
5.2.2.1. Localisation of CB_1R and TH in the rat heart 251
5.2.2.2. CB_1R activation does not affect rat cardiac NTUA uptake 253
5.2.2.2.1. WIN 55,212-2 253

5.2.2.2.2. ACEA ... 253

5.3. Results: rodent mesenteric artery ... 256
5.3.1. Mice ... 256
5.3.1.1. Localisation of CB_1R and TH in the murine mesenteric artery ... 256
5.3.1.2. CB_1R activation does not affect murine periarterial NTUA uptake ... 260
5.3.1.2.1. WIN 55,212-2 ... 260
5.3.1.2.2. ACEA ... 260
5.3.2. Rat ... 263
5.3.2.1. Localisation of CB_1R and TH in the rat mesenteric artery ... 263
5.3.2.2. CB_1R activation does not affect rat periarterial NTUA uptake ... 266
5.3.2.2.1. WIN 55,212-2 ... 266
5.3.2.2.2. ACEA ... 266

5.4. Discussion ... 269
5.4.1. Main findings ... 269
5.4.2. CB_1R activation suppresses cardiac NAT kinetics ... 269
5.4.2.1. Location of neuromodulatory cardiac CB_1R ... 269
5.4.2.1.1. CB_1R: prejunctional localisation ... 270
5.4.2.1.2. CB_1R: non-neuronal localisation ... 272
5.4.2.1.3. Immunohistochemistry protocol ... 272
5.4.2.1.4. Summary ... 273
5.4.2.2. Murine NAT suppression with CB_1R agonists: mechanism of action ... 274
5.4.2.2.1. Prejunctional CB_1R upon NAT ... 274
5.4.2.2.1.1. CB_1R-$G_{i/o}$ signalling ... 274
5.4.2.2.1.2. CB_1R-G_s signalling ... 275
5.4.2.2.1.3. CB_1R-$G_{q/11}$ signalling ... 276
5.4.2.2.2. Retrograde effect upon NAT by postjunctional CB_1R activation ... 276
5.4.2.2.3. Other cannabinoid-sensitive receptors ... 277
5.4.2.2.4. Summary ... 278
5.4.2.3. CB_1R-mediated tonic suppression of NAT: endocannabinoid source ... 278
5.4.2.4. (Patho)physiological relevance in the heart ... 280
5.4.2.5. Species-specific effect of CB_1R-mediated cardiac NAT suppression ... 283
5.4.2.6. Summary ... 283
5.4.3. CB_1R activation does not affect periarterial NAT kinetics ... 284
5.4.3.1. Vascular CB_1R localisation ... 284
5.4.3.1.1. CB_1R: prejunctional localisation ... 284
5.4.3.1.2. CB_1R: non-neuronal localisation ... 285
5.4.3.2. Physiological relevance ... 286
5.4.3.3. Summary ... 287
5.4.4. Therapeutic potential of cannabinoids to treat cardiovascular disease? ... 288

5.5. Overall conclusion ... 290

CHAPTER VI. DISCUSSIONS AND CONCLUSIONS ... 292

General conclusions ... 292

Challenges and limitations ... 293

Future work ... 295
Future applications of the NTUA assay ... 295
What are the interactions between sympathetic neurotransmitter release and reuptake to determine net transmission? ... 296
Do cannabinoids have the therapeutic potential to treat hypertension? ... 297

Concluding remarks ... 298

APPENDICES 300

Appendix A: Cao *et al.* (2020) Dynamic monitoring of single-terminal norepinephrine transporter rate in the rodent cardiovascular system: A novel fluorescence imaging method. 300

Appendix B: Cao *et al.* (2021) Resting cardiac sympathetic firing frequencies suppress terminal norepinephrine transporter uptake. 301

Appendix C: Alzahrani *et al.* (2020) β-Adrenoceptor blockade prevents carotid body hyperactivity and elevated vascular sympathetic nerve density induced by chronic intermittent hypoxia. 302

Appendix 3.1: NTUA labelling of murine cardiac nerve structures by Langendorff retrograde perfusion 303

REFERENCES 304

LIST OF FIGURES

No.	Figure description	Page
1.1	Schematic representation of the ANS for all visceral functions	4
1.2	Anatomical structure of the heart	6
1.3	Anatomical structure of the blood vessel	10
1.4	Anatomy of sympathetic postganglionic neurones	12
1.5	Sympathetic innervation of cardiovascular tissue	15
1.6	Noradrenergic transmission in sympathetic postganglionic nerve terminals	18
1.7	The effect of NAT dysfunction upon NAd overflow at the neuroeffector site	29
2.1	Principle of NTUA	60
2.2	Superfusion delivery system	63
2.3	Standard NTUA superfusion protocol	66
2.4	NTUA fluorescence analysis method	69
2.5	Two methods of NTUA uptake rate analysis	72
2.6	Schematic of Langendorff apparatus	76
3.1	Autofluorescence of murine cardiovascular tissue	95
3.2	NTUA labelling of murine cardiac neuronal structures	96
3.3	NTUA labelling of rat cardiac neuronal structures	97
3.4	NTUA labelling of rodent mesenteric periarterial neuronal structures	99
3.5	Emission profile of NTUA in murine cardiovascular tissue	100
3.6	Cardiac neuronal NTUA fluorescence imaged with multi-photon microscopy	101
3.7	Glyoxylic acid chemofluorescence of murine cardiac noradrenergic neurones	102
3.8	Glyoxylic acid chemofluorescence of rat cardiac noradrenergic neurones	103
3.9	Glyoxylic acid chemofluorescence of rodent mesenteric periarterial noradrenergic neurones	103
3.10	NTUA uptake into murine cardiac neuronal structures is temperature sensitive	105
3.11	Abolition of rodent cardiac neuronal NTUA uptake during NAT inhibition	107
3.12	NAT-dependent uptake of NTUA into the rodent cardiac neurones	108
3.13	Abolition of rodent mesenteric periarterial neuronal NTUA uptake during NAT inhibition	109

3.14	NAT-dependent uptake of NTUA into the rodent mesenteric periarterial neurones	110
3.15	Sympathomimetic amine tyramine augments NTUA washout from murine cardiac neurones	112
3.16	Non-neuronal uptake of NTUA in the murine heart	114
3.17	Cell nuclei morphology of non-neuronal cell types that accumulate NTUA	115
3.18	$Uptake_2$ inhibition prevents NTUA uptake into non-neuronal structures in the murine heart	116
3.19	$Uptake_2$ inhibition abolishes cardiac non-neuronal NTUA uptake	117
3.20	Time course of NAT-mediated neuronal uptake of NTUA in the murine heart	118
3.21	Phototoxicity of frequent imaging protocols on NTUA	120
3.22	Timeline of neuronal NTUA fluorescence detection with 405 nm versus 458 nm excitation laser line	120
3.23	Rodent sacrifice method affects periarterial neuronal NTUA uptake rate	122
3.24	Neuronal NTUA labelling of the rat mesenteric vein, femoral artery, and internal carotid artery	123
3.25	Neuronal NTUA labelling in the rat carotid body	125
3.26	Lack of neuronal NTUA labelling in the human mesenteric artery	126
4.1	Pattern of sympathetic NTUA uptake in each cardiac chamber across the murine heart	157
4.2	Faster sympathetic NTUA uptake rate in the murine heart than in the mesenteric arteries	160
4.3	Faster NTUA sympathetic uptake rate in the rat heart than in the mesenteric arteries	161
4.4	Faster cardiac sympathetic NTUA uptake in the mouse than in the rat	163
4.5	Faster mesenteric periarterial sympathetic NTUA uptake rate in the mouse than rat	164
4.6	Muscarinic acetylcholine receptor activation reduces murine cardiac sympathetic NTUA uptake	167
4.7	Cardiac NTUA uptake is transiently suppressed by sympathetic neuronal activity in a frequency-dependent manner	171
4.8	Measurements of evoked [^{3}H]-NAd release from the isolated murine atrium	173
4.9	Inhibition of α_2-adrenoceptor, but not mAChR, prevents the transient stimulation-evoked NAT suppression in the murine heart	177
4.10	Competition of NTUA with NAd for murine cardiac NAT during uptake	179
4.11	Displacement of NTUA from murine cardiac sympathetic nerve terminals by NAd during washout	181

4.12	Microtubule destabilising agent, colchicine, reduces cardiac sympathetic NTUA uptake in non-stimulating conditions	183
4.13	CIH accentuates cardiac sympathetic NTUA uptake	186
4.14	CIH does not affect mesenteric periarterial sympathetic NTUA uptake	188
4.15	β-adrenoceptor inhibition prevents the CIH-induced increase in mesenteric periarterial sympathetic nerve density	189
4.16	Simplistic schematic diagram of α_2-adrenoceptor-mediated NAT rate suppression during resting sympathetic neuronal activity	218
5.1	Prejunctional CB_1R are not present on murine cardiac sympathetic nerve terminals	239-40
5.2	Nonselective CBR agonist WIN 55,212-2 reduces murine cardiac sympathetic NTUA uptake function via a CB_1R-dependent pathway	243
5.3	Highly selective CB_1R agonist ACEA suppresses murine cardiac sympathetic NTUA uptake rate	246
5.4	Sympathetic nerve activity reduces murine cardiac noradrenergic NTUA uptake via an endogenous CB_1R-dependent pathway	250
5.5	Prejunctional CB_1R are not present on rat cardiac sympathetic nerve terminals	252
5.6	Nonselective CBR agonist WIN 55,212-2 does not affect rat cardiac sympathetic NTUA uptake function	254
5.7	Highly selective CB_1R agonist ACEA does not affect rat cardiac sympathetic NTUA uptake function	255
5.8	Localisation of CB_1R and TH in the murine mesenteric artery	257-8
5.9	Localisation of CB_1R with sympathetic single fibre processes and axonal bundles in the murine mesenteric artery	259
5.10	Nonselective CBR agonist WIN 55,212-2 does not affect murine periarterial sympathetic NTUA uptake function	261
5.11	Highly selective CB_1R agonist ACEA does not affect murine periarterial sympathetic NTUA uptake function	262
5.12	Localisation of CB_1R and TH in the rat mesenteric artery	264-5
5.13	Nonselective CBR agonist WIN 55,212-2 does not affect rat periarterial sympathetic NTUA uptake function	267
5.14	Highly selective CB_1R agonist ACEA does not affect rat periarterial sympathetic NTUA uptake function	268

LIST OF TABLES

No.	Table description	Page
2.1	List of buffers used for immunohistochemistry	85
2.2	List of drugs and reagents used	87
4.1	Changes in chemoafferent sensory activity, cardiorespiratory parameters, and sympathetic nerve function in CIH	226

LIST OF APPENDICES

No.	Appendix description	Page
A	Paper: Dynamic monitoring of single-terminal norepinephrine transporter rate in the rodent cardiovascular system: A novel fluorescence imaging method (2020)	300
B	Paper: Resting cardiac sympathetic firing frequencies suppress terminal norepinephrine transporter uptake (2021)	301
C	Paper: β-Adrenoceptor blockade prevents carotid body hyperactivity and elevated vascular sympathetic nerve density induced by chronic intermittent hypoxia (2020)	302
3.1	Figure: NTUA labelling of murine cardiac nerve structures by Langendoff retrograde perfusion	303

ABBREVIATIONS

2-AG	2-Arachidonoyl glycerol
Δ^9-THC	Δ^9-Tetrahydrocannabinol
αAR	Alpha adrenoceptors
βAR	Beta adrenoceptors
AC	Adenylyl cyclase
ACEA	Arachidonyl-2-chloroethylamide
ACh	Acetylcholine
AEA	Anandamide
AF	Atrial fibrillation
AMI	Acute myocardial infarction
ANOVA	Analysis of variance
ANS	Autonomic nervous system
AP	Action potential
APP^+	4-[4-(dimethyl amino)phenyl]-1-methylpyridinium
ASP^+	4-[4-(dimethyl amino)styryl]-*N*-methylpyridinium iodide
ATP	Adenosine triphosphate
BoNT	Botulinum toxin
BP	Blood pressure
CAD	Coronary artery disease
cAMP	Cyclic adenosine monophosphate
CB	Carotid body
CB_1R	Cannabinoid type 1 receptor
CB_2R	Cannabinoid type 2 receptor
CHF	Chronic heart failure
CIH	Chronic intermittent hypoxia
CNS	Central nervous system
CO	Cardiac output

COMT	Catechol-O-methyltransferase
CVD	Cardiovascular disease
DAT	Dopamine transporter
DHPG	Dihydroxyphenylglycol
DMSO	Dimethylsulphoxide
DSM	Desipramine
EC_{50}	Half maximal effective concentration
eCB	Endogenous cannabinoid
ECS	Endocannabinoid system
EF_{50}	Half maximal effective EFS frequency
EFS	Electrical field stimulation
EJC	Excitatory junctional current
EJP	Excitatory junctional potential
ELISA	Enzyme-linked immunosorbent assay
FA	Femoral artery
FAAH	Fatty acid amidohydrolase
FAGLU	Formaldehyde-glutaraldehyde
FFN	False fluorescent neurotransmitter
GIRK	G protein coupled inwardly rectifying potassium channels
GPCR	G protein coupled receptor
GRAB	GPCR activation-based (sensors)
HIF-1α	Hypoxia inducible factor 1α
HR	Heart rate
ICA	Inner carotid artery
ICNS	Intrinsic cardiac nervous system
IHC	Immunohistochemistry
IP_3	Inositol triphosphate
IQR	Interquartile range

KHB	Krebs-Henseleit buffer solution
LA	Left atria/atrium
LV	Left ventricle
MA	Mesenteric artery
mAChR	Muscarinic acetylcholine receptor
MAGL	Monoacylglycerol lipase
MAO	Monoamine oxidase
MIBG	Metaidobenzylguanidine
mKHB	Modified Krebs-Henseleit buffer solution
MPE	Multi-photon excitation microscopy
MPP^+	1-Methyl-4-phenylpyridinium
MSNA	Muscle sympathetic nerve activity
MV	Mesenteric vein
n	Number of animals
NAd	Noradrenaline
NAT	Noradrenaline transporter
NPY	Neuropeptide Y
n_t	Number of terminals
NTUA	Neurotransmitter Transporter Uptake Assay
OCT	Optimal cutting temperature compound
OSA	Obstructive sleep apnoea
PBS	Phosphate buffered saline
PKA	Protein kinase A
PKC	Protein kinase C
PLC	Phospholipase C
PNMT	Phenylethanolamine-N-methyl transferase
PNS	Parasympathetic nervous system
RA	Right atria/atrium

RDEV	Rotating disk electrode voltammetry
RDN	Renal denervation
ROI	Region of interest
RT	Room temperature
RV	Right ventricle
SCG	Superior cervical ganglion
sEJP	Spontaneous excitatory junctional potential
SEM	Standard error of the mean
SERT	Serotonin transporter
SHR	Spontaneously hypertensive rat
SLC6	Solute carrier 6 transporters
SMA	Superior mesenteric artery
SNA	Sympathetic nerve activity
SNARE	Soluble N-ethylmaleimide-sensitive factor attachment protein
SNS	Sympathetic nervous system
SPG	Sucrose-potassium-glyoxylic acid
SR	Sarcoplasmic reticulum
TH	Tyrosine hydroxylase
TPR	Total peripheral resistance
$TRPV_1$	Transient receptor potential vanilloid type I
TYR	Tyramine
VF	Ventricular fibrillation
VGCC	Voltage-gated Ca^{2+} channels
VMAT	Vesicular monoamine transporter
VSMC	Vascular smooth muscle cells

CHAPTER I. GENERAL INTRODUCTION

1.1. Overview

The sympathetic nervous system (SNS) plays an important role to modulate cardiac function and vasomotor tone. The prejunctional noradrenaline transporter (NAT) is ubiquitously located on sympathetic nerve terminals to efficiently clear noradrenaline (NAd) availability from the neuroeffector junction (Goldstein *et al.*, 1988, Esler *et al.*, 1990). Considerable progress has been made in understanding transporter regulation; however, direct and real-time measurements of NAT function are difficult to achieve and are often confined to a macroscopic scale. As NAT dysfunctions are often implicated in cardiovascular diseases (CVDs) (Liang *et al.*, 1989, Schroeder and Jordan, 2012), new tools to directly investigate the finer and local regulation of the transporter in tissues they innervate are required, as it may provide novel targets to pharmacologically manage treatment-resistant CVDs.

The SNS is one key target for cannabinoid receptor ligands, such as Δ^9-tetrahydrocannabinol (Δ^9-THC) - the principle psychoactive component of *Cannabis sativa* (Mechoulam *et al.*, 2014). However, due to the plethora of receptor targets and the variabilities of the elicited cardiovascular effects (Malinowska *et al.*, 2012), the current understanding of cannabinoids upon sympathetic regulation is less well developed. The classical cardio/vasodepressive effect may be due to inhibition of NAd release from sympathetic nerve endings (O'Sullivan, 2015), though whether these ligands also act at via the NAT in the cardiovascular system is largely unknown. By utilising new tools to exclusively study NAT regulation, further understanding of the peripheral actions of cannabinoids on sympathetic outflow to the heart and vessels can

be achieved. Such tools may also help to identify new drug targets within the endocannabinoid system for CVDs, which is an area of great therapeutic interest (Toczek and Malinowska, 2018).

1.2. Autonomic nervous system

The autonomic nervous system (ANS) provides an intimate regulatory link between the central nervous system (CNS) and the viscera to fine tune homeostasis during periods of rest, stress, and exercise (Jänig, 2006b). Throughout history the connection has been proposed by many scholars, when perhaps the first record between the mind and cardiovascular system was made in AD 30 by Roman physician Celsus, who wrote: "fear and anger and any other state of mind may often be apt to excite the pulse" (Celsus and Spencer, 1935), with an akin statement made in 1628 by physician William Harvey: "for every affection of the mind that is attended with either pain or pleasure, hope or fear, is the cause of an agitation whose influence extends to the heart" (Harvey, 1929).

The anatomical account of the ANS began with Galen in the 2nd century. In the 17th century Thomas Willis had vastly improved the descriptions of autonomic nerves, ganglia, and plexuses previously made by many international scholars, including Vesalius, with bold speculations that the originating point of the vagus and "*nervus intercostalis magnus*" (sympathetic nerve trunk), the cerebellum, controls for involuntary movement. Importantly, Willis provided accurate anatomical accounts of the wandering vagi with cardiac projections, which when resected caused a "great trembling" of the heart, thus demonstrating for a functional link between central sites and the periphery (Oakes *et al.*, 2016). The significance of the latter observation was substantiated when

Eduard and Heinrich Weber first demonstrated the depressive effect of right vagal stimulation upon heart rate in the 1800s (Herring and Paterson, 2021).

From the 19th century onwards, the physiological mechanisms that govern control of the heart from the brain became increasingly elucidated with the use of electrical field stimulation (EFS). As such, the sympathetic and parasympathetic divisions of the ANS are historically based on their neuroanatomical arrangement and opposing efferent outflows observed by nerve stimulation and exogenously applied substances (e.g., NAd, pilocarpine, atropine) (Figure 1.1). For example, the British physiologist John Newport Langley reported that extracts from ground-up adrenal glands paralleled most of the visceral effects induced by electrical stimulation of thoracolumbar fibres in animals, including a rise in blood pressure (BP), thus termed the system 'sympathetic'. Similarly, pilocarpine from the *Rutaceae* plant family mimicked the effects of tectal (mesencephalon), bulbar (medulla oblongta) and sacral (collectively: craniosacral) stimulation, such as a decrease in heart rate (HR), and were jointly termed 'parasympathetic' (Langley, 1905).

As of the 21st century, once regarded as a purely efferent system of outflows (Langley, 1921), the ANS is now appreciated as an intricate feedback system consisting of sensory afferent nerves that relays and integrates information to the CNS for efferent output (Loewy, 1990). The SNS is classically referred to prepare the body for 'fright, fight, and flight' contexts, while the parasympathetic nervous system (PNS) is most active during resting states (Gordan *et al.*, 2015). Although recent genetic studies have suggested for a re-classification of the sacral outflow to one that is 'sympathetic' (Espinosa-Medina *et al.*, 2016), there is currently continued debate (more towards against) of the idea (ISAN, 2017, Jänig *et al.*, 2017, 2018).

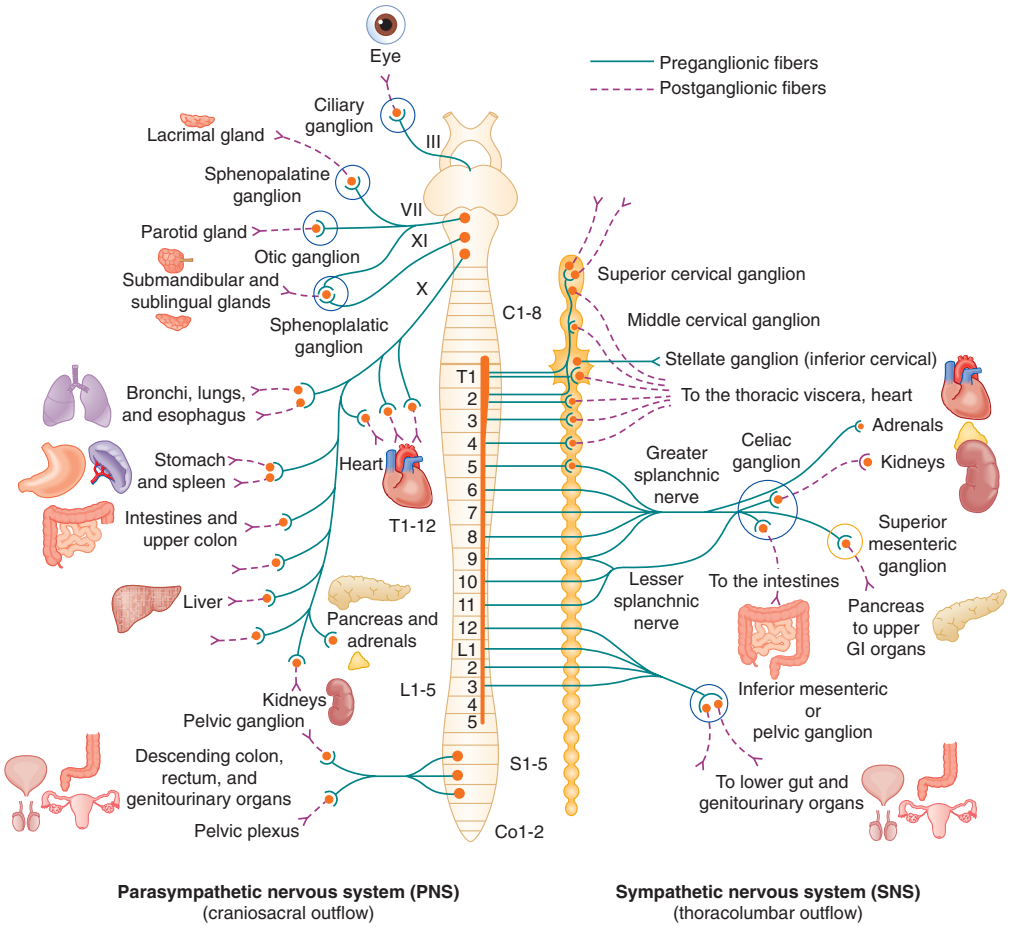


Figure 1.1: Schematic representation of the ANS for all visceral functions
The ANS is historically anatomically divided into two main divisions: sympathetic (left) and parasympathetic (right) outflows. Note the enteric division is not displayed here. Image extracted from: Johnson (2019).

The third division of the ANS is the 'enteric' nervous system, a fully integrated network comprised of a heterogeneous population of afferent, efferent, and local circuit neurones arranged in ganglia that resides in the wall of the gastrointestinal tract to control digestion independently of the CNS (Langley, 1921). Such an elaborate network also resides in the heart [intrinsic cardiac nervous system (ICNS)], where the cardiac ganglia are not merely relay stations but rather local sites for signal modulation and

integration (Armour *et al.*, 1997, Wink *et al.*, 2020), and the bladder (Fehér *et al.*, 1980); thus, the 'intrinsic system' is perhaps a better suited collective nomenclature.

In the periphery, the autonomic efferent nerves innervate all viscera with the exception of skeletal muscle; some tissues receive dual innervation from the SNS and PNS, e.g., the heart, while some are only influenced by one arm, e.g., SNS in most resistance vessels. In dually innervated tissues, the two ANS arms may elicit opposing actions on the same target cells, e.g., in cardiac pacemaker cells - sympathetic (excitatory, cardioacceleration) and parasympathetic (inhibitory, cardiodeceleration), or synergistic actions on neighbouring target cells to control overall function, e.g., pupil diameter - sympathetic (excitatory; radial dilator muscle) and parasympathetic (excitatory; sphincter constrictor muscle) (Jänig *et al.*, 2017).

The SNS is activated during 'fright, fight, and flight' contexts, such as exercise, emotional distress, and haemorrhagic shock, in which the reflex alterations in cardiovascular function ensure the change in metabolic demands of tissues are efficiently met with accurate increases in cardiac output (CO) and peripheral resistance. The effects include increases in HR, cardiac contractility, and arterial tone, and a reduction in venous capacitance (Gordan *et al.*, 2015). Unsurprisingly, there is an undoubted role of chronic sympathetic activation in the pathogenesis and maintenance of several CVDs, as seen with increases in plasma NAd concentrations, sympathetic predominance of cardiac autonomic modulation, and sympathetic nerve firing activity. However, more could be known about the regulation of neurotransmission at the end-organ neuroeffector site (release/reuptake/metabolism) in these diseased states (Jordan and Grassi, 2018).

1.3. Cardiovascular system: basic anatomy and function

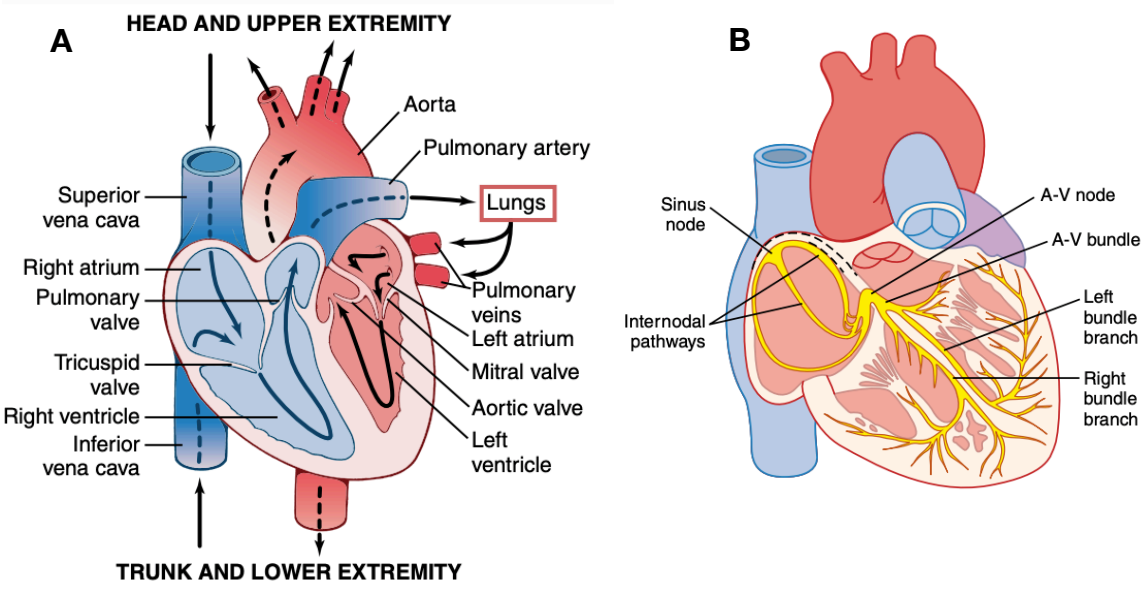


Figure 1.2: Anatomical structure of the heart
Schematic diagram demonstrating the anatomy of the heart: **(A)** cardiac chambers and direction of blood flow, and **(B)** the cardiac conduction system. Images extracted from: Guyton and Hall (2010).

1.3.1. Heart

The mammalian heart is a muscular four-chamber organ located in the lower ventral part of the thoracic mediastinum. Representing as the epicentre of the circulatory system, the heart pumps blood into the pulmonary circulation for oxygenation and into the systemic circulation for tissue perfusion. The heart is anatomically and functionally divided into left- and right halves, with each containing a thin-walled atrium and a thicker walled ventricle (Figure 1.2A). Systemic deoxygenated blood enters into the right atrium (RA) via the superior- and inferior vena cava, and oxygenated blood returns from the lungs into the left atrium (LA) via the pulmonary veins. At each atrial contraction, blood is pumped into the right- (RV) and left ventricle (LV) via the open tricuspid- and mitral

valve, respectively. As the ventricles contract, deoxygenated blood in the RV is subsequently propelled into the pulmonary trunk for oxygenation, and oxygenated blood in the LV into the aortic trunk for coronary and systemic perfusion (Guyton and Hall, 2010) (Figure 1.2A). As the left ventricular contraction has to overcome the high pressures of the systemic arterial circulation, the walls of the LV are considerably thicker than the RV.

The heart is enclosed within a protective pericardium sac, and each chamber wall consists of three layers: the epicardium, myocardium, and endocardium. The epicardium is the visceral layer of the pericardium that is firmly attached to the surface of the heart; the fluid between the serous pericardial membranes provides frictionless sliding during contraction. The myocardium is the middlemost layer and contains striated cardiac muscle fibres arranged end-to-end with intercalated disc gap junctions that enables low-resistance impulse propagation. Finally, the endocardium is comprised of endothelium that forms a continuous layer over the interior of the cardiac chambers, valves, and major blood vessels (Whitaker, 2018).

Cardiac rhythmicity is self-initiated at 100 impulses/min [or beats/min (BPM)] by the cardiac intrinsic conduction system (Figure 1.2B). Starting from the sinoatrial (SA) node located within the superior posterolateral wall of the RA, specialised SA nodal fibres spontaneously generate action potentials (APs) due to their less negative resting membrane potential, which is set by a slow inward movement of Na^+ [the pacemaker current (I_f)] and potentiated by Ca^{2+} entry via T- and L-type voltage-gated Ca^{2+} channels (VGCCs). Because SA nodal fibres connect directly with atrial muscle fibres, APs are spread rapidly into the atrial muscle wall via the internodal pathways at a rate of 0.5 $m.s^{-1}$. At the atrioventricular (AV) node located in the inferior-posterior region of the

interatrial septum, conduction rate slows to 0.05 $m.s^{-1}$ to allow for complete atrial depolarisation and ventricular filling. The impulse then enters the penetrating Bundle of His located between the atria and ventricles and travels down towards the apex via the left- and right bundle branch at 2 $m.s^{-1}$. APs then terminates on the Purkinje fibres that are connected to ventricular myocytes to transmit APs through the entire ventricular muscle mass at 4 $m.s^{-1}$ (Klabunde, 2012) (Figure 1.2B). The rhythmic synchrony of AP propagation allows for organised and deliberate depolarisation of cardiomyocytes to ensure efficient and accurate chamber filling and contraction.

APs that propagate into cardiac fibres initiates the excitation-coupling mechanism; an increase in intracellular Ca^{2+} ($[Ca^{2+}]_i$) entry via myocardial VGCC L-type Ca^{2+} channels trigger the mobilisation of large quantities of Ca^{2+} from the sarcoplasmic reticulum (SR) (Ca^{2+}-induced-Ca^{2+}-release), which in turn facilitates the mechanical shortening of the cardiomyocyte leading to contraction (Klabunde, 2012). In the absence of APs, cardiac contractility is determined by the intrinsic Frank Starling mechanism where the optimal stretch-induced overlap of actin and myosin myofilaments augments the sensitivity of troponin-C (part of troponin complex) to Ca^{2+}, which in turn results in greater cross-bridge attachment and detachment rates, hence matched force generation (Fuchs and Smith, 2001).

The propulsion of blood from the heart is maintained by the synchronous control of cardiac rhythmicity and contractility (Hill and Iaizzo, 2015). While the heart possesses intrinsic mechanisms for both components, it is also highly sensitive to extrinsic factors, such as the peripheral nerves of the ANS (section 1.3) and the ICNS. For example, vagal predominance at rest reduces the autorhythmicity from 100 BPM to ~60 BPM (in young healthy adults). During maximal SNS activation (and PNS withdrawal), HR and cardiac

contractility can each increase by 2- to 3-fold, thereby contributing towards an increase in CO by 4- to 7-fold (Guyton and Hall, 2010).

1.3.2. Resistance arteries

Homeostatic control of the circulatory system is required to ensure optimal delivery of CO to meet the perfusion demands of all tissues and organs. Oxygenated blood is distributed to specific regions of the body via the large conduit arteries and then into the target organs via the resistance vessels (small arteries and arterioles) before splitting into capillaries for diffusion. The resistance vessels are the most important sites to regulate TPR, contributing to ~2/3 of TPR to regulate arterial BP and tissue blood flow (Klabunde, 2012).

The splanchnic vascular bed alone receives about 20-25% of total CO in the unfed state (Matheson *et al.*, 2000), and within this the mesenteric bed receives 50% from the superior mesenteric artery (SMA) (Christensen and Mulvany, 1993), thus any change in mesenteric resistance vessel diameter contributes greatly to TPR and can mediate a vast redirection of blood flow. The resistance vessels contain three layers: the *tunica adventitia*, *tunica media*, and *tunica intima* (Figure 1.3). The adventitia is the outermost layer that consists of fibrous connective tissue, nerve fibres, and lymphatics. The innermost intima layer consists of a single layer of endothelial cells and a basement membrane. Arranged longitudinally in the direction of flow, endothelial cells are able to synthesis vasoactive factors to fine tune vasomotor tone in response to changes in blood flow and shear stress, such as endothelin-1 and nitric oxide (NO) (Guyton and Hall, 2010, Klabunde, 2012).

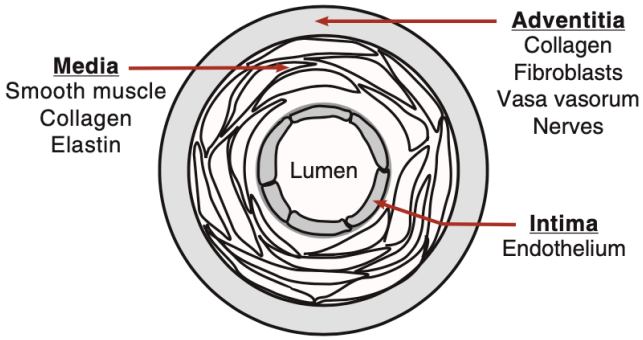


Figure 1.3: Anatomical structure of the blood vessel
Schematic diagram demonstrating the three typical layers of a blood vessel (with the exception of capillaries and post-capillary venules): *tunica adventitia* (outer), *tunica media* (middle), and *tunica intima* (inner). Image extracted from: Klabunde (2012).

Compared to other vessels, the media of resistance vessels contain large amounts of vascular smooth muscle cells (VSMCs) that are arranged concentrically in a few layers. Neighbouring VSMCs are connected by gap junctions to allow for cell-to-cell coordination of membrane potential and exchange of $[Ca^{2+}]_i$. An increase in $[Ca^{2+}]_i$ binds and activates regulatory protein calmodulin, which in return activates myosin light chain kinase to phosphorylate myosin light chain located on myosin heads. As a result, cross-bridge formation between myosin heads and actin filaments facilitates smooth muscle contraction. VSMC contraction occurs in a coordinated fashion to greatly reduce blood vessel diameter; in doing so, the increase in arteriolar resistance to blood flow augments the pressure for a given volume of blood (Guyton and Hall, 2010).

As with cardiac function, the degree of arteriolar vasoconstriction depends upon intrinsic and extrinsic factors in response to a range of electrical, chemical, or mechanical stimuli. SNS activation is a powerful mediator to reduce arteriolar diameter, for example by up to 85% in the microcirculation of skeletal muscle (Marshall, 1982), thus it is as a key influencer of TPR and regional blood flow within the circulation.

1.4. Sympathetic transmission and cardiovascular function

1.4.1. Basic anatomy of efferent SNS

The efferent SNS consists of a sequential two-neurone pathway between the CNS and cardiovascular tissue: the 'preganglionic' and 'postganglionic' neurone. The human cardiac sympathetic preganglionic cell bodies are located in the T_1-T_6 segments of the spinal cord (that extends lower in some animal species) (Coote and Chauhan, 2016). The corresponding myelinated axons project out of the ventral roots and into the paravertebral ganglia, also known as the 'sympathetic chain', and either immediately synapses with multiple postganglionic cell bodies located at the same segmental level or travel rostrally to synapse with those in the stellate ganglia, comprised of the inferior cervical ganglion and the first thoracic ganglion ('cervicothoracic') (Figure 1.1) (Coote and Chauhan, 2016). Postganglionic nerves obliquely approach the heart via the cardiac nerves through the vascular pole; on the arterial side, sympathetic nerves follow the common carotid-, subclavian-, and brachiocephalic arteries towards the aorta, and via the superior vena cava on the venous side (Kawashima, 2005). During development, blood vessels (arteries and veins) guide the innervation by sympathetic nerves in a phenomenon termed 'neurovascular congruence' (Manousiouthakis *et al.*, 2014).

On the other hand, the preganglionic cell bodies for the mesentery originate from T_9-T_{11}; myelinated axons bypass the sympathetic chain and travel via the lesser splanchnic nerve through the diaphragm and celiac ganglion, where it will synapse with postganglionic cell bodies located in the prevertebral superior mesenteric ganglia found in close apposition to the SMA (Loukas *et al.*, 2010) (Figure 1.1). Thereafter, like with cardiac nerves and the vascular pole, the unmyelinated sympathetic postganglionic nerve fibres exit the ganglia and follow the path of the SMA towards the site of

innervation as a bundle or fascicle of axons to the target organ for innervation (Yang *et al.*, 2008) (Figure 1.4A,B).

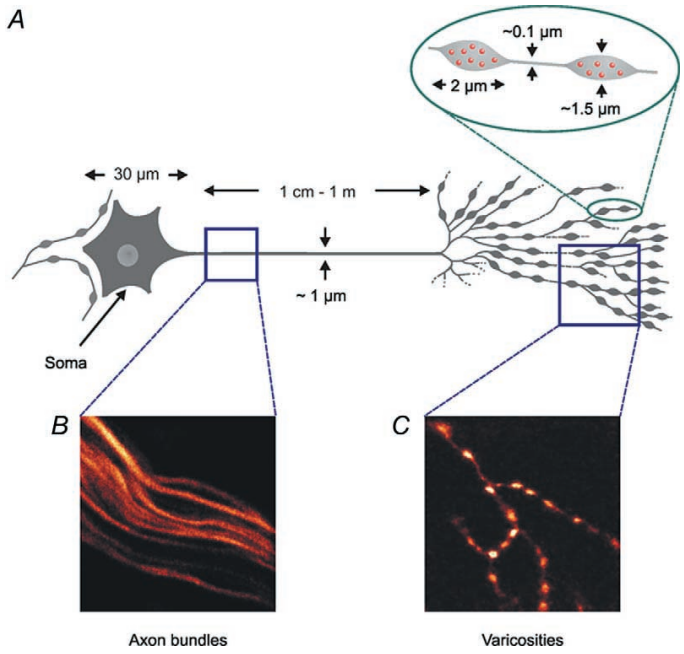


Figure 1.4: Anatomy of sympathetic postganglionic neurones
Schematic diagram demonstrating the sympathetic postganglionic morphology and approximate dimensions of the cell body (ganglia), axon (periphery) and terminal varicose swellings (target end-organ). Images were taken from sympathetic neurones retrogradely labelled with Ca^{2+} indicator Oregon Green 488 BAPTA-1 dextran in the mouse vas deferens. Image extracted from: Jackson *et al.* (2001).

1.4.2. Sympathetic innervation of cardiovascular tissue

1.4.2.1. General morphology

Unmyelinated sympathetic postganglionic fibres exit the ganglion as a fascicle of axons invested by cytoplasmic processes of non-myelinating Schwann cells (Brock and Cunnane, 1993). As the axon reaches the vicinity of the tissue, it courses some distance before branching off repeatedly to form a ground plexus of terminal varicose swellings

('varicosities') joined by intervaricose segments containing neurofilaments (Figure 1.4A,C) (Burnstock, 2008). Each individual sympathetic nerve may give rise to as many as 30,000 varicosities over the total length of innervation (Gabella, 1992), with many losing their Schwann cell investment as it forms neuroeffector junctions with nearby target cells. Sympathetic varicosities can transverse along the membrane of the target cell with non-permanent geometry and groove their surfaces to form neuroeffector junctions with considerable distances (10-2000 nm) depending on the organ (Burnstock, 2008). The neuroeffector junction is arguably an underrecognised site for transmission regulation and net sympathetic tone. However, by investing more research into junctional modulation, one could aim to identify more selective and effective target therapies for CVDs at the site of neuroeffector coupling.

1.4.2.2. Heart

Cardiac sympathetic postganglionic fibres enter the pericardial sac and approaches the base of the heart jointly with cardiac preganglionic vagal branches, with each cardiac chamber receiving bilateral innervation from the left and right stellate ganglion (Figure 1.5A) (Coote and Chauhan, 2016). Upon contact, the sympathetic fibres begin to extensively branch as varicose swellings in the subepicardium, travel along the adventitial surface of great coronary vessels or their major branches, and penetrate depth-wise into the myocardium (Kimura *et al.*, 2012). Within the cardiac conduction system, the highest level of sympathetic innervation is within the SA node with a decreasing gradient down to the apex along the AV node and His-Purkinje system, where some Purkinje cells show no innervation at all (Dahlström *et al.*, 1965, Chow *et al.*, 2001, Kawano *et al.*, 2003). While there is a sympathetic predominance of innervation in the cardiac conduction system during childhood, a transition into co-dominance of sympathetic- and parasympathetic innervation occurs in adulthood

(Chow *et al.*, 2001). Overall, the density of sympathetic innervation in the atria is described to be higher than in the ventricles (Kawano *et al.*, 2003) and that on average, each cardiomyocyte forms multiple neuroeffector junctions with the same sympathetic neurone, but also from different neurones (Zaglia and Mongillo, 2017). The heart also possesses the ICNS, which includes intrinsic cardiac ganglia and a heterogeneous population of associated afferent and efferent nerves arranged in plexuses. The activity of the ICNS can be modulated by sympathetic postganglionic (and parasympathetic preganglionic) inputs for autonomic regulation (Armour, 2008, Allen *et al.*, 2018), such as SA nodal pacemaker regulation (Randall *et al.*, 2003, Zarzoso *et al.*, 2013).

1.4.2.3. Resistance vessels

The periarterial sympathetic nerve fibres of the mesenteric (and other) resistance vessels are located in the adventitial/medial border (Birch *et al.*, 2008) and forms very dense plexuses around the vessel (Figure 1.5B) (Furness, 1973). Perivascular innervation will follow the arterial supply, entering the tissue along the feeding arterioles and ending at the pre-capillary arterioles. The density of sympathetic innervation is inversely correlated with artery diameter, which is possibly due to the highly significant requirement of noradrenergic-mediated tone regulation prior to blood entry into the capillaries for tissue perfusion (Yokomizo *et al.*, 2015).

1.4.2.4. Methodologies to visualise innervation

Current methods that produce anatomical visualisation of sympathetic noradrenergic innervation predominately rely upon fixation methods, such as most of the immunohistochemistry and histochemical techniques. These techniques range from formaldehyde-glutaraldehyde (FAGLU: Furness *et al.* (1978)) and glyoxylic acid (Furness

and Costa, 1975) to detect for catecholamines, to immunoreactivity with NAd synthesis markers such as tyrosine hydroxylase. However, due to the fixation nature of these protocols, physiologically relevant data cannot be obtained in these tissues. In order to selectively measure for sympathetic transmission at the neuroeffector site with preserved physiological function within living tissue, non-toxic and high spatiotemporal methods are required.

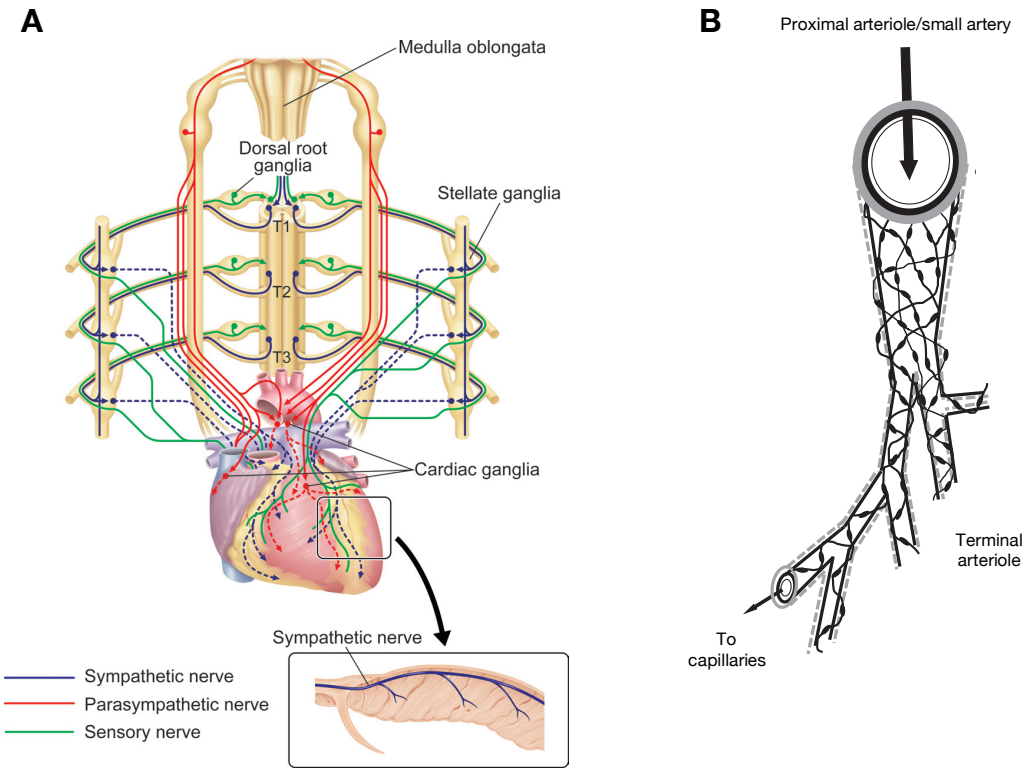


Figure 1.5: Sympathetic innervation of cardiovascular tissue
Schematic diagram demonstrating the sympathetic innervation of **(A)** the heart (with parasympathetic and sensory innervation) and **(B)** the resistance vessels. Images extracted from: **(A)** Kimura *et al.* (2012) and **(B)** adapted from Marshall (2015).

An example of such technological advancement is the fluorescent labelling of intracellular Ca^{2+} in sympathetic nerve terminals, first developed in the murine vas deferens (Brain and Bennett, 1997, Brain and Cunnane, 2008) and later optimised in the rat mesenteric arteries (Hansen *et al.*, 2019) to indirectly monitor AP propagation, exocytotic transmitter release, and the associated effector function. This technique involves retrogradely loading the sympathetic nerve terminals with a dextran-conjugated Ca^{2+} indicator, Oregon Green 488 BAPTA-1 dextran, though the entire mapping of innervation may require extensively long loading periods. Nevertheless, although fluorescent imaging is an advantage for discerning individual synapses and measuring for transmitter release, the repertoire is thus far limited for monitoring the termination of neurotransmission in the cardiovascular system (an important factor later discussed in section 1.5).

1.4.3. Neuroeffector transmission in cardiovascular tissue

1.4.3.1. Autonomic chemical mediators

Chemical mediators are liberated from the autonomic pre- and postganglionic neurones for signal transmission from the CNS to the innervated tissue. Within the autonomic ganglia, preganglionic neurone activation liberates acetylcholine (ACh) to activate postsynaptic excitatory nicotinic acetylcholine receptors on postganglionic neurones (Jänig, 2006b). In the case of the SNS, the postganglionic neurones may integrate signals derived from several convergent preganglionic neurones, with at least one suprathreshold ("strong") and several subthreshold ("weak") inputs (Bonica, 1968, Jänig, 2006a). There is also some evidence for interneurons within the sympathetic ganglia, termed 'small intensely fluorescent cells' (Takaki *et al.*, 2015).

The predominant mediators liberated from the sympathetic and parasympathetic postganglionic nerves are NAd and ACh, respectively. The chemical basis of neurotransmission in the heart was established by Otto Loewi in 1921, who observed a paralleled bradycardic effect in isolated frog hearts treated with the same perfusate collected from second hearts where the right vagus nerve was stimulated (Herring and Paterson, 2021). Initially termed *vagusstoff*, the substance in the perfusate was later identified as ACh by Henry Dale, which then led to the joint award with Loewi for the 1936 Nobel Prize in Physiology or Medicine. Similar studies were later conducted by Loewi into the substance that accelerates HR, which was identified as NAd by Von Euler in 1946, a recipient for the later 1970 Nobel Prize in Physiology or Medicine (Herring and Paterson, 2021).

The majority of sympathetic postganglionic neurones are noradrenergic, and so are able to synthesise and store NAd within vesicles concentrated within the nerve varicosity. In addition, NAd is co-released with co-transmitters adenosine triphosphate (ATP) and neuropeptide Y (NPY), amongst others, in a highly stimulation-dependent manner (Lundberg *et al.*, 1986, Burnstock, 2009). NAd and ATP are stored in small synaptic vesicles [20-60:1 ratio (Klein and Lagercrantz, 1981)], while NPY is stored in large dense-core granular vesicles, though some evidence suggests for their co-localisation with NAd in single vesicles (Svensson *et al.*, 2019). Co-transmission from sympathetic nerve terminals has been well reviewed in Burnstock (2013) and Svensson *et al.* (2019). At neuroeffector junction, the basal laminae of the sympathetic nerve terminal and effector tissue fuse; the small vesicles that contains the neurotransmitter, but not the large vesicles with neuropeptides, predominately aggregate at the thickened plasma membrane at the junctional cleft primed for release (Jänig, 2006b).

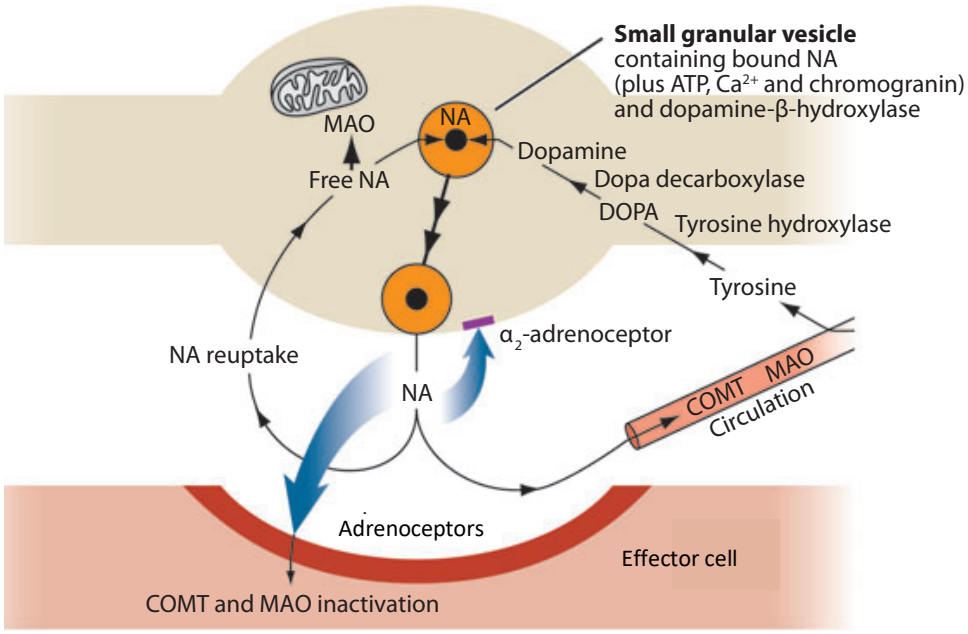


Figure 1.6: Noradrenergic transmission in sympathetic postganglionic nerve terminals

Simplified diagram demonstrating the synthesis, release, reuptake, and degradation pathways for NAd within the sympathetic nerve terminals and neuroeffector junction. Image extracted and adapted from Burnstock (2009).

Abbreviations: DOPA, dihydroxyphenylalanine; NA, noradrenaline; COMT, catechol-O-methyltransferase; MAO, monoamine oxidase.

1.4.3.2. Primary chemical mediator: noradrenaline

The primary sympathetic neurotransmitter, NAd, is synthesised from tyrosine (obtained from the blood) in a 3-step enzymatic conversion process within the nerve terminal (Figure 1.6). The first 2 steps take place within the axoplasm where tyrosine is converted by tyrosine hydroxylase (TH) to DOPA (dihydroxyphenylalanine), and from DOPA to dopamine by DOPA decarboxylase. Dopamine is then actively transported against its concentration gradient into neurotransmitter vesicles by the vesicular monoamine

transporter 2 (VMAT2); its motive force is set by the proton gradient established by the vesicular ATPase. Here, dopamine is finally converted to NAd by the membrane bound dopamine-β-hydroxylase (Figure 1.6) (Burnstock, 2009). Components of the NAd synthesis and storage process have been the therapeutic target for CVDs, such as methyltyrosine and reserpine to inhibit TH and VMAT2, respectively, for the treatment of hypertension (Engelman, 1988).

At least in the rodent vas deferens, each sympathetic nerve terminal contains NAd packaged at high concentrations in vesicles averaging at 15,000 NAd molecules/quantum, dependent upon the size of the vesicle (Dahlström *et al.*, 1966, Stjärne, 2000). Each nerve varicosity contains on average 500 small synaptic vesicles and 25 large dense-core granular vesicles (Stjärne and Stjärne, 1995). The total number of NAd molecules in noradrenergic nerve terminals that innervate one rabbit SA node cell alone is at a magnitude of 65×10^6 (Šćepanović, 2011), thus averaging 8 varicosities per cell. At the site of exocytotic release, the NAd concentration is equivalent to 10-100 mM [dependent on the mode of release; "kiss-or-run" or "complete fusion", (Svensson *et al.* (2019)], which rapidly dissipates into the neuroeffector junction down to 200-300 μM as NAd travels laterally, and finally up to 1 μM at the postjunctional receptor (Stjärne, 1989), as inferred by maximum neurogenic contraction in the rat tail artery (Bao *et al.*, 1993) and atria (Williamson and Broadley, 1989).

1.4.3.3. Action potential-mediated exocytotic release

Neuronal depolarisation elicited by AP propagation activates N-type VGCCs for Ca^{2+}-dependent exocytotic neurotransmitter release (Brain and Bennett, 1997). Exocytosis is a complex coordinated process mediated by a collection of proteins known as SNAREs [soluble NSF (N-ethylmaleimide-sensitive factor) attachment proteins] (Chen and

Scheller, 2001). Prior to fusion, a neurotransmitter vesicle is directed to the target neuronal membrane by the cytoskeleton (Porat-Shliom *et al.*, 2013) and tethered there via the interactions between SNAREs present on the plasma membrane and the vesicular membrane. During AP propagation, Ca^{2+} binds to synaptotagmin and promotes the fusion of the two lipid bilayers to dissipate the vesicular contents out into the extracellular space; vesicles are then rapidly endocytosed into coated pits back to the nerve terminal (Chen and Scheller, 2001). The precise cellular machineries that transport neurotransmitter vesicles to their target site and elicit the excitation-secretion pathway to deliver neurochemical signals in a regulated and timely manner were explored by Randy W. Schekman, James Rothman, and Thomas Südhof, who together were the recipients of the 2013 Nobel Prize in Physiology of Medicine (Ray, 2014). Unsurprisingly, neurotoxic compounds that inhibit transmitter release specifically target components of exocytotic machinery; for example, botulinum toxin cleaves SNAREs (Peng *et al.*, 2013) and colchicine disrupts the cytoskeletal architecture to prevent vesicular movement (Sorimachi *et al.*, 1973).

As assessed by electrophysiological- and fluorescence-based techniques, the release probability of a quantum of ATP from sympathetic nerve terminals (ATP per AP per varicosity) in the rodent urogenital system is very intermittent averaging at 0.01-3% despite undisrupted AP propagation (Brain and Bennett, 1997, Cunnane and Stjärne, 1984, Brain *et al.*, 2002). Furthermore, the release probability is highly heterogeneous with those at low basal release probability exhibiting more facilitation than those with higher probability during short trains of stimulation (Brain and Bennett, 1997, Brain *et al.*, 2002). Whether or not a similar pattern occurs for NAd remains unclear (Stjärne, 2000); although ATP and NAd are released in parallel the proportions are not fixed and are subjected to differential modulation (Stjärne, 2001). Nevertheless, this highlights that

sympathetic transmission is not uniform in tissues and here I speculate whether distinct populations of terminals within a tissue may be present to produce a coordinated response. This further prompts the requirement of high spatial resolution experimental techniques to monitor changes in neurotransmission.

1.4.3.4. Neuromodulatory prejunctional receptors

The sympathetic nerve terminal possesses a plethora of prejunctional regulators for release. Most importantly, released NAd activates prejunctional α_2-adrenoceptors (α_2AR) on the same nerve terminal to prevent further liberation as part of a negative feedback system (Starke, 2001). Interestingly, the α_2AR subtype for autoinhibition is frequency-dependent; in the mouse atria, there is a preference for the α_{2A}-AR and α_{2C}-AR subtype at high and low stimulation frequencies, respectively (Hein *et al.*, 1999). The inhibitory effects of α_2AR are most likely due a suppression of Ca^{2+} influx through VGCCs, and not by G protein-coupled inwardly rectifying K^+ channels (GIRK), as the latter are not expressed in peripheral noradrenergic neurones (Ruiz-Velasco and Ikeda, 1998). Interestingly, prejunctional facilitatory receptors are also present to enhance the release of NAd ($\beta_{1/2}$-adrenoceptor subtype) (Nedergaard and Abrahamsen, 1990), though there is some debate of its physiological relevance (Goldstein, 2010). In addition to NAd-sensitive prejunctional autoreceptors, there are also regulatory mechanisms in place for NPY and the other co-transmitters [for review, see Burnstock (2013)].

Sympathetic nerve terminals also possess heteroreceptors that are activated by ligands other than those that are released, i.e., NAd, ATP, and NPY (Fuder and Muscholl, 1995). An example is the muscarinic acetylcholine receptor (mAChR), which are inhibitory in the pupil (Bernhard *et al.*, 2004), heart (Trendelenburg *et al.*, 2003a, Trendelenburg *et*

al., 2005), and cultured sympathetic neurones (Kubista *et al.*, 2009), though some are also facilitatory in the heart (Costa *et al.*, 1993). Inhibitory mAChR are hypothesised to mediate autonomic cross-inhibition where sympathetic and parasympathetic nerve terminals are in close apposition, such as within the SA node (Ritter *et al.*, 2020).

Other sympathetic heteroreceptors that modulate NAd release include the cannabinoid type I- (CB_1R; section 7), opioid-, adenosine-, and bradykinin receptors (Trendelenburg *et al.*, 2000). A comprehensive review of these receptors can be found in Schlicker and Feuerstein (2017). The plethora of ligands that can modulate NAd release demonstrates for a great diversity of regulatory events that can occur within a neuroeffector junction, and questions whether a similar level of modulation may exist for NAd clearance by NAT.

1.4.3.5. Methods to measure for exocytotic release

Measurements of exocytotic transmitter release from sympathetic neurones in the rodent vas deferens can be resolved at the level of single neuroeffector junctions with electrophysiological- and fluorescent-based approaches. The former approach includes intracellular measurements of excitatory junctional potentials (EJPs) attributed to ATP activation of postjunctional inotropic P_{2X} receptors during trains of nerve stimulation. The electrical differentiation of fluctuations in the EJP rising phases can 'tease out' separate components, termed 'discrete events' (Blakeley and Cunnane, 1979a, 1979b). Each evoked discrete event of a single latency has a similar time course with spontaneous EJPs (sEJPs) thus suggesting for a common site of release. By refining the technique in single cells (poorly electrically coupled cells in a syncytium), it was revealed that evoked EJPs at a single latency can produce multiple matching discrete events that can be grouped into different amplitude classes. Furthermore, as

the time course of discrete events within each amplitude class matched so closely in an all-or-none manner, it would suggest the packet size of a release event is monoquantal (Cunnane and Stjärne, 1984). This technique, as well as measurements for excitatory junctional currents (EJCs), have been used to identify the high intermittence of neurotransmitter release from nerve terminals despite uninterrupted AP propagation. As a result, the technique is commonly used to measure local modulation of neurotransmitter release in response to varying conditions; a comprehensive review can be found in Brock and Cunnane (1993).

Similarly, several fluorescence-based techniques have been developed to measure secretory release events at neuroeffector sites. In addition to dual fluorescent labelling of Ca^{2+} in sympathetic neurones and the target effector tissue (Brain and Bennett, 1997, Brain *et al.*, 2002) (section 1.4.2.4.), some have designed false fluorescent neurotransmitters (FFNs) to directly measure exocytotic fusion and release events from individual presynaptic terminals in the CNS (section 1.6.2.3.) (Gubernator *et al.*, 2009). These techniques provide great understanding into the regulation of transmitter release, where the heterogeneous control of neuroeffector junction events between different varicosities can be resolved (Brain and Bennett, 1997, Brain *et al.*, 2002). However, currently there is a lack of high spatiotemporal techniques to investigate another important determinant of net neurotransmission - neurotransmitter clearance. To better understand the implications of a defunct clearance system, I will firstly discuss the postjunctional physiological effects of sympathetic activation in the cardiovascular system.

1.4.3.6. Postjunctional action of NAd

At rest, the heart is predominated by vagal tone that can reduce the rate of autorhythmicity to ~60 BPM (in young healthy adults) and dictate respiratory sinus arrhythmia. It is important to note that, at all times, autonomic control of cardiac function represents a net balance between vagal- and sympathetic tone. During bouts of exercise, an increase in cardiac function is initiated by vagal withdrawal that contributes to cardioacceleration to HR ≥100 BPM followed by sympathetic predominance (Coote, 2010). Most resistance vessels, on the other hand, are solely supplied by sympathetic nerve fibres and are in a constant state of constrictive 'tone', thus any required change in diameter is evoked by the hyperactivation or withdrawal of sympathetic activity (Klabunde, 2012).

Upon sympathetic nerve activation, NAd released from noradrenergic varicosities diffuses across the junctional cleft and binds onto postjunctional α- and β-adrenoceptors (AR). The αAR subtypes, α_1 and α_2, are $G_{q/11}$- and $G_{i/o}$-coupled, respectively, while the main βAR subtypes, β_1 and β_2 are G_s-coupled. The dominant pathways are driven by 1) phospholipase C (PLC)/inositol triphosphate (IP_3)/protein kinase C (PKC) ($G_{q/11}$) or 2) adenylyl cyclase (AC)/cyclic adenosine monophosphate (cAMP)/protein kinase A (PKA) [upregulated (G_s) or downregulated ($G_{i/o}$)] (Klabunde, 2012). These receptors and pathways can also be activated by circulating catecholamines, NAd and adrenaline, which the former is predominately contributed by sympathetic nerve terminals and both components from the adrenal medulla.

In the heart, NAd predominately activates the β_1AR in the SA nodal fibres to augment pacemaker activity: an increase in cAMP augments the Na^+-mediated I_f and thus earlier opening of L-type VGCC, thereby causing a more positive potential towards the

threshold and consequently an increase in pacemaker frequency (positive chronotropy). Similarly, enhanced ionic permeability in the AV node and Bundle of His reduces the conduction delay between each succeeding section, thereby accelerating the rate of atrial-to-ventricular contraction (positive dromotropy) (Klabunde, 2012). Myocardial β_1AR-induced PKA activation phosphorylates L-type Ca^{2+} VGCCs and the SR to augment $[Ca^{2+}]_i$ for enhanced contractility (positive inotropy). Further to this, PKA can also phosphorylate phospholamban to accelerate sequestration of intracellular Ca^{2+} back into the SR, and regulatory proteins involved in actin-myosin cross-bridging to dissociate Ca^{2+}, thereby increasing the rate of myocardial relaxation (positive lusitropy). NAd can also activate myocardial α_1AR to facilitate a further increase in $[Ca^{2+}]_i$ from the SR by the $G_{q/11}/IP_3$ pathway (Klabunde, 2012, Liu *et al.*, 2021). Interestingly, there is some evidence for the role of postjunctional β_3AR (negative inotropic and chronotropic) in instances of high noradrenergic activity for cardioprotection (Jovanovic *et al.*, 2019).

Despite dual innervation of the cardiac chambers by the right and left stellate ganglion, there appears to be regional specificity of cardiac function based on the location of sympathetic innervation received from the spinal cord. With an isolated innervated rabbit heart preparation, the right sympathetics were shown to predominately modulate rhythm control while the left sympathetics causes a significant inotropic response (Ng *et al.*, 2001, Winter *et al.*, 2012).

In most resistance vessels, NAd preferentially binds onto the α_1AR subtype on VSMCs. $G_{q/11}/IP_3$ activation enhances $[Ca^{2+}]_I$ by its liberation from the endoplasmic reticulum, which in turn mediates the downstream effect of myosin light chain kinase-induced phosphorylation of myosin light chain for cross-bridge formation. Similar vascular responses are seen with postjunctional α_2AR activation by NAd, though the α_1AR are

regarded as the most important αAR subtype. NAd (but more importantly, adrenaline) can also activate β_2AR in skeletal and hepatic vascular beds for vasodilatation, though the effects are usually overpowered by the vasoconstrictive effects of $\alpha_{1/2}$AR at high catecholamine concentrations (Klabunde, 2012).

As a result, SNS activation of the cardiovascular system increases cardiac function and TPR to elevate BP as a homeostatic response to stressful conditions. Following the stimuli, the SNS will gradually withdraw in order to return the physiological state to rest. However, evidence has shown persistent sympathetic activation in several CVDs that carries major prognostic implications, such as autonomic remodelling and end-organ damage. Interestingly, many are associated with dysfunctional noradrenergic termination mechanisms in cardiovascular tissues, namely the neuronal noradrenaline transporter (NAT) (section 1.5.2) (Schroeder and Jordan, 2012).

1.4.3.7. Brief account of noradrenergic termination

The 50-100 ms lifetime of ATP may reflect its rapid inactivation by ATPases in the neuroeffector junction (Zimmermann, 1994). The metabolic enzymes for NAd, on the other hand, are located intracellularly thus NAd is more metabolically stable with a longer lifetime of 1.5-5 s (Gonon *et al.*, 1993, Stjärne, 2000). As NAd is polar and does not diffuse across the plasma membrane, noradrenergic signal termination is entirely reliant upon efficient neuronal- and extraneuronal uptake mechanisms for removal (Stjärne, 1989) (Figure 1.3).

The main mechanism for NAd removal from the junctional cleft is by the NAT, a transporter located ubiquitously on the plasma membrane of sympathetic nerve

terminals (section 1.5.) (Esler *et al.*, 1990). Following reuptake, cytoplasmic NAd is either restored into vesicles by VMAT2 or deaminated by monoamine oxidase (MAO) present on the outer surface of the mitochondria into dihydroxyphenylglycol (DHPG) (Eisenhofer *et al.*, 2004). Thus, there is a dynamic 'sink' within the varicosity where NAd in the cytoplasm and vesicles are equilibrated so that levels in the former are kept to a minimum to prevent toxicity (Goldstein, 2010). Traces of NAd that escapes the NAT is either subjected to extraneuronal uptake ($uptake_2$) in some postjunctional tissues (Iversen, 1965), or liberated into the circulation to other tissues, both of which contains degradative enzymes MAO and COMT (catechol-O-methyltransferase) that can work in synergistically to degrade NAd (Figure 1.6, 1.7). The final metabolic step of NAd results in the end-stage metabolite vanillylmandelic acid (Wehrwein *et al.*, 2016).

1.5. Noradrenaline transporter

1.5.1. Neuronal uptake of biogenic amines

Catecholamines were once thought to be entirely inactivated by enzymatic breakdown akin to that seen with ACh (by acetylcholinesterase) (Axelrod, 1998). However, in the 1950s Julius Axelrod's laboratory observed that tritium labelled NAd ([^{3}H]-NAd) persisted unchanged in peripheral organs rich with sympathetic innervation, even after the evoked physiological effects (Whitby *et al.*, 1961). The intraneuronal localisation of NAd was further implied when the unilateral removal of the superior cervical ganglion from the cat exclusively abolished [^{3}H]-NAd uptake on that one side (Hertting *et al.*, 1961), and that [^{3}H]-NAd liberated by nerve impulses from the cat spleen returned to the same place where it was stored (Hertting and Axelrod, 1961). The direct evidence of NAd storage in sympathetic nerve vesicles was later captured by electron microscopy (Wolfe *et al.*, 1962). Together, these key discoveries (amongst many more)

propelled the scientific understanding of 'the humoral transmitters in the nerve terminals and the mechanisms for their storage, release, and inactivation', which was the topic for the 1970 Nobel Prize for Physiology or Medicine (Nicholls, 2020).

Now as we understand it, the mediator of NAd uptake into sympathetic neurones is by the prejunctional NAT, a member of the solute carrier 6 (SLC6) family (Pacholczyk *et al.*, 1991) (Figure 1.7), which consists of 20 transporter members for neurotransmitters, proteinogenic amino acids, taurine, and creatine, subdivided into the GABA transporter branch, monoamine transporter branch, and two amino acid transporter branches (Bröer and Gether, 2012). Other than NAT (SLC6A2), the members of the SLC6 family for monoamines include the cognate neuronal transporters for dopamine and serotonin [DAT (SLC6A3) and SERT (SLC6A4), respectively] (Bermingham and Blakely, 2016).

1.5.2. NAT (uptake$_1$)

Outside of Axelrod's laboratory, researchers such as Leslie Iversen described the ionic dependence, kinetic properties, and substrate competition of NAT (then described as uptake$_1$) (Iversen, 1967), and in 1991 the human transporter was cloned (Pacholczyk *et al.*, 1991). The NAT is a Na^+/Cl^--dependent transporter consisting of one single polypeptide of 500-600 amino acids that spans the prejunctional membrane in 12 α-helical domains (Kavanaugh, 1998) (Figure 1.7). NAT is exclusively localised on the sympathetic nerve terminal with minimal expression on the intervaricose segments (Schroeter *et al.*, 2000). Driven by the electrochemical gradient of Na^+ generated by the Na^+/K^+ ATPase, NAT pumps extracellularly located NAd in a saturable, secondary active process back into the nerve terminal (Iversen, 1963). One chloride ion is thought to accompany cellular entry alongside 1 NAd and 2 Na^+, though the net influx of positive

ions does not appreciably perturb the resting membrane potential of the cell (Iversen, 2006). The NAT is initially in the outward-facing conformation to bind $2Na^+$ and Cl^- followed by NAd, before transitioning into an inward-facing conformation (Niello *et al.*, 2020). As the ions and substrate dissociates intracellularly, the transporter slowly returns to the outward facing conformation, which is the rate-limiting step of NAd reuptake (Hasenhuetl *et al.*, 2019).

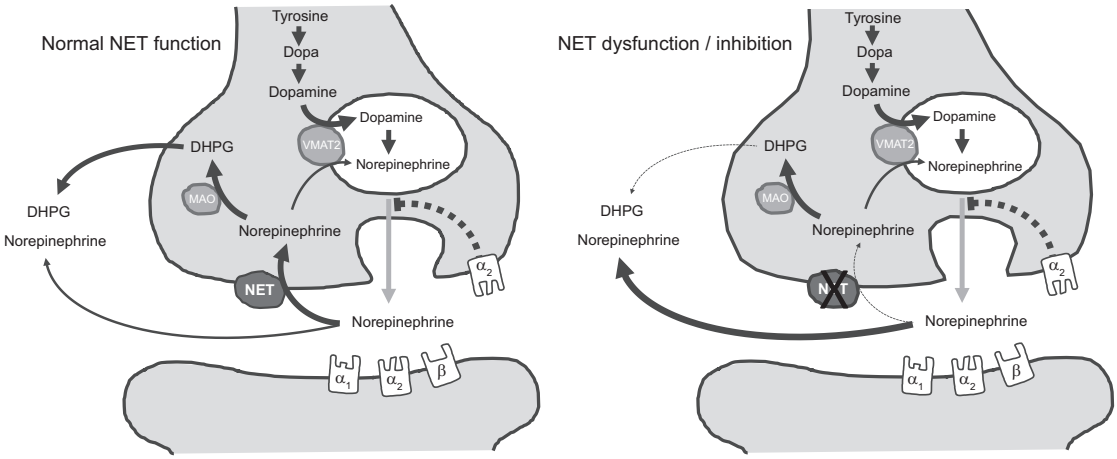


Figure 1.7: The effect of NAT dysfunction upon NAd overflow at the neuroeffector site
Schematic diagram demonstrating the role of NAT to minimise 'spill' of NAd from the junctional cleft into the circulation. NAd taken into the nerve terminal is subsequently transported into the vesicles by VMAT2 or metabolised by MAO into DHPG that is released into the circulation. Any disruptions to NAT function directly increase the amount of NAd that escapes into the plasma and reduce levels of metabolite DHPG. Image extracted from Schroeder and Jordan (2012).

Abbreviations: VMAT2, vesicular monoamine transporter 2; NET/NAT, norepinephrine/noradrenaline transporter; DHPG, dihydroxyphenylglycol; MAO, monoamine oxidase.

In response to stimuli, the NAT is a target for kinases and phosphatases that can alter its transcription or translocation to regulate transporter function (Mandela and Ordway, 2006b). The NAT N- and C-termini are located intracellularly and contains sites for

phosphorylation by PKC and Ca^{2+} calmodulin kinases, particularly on the serine/threonine residues (Bermingham and Blakely, 2016). Additionally, the large extracellular loop located between TM3 and TM4 contains three N-glycosylation sites, and it is the glycosylated form that is preferentially expressed on the membrane surface (Mandela and Ordway, 2006b). These molecular sites are targets for NAT regulation in multiple layers, either by changes in transporter intrinsic rate and/or plasma membrane availability (Savchenko *et al.*, 2003, Habecker *et al.*, 2006).

NAT function is important both centrally and peripherally, where any subtle changes could have profound effects on the human body. In the CNS, NAT is located predominately within the locus coeruleus-NAd system and it is responsible to regulate higher cognitive function, such as memory, learning, arousal/wakefulness, and attention (Mandela and Ordway, 2006b). Low levels of central NAd (and serotonin) is a marker for the monoaminergic deficient state in depression, thus the central NAT (and SERT) is often the target of neuropharmacological agents, such as tricyclic antidepressants, that inhibits NAd reuptake to treat psychiatric disorders (Montoya *et al.*, 2016).

In the periphery, the NAT is highly efficient and critical in the cardiovascular system, such as in the heart, vasculature, and kidneys, where up to 90% of released NAd is transported back into cardiac sympathetic nerve terminals (Goldstein *et al.*, 1988, Esler *et al.*, 1990). Additionally, there is approximately a 20:1 ratio of released NAd that contributes to the 'spill over' of NAd into plasma from the human heart (Kopin *et al.*, 1998). Unsurprisingly, an increase in NAd spillover is often a hallmark for NAT dysfunction (Figure 1.7), and it can be a direct predictor of disease progression in several CVDs such as hypertension, tachycardia, orthostatic intolerance (Schroeder and Jordan, 2012), and heart failure (Kaludercic *et al.*, 2010, Liang *et al.*, 1989). For this

reason, transporter regulation should be studied in conjunction with NAd release to comprehensively understand the dynamic modulation of net sympathetic volume transmission, as it may provide novel pharmacological targets to manage treatment-resistant CVDs.

1.5.3. NAT and cardiovascular disease

1.5.3.1. NAd and cardiovascular disease

The general consensus that overactivation of the SNS contributes to the pathogenesis and maintenance of several CVDs is vastly based on the observation that plasma NAd concentrations is high in human patients and experimental animal models, and that prognosis improves under adrenergic blockade (Grassi and Ram, 2016). This is also demonstrated by the fact that regional NAd spillover into plasma is well correlated with rates of sympathetic nerve activity to the heart, lungs (Yamaguchi *et al.*, 1975), and spleen (Brown and Gillespie, 1957). Under normal conditions, NAd (and adrenaline) fulfils a temporary homeostatic function; however, excessive adrenergic drive in chronic SNS activated states can trigger a number of adverse effects both in a structural and functional sense to induce target end-organ damage in CVDs (Grassi *et al.*, 2015). For example, in coronary artery disease (CAD) where the coronary vessels distal to the stenoses dilate maximally, the persistent increase in SNS-mediated HR and myocardial contractility increases the likelihood for myocardial ischaemia when autoregulation fails. Moreover, αAR-mediated systemic vasoconstriction augments cardiac preload and afterload, thereby increasing cardiac workload and myocardial oxygen consumption, despite reduced coronary blood flow (Florea and Cohn, 2014). In hypertension-related organ damage, the increase in afterload induces LV hypertrophy, in which the reduction in ventricular compliance overtime impairs ventricular filling (diastolic dysfunction) and

thus stroke volume, ultimately leading to heart failure (Grassi and Ram, 2016). At a slower timescale than at the myocardium and vasculature, NAd can also act in the kidneys to increase salt and water retention, leading to augmented blood volume and thus further straining on the heart. Finally, excess NAd can directly mediate tissue injury irrespective of postjunctional α- and β-AR activation; chronic NAd administration has been shown to increase markers for oxidative stress (Neri *et al.*, 2007), which can lead to myocyte apoptosis (Qin *et al.*, 2001), β_1AR downregulation, and damage sympathetic nerve endings (Liang *et al.*, 2000), all of which could exacerbate CVD phenotypes. Therefore, the regulation of net noradrenergic neurotransmission must be adequately understood to approach CVDs therapeutically to prevent end-organ damage. As NAT represents an important determinant of NAd junctional availability, the following sections aim to discuss the several CVDs associated with NAT dysfunction and the importance of identifying new therapeutic approaches associated with the transporter.

1.5.3.2. Atrial fibrillation

Cardiac arrhythmias are characterised by abnormal rhythmicity attributed to the discoordination of electrical impulse propagation in the cardiac conduction system. That present in the atria, termed atrial fibrillation (AF), is the most common sustained cardiac arrhythmia type affecting up to 3% of the United Kingdom (UK) population (Adderley *et al.*, 2019). Despite current management, many AF patients continue to develop cardiovascular pathologies, such as sudden cardiac death, heart failure (HF), and stroke (Marijon *et al.*, 2013). Unfortunately, the prevalence of AF-related hospitalisations continues to rise due to the ageing population and increased survival from preceding conditions such as acute myocardial infarction (AMI) (Friberg *et al.*, 2003). As a result, AF is becoming a major cause for morbidity and mortality, and poses

as a healthcare burden that costs the National Health Service (NHS) in the UK up to 1.6% of its total expenditure (Burdett and Lip, 2020). Therefore, better understanding of AF pathogenesis is required to aid the urgent clinical need for better strategies to prevent and treat AF.

Up to 20% of AMI patients proceed to suffer from AF, which may further hinder CO into the coronary circulation (Gorenek and Kudaiberdieva, 2012). Relevant pathogenic mechanisms include reduced atrial perfusion and stretch-induced LA arrhythmias (Gorenek and Kudaiberdieva, 2012). Whilst the ANS does play a role in AF arrhythmogenesis, the mechanism is less well understood. In AMI, there is a derangement of sympathetic hyperinnervation and denervation in different areas (Yokoyama *et al.*, 2017) paralleled with a reduction in NAT density (Zukela *et al.*, 2015). These findings suggests that atrial electrical instabilities might manifest as a result of inhomogeneities in regional innervation and clearance mechanisms (Yokoyama *et al.*, 2017). What is unclear, however, is whether the observed NAT dysfunction is a direct result of sympathetic denervation or, in fact, due to intrinsic changes in the transporter itself in intact nerve terminals.

It was demonstrated in the late 1990s that, in response to ischaemic stress, NAT enters into reverse transport mode to release vast amounts of NAd as analysed by microdialysis of myocardial interstitial fluid (Kurz *et al.*, 1995, Lameris *et al.*, 2000). The local accumulation of NAd in the ischaemic LV can then lead to nerve sprouting and consequently ventricular arrhythmogenesis, which can be significantly prevented by pharmacological blockade of NAT prior to AMI as a method of myocardial ischemic preconditioning (Wu *et al.*, 2012). Interestingly, in a canine model of LV AMI with sympathetic nerve sprouting in the atria and pulmonary veins, perfusion with

sympathomimetic amine, tyramine, directly initiated AF (Numata *et al.*, 2012). While this merely shows an AF arrhythmogenic effect of liberated NAd in the vulnerable heart, it does probe the question whether NAT reverse transport may also initiate AF in AMI, and if pharmacological blockade (with desipramine, for example) could be used as a preventative measure in those who are susceptible to CAD. To study this further, techniques are required to investigate NAT regulation *ex/in vivo* to understand how they might be affected in pathological states (entering reverse transport mode, for example) and when/how pharmacological agents could intervene to manage AMI-induced AF.

1.5.3.3. Resistant hypertension

Resistant hypertension (RH) is clinically defined by NICE (2019) as the incidence of uncontrolled BP (≥140/90 mmHg) in patients who are already receiving 3 antihypertensive drugs. Despite the enormous progress in understanding hypertension, the current strategies of BP control in clinical trials and in the clinic remain unsatisfactory worldwide even for those without RH (Williams *et al.*, 2018). Thus, RH patients are 50% more vulnerable than non-RH patients to have adverse complications, such as CAD, stroke, and end-organ damage. Consequently, a strive towards adequate BP control in RH patients is even more crucial to prevent the associated increase in morbidity and mortality (Myat *et al.*, 2012).

There is a growing interest in the sympathetic denervation of renal arteries (RDN) to treat RH. The catheter-based radiofrequency procedure destroys perivascular afferent and sympathetic efferent nerve fibres in hope to prevent further vasoconstriction and volume/sodium retention mechanisms (Ram, 2019). Although surgical RDN was shown to be promising to treat hypertension in experimental animal studies and preliminary

human studies (Singh and Denton, 2018), the 2015 results from 7 randomised controlled clinical trials (SIMPLICITY HTN2, 3, FLEX, and JAPAN, OSLO RDN, and PRAGUE-15 DENERHTN) (Fadl Elmula *et al.*, 2015) has prevented its routine clinical use in the UK for RH patients (NHS, 2016). Nevertheless, interest in the procedure remains due to the ongoing debate regarding factors that might have contributed to a lack of an effect, such as population- and procedural variability, as well as the sound pathophysiological understanding of autonomic uncoupling between the kidneys and the CNS in RH (MacIntyre and Webb, 2019).

Interestingly, in a recent study of RH patients that were enrolled in a RDN program, those with a single nucleotide polymorphism within the NAT gene (rs7194256; C→T allele) had significantly higher values of ambulatory BP and NAd plasma concentrations, and lower levels of the DHPG metabolite (indicative of reduced neuronal uptake and metabolism) compared to those without (C allele) (Eikelis *et al.*, 2018). Similarly, the same target allele (T allele) was previously found to be more prevalent in other NAT impairment diseases in humans, such as major depressive disorder, panic disorder, hypertension, and postural orthostatic tachycardia syndrome (Marques *et al.*, 2017). The T-allele is thought to encode a microRNA binding site to repress transporter translation (Marques *et al.*, 2017). This was intriguing as all RN patients (C- and T-allele) had similar MSNA (muscle sympathetic nerve activity) recordings (Eikelis *et al.*, 2018), suggesting the difference in BP was likely due to enhanced junctional availability of NAd. In other words, possessing the T-allele may render an individual more vulnerable to neurogenic hypertension. This could suggest that T-allele RH patients may benefit from an additional prescribed αAR antagonist as their 4th antihypertensive drug, while it would hypothetically not be as useful for those with a C-allele. In order to study this, more

investigations are required to study long term regulatory control of the NAT and thus require more specific and sensitive tools.

1.5.3.4. Chronic heart failure

Chronic heart failure (CHF) is characterised by the inability of the heart to pump effectively to supply tissues with oxygenated blood to meet demand. CHF is not a standalone disease, but rather the chronic endpoint of several CVDs that ultimately impinges upon impairment of cardiac filling and/or ventricular function. CVDs that predispose an individual to CHF include cardiac arrhythmias, MI, and hypertension. Today, CHF affects up to 1.5% of the UK population (NICE, 2018), which will continue to rise due to similar reasons for AF mentioned previously (Braunschweig *et al.*, 2011). However, despite drug- and device-based therapies, the 5-year survival rate of CHF patients remain close to 50% (Stewart *et al.*, 2001). Therefore, it is crucial to thoroughly understand the early mechanisms that govern CHF initiation in order to intervene with disease progression and improve prognosis.

The SNS is hyperactivated in CHF patients as an early compensation mechanism to restore CO and BP (Pepper and Lee, 1999); interestingly, an increase in sympathetic activity is initially detected in the heart before advancing to the skeletal muscles and kidneys. As CHF progresses, sustained SNS leads to progressive increases in preload, afterload, plasma NAd, retention of salt and water, and oedema. In the long term, SNS hyperactivation downregulates myocardial β_1AR and reduces inotropic responses, which further enhances SNS in a vicious cycle (Borovac *et al.*, 2020). The NAT appears to be an important mediator for progressive CHF, as reduced cardiac [^{123}I]-metaidobenzylguanidine (MIBG) uptake can directly predict rates of

hospitalisations and cardiac deaths in CVD patients (Imamura *et al.*, 2001). Moreover, NAT overexpression by adenoviral vector transfer in a paced rabbit model of CHF ameliorated myocardial β_1AR downregulation and improved ventricular diameters to restore systolic function (Münch *et al.*, 2005). However, there is some debate as to whether NAT dysfunction precedes, or is a consequence of, a loss of cardiac sympathetic nerve terminals.

In a salt-induced model of CHF, a reduction in cardiac [^{3}H]-NAd uptake was in fact attributed to a decline in neurotrophic factors (positive NAT regulator) that occurred 10 days prior to a loss of sympathetic nerve terminals (Backs *et al.*, 2001, Kreusser *et al.*, 2008). Similarly, when rat hearts were treated with reserpine for 1 day to mimic the paradoxical mass NAd depletion in HF there was a corresponding post-transcriptional downregulation of cardiac NAT (Kreusser *et al.*, 2017). Such modifications of NAT function in intact nerve terminals could be driven by microRNA mechanisms (Deng *et al.*, 2016), mineralocorticoid- and endothelin receptor activation (Buss *et al.*, 2006), and oxidative species generation by MAOs (Kaludercic *et al.*, 2010, Kaludercic *et al.*, 2014). In contrast, others have attributed NAT dysfunction to a loss of cardiac nerve fibres in other experimental models of CHF, such as volume overload (Kristen *et al.*, 2006) and MI-induced HF (Wang *et al.*, 2019).

In the clinic, inhibitors of postjunctional receptors involved in NAd signalling have been adopted to reduce noradrenergic transmission to treat HF (Bencivenga *et al.*, 2019). However, the wealth of studies that describe a post-translational NAT downregulation in HF identifies a new therapeutic target to hinder CHF disease progression. Indeed, the therapeutic potential of inhibiting negative modulators of NAT has been demonstrated in experimental HF animal models (Backs *et al.*, 2005, Buss *et al.*, 2006). However,

recent evidence also show that a post-translational effect of NAT also occurs in the SMA of HF, though there was an upregulation (rather than downregulation) of transporter function with preserved nerve density (Blanco-Rivero *et al.*, 2021). These results demonstrate that there might be tissue disparities of NAd homeostasis in HF. To elucidate this further, NAT-specific techniques are required to investigate tissue differences in transporter regulation to aim for selective target therapies.

1.5.3.5. Chronic intermittent hypoxia

Obstructive sleep apnoea (OSA) is a sleep disorder characterised by nocturnal episodes of upper airway collapse that corresponds to drastic reductions, or even complete eliminations, in breathing (Prabhakar and Semenza, 2016). Due to the hypoxic stimuli and inability to compensate for an increase in airway resistance, the individual is aroused briefly and cyclically to restore pharyngeal patency, which may repeat up to 60 episodes/hr of sleep (Prabhakar and Semenza, 2016). The resultant cyclic oscillations between tissue hypoxia (15-60 s) and reoxygenation incurs transient ischaemia of tissues and is termed 'chronic intermittent hypoxia (CIH)'. Often OSA patients suffer from sleep fragmentation, which can result in cognitive deficits (Djonlagic *et al.*, 2012) that threaten safety in the workplace (Garbarino *et al.*, 2016). Importantly, OSA poses further public health concerns due to the cardiovascular and cerebrovascular risk associated with CIH-induced heightened sympathetic nerve activation (Dewan *et al.*, 2015).

During an apnoeic episode, the chemoreflex-dependent increase in the SNS is potentiated due to the elimination of the sympathoinhibitory thoracic afferents (Somers *et al.*, 1989, Narkiewicz and Somers, 1997). Upon resumed breathing, venous return

and CO into the vasoconstricted circulation results in a rise in BP at the end of each apnoea (Mansukhani *et al.*, 2014). However, sympathetic hyperactivation appears to carry over into the daytime in OSA patients, as seen with higher sustained MSNA activity and plasma NAd levels compared to healthy controls (Carlson *et al.*, 1993). As a result, OSA patients are particularly vulnerable to the development of various CVDs, such as RH (Jehan *et al.*, 2020), AF, and stroke (Yaranov *et al.*, 2015). It has been suggested that the repeated apnoeic episodes during sleep induces a chronic pathological enhancement of sympathoexcitation that eventually promotes CVD initiation (Prabhakar *et al.*, 2012).

There is a body of evidence to show the CIH-induced augmentations in chemoafferent discharge (Holmes *et al.*, 2019) and central sympathetic outflow (Knight *et al.*, 2013, Shell *et al.*, 2016) drive the maladaptive cardiorespiratory outcomes in OSA. However, limited information is available regarding the dynamic events at the sympathetic neuroeffector junction that could lead to cardiovascular end-organ damage. While one study of acute hypoxia in healthy humans showed an enhancement of NAd clearance, the authors were unsure whether it was secondary to an increase in blood flow to organs with high clearance capacity (Leuenberger *et al.*, 1991). Therefore, specific techniques to detect dynamic changes in NAT-specific clearance are required to help elucidate mechanisms of CIH-dependent CVD initiation and progression to understand prevent end-organ damage and ultimately improve disease prognosis.

1.5.4. Targeting NAT to treat cardiovascular disease?

Most research of the SNS in CVDs have been focused upon sympathetic nerve traffic and plasma NAd as markers for disease (Jordan and Grassi, 2018). However, there is

now an appreciation for the imperative role of NAT dysfunction in CVDs. Afterall, the typical hallmark of enhanced plasma NAd concentration can also be explained by reductions in NAd reuptake. Therefore, the NAT in cardiovascular tissue represents an attractive target to modulate function in CVDs. Targeting NAT pharmacologically in the CNS is common practice for psychiatric disorders (Montoya *et al.*, 2016), though its use in the periphery requires further research.

Prior to this work, there were no experimental tools available to study neurotransmitter clearance independently of release at the level of discrete neuroeffector junctions in living tissue. These tools would be profoundly useful to investigate the role of endogenous and exogenous NAT neuromodulators that could affect net sympathetic transmission. The following sections will explore the existing methodologies that provide insight into NAT-mediated clearance and their associated challenges.

1.6. Existing methodologies to measure NAT function

1.6.1. Radiolabelled NAT substrates

The most common method to assess NAT function is by measuring the overflow or accumulation of radiolabelled NAT substrates, such as [^{3}H]-NAd, in response to stimuli with or without NAT inhibition. The total and regional NAd clearance rate from plasma *in vivo* can be calculated with an intravenous infusion of [^{3}H]-NAd at steady state conditions by assessing the infusion rate and plasma concentration of specific activity (Esler *et al.*, 1984, Eisenhofer *et al.*, 1991a). Plasma NAd clearance can also be contributed by non-neuronal pathways of NAd uptake, termed uptake$_2$ (Lightman and Iversen, 1969); thus, a technique has been refined to measure specific activities of the neuronally sourced NAd metabolite, [^{3}H]-DHPG, alongside [^{3}H]-NAd. However,

measurements are often distant from sites of NAd reuptake into varicosities, thus mechanistic insights at high spatial resolutions are limited. Macroscopically, radioisotopes are useful in a clinical setting, where NAT substrates serve as PET probes, e.g., [^{123}I]-MIBG, to quantify cardiac sympathetic nerve innervation (Miranda *et al.*, 2014) and to identify NAT-expressing tumours such as phaeochromocytomas (Lenders *et al.*, 2014). With this technique, clinical studies have also discovered cardiac regional heterogeneities of reuptake in some CVDs, such as in Brugada syndrome (Wichter *et al.*, 2002). However, the interpretation of detective NAT kinetics is often complicated by concurrent sympathetic remodelling in disease and variations in blood flow-mediated delivery of the radiotracer.

On a microscopic scale in *ex vivo* and *in vitro* radiometric assays, NAT-expressing isolated tissues and cells are exposed to [^{3}H]-NAd and lysed to measure the total cellular accumulation of tritium as a marker for reuptake (Iversen, 1967, Schwartz *et al.*, 2005). While this technique can be conducted in conjunction with desipramine to measure NAT-specific uptake, and radiobinding- and molecular assays to estimate changes in transporter expression and function, it is often limited by its low temporal resolution to measure for real-time, dynamic changes in NAT reuptake rate that could otherwise be overlooked.

1.6.2. Rotating disk recordings

NAd release and NAT-mediated clearance can also be measured with electrochemical techniques, such as rotating disk electrode voltammetry (RDEV). The high temporal resolutions in RDEV are provided by the readiness of NAd oxidation at the carbon fibre microelectrode, and that the detected current flow is directly proportional to the analyte

concentration measured with nanomolar sensitivity in the millisecond domain (Gerhardt and Burmeister, 2000, Eisenhofer, 2001). In RDEV, a rapidly rotating disk is placed near the tissue in solution, which induces a laminar flow to draw solution up to the microelectrode. Here, NAd becomes oxidised, and the oxidised products are then rapidly 'spun away' (Burnette *et al.*, 1996, Hagan *et al.*, 2010). However, applications of RDEV can be limited for several reasons; RDEV lacks analytical specificity between catecholamines, particularly dopamine (Robinson *et al.*, 2003), and other electrochemically active species. Moreover, the site of catecholamine measurement *ex/in vivo* is often distant from neuroeffector junctions, thus analyte measurements are likely to be lower than at the site of release with limited detection sensitivity for endogenously low concentrations of the catecholamine. Thus, the use of voltammetry may be challenging to measure NAT function in mature cardiac sympathetic nerve terminals *ex/in vivo* at the spatial resolution required to measure local regulation of transporter rate.

1.6.3. Quantitative fluorescence microscopy

1.6.3.1. ASP^+/APP^+

The neurotoxin 1-methyl-4-phenylpyridinium (MPP^+) is a high affinity substrate for the biogenic amine transporters NAT, DAT, and SERT (Namura *et al.*, 1987). Interestingly, the MPP^+ analogues, APP^+ [4-[4-(dimethyl amino)phenyl]-1-methylpyridinium] and ASP^+ [4-[4-(dimethyl amino)styryl]-*N*-methylpyridinium iodide] are fluorescent and have been used to study transporter kinetics with the potential for high throughput screening of NAT substrates and inhibitors *in vitro* (Schwartz *et al.*, 2003, Haunsø and Buchanan, 2007). APP^+ is also able to label noradrenergic neurones in mouse midbrain slices *ex vivo* (Karpowicz *et al.*, 2013), thus the compound was of interest to adapt in peripheral

tissues *in vivo*. However, Karpowicz and colleagues (2013) demonstrated that APP^+ is unable to enter the neuronal synaptic vesicular pool via VMAT2 but rather non-specifically aggregates into non-exocytic cellular compartments, such as the nucleoli and mitochondria. As NAT kinetics can be sensitive to changes in VMAT2 function (Trendelenburg *et al.*, 1972), APP^+ may not be a suitable probe to measure transporter regulation. Moreover, the current laboratory was not able to confidently demonstrate positive noradrenergic labelling in isolated organ preparations, such as the murine anococcygeus and vas deferens (Amos, 2007), thus other avenues of fluorescence-based imaging were pursued.

1.6.3.2. False fluorescent neurotransmitters

False fluorescent neurotransmitters (FFNs) are optical tracers designed to monitor neuronal release events. FFNs are optimised to be transported intracellularly by the cell surface transporter and subsequently into vesicles by VMAT2 for exocytosis (Karpowicz *et al.*, 2013, Leopold *et al.*, 2019). The technique has been helpful to monitor activity-dependent synaptic plasticity in the brain *ex vivo* (Gubernator *et al.*, 2009) and *in vivo* (Rodriguez *et al.*, 2013, Dunn *et al.*, 2018). However, to my knowledge, the application of FFNs is primarily for studies into exocytotic release, and not yet to be extended or validated to monitor NAT function in the peripheral nervous system.

1.6.3.3. GPCR activation-based NAd sensors

In the late 2010s, a new type of technology was developed involving fluorescent sensors genetically scaffolded onto G protein coupled receptors (GPCRs) to detect for NAd concentrations (Feng *et al.*, 2019). These GPCR activation-based sensors (GRABs) takes advantage of the large conformational change that GPCRs undergo during ligand

binding (Jing *et al.*, 2019), and have been demonstrated to provide analyte quantification at very high spatiotemporal resolutions *in vivo* within the nanomolar range of detection (Feng *et al.*, 2019). In the case for NAd, the α_2AR subtype was chosen for GRAB scaffolding (Feng *et al.*, 2019), and it is quite possible these sensors would be useful in the future to measure NAT function in conjunction with desipramine. However, it would perhaps only provide an indirect measurement of NAT function secondary to the total junctional availability of NAd.

1.6.3.4. Neurotransmitter Transporter Uptake Assay

The Neurotransmitter Transporter Uptake Assay (NTUA) is a commercially available kit (Molecular Devices), which contains a proprietary fluorescent substrate that mimics the biogenic amines (NAd, dopamine, and serotonin). Developed within cell-based systems, the novelty of NTUA also resides within a mixed-in masking dye that extinguishes extracellular fluorescence until the substrate has been transported intracellularly (R8173, Molecular Devices, Berkshire, UK; U.S. Patent # 6420183, 7063952, 7138280 and European Patent # 0906572). The NTUA assay can therefore be used to detect the activity of their corresponding transporters (NAT, DAT, and SERT, respectively).

The use of NTUA to accurately determine NAT function has been validated in cell culture systems, where the K_i values of known inhibitors have been comparable to those within the literature, particularly in the gold standard radiometric assays (Jørgensen *et al.*, 2008, Zwartsen *et al.*, 2017). In contrast to the latter, NTUA is straightforward to use, does not require specific facilities nor professional personnel, and is more cost efficient. The technique has also been adapted to measure active VMAT2-mediated uptake into vesicles following reuptake by DAT (Bernstein *et al.*, 2012).

The current laboratory has previously demonstrated the use of NTUA to label sympathetic nerve terminals and monitor NAT activity in the intact murine vas deferens *ex vivo* (Parker *et al.*, 2010), an organ commonly used to model sympathetic co-transmission (Burnstock and Verkhratsky, 2010). Given its success, it is of particular interest to adapt the technique for the rodent cardiovascular system. This would overcome the challenges faced by existing techniques to measure NAT function *ex vivo* and be a step forward in understanding how neurotransmitter clearance regulation may be dysfunctional in CVDs. One particular class of sympathetic modulators that may have therapeutic potential for CVDs are the cannabinoids.

1.7. Cannabinoids

The earliest record for the medicinal use of the cannabis plant (*Cannabis sativa*) was made in the 18th century BCE in an herbarium published by the Chinese Emperor Sheng Nong for its anti-inflammatory benefits and alleviation of symptoms associated with absent-mindedness, gout, and stroke (Yang, 1998). Now, cannabis is widely used in both therapeutic and recreational contexts for its sedative, relaxant, anxiolytic, and analgesic properties (Kalant, 2001) with over 203 million users worldwide (Degenhardt and Hall, 2012). Despite its apparent use throughout history, it was only in the 1960s when its principle psychoactive constituent, Δ^9-tetrahydrocannabinol (Δ^9-THC), was isolated (Gaoni and Mechoulam, 1964), and since then 113 other cannabinoids were discovered (Pacher *et al.*, 2018).

The 'cannabinoids' refer to the ligand compounds that can activate the endocannabinoid system (ECS; section 1.7.2) in a functionally similar manner as Δ^9-THC; they can be naturally occurring (phytocannabinoids), endogenously present

(endocannabinoids; eCB), or synthetic (Pertwee, 2005). Other components of the ECS include its receptor targets, transporters, degradative enzymes, and degradative products. Cannabinoids can exert a plethora of actions centrally and peripherally, which the mechanisms have been extensively examined and reviewed from the 1990s following on from the discovery of the first cannabinoid receptor a few years prior (Malinowska *et al.*, 2012). However, despite an increase in usage globally and changing attitudes towards expanding its legalisation, much of the available data on Δ^9-THC is focused on its neurological properties, with very little information on its cardiovascular effects (Subramaniam *et al.*, 2019). Interestingly, available research indicates the effects of cannabinoids on the cardiovascular system can be related to the modulation of sympathetic transmission.

1.7.1. Cannabinoids and the cardiovascular system

Cannabinoids elicit complex and variable actions on the cardiovascular system, which are highly dependent upon ligand type, activated receptor type, dose, route of administration, experimental setting (*ex/in vivo,* isolated vessel vs. perfused vascular bed), and if in experimental animals, whether a state of anaesthesia is incurred, and the type of anaesthetic (Randall *et al.*, 2002, Malinowska *et al.*, 2012). Despite these variabilities, the most important features of systemic administration of cannabinoids at high doses *in vivo* are bradycardia and hypotension (Randall *et al.*, 2002).

In anaesthetised animals, the cardiovascular effects of cannabinoids occur as a triphasic response - a short-lived reduction in HR and BP (phase I), followed by a brief pressor response (phase II) that finalises upon a prolonged bradycardic and hypotensive effect (phase III). Phases I and II are also present in conscious animals,

though phase III is only evident in pre-emptive states of high sympathetic tone. In man, acute exposure to cannabinoids induces an immediate tachycardic response and a small pressor effect, while orthostatic hypotension is pronounced in those with hypertension or elevated SNS phenotypes. Chronic use of cannabinoids, on the other hand, can elicit significantly long-lasting reductions in HR and BP. The different physiological effects imposed by cannabinoids *in vivo* are mediated by the variety of receptors in central and peripheral sites that become activated, including those that modify autonomic outflow (Randall *et al.*, 2002).

Functional studies have suggested that phase III of cannabinoids could be contributed by the prejunctional suppression of NAd release from sympathetic nerve terminals in the heart and vasculature (O'Sullivan, 2015). However, there is currently little evidence of the effect of cannabinoids on NAT-mediated reuptake; interestingly, the current laboratory did demonstrated for a cannabinoid-mediated reduction in NAT function in the murine urogenital system (Kennard, 2015); whether a similar action is present in the cardiovascular system is largely unknown. Regardless, one must not forget that there are also alternative modes of action that may explain for phase III of cannabinoid exposure; thorough reviews of the extensive physiological effects of cannabinoids can be found in Randall *et al.* (2002) and Malinowska *et al.* (2012).

1.7.2. Cannabinoid receptors

Within the cannabinoid receptor family, the cannabinoid type I- (CB_1R) and II (CB_2R) receptors are the GPCRs best known to mediate the effects of cannabinoids (Pertwee *et al.*, 2010). CB_1Rs primarily modulate neurotransmitter release and are most highly expressed within the CNS in regions associated with higher cognitive function, such as

memory and learning (hence the psychoactive effects of Δ^9-THC), and at lower levels in peripheral organs (Di Marzo, 2008). Importantly, CB_1R is the dominant (if not only) subtype found prejunctionally on sympathetic nerve terminals in the heart and vasculature (Malinowska *et al.*, 2012), though to my knowledge there is no morphological evidence to confirm this. CB_2R, on the other hand, are mostly associated with immune cells to mediate the anti-inflammatory effects of cannabinoids (Di Marzo, 2008) and shares about 66% homology with CB_1R in the murine species (Shire *et al.*, 1996).

The major signal transduction pathways for CB_1R and CB_2R activation are mediated by $G_{i/o}$-coupled proteins. Upon stimulation, cannabinoid receptors modulate intracellular activity by the downstream effectors associated with the inhibition of AC and reduced levels of cAMP. In the case of CB_1R, but not CB_2R, receptor activation inhibits ion channels VGCC (N- and P/Q-type) and activates GIRK. However, the physiological effects of cannabinoids can be complicated by promiscuous G-protein coupling with G_s- and $G_{q/11}$-proteins dependent upon the ligand and its concentration (Wouters *et al.*, 2019).

Another cannabinoid-sensitive target is the transient receptor potential vanilloid type I ($TRPV_1$); $TRPV_1$ is a ligand-gated non-selective cation channel expressed on peripheral neurones that is best known to mediate phase I of the *in vivo* effects of cannabinoids in animals. Cannabinoids activate $TRPV_1$ present on cardiac vagal afferents to elicit the Bezold-Jarisch reflex for cardio/vasodepression (Aviado and Guevara Aviado, 2001, Pacher *et al.*, 2005a), and on perivascular sensory nerve terminals to release calcitonin gene-related peptide for vasorelaxation (Ralevic and Kendall, 2009). The cannabinoid

receptor type responsible for phase II effects is unclear, though some suggest $TRPV_1$ and/or centrally located receptors (Malinowska *et al.*, 2012).

Other cannabinoid sensitive receptors that are found to modulate cardiovascular effects include the NMDA receptors, β_2AR, thromboxane A_2 receptors, α_7-nicotinic ACh receptors, and endothelial cannabinoid receptors (CB_xR). However, a thorough discussion is beyond the scope of this thesis; thus, a comprehensive review of these non-CB_1R/CB_2R/TPRV1 receptors (and others) can be found in Malinowska *et al.* (2012) and Bondarenko (2014).

1.7.3. CB_1R at the sympathetic neuroeffector site

Several studies have attributed phase III of cannabinoids to CB_1R. Firstly, intravenous infusion of CB_1R inverse agonist, SR141716A, into wild-type mice prior to cannabinoid exposure had no effect upon phase I or II but abolished the reductions in cardiac contractility and TPR in phase III (Pacher *et al.*, 2004). Similarly, while the haemodynamic profiles of phase I and II were absent in $TRPV_1$ knockout mice, the persistence of phase III was eventually antagonised by SR141716A (Pacher *et al.*, 2004) and CB_1R knockout mice (Ledent *et al.*, 1999). Finally, there is a positive correlation between the binding affinities of cannabinoids and the EC_{50} of the elicited phase III effects (Lake *et al.*, 1997).

With the use of [^{3}H]-NAd in isolated tissues and pithed animals, the CB_1R that mediate a cardio/vasodepressive effect were found to be located prejunctionally on sympathetic nerve terminals in the rodent heart (Malinowska *et al.*, 2001), tail arteries (Malinowska *et al.*, 1997), mesenteric bed (Ralevic and Kendall, 2002), and renal arteries (Deutsch *et al.*,

1997). However, to my knowledge, there is little information of its effect on NAT kinetics in the neuroeffector junction. Moreover, within the literature the use of NAT inhibitors is inconsistent in [^{3}H]-NAd overflow experiments, thus any assumptions of an effect cannot be inferred. As the NAT would be present at the same location as the release-inhibiting CB_1R, it is reasonable to assume cannabinoids may also affect NAd clearance concomitantly with NAd release. These investigations could also provide further insight and possibly explain for cardiovascular effects of cannabinoids that are atypical of phase I-III. In this thesis, the NTUA technique shall be used to investigate exclusive effects of cannabinoids upon the NAT in cardiovascular tissue.

1.7.4. Endocannabinoids and its therapeutic potential

The endocannabinoid system (ECS) includes the CBRs, eCBs, reuptake transporters and ligand degradation enzymes. The eCBs are derivatives of arachidonic acid that are enzymatically synthesised 'on demand' from membrane phospholipids. A postsynaptic depolarisation-induced increase in $[Ca^{2+}]_i$ or $G_{q/11}$-mediated Ca^{2+} mobilisation will trigger the synthesis and release of 2-arachidonoyl glycerol (2-AG) and anandamide (AEA) (the two main eCBs), which can act retrogradely to induce 'depolarisation-induced suppression of inhibition/excitation' (Szabo and Schlicker, 2005, Di Marzo, 2008). 2-AG is a full agonist at both CB_1R and CB_2R with no affinity towards $TRPV_1$, though AEA is a partial agonist at CB_1R and $TRPV_1$ but a weak agonist at CB_2R (Pertwee *et al.*, 2010). Upon release, eCBs have a short half-life *in vivo*, owing to its rapid transport intracellularly and metabolism by degradation enzymes FAAH (fatty acid amidohydrolase, for AEA) and MAGL (monoacylglycerol lipase, for 2-AG) (Pacher *et al.*, 2018).

Given the prominent cardiovascular effects exerted by cannabinoids, it is surprising that global knockout of CB_1R, CB_2R, and FAAH mice have normal BP, myocardial contractility, and baroreflex sensitivity, indicating the minimal role of the ECS in normal cardiovascular regulation (O'Sullivan, 2015). Interestingly, the role of eCB to induce cardio/vasodepressive effects only becomes blatant in states of sympathetic overactivity, such as hypertension, which is thought to be cardioprotective (Haspula and Clark, 2020). For example, an increase in plasma AEA by FAAH inhibition normalises cardiac contractility and BP in a CB_1R-dependent manner in spontaneously hypertensive rats (SHR), while no effect is observed in normotensive animals (Bátkai *et al.*, 2004). Similarly, other components of the ECS are also upregulated in hypertension (experimental animals and patients), such as circulating eCB (Li *et al.*, 2009), CB_1R expression (Wang *et al.*, 2017a), and the elicited functional effect (Toczek *et al.*, 2015).

The cardio/vasodepressive effect of CB_1R activation in hypertensive states appear to be mediated peripherally, rather than centrally. For example, the SR141716A-mediated accentuation in BP and cardiac contractility in SHR was not observed with intracerebroventricular administration (Bátkai *et al.*, 2004). Moreover, CB_1R antagonist AM251 treatment alone enhanced the neurogenic vasopressor response to electrical stimulation in the pithed and vagotomised DOCA-salt hypertensive rats, but not the normotensive counterparts (Toczek *et al.*, 2015), thus also indicating the mechanism of BP control by an overactive ECS in hypertension is by a prejunctionally-mediated inhibition of sympathetic transmission. However, what is unclear is whether CB_1R also acts upon NAd clearance mechanisms, such as the NAT. This would be an important factor to consider as the net junctional NAd concentration is dynamically determined by the balance between NAd release and reuptake. As such, it is pertinent to discover CB_1R modulation of NAT function in healthy states (if any) to understand the dynamics

of junctional transmission, and whether this also becomes altered in pathological conditions such as hypertension. These are important questions to tackle particularly due to the growing interest in enhancing the ECS pathways for future therapeutic approaches.

1.8. Objective and aims

Based on the work of others, studies of NAT function on a macroscopic scale have allowed for the investigation into the net effects of transporter function in cardiovascular pathophysiology. However, to be able to identify key modulators that govern the finer and local control of the NAT in the cardiovascular system require techniques with high spatiotemporal resolutions. By understanding how NAT function is modulated at the neuroeffector site, these methods will allow us to better understand the mechanisms of sympathetic regulation within the cardiovascular system and be able to assess novel therapeutic targets, for example the CB_1R. As such, the aims and objectives of the present thesis are:

1. To optimise a fluorescence-based technique, the NTUA assay, to label sympathetic nerve terminals and concomitantly monitor for single-terminal NAT function in the rodent cardiovascular system *ex vivo*, namely the heart and mesenteric periarterial vessels. I will also assess the usability of NTUA in other rodent tissues and its translation into human tissues. These aims are explored in Chapter 3.

2. Apply the NTUA methodology to understand how single-terminal NAT function may differ across species between mice and rats, and whether transporter

function is heterogeneous in different tissues, namely the rodent heart and blood vessels. These aims are explored in Chapter 4.

3. Apply the NTUA methodology to investigate whether the single-terminal cardiac NAT function is altered by autonomic activity as mimicked by either nerve stimulation or application of exogenous agonists. If there are changes, I will attempt to dissect key mechanisms that govern this. These aims are explored in Chapter 4.

4. Apply the NTUA methodology to investigate whether single-terminal NAT function and/or sympathetic nerve density in the heart and mesenteric periarterial vessels are altered in a pre-clinical model of OSA, a disease with complex cardiovascular complications. These aims are explored in Chapter 4.

5. Apply the NTUA methodology to investigate single-terminal NAT function in the heart and mesenteric periarterial vessels in response to CB_1R agonists. I will also assess whether there is an endogenous ECS tone in the heart to modulate NAT function. These assessments are paralleled with immunohistochemical techniques to investigate the prejunctional localisation CB_1R in cardiovascular tissue. These aims are explored in Chapter 5.

CHAPTER II. MATERIAL AND METHODS

2.1. Ethical statement

All animal procedures were undertaken in accordance with ethical guidelines set out by the UK Animals (Scientific Procedures) Act 1986 and the Animal Welfare and Ethical Review Body (AWERB) at the University of Birmingham. Procedures were approved by the Home Office (mice: PPL PFDAAF77F; rat: PPL PF4C074AD). Animals were housed in individually ventilated cages (n=4 maximum per cage) in the Biomedical Services Unit at the University of Birmingham under standard conditions: 12:12 h light/dark cycle (with light beginning at 07:00), 22°C and 55% humidity. Standard laboratory chow and water were available *ad libitum*.

2.2. Physiological saline solutions

For all experiments, tissues were maintained in standard bicarbonate buffered Krebs-Henseleit (KHB) solution containing (in mM): NaCl 118, $NaHCO_3$ 25, KH_2PO_4 1.2, glucose 11, EDTA 0.5, $MgSO_4$ 1.2, $CaCl_2$ 2.5 and KCl 4.7 and equilibrated with 95% O_2/5% CO_2, pH of 7.4, unless otherwise stated.

2.3. Animals

Experiments were performed on adult animals: C57BL/6 mice [some bred at the University of Birmingham, and some purchased from Charles River Laboratories (Margaret, UK)] and adult Wistar rats (Charles River Laboratories, Margate, UK). During this work, there was ongoing research elsewhere in the College on an experimental rodent model of chronic intermittent hypoxia (CIH) conducted by Mr Abdulaziz Alzahrani, PIs Dr Andrew Coney, and Dr Andrew Holmes in the Birmingham Hypoxia and Arterial

Chemoreceptor group (male Wistar rats from Charles River Laboratories, Margate, UK). Rat hearts and mesenteric arteries (MAs) were kindly donated for my investigations into sympathetic nerve function in response to CIH exposure. A brief description of the animals, CIH induction paradigm, and drug administration process is outlined in section 2.7.1.; tissues were isolated and dissected with the methods described below.

2.4. Tissue isolation

Animal tissues were isolated either during deep terminal anaesthesia (Home Office regulated procedure) or after an approved Home Office Schedule 1 method (cervical dislocation or CO_2 inhalation) with death confirmed by cessation of circulation.

2.4.1. Rodent heart isolation

2.4.1.1. Anaesthesia

Each spontaneously breathing rodent was initially placed into a red induction chamber with 99.5% O_2 delivered at a constant flow rate of 2 $L.min^{-1}$ from an O_2 generator. Concomitantly, the gaseous delivery system was primed to an activated charcoal canister (Veterinary Fluosorber, Harvard Apparatus, UK) to scavenge any excessive gaseous anaesthesia for removal. Isoflurane (3-5%, Isoflo, Zoetis, Tadworth, UK) was then vaporised (Tec-3, Protech), mixed in with O_2, and co-administered into the induction chamber until the animal was recumbent and exhibited slow and shallow breathing. The animal was maintained in these conditions until it began to gasp - indicative of deep depth anaesthesia. At this point, the righting reflex was tested by tilting the induction chamber side to side; a negative result confirms sufficient anaesthesia had been reached.

The rodent was quickly removed from the induction chamber and placed onto a cork board in the supine position with its mouth and nose fully positioned within the anaesthesia mask. The mask was connected to a non-rebreathing Bain's circuit where vaporised anaesthetic was delivered by the inner ring and scavenged by the outer ring. Once a negative result of the pedal reflex was confirmed, the body of the animal was straightened and slightly stretched with its forepaws and hindpaws secured onto the cork board with tape.

2.4.1.2. Murine heart isolation

The skin above the sternum was drawn up with forceps and a midline incision was made with surgical scissors to expose the underlying thoracic wall. Cutting through the thoracic wall revealed both the ribcage and sternum; the latter was held up with serrated forceps and the stretched diaphragm was perforated on each side of the ribcage with a pair of surgical scissors. These bilateral cuts were extended anteriorly to expose the thoracic cavity. With the sternum held up, the diaphragm was cut laterally to allow access to the thoracic organs. The beating heart was lifted up by the lungs and collectively dissected away by severing the vessels as close as possible to the dorsal thoracic wall in a strictly parallel fashion to avoid damage to the heart. The tissues were then quickly submerged in ice-cold gassed KHB to cause temporary cessation of cardiac activity. This procedure was conducted with compliance to PPL PFDAAF77F.

2.4.1.3. Rat heart isolation

As the terminal heart isolation procedure was not approved for the rat species, the heart was obtained in different circumstances. The first being after confirmed death under PPL PF4C074AD for its intended Home Office approved purpose(s). Briefly, the rats

were anaesthetised for carotid body (CB) isolation and then subsequently sacrificed; the heart was then rapidly isolated thereafter. It took approximately 1 hr from anaesthesia induction to heart dissection. The second was after a Home Office Schedule 1 sacrifice. Rats were sufficiently anaesthetised then sacrificed by cervical dislocation with the use of a metal bar positioned just caudal to the skull. Death was confirmed by the cessation of circulation prior to heart isolation.

2.4.2. Rodent mesenteric artery isolation

Rodent mesenteric arteries (MAs) were rapidly isolated from sacrificed animals. A midline incision was made in the abdominal area through the skin and underlying wall to expose the abdominal cavity. Ice-cold gassed KHB was applied into the cavity intermittently with a disposable transfer pipette to prevent tissues from drying out, otherwise tissues were difficult to manipulate as they were prone to 'sticking' together and tearing. Segments of the mesentery were pulled out and stretched outwards to reveal the transparent membranous mesenteric windows between individual artery/vein pairs that supply the intestinal wall. Throughout the mesenteric arcade, artery/vein pairs from the superior mesenteric artery branched out into first-, second- and third-order levels before reaching the intestinal wall (Furness, 1973).

Third-order artery/vein pairs that supply the intestinal wall were difficult to isolate thus tissue dissections were confined to first- and second-order pairs only. Mesenteric windows on either side of the artery/vein pair were perforated with the blunt end of forceps by gently 'scraping' the surface. Each end of the artery/vein bundle, including perivascular adipose tissue, was collectively tied off with black braided silk suture (rat:

3-0, mouse: 6-0; Ethicon) and isolated by making incisions beyond the suture ties. The vessel bundle was then submerged into ice-cold gassed KHB.

2.5. Measurement of single-terminal noradrenaline transporter rate

2.5.1. Neurotransmitter Transporter Uptake Assay (NTUA)

To dynamically measure for single-terminal noradrenaline transporter (NAT) rate, the commercially available Neurotransmitter Transporter Uptake Assay (NTUA; R8173, Molecular Devices, Berkshire, UK; U.S. Patent # 6420183, 7063952, 7138280 and European Patent # 0906572) was utilised. According to the manufacturer, NTUA contains a novel fluorescent substrate that mimics biogenic amine neurotransmitters noradrenaline (NAd), dopamine, and serotonin for the detection of their corresponding transporter activity: the NAT, dopamine- (DAT), and serotonin transporter (SERT), respectively. The NTUA assay also contains a cell-impermeant masking dye that extinguishes extracellular fluorescence (Figure 2.1). NTUA has been validated to detect NAT activity in cell culture systems with similar K_i values previously reported in the literature with radiolabelled assays (Jørgensen *et al.*, 2008).

2.5.2. NTUA preparation

The NTUA assay arrived in individual vials containing lyophilised powder of fluorescent substrate/masking dye mix and was stored at -20°C. Stock solutions at a 1:1 ratio was made up by adding 10 mL gassed KHB into each defrosted vial and vortexed to ensure thorough mixing. NTUA was subsequently split into 200 μL aliquots and stored at -20°C until the day of use. Freeze-thaw cycles were avoided throughout. On the day of use, frozen aliquots of NTUA were defrosted and added to appropriate volumes of gassed KHB to yield working concentrations for the experimental purpose. Any

glassware/tubes containing NTUA were wrapped in aluminium foil to minimise exposure to light.

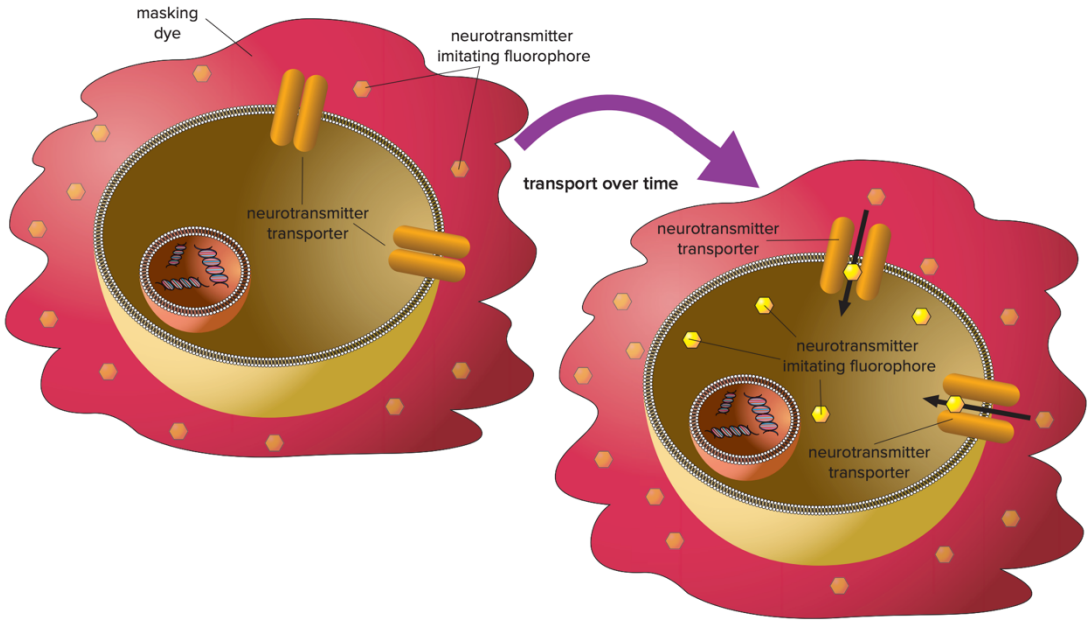


Figure 2.1: Principle of NTUA
The NTUA assay contains a fluorescent substrate that mimics biogenic amine neurotransmitters NAd, dopamine, and serotonin (hexagons), and a cell impermeant masking dye (red overlay). In principle, fluorescence is extinguished by the masking dye when the substrate is in the extracellular space (faint orange hexagons). As the substrate is transported across the cellular membrane by the monoamine transporters (NAT, DAT, and SERT), it becomes separated from the masking dye and the fluorescence is emitted (solid yellow hexagons). Figure extracted from: Molecular Devices NTUA datasheet.

2.5.3. Tissue preparation for NTUA superfusion

2.5.3.1. Heart preparation

The isolated heart was transferred into a petri-dish containing ice-cold gassed KHB. The thymus, adipose tissue, lungs, and pulmonary vessels were lifted with a pair of serrated forceps and individually dissected away from the body of the heart with fine surgical scissors. The left- (LA) and right atrium (RA) were then dissected free by incisions made as close to the body of the heart as possible (Holmes *et al.*, 2016). A

pair of closed thin-tipped forceps was inserted into the right ventricle (RV) and opened until it could not be stretched further; incisions were made at the interventricular septum to free the RV; the same process repeated for the left ventricle (LV).

2.5.3.2. Mesenteric artery preparation

The isolated artery/vein bundle was transferred to a Sylgard-lined dish containing ice-cold gassed KHB. With the use of fine entomology pins, sutures on each end of the artery/vein pair were secured onto a Sylgard so that the vessel preparation was slightly taut. Using two fine-tipped tweezers, the surrounding periarterial fat was gently teased away and removed with micro-scissors with special care to not damage the adventitia. Often it was easier to securely hold onto an adequate portion of adipose tissue with forceps and gently tug it upwards/downwards in a parallel longitudinal fashion along the ipsilateral side of the vessel to ensure its complete removal. The residual blood within the vessels (due to tied sutures) allowed for identification of the artery: the artery held onto proportionally less blood volume than the vein due to its thicker vessel wall. The vein was then removed with micro-scissors, leaving the artery behind between the two sutures.

2.5.3.3. Implementation of the ‘reduce’ principle in animal research

Each isolated LA from an animal could be cut into two and utilised within 1 hr in between. Similarly, the sacrifice of one rodent would provide multiple mesenteric artery/vein pairs for experiments. To minimise the total number of animals used in this thesis, each piece of LA or MA from the same animal was utilised for different experimental purposes in a randomised order; for example, one for control conditions and another for drug treatment. This method avoided the duplication of the same animal within a dataset. In between experiments, tissues were kept in room temperature (RT) gassed KHB. At

times, any remaining tissues were stored accordingly for other experimental procedures such as immunohistochemistry.

2.5.4. Superfusion delivery system

Isolated cardiac chambers and MAs were transferred to a Sylgard-lined imaging chamber (~1.5 mL volume) and securely pinned down as flat as possible with short sections (1-2 mm) of fine silver wire (50 μm diameter). A central reservoir contained gassed RT KHB, with the inflow from the reservoir to the imaging chamber powered by a low-pulse peristaltic pump (MINIPULS 3, Gilson). The outflow ran via the same pump from the chamber to waste (Figure 2.2). Prior to the imaging chamber, the inflow ran through a bubble trapper (Labtech Ltd, United Kingdom) to ensure constant, undisrupted flow (that would otherwise cause rippling and compromise imaging) and then a heating module (Figure 2.2). The heating module consisted of an aluminium clad wire wound resistor with four stainless steel pipes fitted into the housing in which four pieces of PVC tubing allowed the inflow solution to run through four times for heating. The heating module was constructed by Martyn Preston (Department of Pharmacology, Oxford University, UK). The temperature on the heating module was always set higher than the desired chamber temperature as there was a length of PVC tubing between the heater and imaging chamber where cooling would have occurred. The set temperature was decided empirically prior to experiments depending on the RT; once the inflow enters the imaging chamber the final temperature would be between 35-37°C at a continuous superfusion rate of 2 $mL.min^{-1}$. An independent thermocouple was used frequently to monitor the temperature within the imaging chamber as close to the pinned tissue as possible.

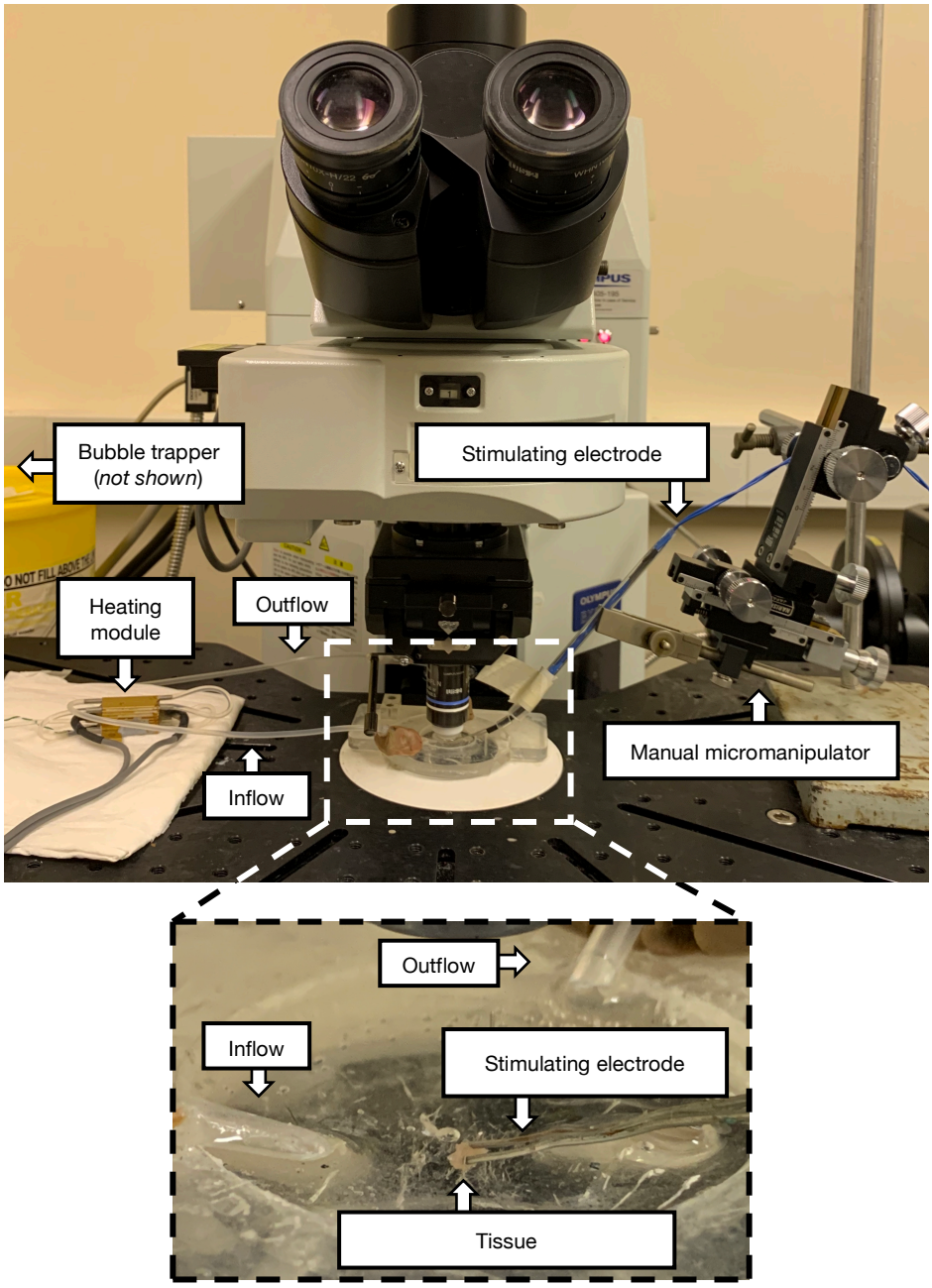


Figure 2.2: Superfusion delivery system

The superfusion system was set up beneath an upright confocal microscope. Tissues were pinned in a Sylgard-lined imaging chamber with KHB superfused at a rate of 2 mL.min^{-1}. Bubbles in KHB were removed with a bubble trapper; KHB was warmed prior to entry into the chamber with the use of a heating module, set at a temperature determined empirically before the experiment so that the final bath temperature was 35-37°C. The temperature of the chamber was checked throughout the experiment with an independent thermocouple. The placement of a pair of silver stimulating electrodes was carefully lowered on top of the tissue with a manual micromanipulator, taking care not to obstruct the lowering of the immersion microscope lens.

2.5.5. Imaging and NTUA superfusion protocol

2.5.5.1. NTUA imaging with confocal microscopy

The imaging chamber was positioned underneath an upright confocal scanning microscope (Olympus Fluoview FV1000) onto a XY motorised translation stage (Scientifica, Germany). The stage was powered by a control cube which each wheel corresponded to an axis of movement; this allowed for fine control of travel distance at a minimum step-size of 0.1 μm. To move in the Z direction, a separate controller allowed for the control of focal point that toggled between 'fine' and 'coarse' movement of the lens objective. For the purpose of NTUA experiments, all experiments were carried out with a water-immersion objective: 40× 0.8 NA (Olympus).

The imaging software (Olympus FV10-ASW, v4.2) was configured to take 512×512-pixel images on a one-way mode at 2.0 μs/pixel. The NTUA fluorophore was excited at 405 nm (*circa* 1% laser power) and detected by an emission bandwidth of 460-560 nm as determined by lambda scanning. *Z*-stacks at 1 μm step-size intervals were captured using the *z*-scanning facility; an average of 12 slices were captured to allow for focal plane drift which was often observed over the course of experiments.

The 512×512-pixel images were initially acquired at a dimension of 320×320 μm, a resolution too low to accurately monitor individual nerve terminals [2×1.5 μm (Jackson *et al.*, 2001)]. To overcome this, an area of sympathetic innervation was zoomed in 5-fold by manipulating the microscope hardware within the software; this consisted of changing the area and speed in which the laser travels over the tissue. As a result, the resolution of 64×64 μm on a 512×512-pixel image was sufficient to quantify fluorescence intensities of multiple individual nerve structures.

To minimise photobleaching of the fluorophore, no line averaging was utilised. If necessary, visualisation was enhanced by widening the pinhole diameter and by manipulating the detector sensitivity in order to increase the emitted light signal received by the photomultiplier tubes. Special care was taken while controlling these parameters to prevent pixel saturation of the final images during NTUA accumulation.

2.5.5.2. NTUA superfusion protocol

Prior to the addition of NTUA, a field of interest was roughly established using white light with a 10× 0.4 NA air objective (Olympus). Then, the field was closely observed with a 40× 0.8 NA water immersion objective (Olympus); if the tissue became solely focused on the X or Y direction as the focal plane is moved in the *Z* direction it would indicate the tissue is slanted. To capture a true representation of nerve distribution in the *Z* axis, it was important to identify an area of tissue that was relatively flat.

The NTUA protocol used throughout this thesis was adapted from previous *ex vivo* work on the murine vas deferens by the laboratory (Parker *et al.*, 2010). Unless otherwise stated, a two-step process was used: 1) the isolated tissue preparation was superfused with a lowly concentrated NTUA solution (1:100, 10 mL) to reveal areas of innervation and then 2) superfused with a highly concentrated NTUA solution (1:20) while imaging regularly. As NTUA is a NAT substrate, the rate of increase in NTUA fluorescence from 1:100 NTUA → 1:20 NTUA can provide an index for NAT reuptake rate. Both solutions were continuously gassed with 95% O_2/5% CO_2. As the nerve terminals do not exhibit autofluorescence, the initial 1:100 NTUA superfusion period was a pertinent step to identify areas of innervation, otherwise a random imaging area may have few or no

terminals present. A concentration of 1:20 NTUA was chosen as it was more economically efficient than 1:10 NTUA for the number of experiments intended.

Tissues were allowed to stabilise for at least 20 min prior to *ex vivo* studies. When the inflow line was swapped from the central KHB reservoir to the 1:100 NTUA reservoir, it took approximately just under 1.5 min for the solution to reach the chamber. At this point, the outflow PVC line was then redirected from waste to the 1:100 NTUA reservoir for recirculation. Areas of innervation became apparent after 2 min for the mouse and 5 min for the rat. A region with the highest innervation was then identified, and the start and end positions for the *z*-stack was determined by manipulating the focal knob.

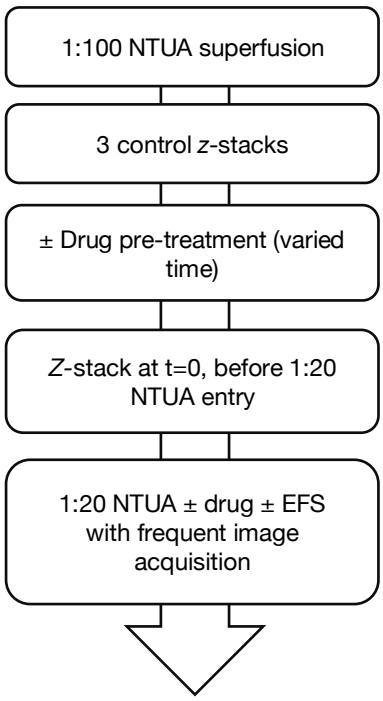


Figure 2.3: Standard NTUA superfusion protocol
The NTUA superfusion protocol was as follows. The tissue was initially incubated in 1:100 NTUA for the mere identification of innervated tissue areas. Once an area of sufficient innervation was located, three control *z*-stacks were acquired. Depending on the experiment at hand, in some cases there was a drug pre-treatment period. Right before 1:20 NTUA enters the imaging chamber, a *Z*-stack at t=0 is captured. In some experiments, 1:20 NTUA was simultaneously delivered with a drug of interest and/or electrical field stimulation (EFS).

Once an area of innervation was identified with 1:100 NTUA, the inflow tubing line was transferred into the 1:20 NTUA reservoir and immediately three control *z*-stacks were taken. It was timed that by the end of the third control *z*-stack image requisition, the

1:20 NTUA solution would have just entered the imaging chamber thus this was deemed as t=0. Image stacks were taken in varied durations depending on the experimental protocol (Figure 2.3).

2.5.6. Image analysis of NTUA uptake rate

2.5.6.1. Quantification of single-terminal fluorescence intensity

Image analysis of single-terminal fluorescence intensity was performed with Fiji (version 1.52a; https://fiji.sc) on unmerged *z*-stacks. As NTUA fluorescence was captured in the blue wavelength of the electromagnetic spectrum, the image contrast was improved by changing the look up table to 'Green'. To quantify raw fluorescence exerted by NTUA, a region of interest (ROI) was drawn around a single nerve terminal at its brightest amongst the first control *z*-stack and the mean intensity was recorded (Figure 2.4). The same ROI (type and size) was then restored in the subsequent time stacks; the ROI position may have changed with focal drift and, if so, it was manually restored to the same slice - the brightest point being the reference point for all stacks (Figure 2.4). In the instance where there was pixel saturation with 1:20 NTUA (checked with Fiji look up table: Highlo), an out-of-focus plane was chosen, and this section was restored in all preceding *z*-stacks (Figure 2.4). For background subtraction, an area unlabelled by NTUA immediately beside the nerve terminal was quantified and subtracted from raw ROI value.

2.5.6.2. Normalisation of single-terminal fluorescence intensity

It was not possible to maintain the same confocal detector parameters for all experiments within a dataset as 1) it may not have been sufficient to detect nerve terminals during the 1:100 NTUA superfusion phase or 2) it risked pixel saturation in the

subsequent 1:20 NTUA superfusion phase. To control for differences in fluorescence detection settings, raw fluorescence intensities in the test period (1:20 NTUA, $F_{1:20,t}$) at each time point (t) were normalised to the average of its three control stacks acquired prior (1:100 NTUA, $F_{1:100}$), thus providing relative changes in NAT reuptake rate to accumulate NTUA with time (equation 2.1, Figure 2.5). All calculations of fluorescence were carried out in Microsoft Excel.

Equation 2.1: $$\Delta F_{1:20,t} = \frac{F_{1:20,t} - F_{1:100}}{F_{1:100}}$$

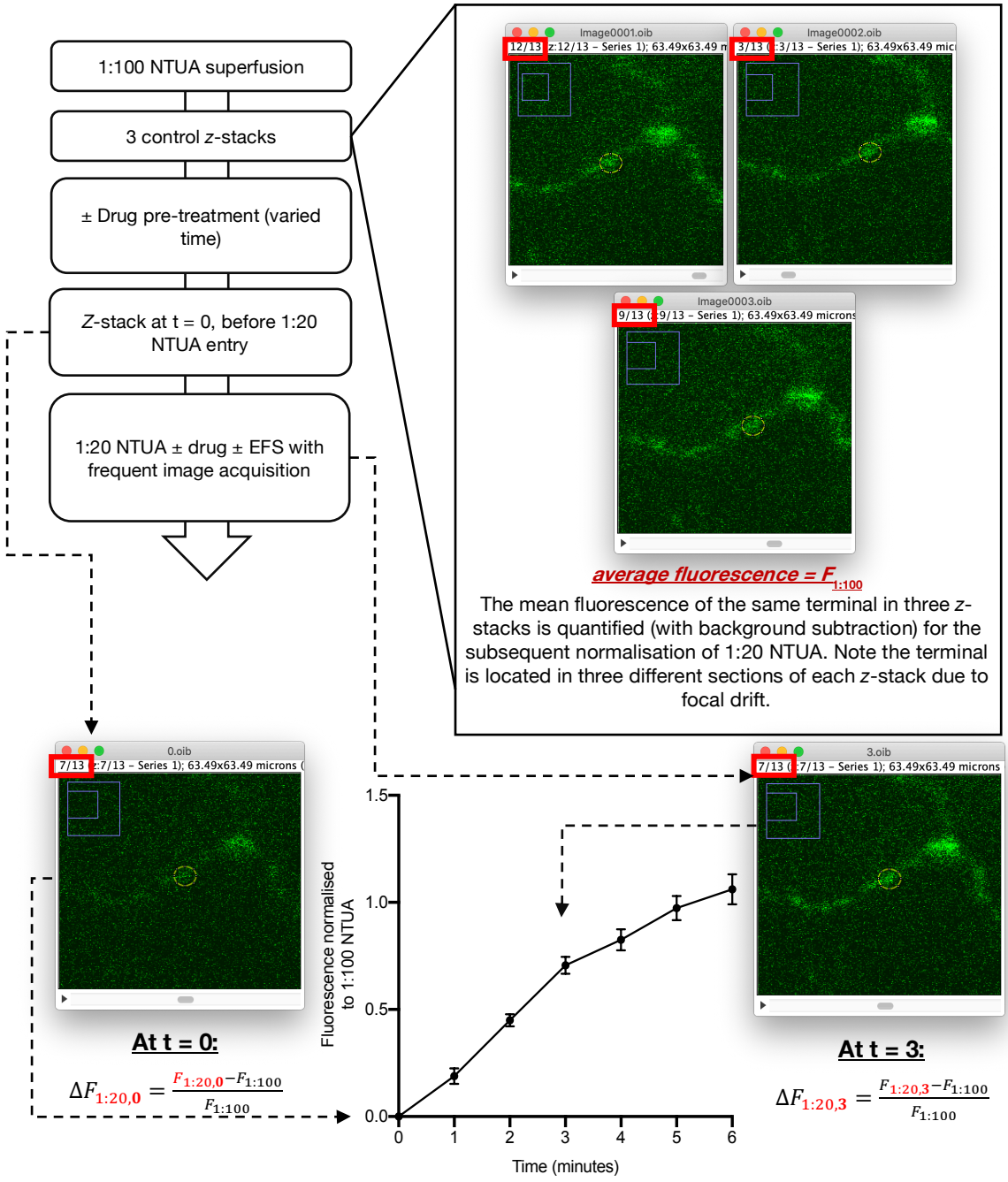


Figure 2.4: NTUA fluorescence analysis method

A nerve terminal is selected in the unmerged *z*-stack in 1:100 NTUA conditions. The mean fluorescence was noted and corrected with background subtraction from an area of unlabelled tissue immediately nearby. This process is repeated for the other 2 control *z*-stacks. Note that focal drift can occur, and the specific section can be relocated within the ~12 slices taken within the stack (red). The mean fluorescence across three control stacks is utilised as a normalisation reference for subsequent 1:20 NTUA fluorescence analysis. The analysis method would allow for comparisons between the experiments where the detection settings differed.

2.5.6.3. Analysis of NTUA uptake rate

2.5.6.3.1. Straight-line analysis

The linear rate of NTUA accumulation can be adopted as a measure of NAT reuptake rate (Parker *et al.*, 2010). To do this, normalised NTUA fluorescence data was exported from Microsoft Excel into GraphPad Prism (version 8.4; GraphPad Software Inc., San Diego, CA, USA), and Equation 2.2 was fit through all timepoints of the data where a linear increase in fluorescence was observed (Figure 2.5A, B). NAT reuptake rate was determined by the trendline gradient variable (equation 2.2: m) and expressed as a percentage over time (Figure 2.5C). The same equation was also used to calculate the decline in fluorescence during the washout phase.

$$Equation\ 2.2: \quad y = mx + c$$

2.5.6.3.2. Non-linear curve fit

NAT reuptake rate was also determined by fitting a non-linear curve fit model to the data, particularly when an early plateau was observed. The 'one phase association' curve fit (equation 2.3; GraphPad Prism pre-set equation) describes the first-order kinetics between an enzyme and substrate, and the resulting 'rate constant' value was utilised as a measure of NAT reuptake rate. The 'plateau' value was also noted as a measurement of the maximum detection of NTUA fluorescence within the experiment timeframe.

An example of its use is shown in Figure 2.5, where treatment 2 appears to reduce the maximum NTUA fluorescence compared to treatment 1 (Figure 2.5A). In many cases, GraphPad Prism could not fully establish a curve fit due to the limited timepoints

available, and so the number of outputs from the model were significantly less than the input (Figure 2.5E). To work around this, the model was constrained to known plateau values where the non-constrained curve fit was established (Figure 2.5D, F) - this maintained the use of nearly all terminals measured (Figure 2.5G).

In the one phase association model (equation 2.3), $Y0$ and $plataeu$ refers to the normalised fluorescence value at t=0 and t=end of experiment, respectively, and t being time. The resulting rate constants (k) were extracted as a measure of NAT reuptake rate with respect to time.

$$\underline{Equation\ 2.3:} \qquad y = Y0 + (Plateau - Y0) \cdot (1 - e^{-kt})$$

The 'one phase decay' curve fit (GraphPad Prism pre-set equation; equation 2.4) was used to measure the rate of NTUA washout from terminals. This equation describes the dissociation of ligands from their receptors. After the tissues were treated with 1:20 NTUA, a KHB washout phase took place in which the normalised fluorescence value steadily declined past 1:100 NTUA and towards -1.0 where terminals could no longer be seen. The model was constrained to a $plataeu$ value of -1.0 and the resulting rate constants (k) were extracted.

$$\underline{Equation\ 2.4:} \qquad y = (Y0 - Plataeu) \cdot e^{-kt} + Plataeu$$

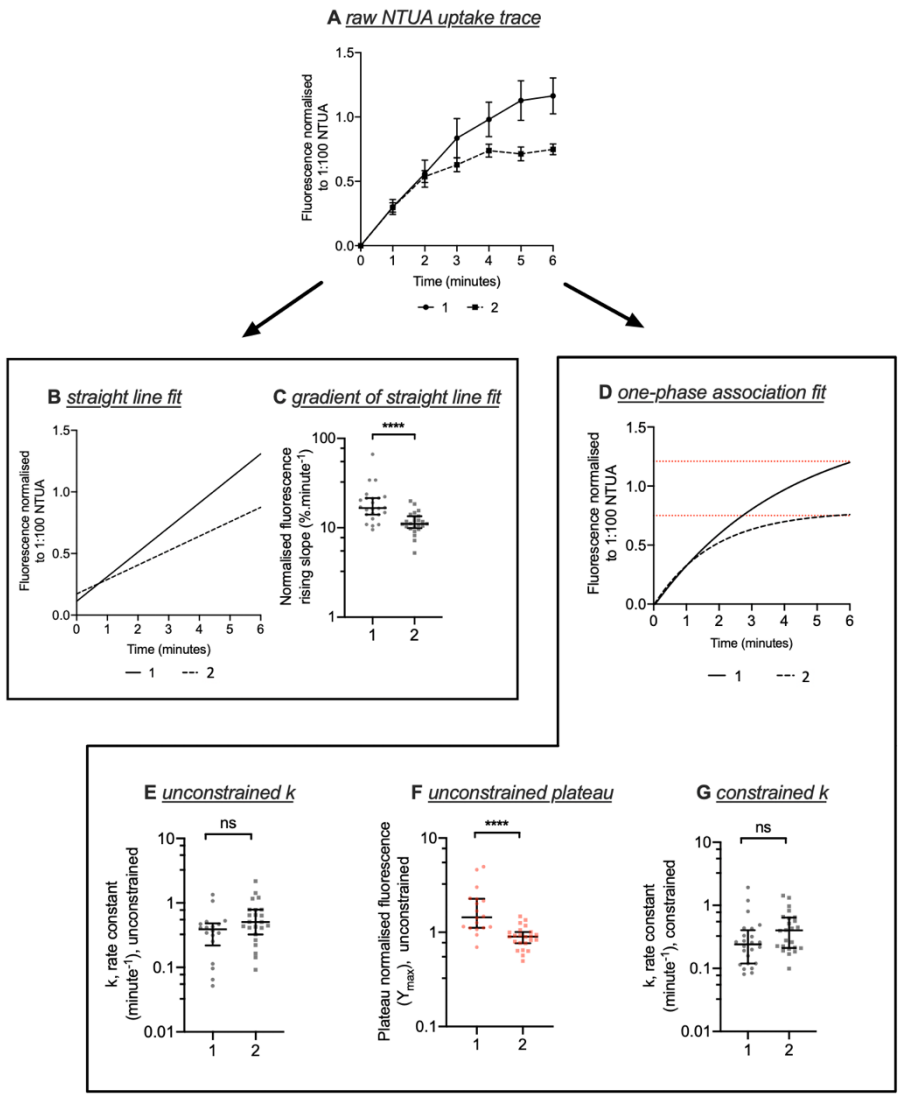


Figure 2.5: Two methods of NTUA uptake rate analysis

Analysis methods for condition 1 (control) and 2 (drug): straight line fit and non-linear one-phase association fit.

(A) 24 terminals/group were analysed. In condition 1, NTUA accumulation occurred in a linear fashion through all timepoints, whereas it was restricted to the first 2-3 min in condition 2.

(B) A straight-line fit was applied to both condition 1 and 2 throughout all timepoints. **(C)** The gradient of accumulation is extracted as a measure of NTUA uptake rate. This method retains all 24 terminals/group, though the linear uptake rate in condition 2 would be inaccurate.

(D) A 'one-phase association' fit is applied onto the data, with the red dotted lines corresponding to the maximum NTUA accumulation fluorescence. **(E)** Due to the limited timepoints available, some terminals were omitted in the unconstrained model, though a value of maximal NTUA fluorescence was provided **(F)**. **(G)** By constraining the model to known plateau values in (F), more terminals are retained for analysis.

2.5.7. Electrical field stimulation and NTUA uptake

Experiments were conducted to investigate the effect of sympathetic postganglionic nerve action potential (AP) propagation on NAT reuptake rate in the murine heart. A custom pair of parallel silver stimulating electrodes was placed on top of the pinned LA in the imaging chamber to deliver electrical field stimulation (EFS). Careful placement was required to ensure minimal obstruction to the lowered immersion microscope lens. The stimulating electrode was mounted on a manual micromanipulator to allow for fine control (Figure 2.2).

Prior to the superfusion of 1:100 NTUA, the stimulation threshold voltage that reliably elicited cardiomyocyte contraction was empirically determined. In order to optically monitor noradrenergic terminals in the absence of contraction artefacts, the threshold voltage was reduced by 20% to allow for neuronal depolarisation only. The chosen EFS parameters were based on the greater excitability of neurones compared to cardiac muscle, as demonstrated by the approximate ten-fold briefer chronaxie (Struik, 2017) and the ten-fold lower rheobase (Reilly and Diamant, 2011).

The standard NTUA superfusion protocol was then followed through with square-wave pulse stimuli delivered concomitant with 1:20 NTUA entry into the imaging chamber (t=0; 0.1-0.2 ms pulse duration). EFS was delivered at varying frequencies (0.2, 0.5, 1, 2, 5, and 10 Hz) until the end of the experiment. These frequencies represent the physiological range of resting and maximal sympathetic activity in the rodent, usually between 0.3-2.4 Hz and 4-8 Hz, respectively (Häbler *et al.*, 1994, Nilsson *et al.*, 1985). Stimuli were delivered by an isolated voltage stimulator (DS2A, Digitimer, Hertfordshire, UK) connected to a digital stimulus trigger unit. At the end of the protocol, the stimulation voltage was returned to 100% cardiomyocyte contraction threshold to

ensure the intended stimuli were delivered throughout the protocol. In non-stimulating conditions, tissues were exposed to the same electrodes but were not stimulated.

Stimulus-response data were evaluated by sigmoidal curve fitting to median values to yield the inhibitory EF_{50} (EFS frequency inhibiting the half maximal reuptake effect) with a constrained Hill Slope of 1. Tissues were pre-treated with yohimbine [1 μM, Kazanietz and Enero (1989)] and atropine [1 μM, Nishimaru *et al.* (2000)] for 20 min prior to 2 Hz EFS to assess the prejunctional roles of the α_2-adrenoceptors (α_2AR) and muscarinic acetylcholine heteroreceptors (mAChR), respectively, on NTUA uptake rate during EFS.

2.5.8. Drug-induced effects of NTUA uptake

The NTUA superfusion protocol was adapted to investigate the effect of numerous drugs on NAT function. Unless otherwise stated, after the three control *z*-stacks were taken, tissues were exposed to a drug pre-treatment period (time was specific for the experiment and drug type) (Figure 2.3). In these experiments, both the pre-treatment solution and the 1:20 NTUA test solution would contain the drug(s) of interest. In some experiments, the effect of drugs on the wash-out phase of NTUA was also investigated; following the 1:20 NTUA test period, the inflow line was switched to a reservoir containing KHB only or KHB with the drug(s) of interest.

2.5.9. Langendorff delivery system

2.5.9.1. Aortic cannulation

While superfusion was the primary method of administering NTUA to the heart, it was of particular interest to investigate whether a similar result could be achieved with Langendorff perfusion. Following murine heart isolation under terminal anaesthesia, the heart was immediately transferred to a 60 mm petri-dish containing ice-cold buffered

KHB. Here, connective tissues were carefully trimmed away underneath a dissection microscope to expose the aorta; in cases where the aorta began to branch off, an incision was made below the brachiocephalic artery. The heart was then transferred to another filled petri-dish, where a 2 mL syringe filled with ice-cold KHB was mounted on the edge with an attached 19 G (1 mm outer diameter) metal cannula submerged in KHB. A loosely tied 5-0 black braided silk suture was positioned on the shaft of the cannula.

With the use of two pairs of hooked-tipped tweezers, the aorta was slipped onto the metal cannula at an adequate depth; too deep would risk puncturing the aortic valve but too shallow would not sufficiently perfuse the left- and right coronary ostia. Once in place, the loosely tied suture was brought down and secured around the aorta. Ice-cold KHB was then retrogradely perfused into the heart to remove traces of blood.

2.5.9.2. Langendorff retrograde perfusion of NTUA

The cannulated heart was attached onto a vertical Langendorff apparatus (Hugo Sachs, Germany) (Figure 2.6) with a flow rate of 4 $mL.min^{-1}$. As the apparatus was flow-constant, pins were inserted into the LV and RV to relieve pressure build-up by any excess solution. The flow of warmed KHB (36-37°C) was maintained for 5 min where cardiac contraction was continuously monitored; any pale or white discolouration of the heart was indicative of ischemic injury due to poor cannulation and the preparation was discarded.

On the day of use, a 1 ml 1:4 NTUA dilution was prepared, drawn into a syringe and administered through a bolus port just above the cannulated heart over a period of 5 min (Figure 2.6). In conjunction with the flow rate of 4 $mL.min^{-1}$, the heart was subjected

to a final concentration of 1:80 NTUA. This method was adopted from the work of O'Shea *et al.* (2019) for a voltage dye. Once NTUA perfusion was complete, the heart was detached from the cannula, subjected to dissection, and transferred to an imaging chamber positioned underneath the confocal microscope as previously described.

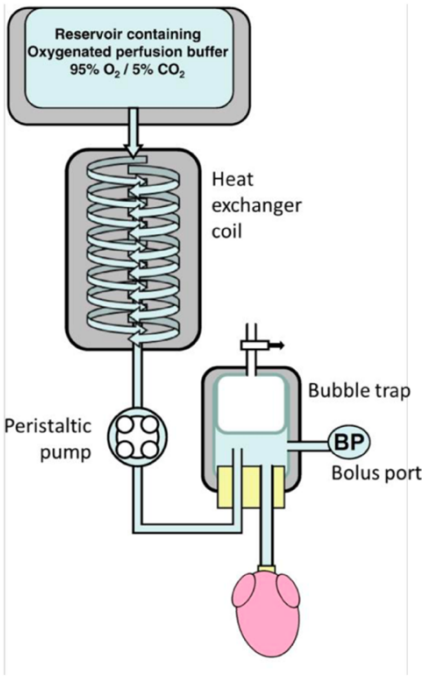


Figure 2.6: Schematic of Langendorff apparatus
A simplified schematic of the apparatus consists of double-coated glassware to maintain the temperature of KHB at 36-37°C, a peristaltic pump that directed KHB from the reservoir to the output port at 4 $mL.min^{-1}$, a bubble trapper, and a bolus port that allowed for administration of NTUA just before the cannulated heart. Figure extracted from: Yu (2015).

2.5.10. Multi-photon microscopy

In addition to confocal laser scanning microscopy, NTUA fluorescence was also visualised with multiphoton laser scanning microscopy. The mouse LA was initially superfused with NTUA (1:1) as described, then pinned in a Sylgard-lined chamber placed underneath an upright multiphoton microscope (Olympus FVMPE-RS). The

image acquisition software (Olympus Multipoint and Mapping Software module) was configured to capture 640×640-pixel images at 2-8 μs/pixel with a 25× 1.05 NA water-immersion objective (Olympus FV30-AC25W). The NTUA fluorophore was excited by 775 nm (*circa* 1% laser power) and fluorescence was detected by an emission bandwidth of 410-460 nm or 495-540 nm. *Z*-stacks at 1 μm step-size intervals were acquired with the *z*-scanning facility. Images were acquired by Dr Dean Kavanagh at the University of Birmingham.

2.5.11. Human tissue

NTUA was applied onto human mesenteric arteries to label noradrenergic nerve terminals. Human samples were obtained through the Human Biomaterials Resource Centre (HBRC), a Research Tissue Bank at the University of Birmingham operating under HTA License 12358. Ethical approval was gained via the HBRC's generic approval (North West - Haydock Research Ethics Committee; Ref 20/NW/0001) under project designation MV-010, in accordance with the UK Policy Framework for Health and Social Care Research, and the Human Tissue Act 2004. All patients gave written informed consent. Data was processed in accordance with the EU General Data Protection Regulation and the UK Data Protection Act 2018, on a legal basis of 'public interest'.

Two human mesenteric artery/vein bundles (at an unknown level of the mesenteric cascade) were obtained from patients during bowel surgery. The diagnosis in these patients included a confirmed case of bowel pathology of diverticulosis and polyps (patient #1) and an active case of undefined bowel cancer (patient #2). Following surgical resection artery/vein pairs were transferred to pathology for prognosis, placed

in standard RPMI cell culture media RT solution (of an unknown time duration), and dispatched for collection. Upon collection, the sample in solution was immediately placed on ice and transported to the laboratory.

Segments of the artery and vein were carefully dissected with the use of a dissection microscope and micro-scissors. Vessels were dissected free of excess fat and connective tissue; the artery was identified by its thicker wall and cut longitudinally. Arterial segments were initially allowed to equilibrate in warmed (35-37°C) and gassed KHB for 20 min, before exposure to highly concentrated (1:1) NTUA. NTUA fluorescence was viewed with confocal laser scanning microscopy as previously described.

2.6. Noradrenaline release

2.6.1. [^{3}H]-NAd overflow

To determine whether cardiac sympathetic neurones were indeed stimulated in conditions of EFS, i.e., at 80% cardiomyocyte contraction threshold (section 2.5.7.), the overflow of tritiated NAd ([^{3}H]-NAd) was measured in similar experimental conditions. The method was based on those previously described with modification (Trendelenburg *et al.*, 2000, Buttgereit *et al.*, 2016). In these experiments, modified KHB (mKHB) contained Na_2EDTA 0.03 mM and ascorbic acid 0.57 mM and was equilibrated with 95% O_2/5% CO_2 to reach pH 7.4. Unless otherwise stated, the 2 mL capacity bath was superfused with mKHB at a rate of 2 mL.min^{-1} to reach 35-37ºC.

The isolated mouse LA was initially allowed to equilibrate for 20 min within the superfusion system. For the next 30 min, the LA was superfused with recirculated mKHB containing [^{3}H]-NAd (levo-[ring-2,5,6-^{3}H]-NAd, specific activity: 60 Ci/mmol,

American Radiolabelled Chemicals, ART1563; 0.2 μM; 4 mL) for loading. During this time, to assist with the evoked release of endogenous neuronal NAd and facilitate the entry of [^{3}H]-NAd into vesicular stores, the LA was subjected to EFS at 2 Hz (cardiomyocyte contraction threshold, 1 ms pulse width) via a pair of parallel silver stimulating electrodes. Afterwards, tissues were washed out for 30 min with mKHB containing 1 μM desipramine to remove excess [^{3}H]-NAd and to inhibit NAT-mediated reuptake in subsequent EFS events.

Analogous to section 2.5.7., the stimulation voltage threshold to induce cardiomyocyte contraction was empirically determined at 0.1-0.2 ms pulse widths, which was then reduced by 20% for neuronal depolarisation only. Following the washout period (t=0), 500 μL superfusate was collected and added to 4.5 mL scintillation liquid (Ecoscint A, National Diagnostics) every 2 min until the end of the experiment.

At the 17th (S_1) and 43rd (S_2) min, EFS was delivered for 6 min (0.1-0.2 ms pulse width) at 2 Hz at a voltage of either 1) 100% cardiomyocyte contraction threshold or 2) 80% of cardiomyocyte contraction threshold. At the end of the experiment, the amount of radioactivity (counts/min, CPM) in the collected superfusate/liquid scintillation mix was measured using a liquid scintillation β spectrophotometer counter (PerkinElmer, Tri-Carb 2910TR) at a requisition time of 5 min per sample.

2.7. The use of NTUA to quantify vascular sympathetic nerve density

During this work, there was ongoing research elsewhere in the College (Birmingham Hypoxia and Arterial Chemoreceptor group) into the chemoreception of an experimental rodent model of obstructive sleep apnoea (OSA). Tissues were kindly donated for

investigations into chronic intermittent hypoxia (CIH)-mediated changes in NAT regulation and vascular sympathetic nerve density in these animals.

2.7.1. Chronic intermittent hypoxia model

12-week-old male Wistar rats were used in this current study. Animals were split into three groups: normoxic group (N), CIH group (CIH), and a CIH group treated with β-adrenoceptor blocker propranolol (CIHP). In brief, CIH induction occurred for 8 hr/day (08:00-16:00) for 21 days; cages were placed in dedicated small animal chambers and the animals were exposed to 8 cycles/hr, totalling to 64 hypoxia cycles delivered per day. Each cycle consisted of a slow reduction from 21% O_2 to 5% O_2 over a period of 150 s; 5% O_2 was held for 15 s before returning to 21% O_2. In N conditions, rats were placed in their home cage for the 21 days. Propranolol was mixed in with drinking water for a final concentration of 40 $mg.day.^{-1}kg.^{-1}$ and were provided to animals 10 days prior to and during CIH induction (two bottles shared between 2 animals). The dosage was determined based on the average daily water consumption of the animals, the targeted drug dose, and the total animal weight in the cage. Full methodological details can be found in Alzahrani *et al.* (2020) and Appendix C.

2.7.2. Image acquisition

After measurements of single-terminal periarterial NAT reuptake rate with NTUA at high magnifications (as described in section 2.5), the magnification level was reset so that the entire width of the vessel can be seen. The imaging parameters (laser power, pinhole diameter, detector sensitivity) were manipulated to ensure individual nerve fibres could be easily identified. A *z*-stack just above the adventitial layer down towards to the lumen (where nerve terminals were confined to the outermost edges) were acquired in 1 μm

intervals. This process was repeated twice more on different areas of the same vessel. The *z*-stacks were imported into Fiji and the optical sections were combined to demonstrate overall nerve innervation. Areas that did not contain structures reminiscent of nerve fibres, e.g., tissue debris or damaged areas, were omitted from the analysis. Two nerve density analysis protocols were adapted from Omar and Marshall (2010): vascular fluorescent area and surface density.

2.7.3. Image analysis

2.7.3.1. Vascular fluorescent area

The 'vascular fluorescent area' was defined as the percentage of image pixels detected as nerve fibres (labelled by NTUA) out of the total surface area of the vessel. Taking the combined *z*-stack, the fluorescence intensities of three random areas that were not labelled by NTUA ('non-NTUA') were quantified with their mean and standard deviation noted. Non-NTUA fluorescence intensities 3 standard deviations above the mean were subtracted from the entire image as a method of background subtraction.

The remaining fluorescence was deemed representative of NTUA-induced fluorescence in noradrenergic nerves and the proportion of its area relative to the whole vessel area was expressed as a percentage. Note the outermost edge of the vessel was omitted from analysis; this was because in the merged *z*-stack format, the outer edge contained multiple nerve fibres overlaying each other from different focal planes. This process was repeated on the two other areas of the same vessel; the mean vascular fluorescent area of the three images were noted for 1 animal in the final statistical analyses.

2.7.3.2. Surface density

The 'surface nerve density' parameter was defined as the total number of nerve fibre intercepts per μm of tissue on a superimposed grid. Taking the combined *z*-stack, a grid consisting of 25×25 μm squares was superimposed onto the image. Squares containing the outermost edge of the vessel was omitted from analysis; this was because in the merged *z*-stack format, the outer edge contained multiple nerve fibres overlaying each other from different focal planes.

The number of times individual nerve fibres intercepted each horizonal and vertical line in a square was counted, with special care taken of what was defined as one nerve fibre: 1) those that appeared distinctly as one were counted as 'one', 2) those that ran in parallel with others that were resolved into single fibres were counted as 'one' and 3) those that couldn't be resolved were counted as 'one'. The total number of intercepts in each image was counted three times on different (non-consecutive) days and the mean was noted; this process was repeated on the two other areas of the same vessel. The mean nerve intercepts of the three images were noted for 1 animal in the final statistical analyses. The surface density (S_v) of noradrenergic nerve fibres was calculated by dividing the total number of nerve intercepts across the horizonal and vertical lines (P_i) by the product of the distance between each horizontal and vertical grid lines (25 μm; d) and the total number of horizontal and vertical grid intersections in the field of measurement (P_t) with the following equation:

$$\underline{Equation\ 2.5:} \qquad S_v = \frac{P_i}{d \cdot P_t}$$

2.8. Histochemistry

2.8.1. Chemofluorescence

To visualise noradrenergic catecholamines with an alternative fluorescence-based technique, rodent hearts and MAs were subjected to a sucrose-potassium-glyoxylic acid (SPG) protocol where fluorophores were formed in a condensation reaction (De la Torre, 1980). The SPG solution (1% w/v glyoxylic acid, 0.236 M KH_2PO_4, 0.2 M sucrose, pH 7.4) was prepared by dissolving 1.5 g glyoxylic acid, 4.8 g KH_2PO_4 and 10.2 g sucrose in 100 mL distilled water. The pH of the solution was corrected by the addition of aqueous 10 M NaOH; distilled water was added to make up the total solution to 150 mL.

Rodent hearts were isolated, freed from connective tissue, and embedded in cryoprotectant [optimal cutting temperature compound (OCT), Tissue-Tek] on a cork disc with the cardiac chamber of interest facing up. A syringe needle was often inserted into the disc to help orientate the tissue prior to freezing. The tissue sample was then quickly frozen in cooled isopentane (Merck) in liquid nitrogen. Cryosections of 8-10 μm thick were cut and transferred to positively charged slides (Histobond, Marienfeld) by nearing the slide to the cryostat knife.

Slides were immediately dipped in room temperature SPG for 3 s (1 dip.s^{-1}). Isolated MAs were submerged in SPG solution for 40 min and stretched out on slides making sure the vessels weren't twisted. Tissue slides (heart sections and MAs) were placed in front of a desk fan and strongly air-dried until a ground-glass appearance. To develop catecholamine fluorescence, tissues were mounted with one or two drops of mineral oil and placed in a pre-heated oven at 75°C for 30 min. Any excess oil was wiped off the

edges of the slides and fresh mineral oil was added. Slides were cover-slipped and sealed with clear nail polish. Chemofluorescence were captured with a confocal microscope fitted with an oil objective (40× 1.3 NA, Olympus) with wavelength filter set: excitation 405 nm/emission 460-560 nm.

2.8.2. Immunohistochemistry

All regents and wash buffers can be found in Table 2.1. To detect for prejunctional cannabinoid type I receptor (CB_1R) on sympathetic nerve terminals, immunohistochemistry (IHC) protocols consisted of dual labelling for CB_1R and tyrosine hydroxylase (TH). Rodent hearts and first- and second-order MAs were excised and immediately fixed for 24 hr at 4°C. Tissues were then rinsed in 1X PBS. Hearts were transferred to a 30% sucrose/1X PBS cryoprotection solution overnight at 4°C and MAs were stored in 70% ethanol at 4°C until day of processing.

Once the hearts had sunk to the bottom in cryoprotectant, they were embedded in OCT, frozen in liquid nitrogen, and cryosectioned onto positively charged slides (Histobond, Marienfeld). Heart tissue sections were then air-dried at RT overnight. Once the heart sections had dried, a hydrophobic barrier was applied to the perimeter of the tissue section with a PAP pen (#ab2601, Abcam, Cambridge, UK). The MAs were rinsed in 1X PBS and pinned down into a custom made Sylgard-lined dish with short silver wires. The Sylgard-lined dish was made by filling a 35 mm petri-dish with Sylgard and cutting out a small square with a scalpel. The hollow square was then partially refilled with Sylgard with a final volume of ~800 µL.

(A) Solutions	Components
Fixative	4% Paraformaldehyde in PBS, pH 7.4 (#15434389 Alfa Aesar)
1X PBS	In mM: NaCl 137, KCl 2.7 (Merck)
Antibody buffer	1% Normal donkey serum (Jackson Laboratories) 0.1% Tween20 (Promega) 1X PBS
Antibody wash buffer	0.01% Tween20 (Promega) 1X PBS
Permeabilising blocking solution	0.3% Triton X100 (Merck) 5% Normal donkey serum 0.05% Tween20 1X PBS

Table 2.1: List of buffers used for immunohistochemistry

Rodent heart sections and whole MAs were first incubated in permeabilising blocking buffer for 1 hr at RT followed by washing in 1X PBS. Tissues were exposed to mixed antibody buffer containing primary antibodies targeting the CB_1R (N-terminus; 1:100, rabbit host, #ab3558, Abcam, Cambridge, UK) and intracellular TH (1:500, sheep host, #ab113, Abcam, Cambridge, UK) for 24 hr at 4°C in a humidified chamber. Primary antibodies were omitted in control experiments.

Tissues were then washed in antibody wash buffer and incubated in mixed antibody buffer containing with fluorophore-conjugated secondary antibodies (1:250, donkey host anti-sheep IgG Alexa Fluor 488, #ab150177, Abcam, Cambridge, UK; 1:250, donkey host anti-rabbit IgG Alexa Fluor 647, #ab150075, Abcam, Cambridge, UK) for 1 hr in a dark humidified chamber at RT and washed again in antibody wash buffer.

In some preparations, cell nuclei were stained with 300 nM DAPI (Merck; dissolved in 1X PBS) and washed in 1X PBS thereafter. MAs were removed from the Sylgard-lined

dishes and placed onto slides, allowing some time to dry for tissue adherence. All tissue preparations were then mounted with Fluoroshield anti-fade mounting medium (#ab104135, Abcam, Cambridge, UK), coverslipped and sealed with clear nail polish. They were then stored in the dark at 4°C.

All tissue washes consisted of 3×10 min in the appropriate wash buffer. All incubations in blocking solution(s) and antibodies took place in dark, humid chambers. To prevent tissue dehydration, heart tissue sections were placed in black slide moisture chambers (76278-848, VWR), and the custom-made Sylgard petri-dishes containing MAs were placed in an enclosed 60 mm petri-dish with wet towel tissue surrounding the inside perimeter.

Images were captured with an upright confocal laser scanning microscope (Olympus Fluoview FV1000) fitted with an oil immersion objective lens (40× 0.3 NA, Olympus) on an imaging acquisition software (Olympus FV10-ASW, v4.2). A drop of mineral oil was placed on top of the coverslip and the objective lens was lowered. *Z*-stacks of various number of slices were captured with the following wavelength filter sets: DAPI (excitation/emission: 405 nm, 450-470 nm), TH (excitation/emission: 488 nm, 510-530 nm), CB_1R (excitation/emission: 647 nm, 655-675 nm). Excitation laser powers were kept as low as possible to prevent photobleaching.

2.9. Drugs

Drug name	Target/use	Company	Solvent
L-Ascorbic acid	Antioxidant	Sigma	dH_2O
Desipramine hydrochloride*	Noradrenaline transporter inhibitor	Sigma	
Tyramine hydrochloride	Sympathomimetic amine	Sigma	
Carbachol*	Muscarinic acetylcholine receptor agonist	Sigma	
Atropine*	Muscarinic acetylcholine receptor antagonist	Sigma	
Atropine sulfate monohydrate		VWR	
(-) Noradrenaline (+)-bitartrate salt monohydrate	NAT substrate	Sigma	
Colchicine	Microtubule destabilising agent	ACROS Organics	
Yohimbine hydrochloride	α_2-Adrenceptor antagonist	VWR	
Propranolol	β-Adrenoceptor antagonist	Sigma	
Corticosterone*	$Uptake_2$ inhibitor	Sigma	DMSO
(R)-(+)-WIN 55,212-2*	Non-selective cannabinoid receptor agonist	Sigma	
SR141716A*	Selective cannabinoid CB_1 receptor antagonist	*Unknown*	
SR141716A		Sigma	
ACEA	Selective cannabinoid CB_1 receptor agonist	Tocris	EtOH
(-)-[ring-2,5,6-^{3}H]-Noradrenaline (Specific activity: 60 Ci/mmol)	Tritium-labelled noradrenaline transporter substrate	American Radiolabelled Chemicals	0.2 N acetic acid:EtOH
Glyoxylic acid monohydrate	Chemofluorescence of catecholamines	Sigma	

Table 2.2: List of drugs and reagents used

* *Drugs that were not brought in new during the PhD.* Description from IUPHAR/BPS Guide to Pharmacology database (Armstrong *et al.*, 2019)

The full list of drugs used in this thesis is tabulated in Table 2.2. Unless stated otherwise, all drugs were dissolved to 10 mM and immediately aliquoted and stored at -20°C until use. On the day of use, drugs were further diluted in KHB as required. Multiple freeze-thaw cycles were avoided. Control experiments were performed in the presence of drug-free solvents, using identical conditions applied for drug application.

2.10. Statistical analyses

Normality of data were checked with a Kolmogorov-Smirnov test. Normally distributed data were expressed as mean±SEM, otherwise data were expressed as median (IQR: Q1, Q3). When reporting percentage differences between mean±SEM data (in the form of '$x \pm \Delta x$ is greater than $y \pm \Delta y$ by $z \pm \Delta z$ %'), the errors of the data were combined as the square root of the sum of squares of relative errors (equation 2.6). This method of error propagation is termed 'summing errors in quadrature' and it is used often in biophysical sciences (Palmer, n.d.).

Equation 2.6: $$\frac{\Delta z}{z} = \sqrt{\left(\frac{\Delta x}{x}\right)^2 + \left(\frac{\Delta y}{y}\right)^2}$$

As this method of combining errors was difficult to do with median (Q1, Q3), percentage differences were simply reported by differences in median only, e.g., 'x $(IQR: xQ3 - xQ1)$ is greater than y $(IQR: yQ3 - yQ1)$ by z%'.

In data consisting of 2 groups of equal variances, the parametric unpaired Student's *t*-test was used; otherwise, a Welch's *t*-test was adopted. Alternatively, the non-parametric Mann Whitney test was used. In data consisting of >2 groups, the parametric Friedman one-way ANOVA test followed by Dunn's multiple comparison *post-hoc* test

was carried out, otherwise the Kruskal-Wallis test was used as a non-parametric alternative. A value of $p<0.05$ was considered statistically significant.

All statistical analyses were carried out on GraphPad (version 8.4; GraphPad Software Inc., San Diego, CA, USA). Several n abbreviations are used in the text: (i) n is the number of animals and (ii) n_t is the number of individual terminals. Statistical analysis was performed on 'n_t' numbers.

CHAPTER III. OPTIMISATION OF A FLUORESCENCE-BASED TOOL TO STUDY SINGLE-TERMINAL NORADRENALINE TRANSPORTER FUNCTION

3.1. Introduction

3.1.1. Overview

Sympathetic noradrenergic volume transmission depends on the interplay between noradrenaline (NAd) release and its subsequent clearance from the junctional cleft. In the heart, the prejunctional noradrenaline transporter (NAT) mediates a Na^+/Cl^--dependent secondary active process (Iversen, 1967) that reuptakes up to 90% of released NAd back into the nerve terminal (Esler *et al.*, 1990). Hence, the NAT is an important determinant of junctional NAd availability and the extent of the elicited postjunctional effects. However, direct measurements of the dynamic changes in NAT rate in mature sympathetic nerve terminals are difficult to achieve, relying on indirect measurements such as NAd overflow (with and without NAT inhibition) (Esler *et al.*, 1988) and total tissue uptake of radioactive NAd analogues (Wichter *et al.*, 2002).

Fluorescence-based imaging is useful to discern individual nerve terminals at high spatiotemporal resolutions (Mondal, 2014). However, this technique could be complicated in tissues that are innervated by a mix of peripheral neuronal types. For example, in addition to noradrenergic innervation, the heart also possess a combination of cholinergic, nitrergic, and sensory neurones (Shivkumar and Ardell, 2016) that are all

morphologically similar (Mitchell, 1953). Thus, specific tools are required to exclusively label noradrenergic nerve terminals and simultaneously monitor for NAT function at the neuroeffector site, which could provide great insight into the pathogenesis of several cardiovascular diseases (CVDs) where NAT is defective (Schroeder and Jordan, 2012).

The laboratory previously developed a fluorescence-based technique to monitor NAT function in the murine urogenital system *ex vivo* (Parker *et al.*, 2010). Given that it was the first to exclusively label peripheral noradrenergic nerve terminals and simultaneously measure for NAT reuptake rate in living tissue, it is of high interest to adapt the technique to the cardiovascular system where the implications of NAT function are vast.

3.1.2. Objectives and aims

Therefore, I aim to address the following objectives:

1. Optimise the NTUA assay to exclusively label sympathetic nerve terminals in the rodent (mice and rat) heart and mesenteric arteries *ex vivo*
2. Optimise approach (1) to dynamically monitor NAT reuptake rate in cardiovascular tissues
3. Assess any non-neuronal labelling by the NTUA fluorescent substrate
4. Test whether NTUA would be useful to label noradrenergic neurones in other tissues (including human)

3.2. Results

3.2.1. NTUA labelling in rodent cardiovascular tissue

3.2.1.1. Confocal microscopy: NTUA labelling of neuronal structures

The use of NTUA to label sympathetic neurones *ex vivo* has already been validated in the murine urogenital system (Parker *et al.*, 2010). To test whether cardiovascular sympathetic neurones could also be labelled with NTUA, rodent hearts and mesenteric arteries (MAs) were superfused with high concentrations of NTUA and subjected to confocal microscopy.

In the absence of NTUA, no varicose structures that resemble nerve terminals were observed in the heart and MAs in either species, though autofluorescence was observably more prominent in the heart than vasculature (Figure 3.1A-E). Lambda scanning of the tissue autofluorescence revealed an emission bandwidth of 425-550 nm with the 405 nm laser line (Figure 3.1F).

NTUA incubation revealed intricate networks of cardiac- and periarterial neuronal innervation; coursing bundles were seen branching out into thinner bundles and ultimately into individual thin varicose fibres [Figure 3.2 (mouse heart); Figure 3.3 (rat heart); Figure 3.4 (rodent MAs)]. The latter structures exhibited the classic 'beads on a string' morphology of neuronal fibres: highly fluorescent punctate nerve terminals joined by fainty labelled thin intervaricose segments [Figure 3.2 (left panels); Figure 3.3 (top panels); Figure 3.4 (left panels)]. In the heart, the distribution of neuronal structures was disorderly and intertwined with non-neuronal cell types [Figure 3.2 (right panels); Figure 3.3 (bottom panels)], observed at an optical depth of ≤10 μm. On the other hand, mesenteric periarterial neuronal fibres appear to run parallel or perpendicular to the

longitudinal axis, forming organised dense plexuses that surrounds the entire surface of the vessel [Figure 3.4 (right panels)]. Non-neuronal NTUA fluorescence was often evident in many images, particularly in the heart (Figure 3.2, 3.3). Lambda scanning of NTUA fluorescence revealed an emission bandwidth that overlaps with tissue autofluorescence: 410-550 nm (Figure 3.5).

To investigate whether cardiac neuronal labelling by NTUA was limited by depth penetration of the fluorophore, NTUA was also loaded into murine hearts by Langendorff retrograde perfusion. This resulted in similar neuronal labelling at a depth limit of ≤10 μm (n=2, Appendix 3.1). These observations demonstrate NTUA delivery by either superfusion or perfusion to cardiovascular tissue labels structures reminiscent of autonomic nerves. However, in the heart, such labelling is confined to about 10 μm from the tissue surface.

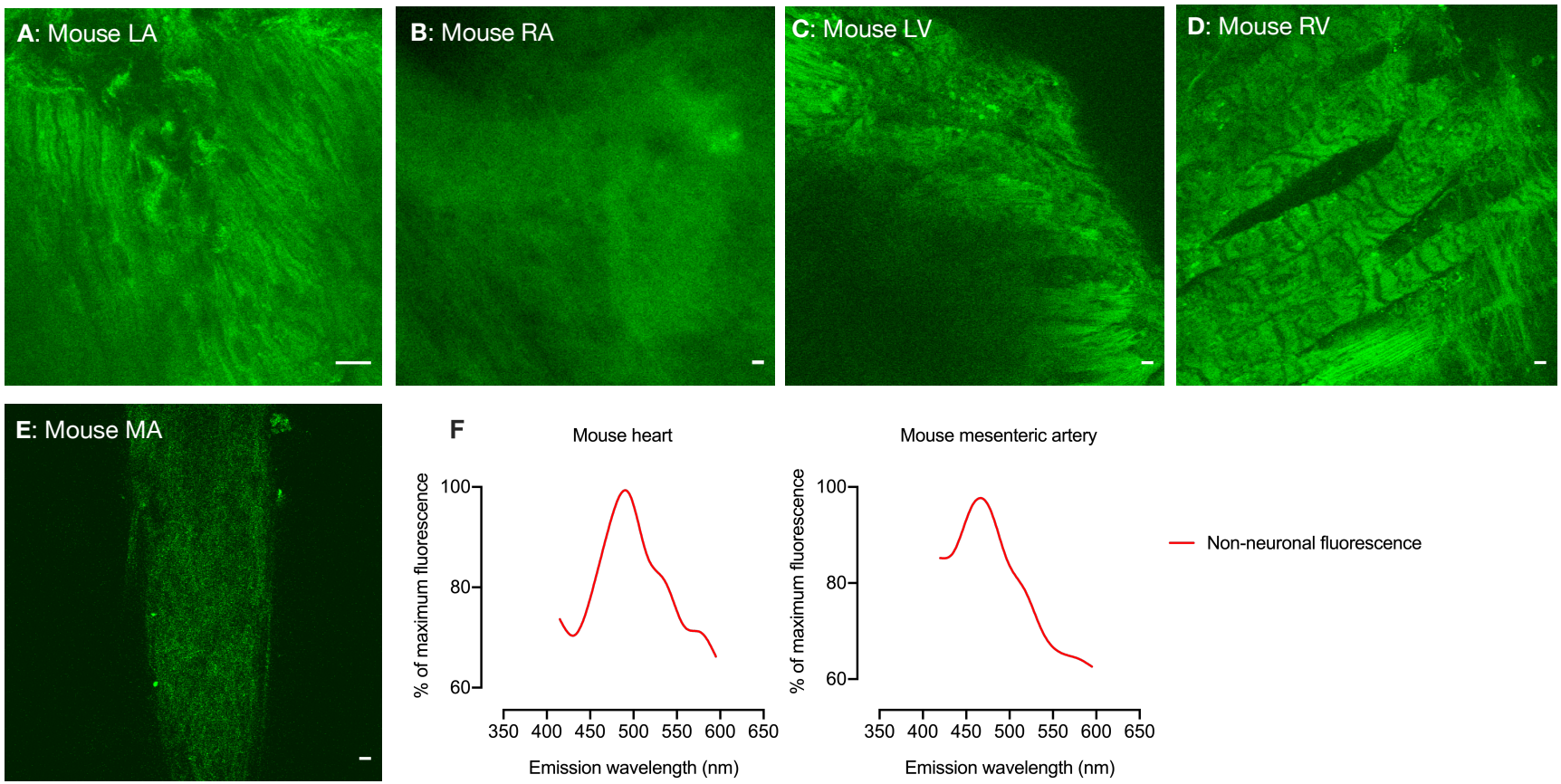


Figure 3.1: Autofluorescence of murine cardiovascular tissue

Tissue autofluorescence of the murine heart and vasculature. **(A-D)** Isolated cardiac chambers and **(E)** MAs were imaged without NTUA. No structures reminiscent of varicose neuronal structures were seen. This was also applicable to the rodent (*data not shown here*). **(F)** Lambda scanning revealed the emission bandwidth of autofluorescence was 425-550 nm with the 405 nm excitation line. All micrographs, bars = 10 µm
Abbreviations: LA (left atrium), RA (right atrium), LV (left ventricle, RV (right ventricle), MA (mesenteric artery)

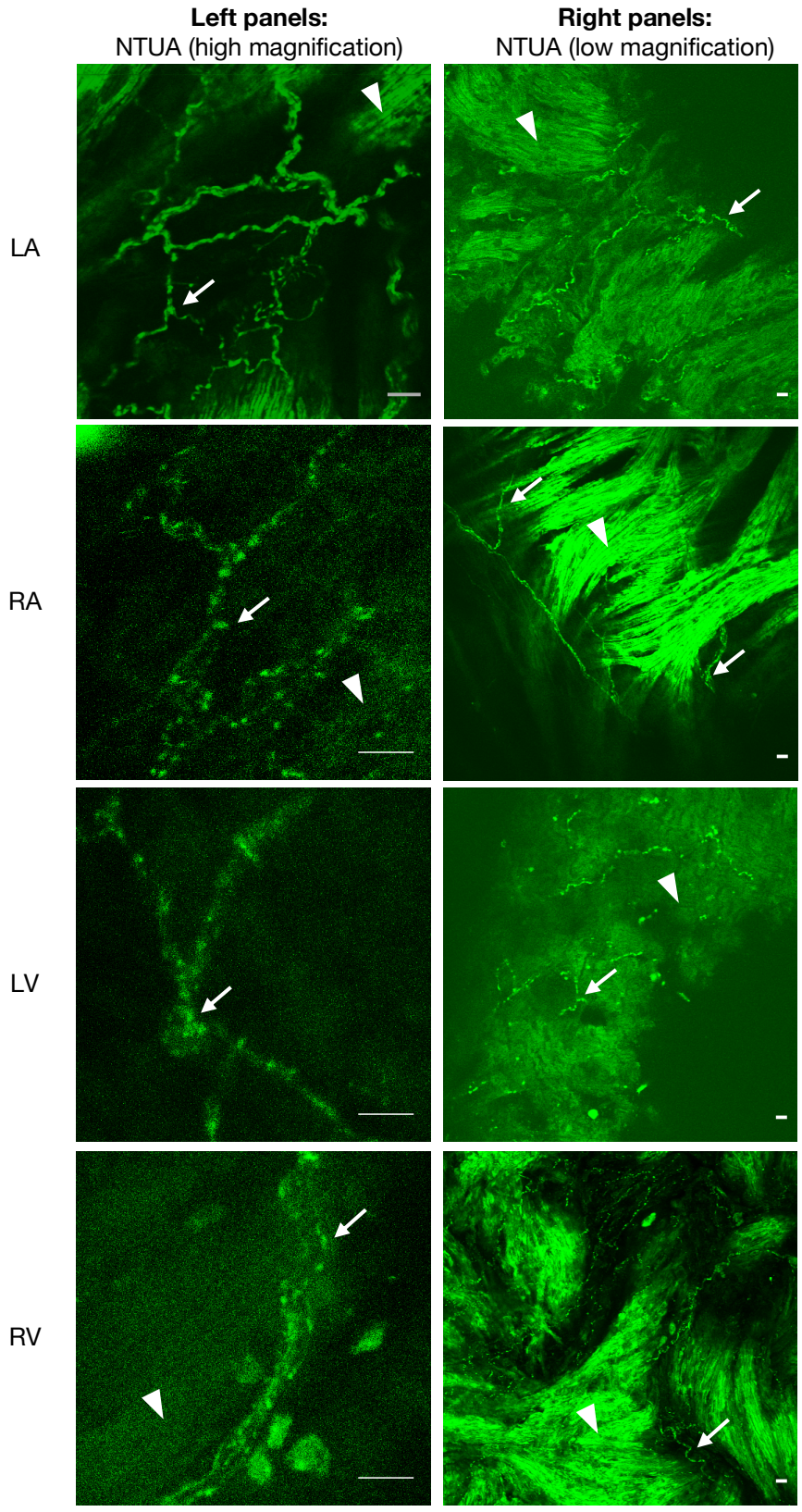
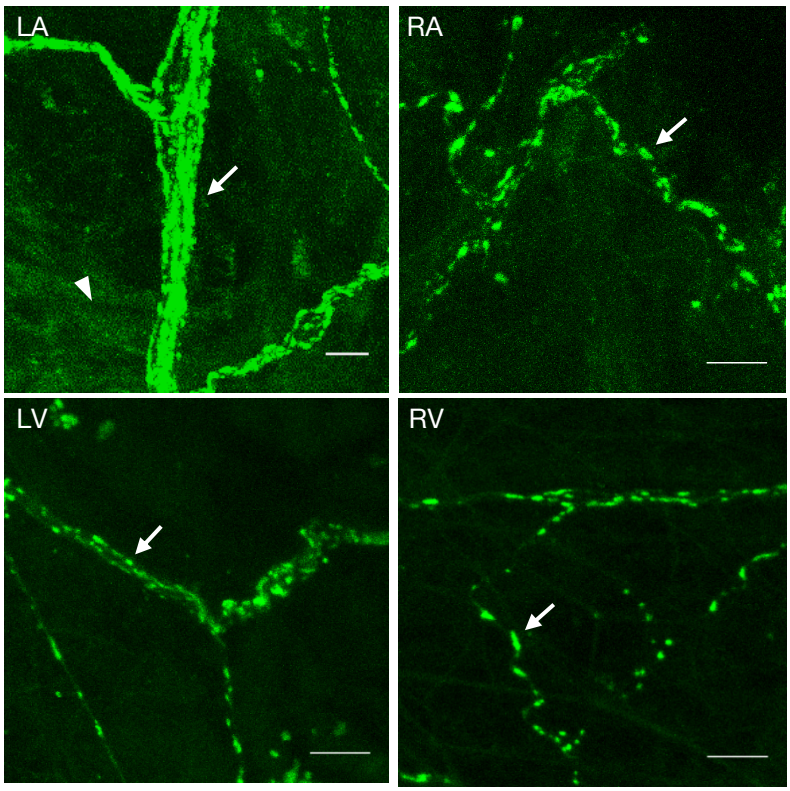


Figure 3.2: NTUA labelling of murine cardiac neuronal structures
Please refer to the following page for the figure legend. All micrographs, bars = 10 μm.

Top panels: NTUA (high magnification)



Bottom panel: NTUA (low magnification)

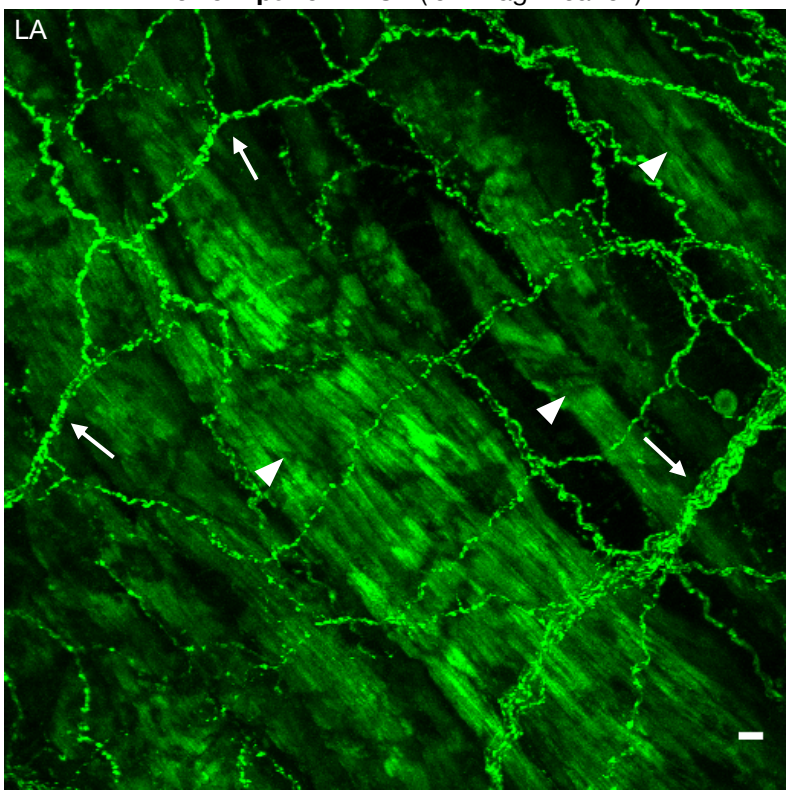


Figure 3.3: NTUA labelling of rat cardiac neuronal structures

Please refer to the following page for the figure legend. All micrographs, bars = 10 μm.

Description for the figures on the previous pages.

Abbreviations: left atrium (LA), right atrium (RA), left ventricle (LV) and right ventricle (RV).

Figure 3.2: NTUA labelling of murine cardiac neuronal structures
Murine cardiac nerve terminals labelled by NTUA. **(Left panels)** At high magnifications, the neuronal bundles labelled by NTUA can be seen branching off into single fibres with punctate swellings of neuronal terminals (white arrows). **(Right panels)** At low magnifications, these structures can be seen in very close proximity with non-neuronal structures (white arrow heads) similar to those with autofluorescence.

All micrographs, bars = 10 μm. The low- and high magnification images were not captured in the same field of focus.

Figure 3.3: NTUA labelling of rat cardiac neuronal structures
Rat cardiac nerve terminals labelled by NTUA. **(Top 4 panels)** At high magnifications, NTUA-labelled noradrenergic neuronal bundles can be seen branching off into single fibres with punctate swellings of neuronal terminals (white arrows). **(Bottom panel)** At low magnifications, these structures can be seen in very close proximity with non-neuronal structures (white arrow heads) similar to those with autofluorescence.

All micrographs, bars = 10 μm. The low- and high magnification images were not captured in the same field of focus.

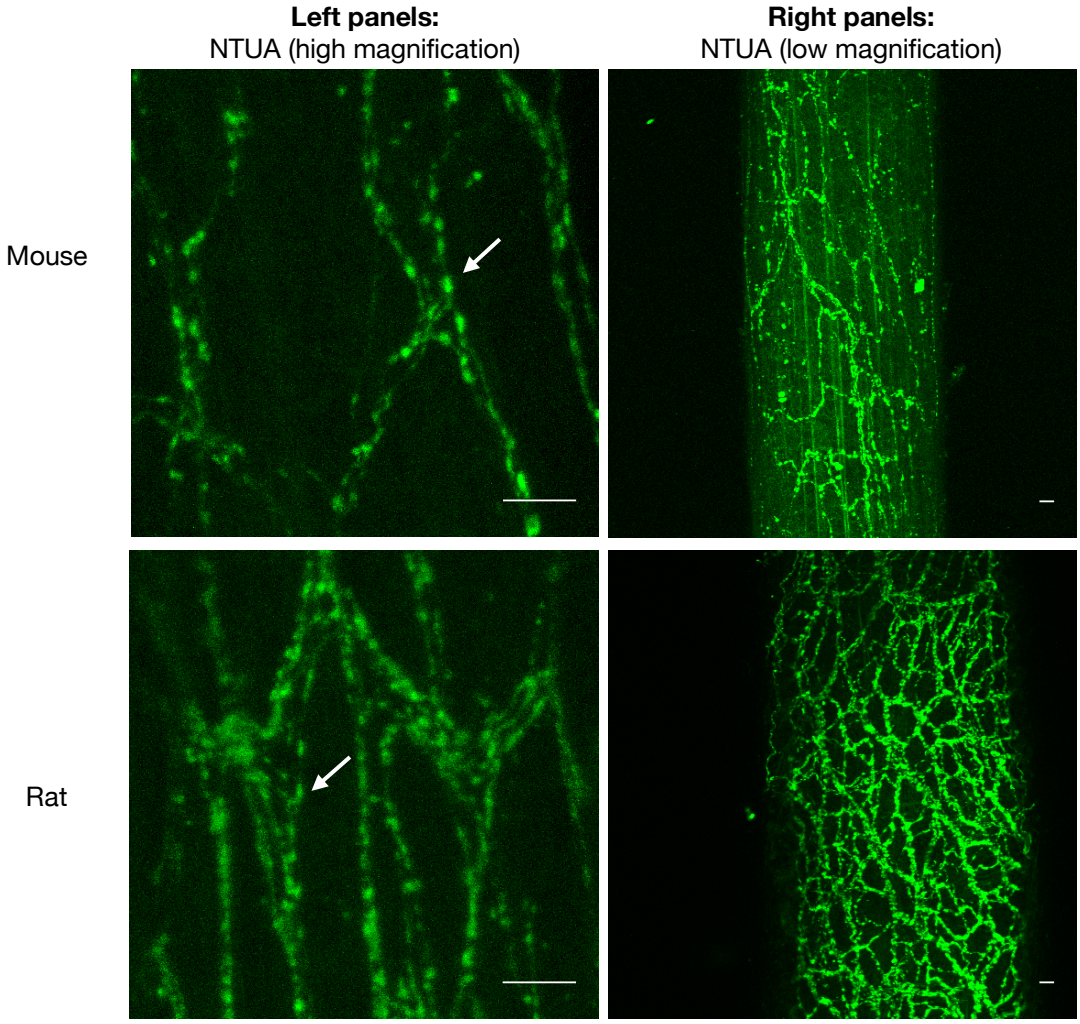


Figure 3.4: NTUA labelling of rodent mesenteric periarterial neuronal structures
Periarterial nerve terminals labelled by NTUA. **(Left panels)** At high magnifications, NTUA-labelled neuronal structures can be resolved at the level of single terminals. **(Right panels)** At low magnifications, the organisation of NTUA labelled neuronal structures were observed in thick bundle arrangements that wraps around the entire surface of the vessel.

All micrographs, bars = 10 µm. The low- and high magnification images were not captured in the same field of focus.

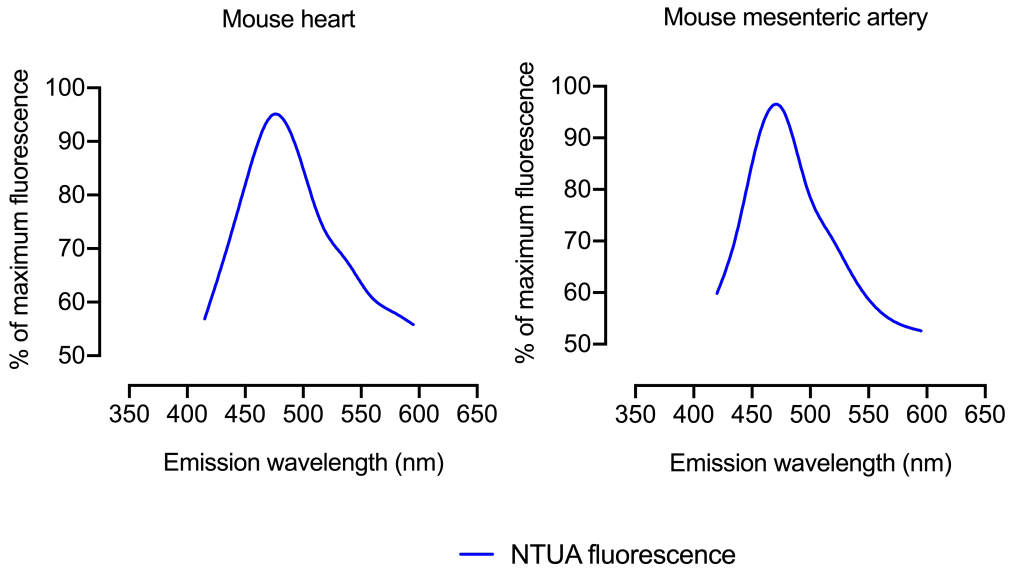


Figure 3.5: Emission profile of NTUA in murine cardiovascular tissue
Spectral scanning of NTUA neuronal fluorescence in the murine heart and vascular tissue. Lambda scanning revealed emission bandwidth 425-550 nm.

3.2.1.2. Multi-photon microscopy: NTUA labelling of neuronal structures

To investigate whether the limited depth detection of NTUA fluorescence in the heart was due to the technical shortcomings associated with confocal microscopy, the murine LA was exposed to NTUA at similarly high concentrations and subjected to multi-photon excitation microscopy (MPE). MPE yielded *z*-stacks at a greater depth (>15 μm) than confocal microscopy (≤10 μm). Furthermore, high resolution of NTUA fluorescence was achieved at lower laser powers in MPE than confocal microscopy (0.6% vs. >1%, respectively) (Figure 3.6). Interestingly, nuclei-like shadows were dispersed throughout non-neuronal structures (Figure 3.6).

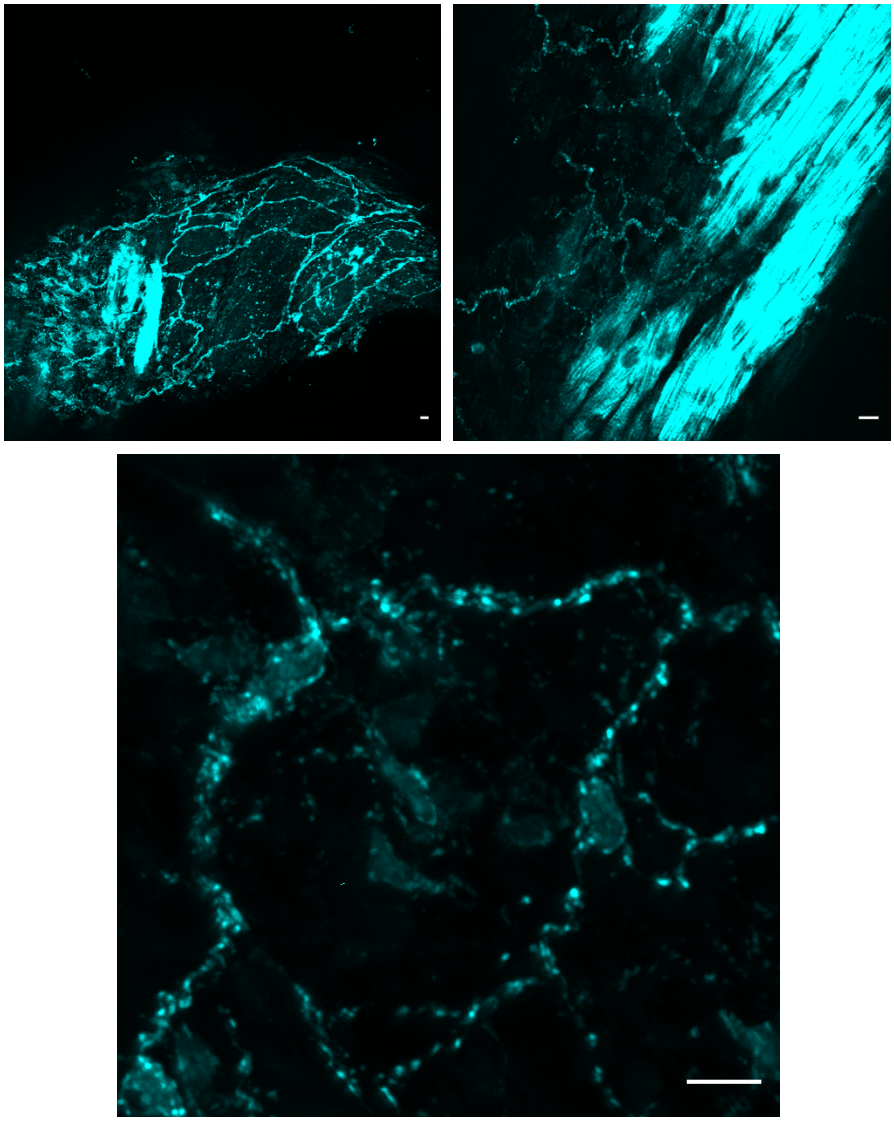


Figure 3.6: Cardiac neuronal NTUA fluorescence imaged with multi-photon microscopy
Murine cardiac nerve terminals labelled by NTUA and imaged with multi-photon microscopy (n=1). NTUA revealed a supply of neuronal innervation in the heart, which could be seen at greater depths compared to confocal microscopy. As with confocal microscopy, non-neuronal fluorescence can be seen. However, multi-photon microscopy also revealed cell nuclei-like structures dispersed throughout non-neuronal cells. All micrographs: bar = 10 μm.

3.2.1.3. Glyoxylic acid-induced chemofluorescence of neuronal catecholamines

To visualise cardiac- and periarterial noradrenergic nerve fibres with a validated fluorescence-based technique, tissues were subjected to sucrose-potassium-glyoxylic acid (SPG) mix. In the cryosectioned heart, SPG revealed only an occasional supply of individual catecholaminergic varicose neuronal fibres, with no nerve bundles in sight [Figure 3.7 (mouse); Figure 3.8 (rat)]. In the whole mount MAs, SPG labelled very dense nerve plexuses, though individual fibres could not be easily resolved (Figure 3.9) and appeared 'scrunched' compared to their NTUA-labelled counterparts (Figure 3.4).

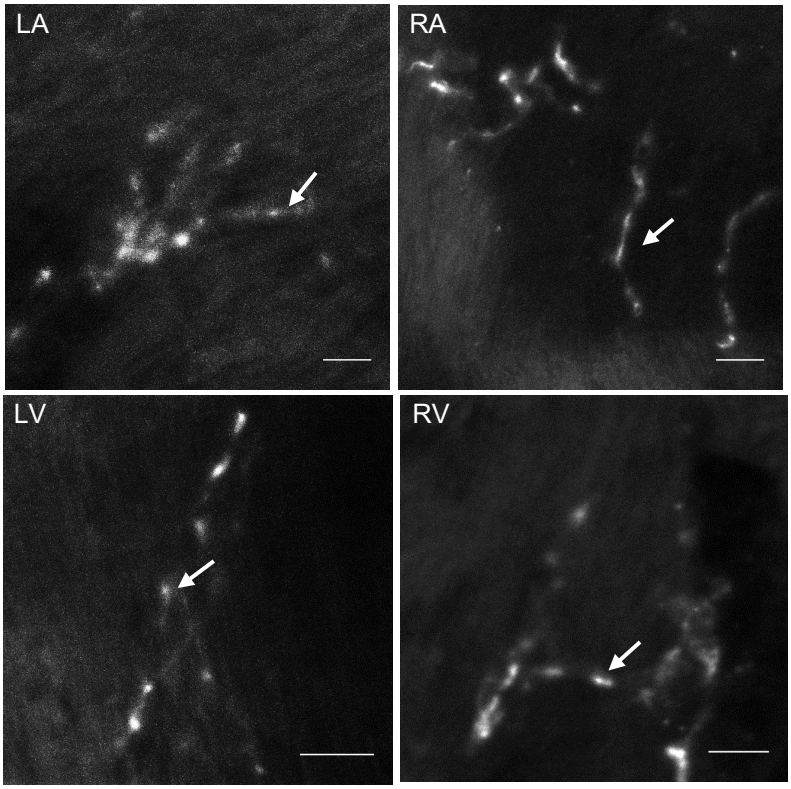


Figure 3.7: Glyoxylic acid chemofluorescence of murine cardiac noradrenergic neurones
The chemofluorescence of cryosectioned murine cardiac noradrenergic neurones revealed only single varicose neuronal fibres (white arrows) joined by very faintly fluorescent intervaricose segments.
All micrographs, bar = 10 μm.

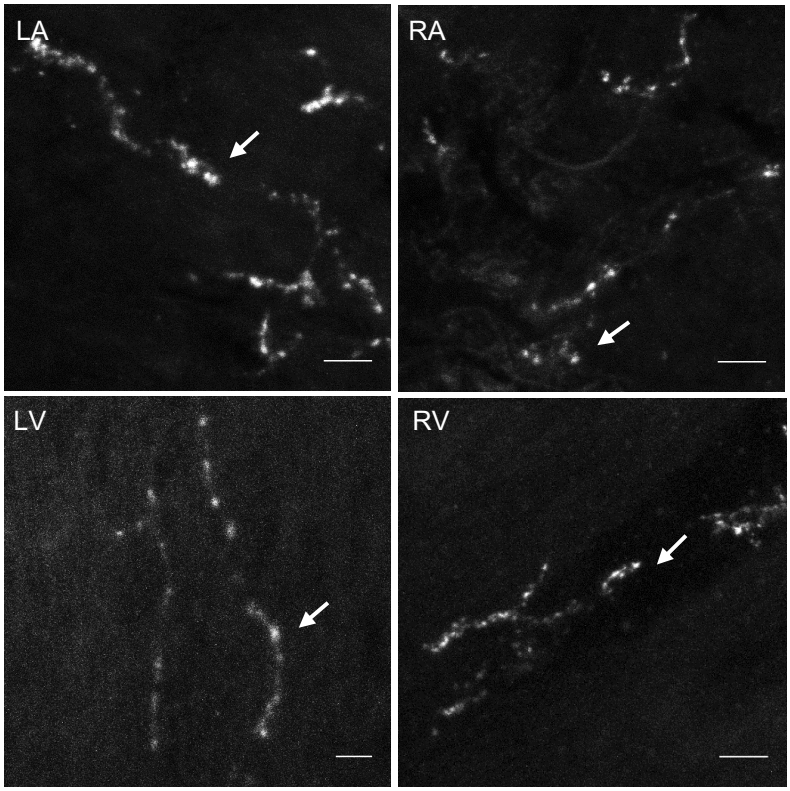


Figure 3.8: Glyoxylic acid chemofluorescence of rat cardiac noradrenergic neurones
The chemofluorescence of cryosectioned rat cardiac noradrenergic neurones revealed only single varicose neuronal fibres (white arrows) joined by very faintly fluorescent intervaricose segments.
All micrographs, bar = 10 μm.

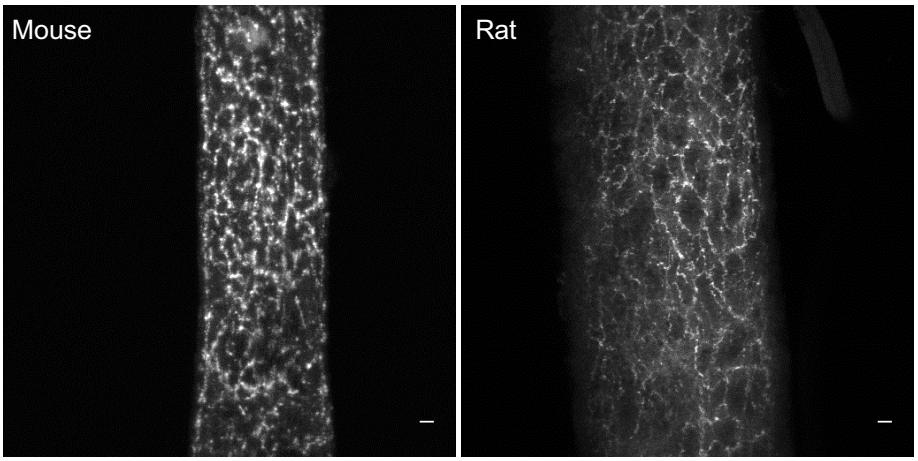


Figure 3.9: Glyoxylic acid chemofluorescence of rodent mesenteric periarterial noradrenergic neurones
Chemofluorescence of noradrenergic neurones in whole mount MAs revealed dense plexuses of innervation that surrounds the entirety of the vessel, though structures appear 'scrunched' compare to NTUA-induced fluorescence.
For all micrographs, bar = 10 μm.

3.2.1.4. NTUA uptake is temperature sensitive

To investigate whether the neuronal accumulation of NTUA occurs through a passive diffusion or active transport mechanism, the murine LA were cooled by 10ºC in the period of 6 min prior to the 1:20 NTUA test period. At 35-37ºC, cardiac neuronal structures accumulated NTUA in a linear fashion for 6 min. In cooled conditions, the linear accumulation of NTUA was comparably shallower (Figure 3.10A).

As a result, the linear NTUA uptake rate was significantly reduced by 59% in cooler temperatures compared to physiological temperatures [control: 17 (14, 22)%.min^{-1} (n=4, n_t=24) vs. cooling: 7 (3, 9)%.min^{-1} (n=4, n_t=24) ; p<0.0001, Figure 3.10B]. This suggests for a temperature-sensitive mechanism of cardiac neuronal uptake of NTUA. Interestingly, the starting fluorescence at t=0 was higher in the cooled group compared to the control group [control: 0.10±0.05 (n=4, n_t=24) vs. cooled: -0.17±0.03 (n=4, n_t=24); p<0.0001, Figure 3.10A].

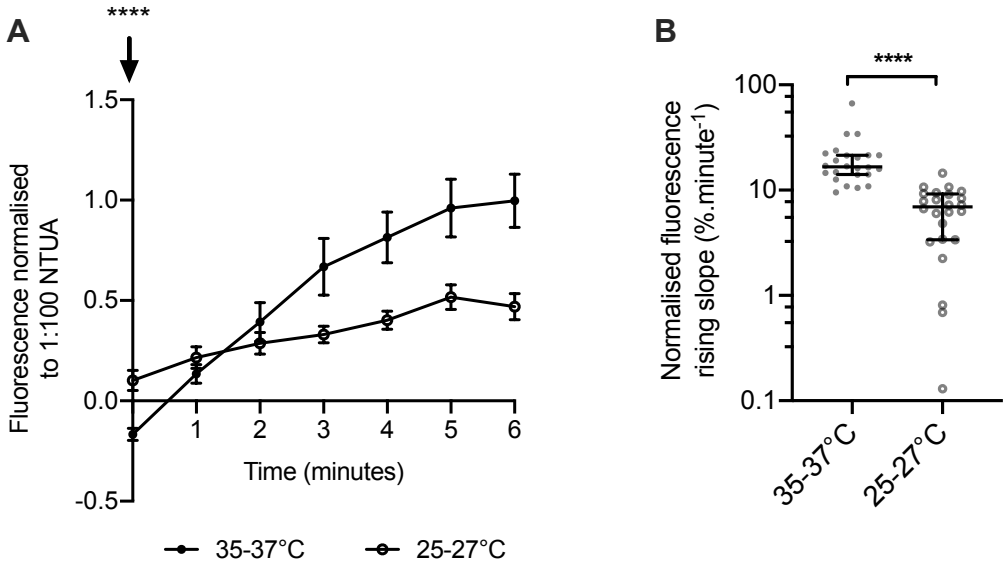


Figure 3.10: NTUA uptake into murine cardiac neuronal structures is temperature sensitive

Uptake rate of NTUA into murine cardiac nerve terminals is slower in cooled temperatures than in physiological (control) temperatures. **(A)**. Prior to the 1:20 NTUA test period, there was a 6-min cooling period. The starting fluorescence after the cooling period (t=0) was higher than in control conditions than in cooled conditions. NTUA accumulation thereafter was significantly shallower than at physiological conditions. Data presented as mean±SEM. **(B)** NTUA uptake rate was significantly lower in cooled conditions, compare to control conditions. Data presented as median (IQR). Each datapoint corresponds to a single nerve terminal.

Statistical analyses:
(A) t=0, Welch's *t*-test.
(B) NTUA uptake rate, Mann-Whitney test
**** denotes $p<0.0001$

3.2.1.5. NTUA uptake is mediated by the noradrenaline transporter

3.2.1.5.1. Desipramine

To investigate if the uptake of NTUA into neuronal structures of the rodent heart and periarterial vessels were attributed to NAT, tissues were pre-treated with NAT inhibitor, desipramine (DSM, 1 μM), for 6 min prior to and during the 1:20 NTUA test period.

In the absence of DSM, there was a time-dependent linear increase in neuronal NTUA fluorescence in the rodent LA (Figure 3.11, 3.12A, B) and MAs (Figure 3.13, 3.14A, B). In the presence of DSM, the rise in nerve terminal fluorescence was prevented. As a result, DSM significantly abolished the NTUA uptake rate in the mouse LA [control: 28.4±4.1%.min^{-1} (n=4, n_t=24) vs. DSM: -2.5±0.5%.min^{-1} (n=4, n_t=24), p<0.0001, Figure 3.12C], rat LA [control: 7.2±1.1%.min^{-1} (n=4, n_t=25) vs. DSM: -1.3±0.2%.min^{-1} (n=4, n_t=23), p<0.0001, Figure 3.12D], mouse MA [control: 18.4±4.8%.min^{-1} (n=4, n_t=24) vs. DSM: 0.3±0.8%.min^{-1} (n=4, n_t=24), p<0.0001, Figure 3.14C], and rat MA [control: 3.2±0.3%.min^{-1} (n=4, n_t=24) vs. DSM: -1.2±0.3%.min^{-1} (n=4, n_t=23), p<0.0001, Figure 3.14D]. The complete abolishment of neuronal NTUA uptake by a NAT-specific inhibitor demonstrates NTUA specificity for NAT in cardiovascular tissue, thus indicating the noradrenergic nature of these neurones.

Interestingly, in both the control and DSM conditions of NTUA exposure, there was also a time-dependent increase in cardiac non-neuronal fluorescence in similar areas (Figure 3.11) that exhibited tissue autofluorescence (Figure 3.1).

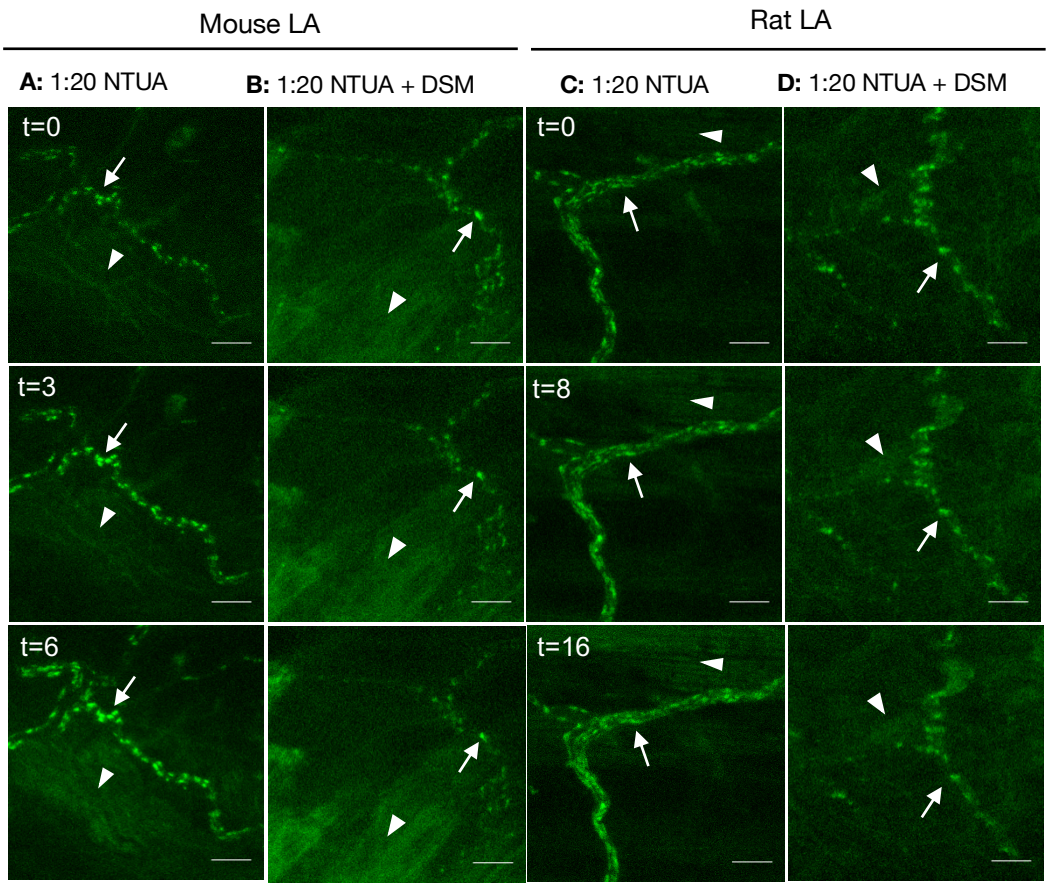


Figure 3.11: Abolition of rodent cardiac neuronal NTUA uptake during NAT inhibition
The uptake of NTUA into rodent cardiac nerve terminals in left atria (LA) is prevented by NAT inhibitor desipramine (DSM, 1 μM). **(Columns A, C)** In control conditions, there was a time-dependent increase of NTUA fluorescence into cardiac neuronal structures in the mouse and rat (white arrows). **(B, D)** In the presence of DSM, the neuronal accumulation of NTUA fluorescence was abolished.

There was also an increase in non-neuronal fluorescence during 1:20 NTUA exposure (white arrowheads) in both control and DSM conditions.

All micrographs, bars = 10 μm

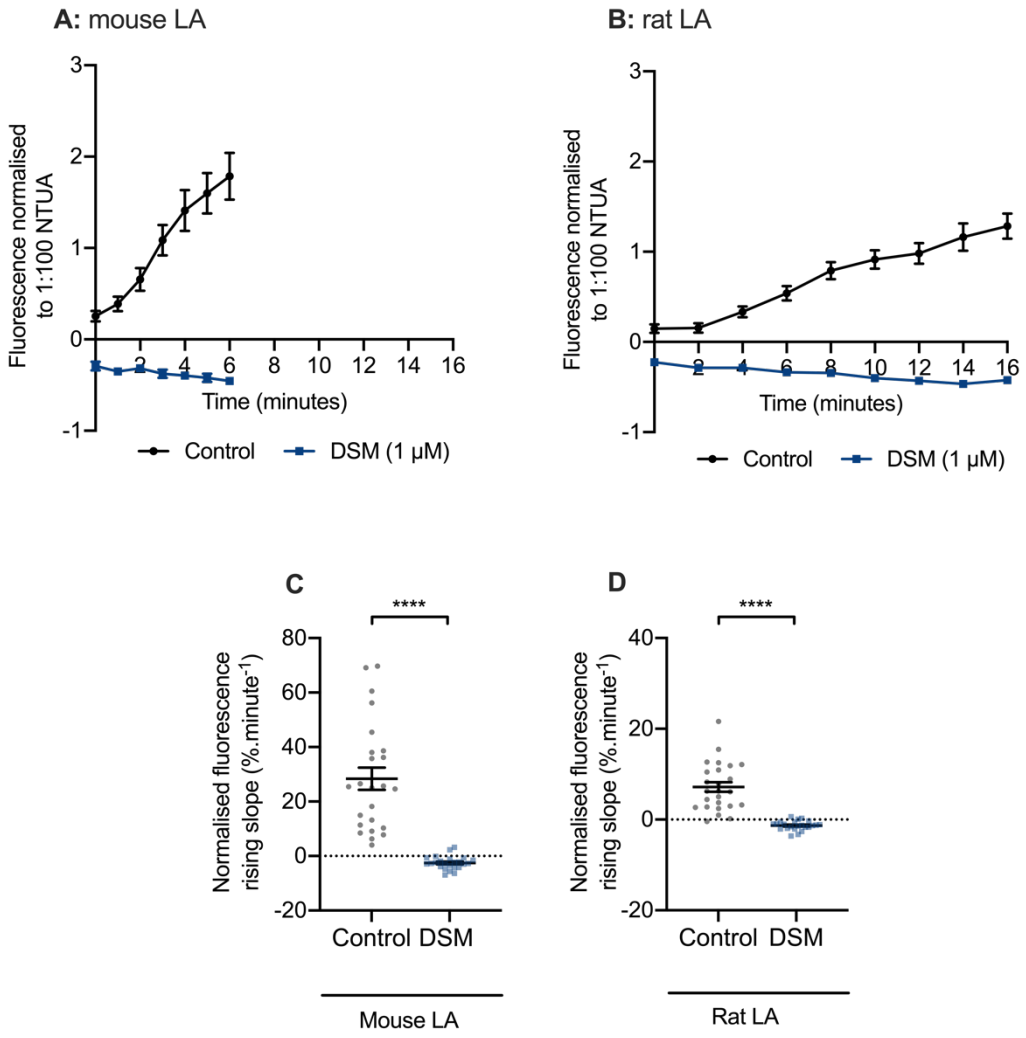


Figure 3.12: NAT-dependent uptake of NTUA into the rodent cardiac neurones

Time-dependent uptake of NTUA into nerve terminals of the rodent left atria (LA) with or without NAT inhibitor desipramine (DSM, 1 μM) treatment. **(A, B)** In the absence of DSM, there was a linear accumulation of NTUA into cardiac neurones in the mouse and rat. Such accumulation was abolished after DSM treatment throughout all time points of 1:20 NTUA exposure. Data presented as mean±SEM. **(C, D)** The linearity of NTUA accumulation was quantified as NTUA uptake rate. The latter was abolished in the presence of DSM. Data presented as mean±SEM. Each datapoint corresponds to a single nerve terminal.

Statistical analyses:
(C, D) Welch's *t*-test; **** denotes $p<0.0001$

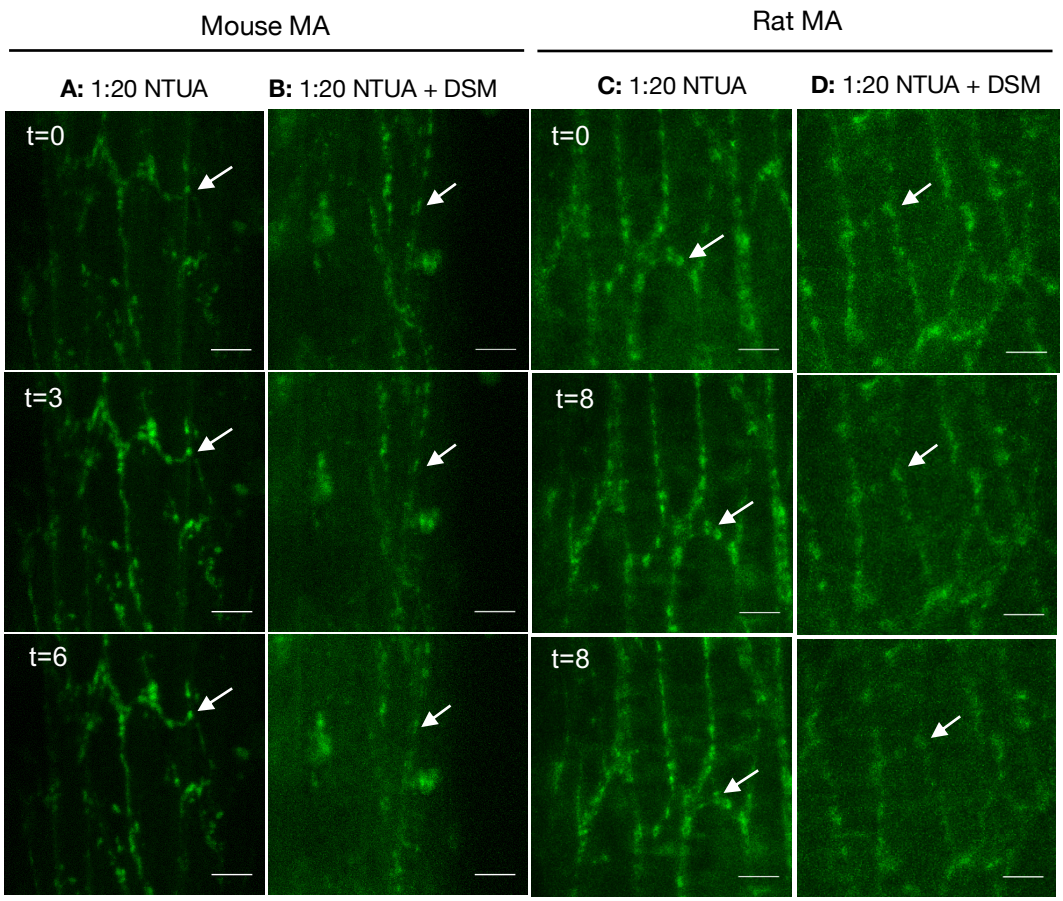


Figure 3.13: Abolition of rodent mesenteric periarterial neuronal NTUA uptake during NAT inhibition

Time-dependent uptake of NTUA into mesenteric periarterial nerve terminals with or without NAT inhibitor desipramine (DSM, 1 μM) treatment. **(A, C)** In the absence of DSM, there was a time-dependent increase in NTUA fluorescence into periarterial neuronal structures in the mouse and rat (white arrows). **(B, D)** In the presence of DSM, the accumulation of NTUA fluorescence was abolished.

In contrast with NTUA uptake into cardiac non-neuronal structures, there were no obvious changes in non-neuronal fluorescence in the rodent MAs during 1:20 NTUA superfusion. All micrographs, bars = 10 μm

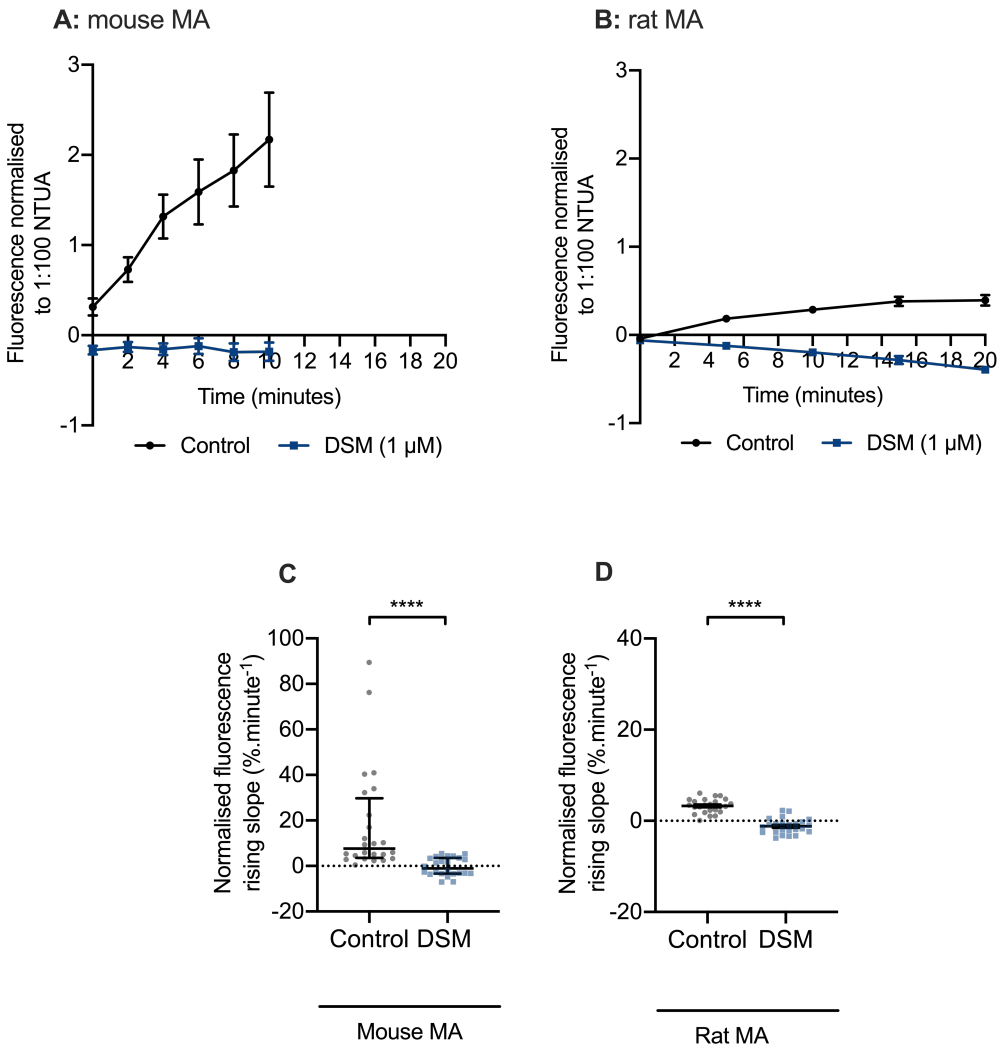


Figure 3.14: NAT-dependent uptake of NTUA into rodent mesenteric periarterial neurones

Time-dependent uptake of NTUA into the rodent mesenteric periarterial nerve terminals with or without NAT inhibitor desipramine (DSM, 1 μM) treatment. **(A, B)** In the absence of DSM, there was a linear accumulation of NTUA into periarterial neurones in the mouse and rat. Such accumulation was abolished after DSM treatment throughout all time points of 1:20 NTUA exposure. Data presented as mean±SEM. **(C, D)** The linearity of NTUA accumulation was quantified as NTUA uptake rate. The latter was abolished in the presence of DSM. Data presented as median (IQR) and mean±SEM, respectively. Each datapoint corresponds to a single nerve terminal.

Statistical analyses:
(C) Mann-Whitney test; **(D)** Unpaired *t*-test
**** denotes $p<0.0001$

3.2.1.5.2. Tyramine

To further investigate NTUA specificity for NAT, the murine LA were loaded with 1:20 NTUA and exposed to sympathomimetic amine tyramine (TYR; 10 μM; enters via NAT and induces reverse transport) during the washout phase with KHB. In the absence of TYR, there was a gradual loss of neuronal NTUA fluorescence towards the 1:100 NTUA starting fluorescence over the span of 5 min (Figure 3.15A, B). In the presence of TYR, the 1:100 NTUA fluorescence was reached by 2 min with no terminals left visible by the end of the washout period (Figure 3.15A, B). As a result, TYR significantly increased the rate of NTUA loss by 117±44% between t=8-10 [control: -12±2%.min^{-1} (n=4, n_t=24) vs. TYR: -26±3%.min^{-1} (n=4, n_t=24), p<0.0001, Figure 3.15C]. The loss of NTUA fluorescence induced by NAT reverse transport further suggests the NTUA specificity for NAT.

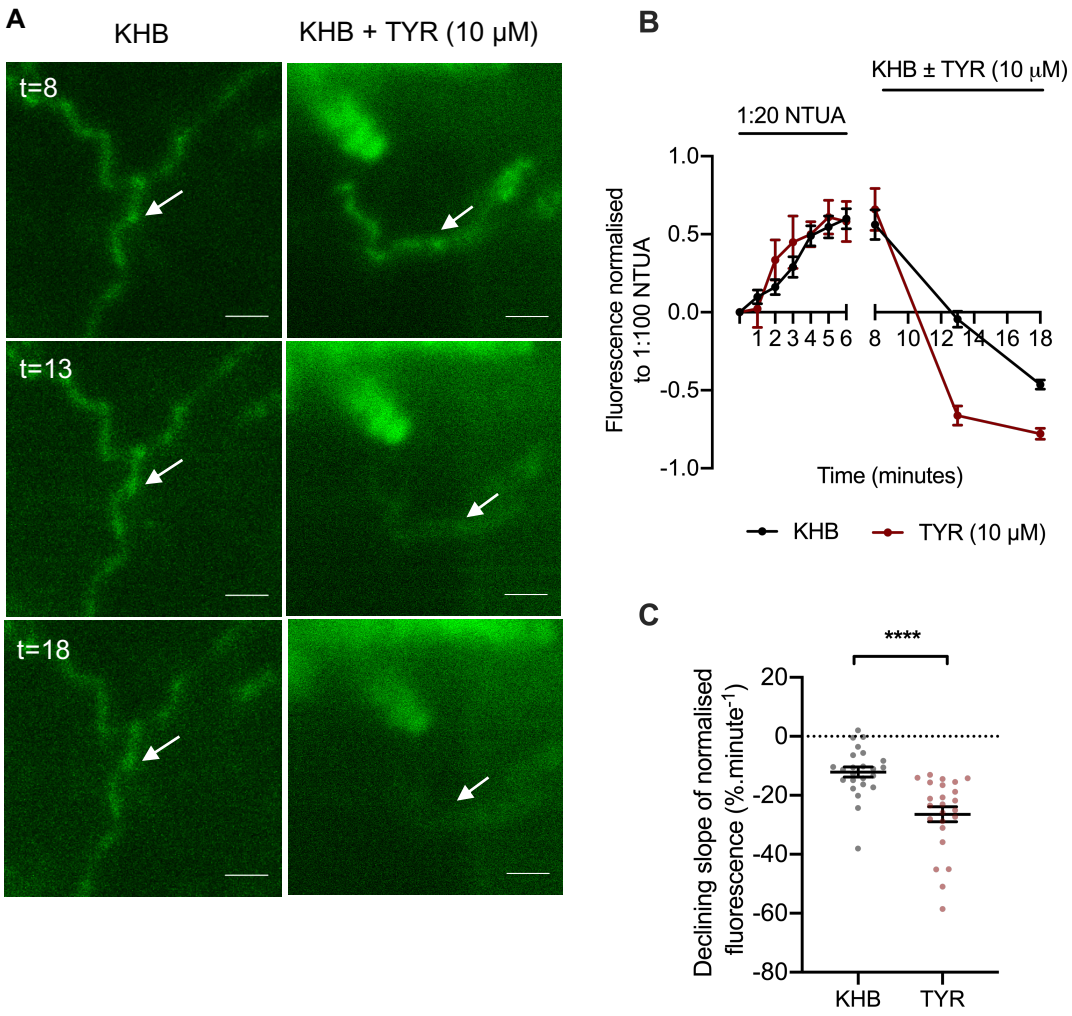


Figure 3.15: Sympathomimetic amine tyramine augments NTUA washout from murine cardiac neurones

The extrusion of NTUA is enhanced by sympathomimetic amine tyramine (TYR; 10 µM) from murine cardiac nerve terminals. **(A)** The loss of NTUA from neuronal structures with KHB alone was gradual, where the terminals remained visible after 10 min. The presence of TYR accentuated fluorescence loss, where terminals were no longer visible by the end of the experiment. **(B)** The loss of neuronal fluorescence in the presence of TYR occurred at a faster rate. Data presented as mean±SEM. **(C)** The rate of fluorescence loss was significantly greater than with KHB alone (t=8-12). Data presented as mean±SEM. Each datapoint corresponds to a single nerve terminal.

All micrographs, bars = 10 µm.

Statistical analysis
(C) Unpaired *t*-test
**** denotes $p<0.0001$.

3.2.1.6. Non-neuronal NTUA uptake into myocyte-like structures

NTUA was consistently seen to accumulate into non-neuronal structures in the rodent heart but not MAs. However, due to the high magnifications required to discern individual nerve terminals, the morphology of these cardiac non-neuronal structures was unclear.

To investigate this further, an area of the mouse LA was identified at low magnifications in the absence of NTUA. Thereafter, the same area was monitored throughout NTUA superfusion. In addition to the appearance of noradrenergic neurones, non-neuronal areas also began to accumulate NTUA fluorescence. These non-neuronal cell types were very large, elongated, irregularly conjoined with others (Figure 3.16), and were reminiscent of those observed with MPE (Figure 3.6). Non-neuronal cell nuclei were also visible as with MPE (Figure 3.6).

The non-neuronal structures were hypothesised to be cardiomyocytes due to their size and shape (Jansen and Rose, 2019). After the identification of an area of non-neuronal cell types that accumulated NTUA, the rat LA was incubated with DAPI which revealed central and elongated nuclei (Figure 3.17). DAPI also revealed nuclei of a different morphology around a neuronal bundle (Figure 3.17). The cell population could be Schwann cells due to the near localisations with rat mesenteric periarterial noradrenergic neurones (Hansen *et al.*, 2019), though this was not investigated further.

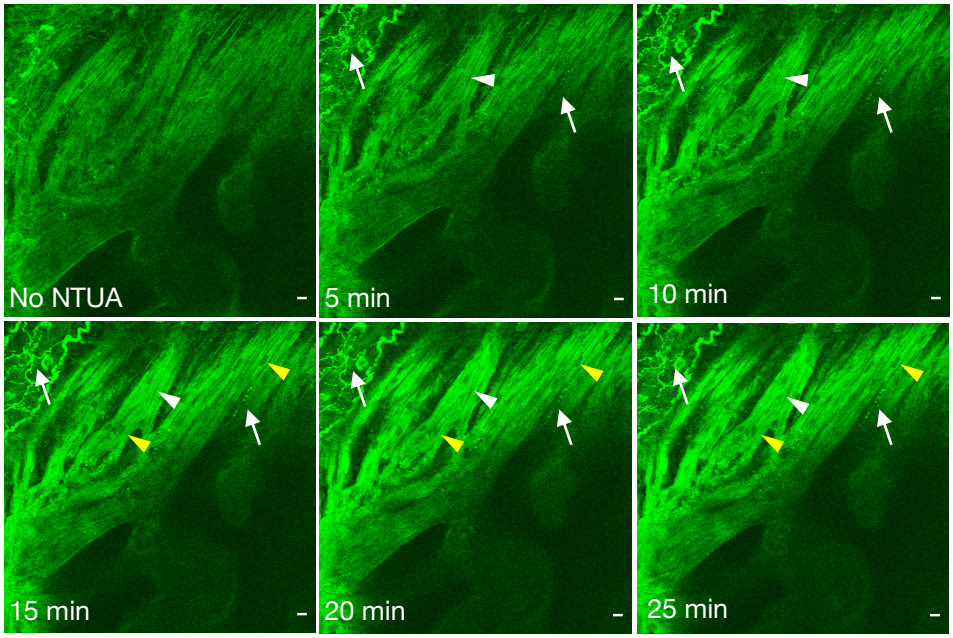


Figure 3.16: Non-neuronal uptake of NTUA in the murine heart
NTUA was detected to accumulate in non-neuronal structures in the murine heart. A region at low magnifications was selected and monitored throughout NTUA superfusion. NTUA labelled sympathetic nerve terminals (white arrows), but also non-neuronal structures with elongated and conjoined brick-like cell types (white arrowheads). In some non-neuronal cells, a faint shadow can be seen within the cell that appears like cell nuclei (yellow arrowheads).

All micrographs, bars = 10 µm

Non-neuronal uptake of NAd, termed uptake$_2$, is well-explored in the rat heart and can be inhibited by corticosterone (Iversen, 1965). Here, the mouse LA was pre-treated with corticosterone (10 µM) to investigate the mechanism of NTUA uptake. In the same areas that accumulated NTUA, corticosterone pre-treatment reduced uptake in subsequent NTUA exposure events by 76% [vehicle control: 29 (17, 38)%.min^{-1} (n=2, n_{ROI}=27) vs. corticosterone: 7 (-6, 11)%.min^{-1} (n=2, n_{ROI}=27), p<0.0001, Figure 3.18,19]. In all conditions, neuronal NTUA accumulation was maintained.

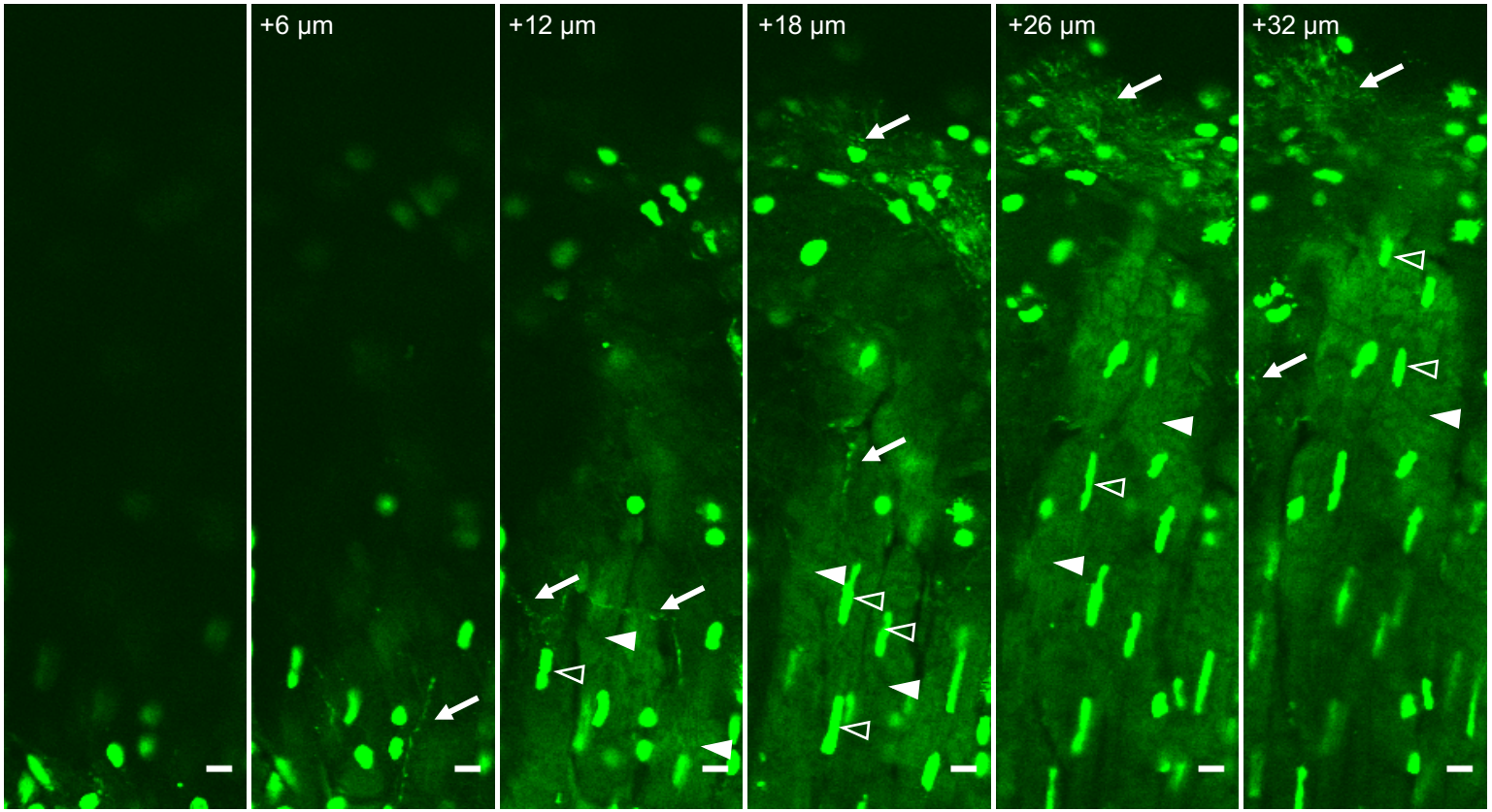


Figure 3.17: Cell nuclei morphology of non-neuronal cell types that accumulate NTUA

A non-neuronal area of the rat heart (LA) that accumulated NTUA was exposed to DAPI. These cells were elongated, brick-like, irregularly shaped, and in close proximity with sympathetic nerve terminals (white arrows). DAPI loading revealed the elongated nuclei (open arrowheads) of non-neuronal structures of interest. A subpopulation of nuclei with a different morphology can also be seen at the top of these images surrounding a neuronal bundle. This *z*-stack spanned by just over 30 µm depth-wise due to the uneven tissue surface. All micrographs, bars = 10 µm

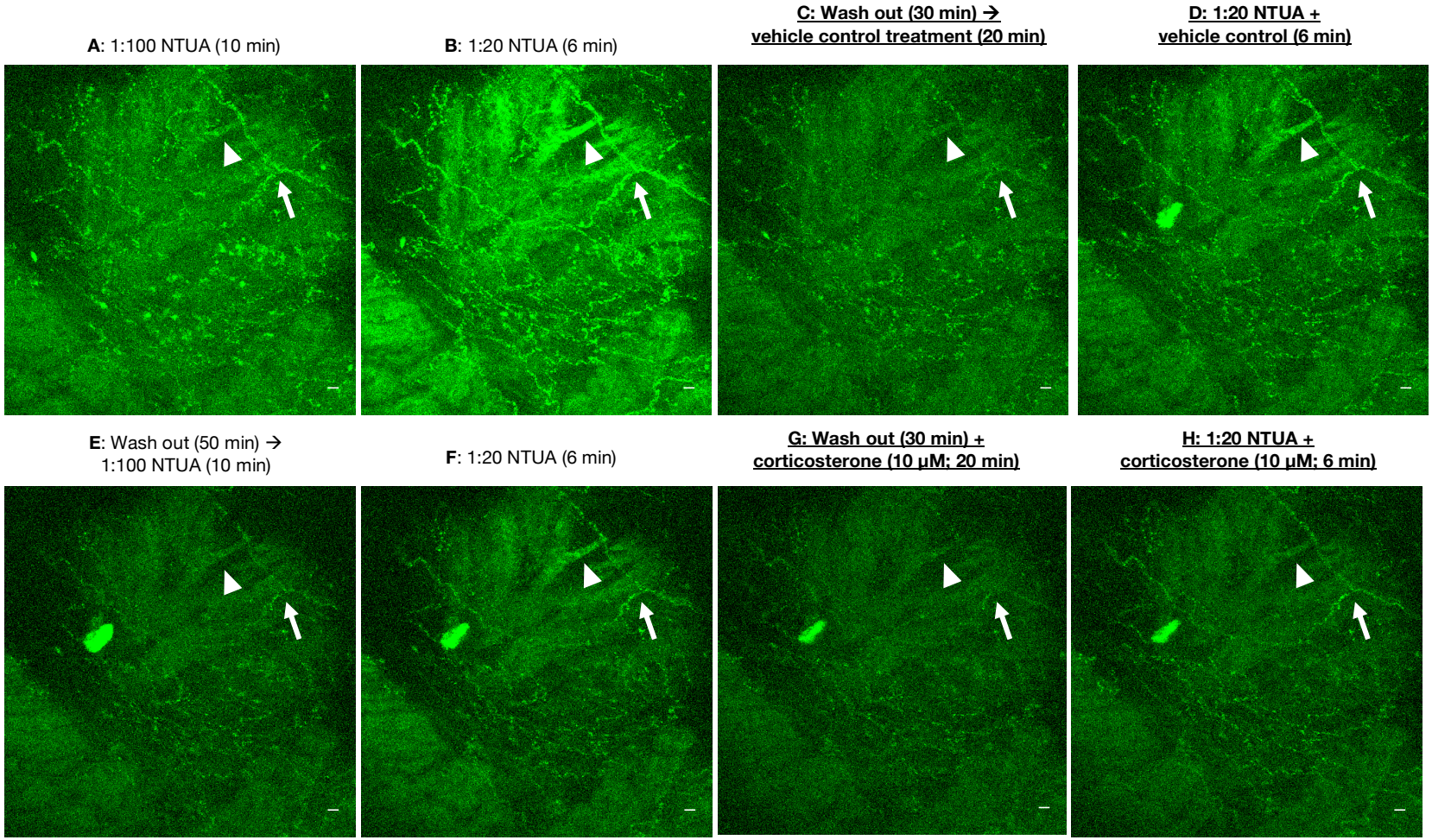


Figure 3.18: Uptake$_2$ inhibition prevents NTUA uptake into non-neuronal structures in the murine heart

Please refer to the following page for the figure legend. For all micrographs, bars = 10 µm.

Description for the figure on the previous page.

Figure 3.18: Uptake$_2$ inhibition prevents NTUA uptake into non-neuronal structures in the murine heart

Investigation of the non-neuronal NTUA uptake mechanism in the murine heart with uptake$_2$ inhibitor, corticosterone. **(A)** A large area of the murine LA labelled with 1:100 NTUA was captured at low magnifications. NTUA accumulated in both neurones (white arrows) and non-neuronal cell types (white arrowheads). **(B)** Neuronal and non-neuronal structures simultaneously accumulated NTUA at higher concentrations (1:20 NTUA) **(C)** Tissues were washed with KHB for 30 min and treated with vehicle control for 20 min. **(D)** Exposure of the mouse LA to 1:20 NTUA once again increased neuronal and non-neuronal fluorescence.

(E) Washout period of 50 minutes to remove 1:20 NTUA, followed by 1:100 NTUA exposure event to restore neuronal fluorescence. **(F)** Re-exposure of tissue to 1:20 NTUA saw another increase in neuronal- and non-neuronal fluorescence. **(G)** NTUA fluorescence was washed out for 30 min and treated with corticosterone for 20 min. **(H)** In corticosterone-treated tissue, 1:20 NTUA exposure led to an increase in neuronal fluorescence, but not non-neuronal fluorescence.

All micrographs, bars = 10 µm.

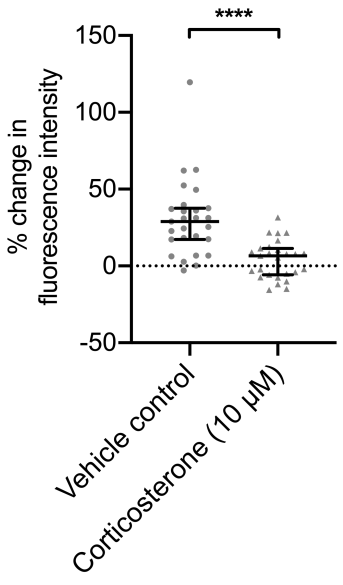


Figure 3.19: Uptake$_2$ inhibition abolishes cardiac non-neuronal NTUA uptake

The fluorescence of several individual non-neuronal structures (region of interest, ROI) was quantified in response to 1:20 NTUA exposure with and without corticosterone pre-treatment. This was calculated as a percentage difference between Figure 3.18 C, D and G, H. Data presented as median (IQR).

Mann-Whitney test
**** denotes $p<0.0001$.

3.2.1.7. Investigating different experimental conditions on NTUA uptake

3.2.1.7.1. Time course of NTUA uptake

Thus far, quantifications of NTUA uptake rate focused on the linear neuronal accumulation of NTUA. To investigate the time course of NTUA accumulation beyond the critical time point, the mouse LA was superfused for 20 min with a continuous supply of fresh NTUA. As per previous experiments, the linear phase of NTUA uptake took place in the first 6 min. Thereafter, NTUA fluorescence was gradually lost at each time point until the end of the experiment (Figure 3.20).

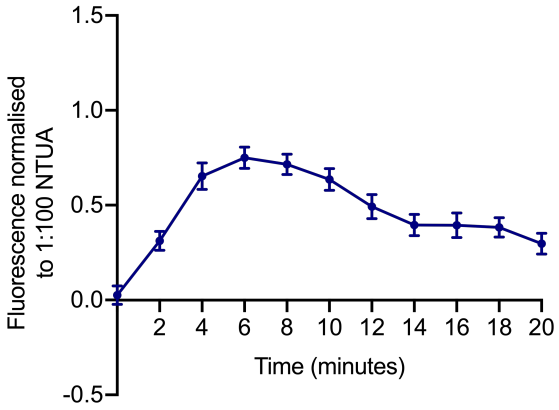


Figure 3.20: Time course of NAT-mediated neuronal uptake of NTUA in the murine heart
The mouse LA was exposed to 1:20 NTUA for an extended duration to investigate the time course of neuronal NTUA accumulation. Following a sharp upstroke of an accumulation of fluorescence into sympathetic nerve terminals, there was a steady decline for the remainder of the experiment despite continuous superfusion of NTUA. Data presented as mean±SEM.

3.2.1.7.2. NTUA fluorophore is photosensitive

To assess whether the decline in fluorescence in Figure 3.20 was due to photobleaching of the NTUA fluorophore, the mouse LA was exposed to NTUA and imaged in similar conditions as Figure 3.20, though illumination 8-18 min was omitted. The NTUA

fluorescence detected at the experiment endpoint was higher in reduced imaging conditions than constant imaging conditions, where the relative change between the t=6 and the endpoint was negative in the latter group [constant: -0.47±0.07 (n=4, n_t=19) vs. reduced: 0.25±0.09 (n=4, n_t=24); p<0.0001, Figure 3.21B].

NTUA photosensitivity was also investigated with different laser excitation wavelengths. Pilot experiments were conducted to assess neuronal NTUA accumulation in the rat MA with the 405 nm and 458 nm excitation laser line. Terminals exposed to 405 nm exhibited a similar NTUA uptake time course trace as in the heart (Figure 3.20); however, the gradual loss of fluorescence was prevented with the 458 nm excitation laser line (Figure 3.21). However, these results are preliminary as 1) the excitation wavelength laser power differed (405 nm: 2%; 458 nm: 30%) and 2) the n numbers were low [i.e., n=1, n_t=6 (405 nm) and n=2, n_t=12 (458 nm)], thus more experiments are required to validate this observation.

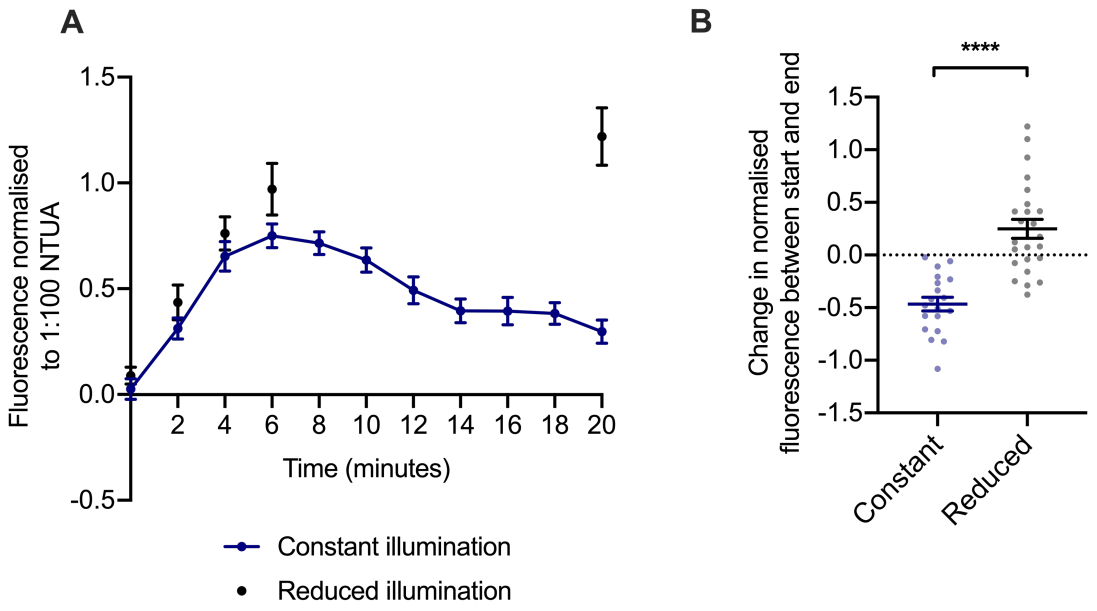


Figure 3.21: Phototoxicity of frequent imaging protocols on NTUA

Continuous exposure of NTUA to imaging protocols underestimates its accumulation. The murine LA was exposed to NTUA and imaged either 1) every 2 min for 20 min or 2) absent illumination protocol t=8-18. **(A)** NTUA fluorescence beyond the initial uptake phase (t=6 onwards) declined steadily in constant illumination conditions. The reduction was prevented by the absence of illumination. Data presented as mean±SEM. **(B)** Constant imaging conditions resulted in a significant attenuation of fluorescence intensity t=6-20, though fluorescence intensity was maintained in the absence of frequent imaging protocols. Data presented as mean±SEM. Each datapoint corresponds to a single nerve terminal.

Statistical analysis:
(B) Unpaired Student's *t* test.
**** denotes $p<0.0001$

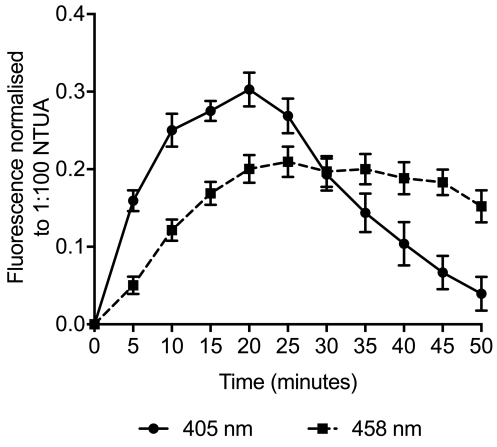


Figure 3.22: Timeline of NTUA fluorescence detection with 405 nm versus 458 nm excitation laser line

Over 20 min, the detection of NTUA fluorescence in the murine LA depletes faster with shorter excitation wavelength (405 nm), compared to maintainence with a longer wavelength (458 nm).

3.2.1.7.3. Rodent sacrifice method affects NTUA uptake rate

Prior to my rodent sacrifice training, tissues were obtained from other researchers within the College. Animals were sacrificed by different methods, such as 1) an inhalation overdose of CO_2 for 10 min or 2) under terminal anaesthesia with isoflurane. To investigate whether method of sacrifice perturbs NAT function *ex vivo*, NTUA uptake rate was assessed in the heart and mesenteric vasculature. NTUA uptake rate did not differ in the rat LA between the sacrifice methods [isoflurane: 8.5±0.9%.min^{-1} (n=4, n_t=24) vs. CO_2: 6.7±0.6%.min^{-1} (n=4, n_t=24), p>0.05; Figure 3.23A, C), though CO_2 overdose significantly attenuated NTUA uptake in MAs by 43±9% compared to those exposed to isoflurane [isoflurane: 7.7±1.0%.min^{-1} (n=2, n_t=12) vs. CO_2: 4.4±0.4%.min^{-1} (n=4, n_t=24), p<0.01; Figure 3.23B, C].

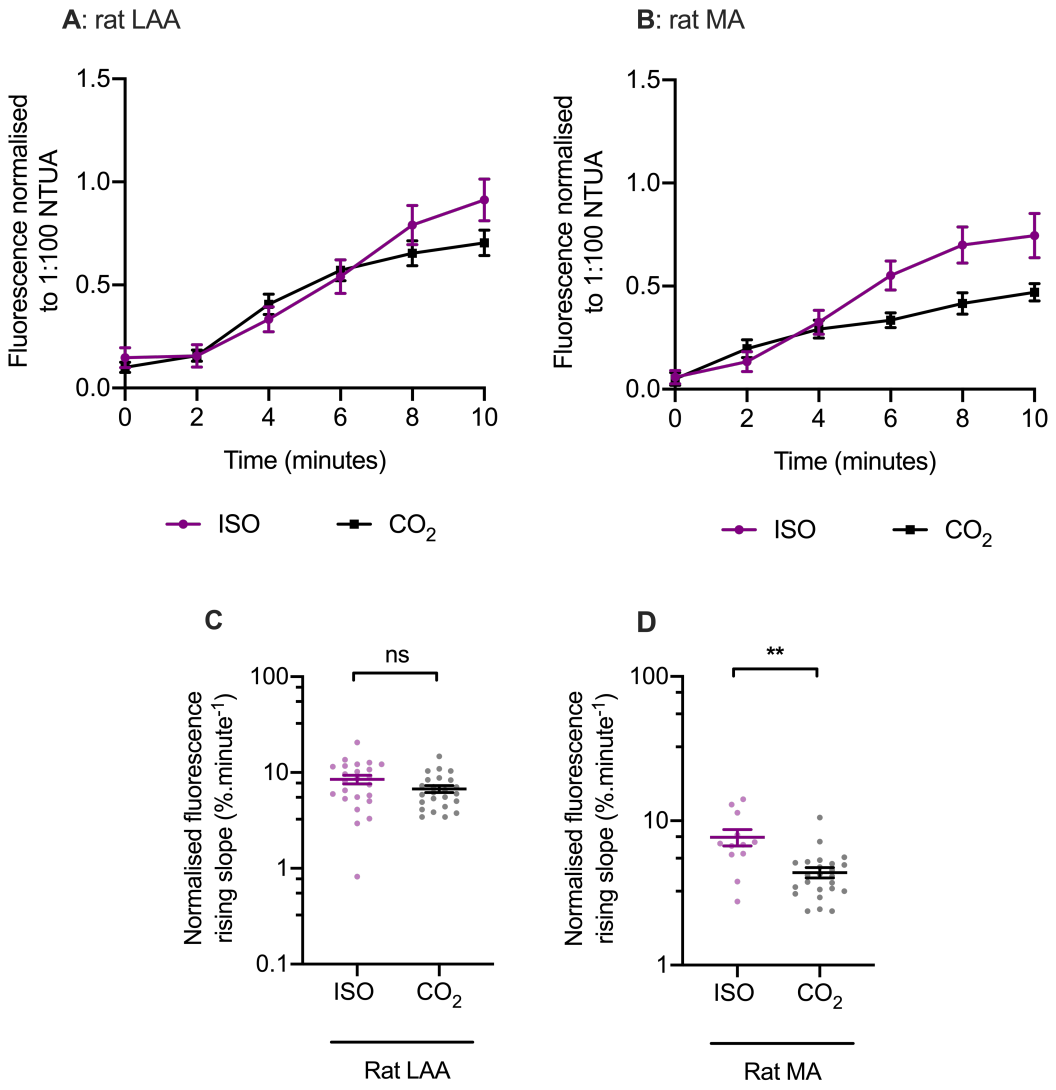


Figure 3.23: Rodent sacrifice method affects periarterial neuronal NTUA uptake rate
The ability of mesenteric periarterial sympathetic nerve terminals to accumulate substrates is perturbed by the animal sacrifice method. Rats were culled either under terminal anaesthesia with isoflurane (ISO) or with an overdose inhalation of CO_2. Data presented as mean±SEM. **(A, C)** Cardiac (LA) NTUA uptake was unaffected by either method. **(B, D)** However, NTUA uptake rate into mesenteric periarterial sympathetic nerve terminals were attenuated in CO_2 overdosed rats compared to ISO-sacrificed animals.

Statistical analyses
(C, D) Welch's *t*-test
** denotes $p<0.01$, ns denotes $p>0.05$.

3.2.2. Neuronal NTUA labelling in other rodent tissues

3.2.2.1. Vascular tissue

NTUA was also applied onto other tissues: the rat mesenteric vein (MV), femoral artery (FA), internal carotid artery (ICA) and carotid body (CB). NTUA labelling of the MV revealed a sparse neuronal supply (Figure 3.24A) compared to that seen with the counterpart MAs (Figure 3.4). Additionally, perivascular neurones of the MV were orientated circumferentially around the vessel. There was also dense innervation labelling in the FA amongst thick organisation of connective tissue (Figure 3.24B), though labelling was devoid in the ICA (Figure 3.24C).

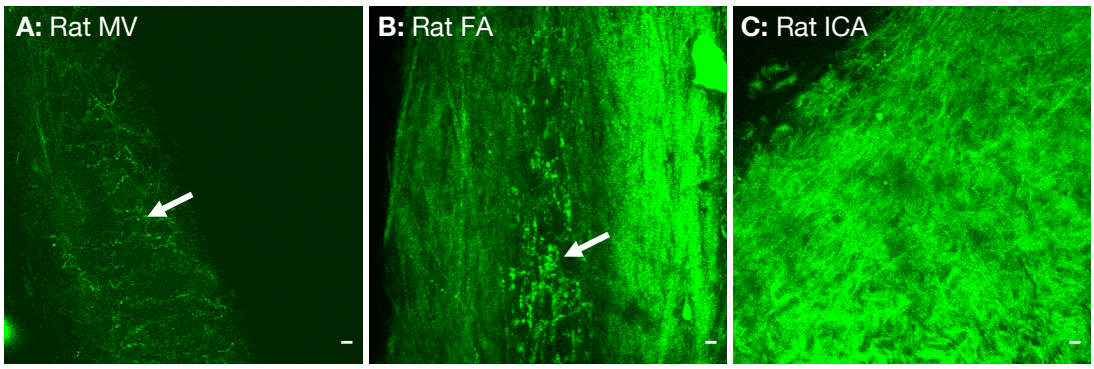


Figure 3.24: Neuronal NTUA labelling of the rat mesenteric vein, femoral artery, and internal carotid artery
The rat mesenteric vein (**A**; MV), femoral artery (**B**; FA) and inner carotid artery (**C**; ICA) were isolated and exposed to NTUA. Perivascular neuronal structures were readily seen on the MV and FA (white arrows) but not in the ICA.

For all micrographs, bars = 10 µm

3.2.2.2. Carotid body

NTUA is also a substrate for the dopamine transporter (DAT). As dopamine is a key neurotransmitter released from the carotid body (CB) type I glomus cells (Gonzalez *et al.*, 1994), it was hypothesised that these cell types may express DAT for signal

termination and thus accumulate NTUA. The rat CB was isolated (by Dr Andrew Holmes, University of Birmingham) and exposed to increasing concentrations of NTUA. Exposure of the rat CB to NTUA did not reveal glomus-like cell types, though a dense network of neuronal terminals was revealed in a time-dependent manner (Figure 3.25). However, it is unknown whether these neuronal structures were noradrenergic as NAT specificity experiments with NAT inhibitor were not conducted.

3.2.3. Negative NTUA labelling in human vessels

The ability of NTUA to label rodent periarterial noradrenergic neurones prompted its application to the human MAs. Human mesenteric artery/vein bundles were acquired during bowel surgery in patients (n=2) through The Human Biomaterials Resource Centre at the University of Birmingham. Once isolated free and cut longitudinally, the artery preparations were stretched and pinned out in the imaging chamber with the adventitial surface facing up. The MA was then superfused with a highly concentrated NTUA solution. Prominent autofluorescence of woven meshwork-like structures of fibres were seen. However, no varicose neuronal endings were detectable in either sample (Figure 3.26).

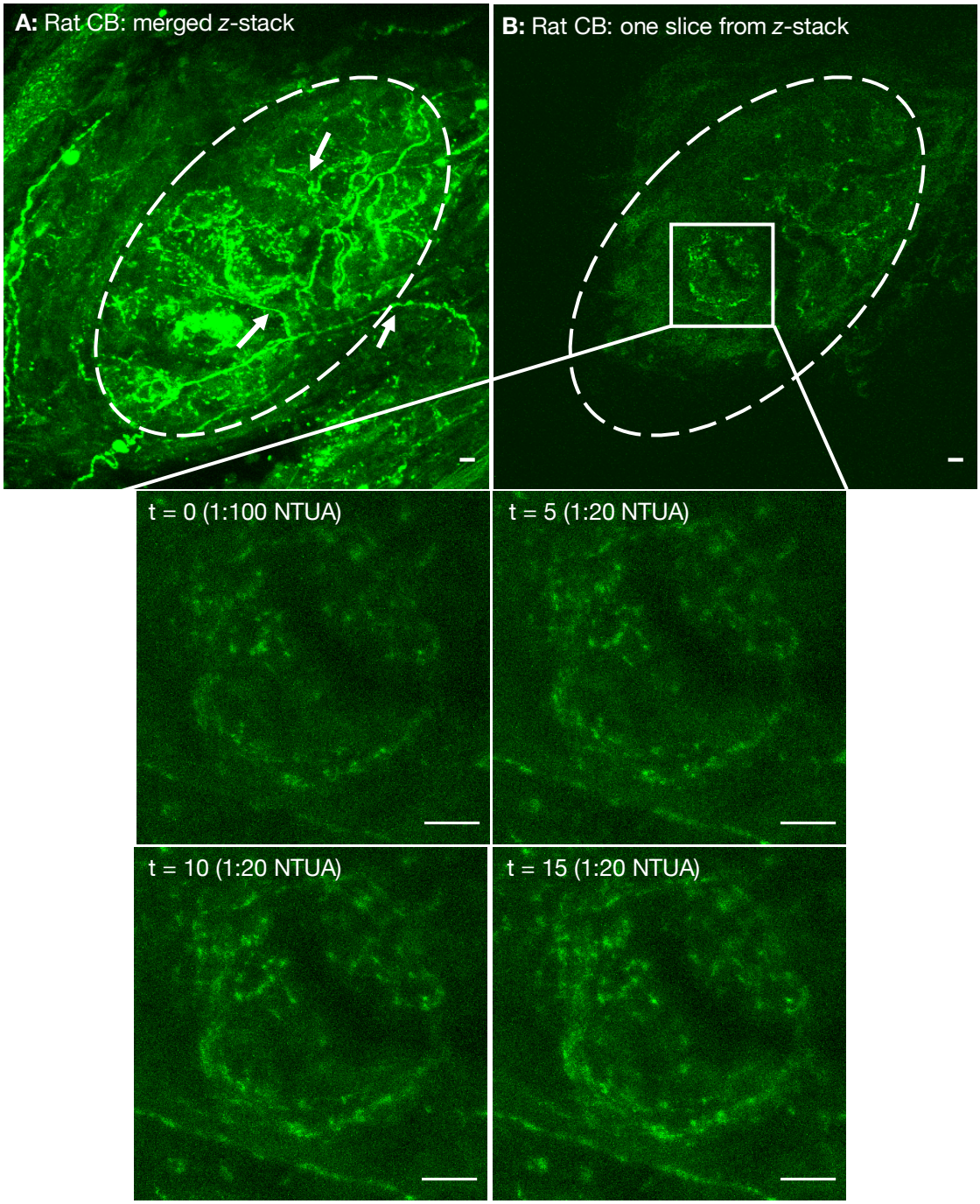


Figure 3.25: Neuronal NTUA labelling in the rat carotid body
NTUA accumulated in nerve terminals in close proximity to the rat carotid body (CB) in a time-dependent manner (1:100 NTUA in t=0 and 1:20 NTUA thereafter) (n=1). **(A, B)** At low magnifications (CB identified in dashed oval square), neuronal terminals joined by intervaricose segments can be seen distributed throughout the tissue, though it is unknown whether they were noradrenergic nerve fibres. **(Bottom panels)** The neuronal accumulation of NTUA occurred in a time-dependent manner.

All micrographs, bars = 10 μm

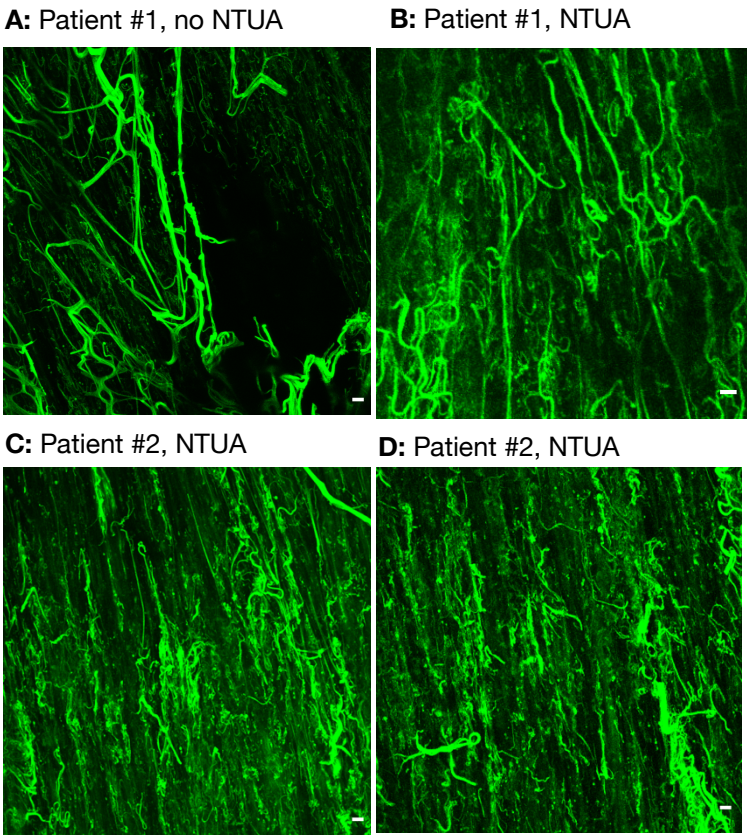


Figure 3.26: Lack of neuronal NTUA labelling in the human mesenteric artery
NTUA exposure to the human mesenteric arteries (MAs) did not reveal neuronal-like structures. Human MAs were isolated from artery/vein bundles from patients underwent bowel surgery. Autofluorescence of a mesh-like network of fibres were prominent in the absence of NTUA. However, no varicose structures were observed with NTUA superfusion. The longitudinal axis of the vessel is from top to bottom of the image.

All micrographs, bars = 10 µm

3.3. Discussion

3.3.1. Main findings

In this Chapter, the commercially available fluorescence-based assay, NTUA, was adapted to dynamically monitor NAT reuptake rate in the rodent cardiovascular tissues at the spatiotemporal resolution of single sympathetic nerve terminals. Thus far, this technique has been validated in NAT-expressing cell culture systems (Jørgensen *et al.*, 2008) and adapted for cultured rat sympathetic postganglionic somata *in vitro* (Shanks *et al.*, 2013a) and the isolated mouse vas deferens *ex vivo* (Parker *et al.*, 2010). Here, the NTUA assay was further adapted to the rodent cardiovascular tissue (murine and rat) *ex vivo*. Moreover, I investigated non-neuronal labelling by NTUA and how measurements of NAT kinetics could be confounded by experimental and technical protocols, such as phototoxicity during imaging.

3.3.2. Radiotracers and NAT function

The NAT plays a key role to clear NAd from the neuroeffector junction. Classically, NAT function is measured with radiolabelled NAd analogues, notably iodine-123-labelled metaidobenzylguanidine ([^{123}I]-MIBG) (Nakajima *et al.*, 2018) and tritium-labelled NAd ([^{3}H]-NAd) (Mandela and Ordway, 2006b). These agents are invaluable for cardiac clinical imaging studies and high throughput studies for discovering new transporter substrate and inhibitors. However, radiotracer studies are often limited in their spatiotemporal resolution and so are insufficient to detect rapid changes in NAT function at discrete neuroeffector junctions. Therefore, new tools are required provide insight into transporter regulation and help elucidate how physiological, pathological and pharmacological conditions may alter cardiovascular function.

3.3.3. The use of fluorescence to monitor NAT function

Fluorescence-based imaging is a promising avenue to study transporter function at discrete synapses; its use to study biogenic amine release and synaptic plasticity in the central nervous system has been demonstrated in recent years (Dunn *et al.*, 2018, Feng *et al.*, 2019). Those that are applicable for NAT function are the analogues of neurotoxin 1-methyl-4-phenylpyridinium (MPP^+) (Namura *et al.*, 1987): APP^+ [4-[4-(dimethyl amino)phenyl]-1-methylpyridinium] and ASP^+ [4-[4-(dimethyl amino)styryl]-*N*-methylpyridinium iodide], and the false fluorescent neurotransmitters (FFNs).

Within the literature ASP^+ and APP^+ have been useful to measure NAT activity *in vitro* (Schwartz *et al.*, 2003, Haunsø and Buchanan, 2007) and to label the noradrenergic neurones in acute brain slices (Karpowicz *et al.*, 2013). However, the several attempts to label sympathetic nerve terminals with ASP^+ in the murine urogenital system (anococcygeus and vas deferens) by former colleagues within the laboratory were unsuccessful (Amos, 2007), thus this avenue of noradrenergic labelling in the rodent cardiovascular system was not pursued in this thesis.

The use of FFNs to study the vesicular storage and release properties of individual noradrenergic nerve terminals have been successful in *in vitro* and *in vivo* settings (Dunn *et al.*, 2018). FFNs are loaded into terminals via the biogenic amine transporters, and so it had been an attractive option for the objectives of this thesis. However, the use of FFNs in many studies were optimised in the central nervous system to assess exocytotic events only (Dunn *et al.*, 2018) thus its adaptation for monitoring NAT function in the peripheral nervous system may be challenging.

The current laboratory has recently optimised the use of a commercially available fluorescence-based kit, NTUA, to monitor NAT function the murine urogenital system (Parker *et al.*, 2010). The vas deferens is a highly sympathetically innervated organ and it is often used to model sympathetic co-transmission (Burnstock and Verkhratsky, 2010). Therefore, the promising adaptation of NTUA to other sympathetically innervated peripheral organs, such as cardiovascular system, *ex vivo* led to the current body of work. Here, the focus was to optimise NTUA for the rodent heart and mesenteric arteries.

3.3.4. NTUA: a fluorescence-based method to label sympathetic nerve terminals in rodent cardiovascular tissue

3.3.4.1. Morphology of sympathetic nerve terminals

The morphology of cardiac- and periarterial neurones labelled by NTUA are analogous to sympathetic nerve terminals described elsewhere (Freeman *et al.*, 2014, Yokomizo *et al.*, 2015). The periodic varicose structures, indicative of sites of junctional release (Bennett, 1993, Brain *et al.*, 1997), are joined by very thin intervaricose segments at varying lengths. The main benefits of the NTUA protocol are that the tissues remain viable, and the collection of physiological data is rapid. NTUA labelling can be seen within 10 min after tissue dissection, compared to the hours to days duration of traditional techniques. Such advantage is further shown in section 4.2.6.3., where NTUA was utilised to rapidly measure mesenteric periarterial sympathetic density immediately after NAT function studies.

However, establishing the cardiac sympathetic nerve distribution with NTUA was challenging due to difficulties of securing the tissue flat; simply merging the *z*-stacks (as with the MAs) would combine different focal planes within each individual slice and the

end image would not truly represent nerve distribution within the tissue. To overcome this, future studies could utilise realignment tools/protocols. For example, the 'tile scan' feature in the image requisition software could help to reset the z-stack positions for each area within a superimposed grid, or the realignment features in the image analysis software such as Fiji (ImageJ) and XuvTools (Emmenlauer *et al.*, 2009) would be useful post-acquisition.

3.3.4.2. Depth penetration of NTUA fluorescence

In the heart, morphological studies show the extensive branching of large noradrenergic neuronal bundles into smaller neuronal bundles as it penetrates from the epicardium into the myocardium (Kawano *et al.*, 2003). However, the sympathetic nerve distribution through the cardiac wall with NTUA was difficult to determine as neuronal fluorescence could only be seen to a depth of ≤10 μm. One possible reason is the failure of the NTUA dye to penetrate deep into the tissue from the epicardial surface. However, while retrograde perfusion of NTUA also labelled noradrenergic terminals, visualisation was also limited by a maximum of 10 μm from the outer surface.

Thus, the next likely reason is the limited depth penetration of confocal laser microscopy under current recording conditions (Pawley, 2006). In this work, the visualisation of murine cardiac sympathetic nerve terminals with MPE was beyond 10 μm within a flat surface of tissue, though the sample size was limited (n=1). The importance of being able to monitor NAT reuptake rate through the cardiac wall is suggested by studies that show a transmural defect in uptake activity in failing hearts. Beau and Saffitz (1994) show that, while there was a homogenous distribution of [^{3}H]-NAd uptake throughout the subepicardial- and subendocardial wall of the healthy human LV, the latter was 5-fold lower than the former in failing hearts. Similarly, in the Dahl salt-sensitive rat,

[^{123}I]-MIBG uptake progressively declined selectively in the endocardial regions compared to the epicardial regions (Nozawa *et al.*, 1998). As NTUA could potentially become a useful tool to measure noradrenergic neuronal distribution in the three-dimensional space, more experiments are required to confirm the penetrability of NTUA into cardiac tissue in order to elucidate changes in NAT reuptake rate in disease states.

However, the focus of the current work was to optimise an optical technique to monitor single-terminal NAT regulation, rather than assess the nerve innervation or quantify transmural differences in uptake. Thus, new methods to overcome uneven confocal *z*-stacks and increase the depth penetration of NTUA measurements in the heart (such as by MPE) forms the basis for future work. Furthermore, while measurements of global NTUA fluorescence during Langendorff perfusion could provide insight into total NAT function, it would be less suitable to study terminal-specific transporter kinetics due to movement artefacts imposed by perfusion.

3.3.4.3. Advantage of NTUA over other techniques

A significant advantage of the NTUA assay over conventional histochemical techniques to label sympathetic nerve terminals is that it does not require mechanical tissue sectioning protocols. In the present study, NTUA-labelled cardiac noradrenergic neuronal bundles were seen coursing through the tissue before branching off into individual nerve fibres deeper in the tissue. However, only the latter was observed in the glyoxylic acid-induced chemofluorescence protocols. If neuronal bundles are indeed primarily located in the epicardial surface that decreases in an epicardial-to-endocardial transmural gradient (Kimura *et al.*, 2012), then accidentally cryosectioning past the nerve bundles during the tissue preparation stage would explain why they were lost in

the chemofluorescence protocol in the current study. An interesting question is whether NTUA fluorescence could be sustained in fixed tissue to allow for a three-dimensional reconstruction of cardiac sympathetic nerve innervation; however, existing techniques are already present to allow for sensitive quantification, in cleared tissues for example (Yokoyama *et al.*, 2017).

Another advantage of NTUA labelling is that tissues do not suffer from shrinkage artefacts associated with the dehydration steps of traditional fixation methods. Tissue shrinkage is likely to explain for the appearance of compressed and 'scrunched' mesenteric perivascular noradrenergic bundles observed with the glyoxylic acid protocol (Figure 3.9). Thus, careful tissue stretching is required for accurate perivascular nerve density measurements (Omar and Marshall, 2010). This disadvantage is significantly overcome by NTUA as the tissue is bathed in isotonic conditions during noradrenergic nerve labelling, and so the architecture of observed neurones is preserved during image acquisition. The usefulness of this NTUA technique to quantify periarterial nerve density is demonstrated in section 4.2.6.3.

3.3.4.4. Summary

In summary, the significant advantages of the NTUA technique over conventional histological protocols are the preservations of tissue viability as well as the continuity of neuronal structures and architecture in whole mount tissues. Thus, NTUA would serve well as a candidate intravital stain during *in vivo* imaging. Future experiments with NTUA could optimise MPE parameters for *ex vivo* and *in vivo* studies as this would help with the three-dimensional reconstruction of the topological morphology of sympathetic neurones, particularly in the heart.

3.3.5. Mechanisms of neuronal NTUA uptake (uptake$_1$)

3.3.5.1. Carrier-mediated transport

The NAT-mediated reuptake of NAd is driven by a Na^+/Cl^--dependent secondary active process, termed 'uptake$_1$' (Iversen, 1965). Several studies have demonstrated for the active mechanism of NAT with NAT substrates. For example, cooling transfected HEK293 cells with hNAT by 17ºC significantly reduced the uptake of fluorescent NAT substrate ASP^+ (Schwartz *et al.*, 2003), and that 96% of [^{3}H]-NAd uptake by NAT-expressing rat astrocytes were accounted by an active mechanism (Inazu *et al.*, 2003). However, while the energy-dependent uptake$_1$ mechanism dominates NAd clearance at lower concentrations, Lashford *et al.* (1991) observed passive diffusion of [^{123}I]-MIBG into a neuroblastoma cell line in the presence of NAT inhibitor desipramine at higher concentrations. Thus, the effect of temperature on NTUA accumulation into neuronal structures was investigated in the current study.

The current study reports an over 2-fold reduction in cardiac NAT reuptake rate in conditions that are 10ºC cooler than physiological temperatures. This is similar to Q_{10} values (ratio of transporter activity at temperatures differing by 10ºC) previously reported for NAT *in vitro* with ASP^+ (2.1) (Mason *et al.*, 2005, Schwartz *et al.*, 2005) and *ex vivo* in the cat spleen with NAd (2.5) (Kirpekar and Wakade, 1968a). The most compelling evidence for NAT (active)-mediated uptake is abolition of neuronal NTUA accumulation in the presence of desipramine (see below). Together, these results confirm a carrier-mediated, rather than passive, pathway of NTUA entry into neuronal structures.

3.3.5.2. NTUA specificity for NAT

Other than the NAT, two other energy-dependent mechanisms that can accumulate NTUA are the dopamine- and serotonin transporters [DAT and SERT (Molecular Devices)], respectively. However, while DAT expression has been detected in the guinea pig heart (Palomar *et al.*, 2011) and in the rabbit celiac artery (Amenta and Ferrante, 1983), there is currently no evidence for its presence in mice and rat cardiovascular tissues (Mitsuma *et al.*, 1998). Furthermore, desipramine is a more potent inhibitor of NAT (K_i=7.36 nM) than DAT (K_i>10,000 nM) (Zhou, 2004), thus the complete abolition of neuronal NTUA accumulation with desipramine in this study suggests against the role of the DAT.

Although the SERT has been observed in the rodent cardiovascular system, they are commonly present on the cardiac valves (Pavone *et al.*, 2008), endocardium (Mekontso-Dessap *et al.*, 2006), and on arterial smooth muscle cells (Ni *et al.*, 2004), with no evidence for its presence on cardiac nerve terminals. Thus, the role of SERT to uptake NTUA into neuronal structures in the current study is likewise unlikely.

Parasympathetic and sensory nerve terminals also exhibit 'beads on a string' morphology (Rysevaite *et al.*, 2011). However, these structures are unlikely candidates of NTUA uptake as 1) previous work by the laboratory demonstrated cholinergic terminals in the mouse vas deferens do not accumulate NTUA (Parker *et al.*, 2010) and 2) the profound sensitivity of desipramine to prevent NTUA accumulation in all present experiments suggests against uptake mechanisms other than NAT, including sensory neuronal uptake. From these results, it can be established that NAT was the most likely neuronal uptake mechanism of NTUA into the rodent cardiovascular system in the current study.

3.3.5.3. Nerve terminal localisation of NTUA

NTUA labelling and glyoxylic acid-induced chemofluorescence revealed highly fluorescent noradrenergic terminals. Following NAd reuptake, the majority of NAd is sequestered into secretory vesicles by the action of vesicular monoamine transporter 2 (VMAT2) (Goldstein, 2010). Secretory vesicles are primarily located in the nerve terminal, as detected by the co-localisation of synaptotagmin (Brain *et al.*, 1997) and VMAT2 (Savchenko *et al.*, 2003) exclusively within varicose structures. Thus, given that NTUA is also a substrate for VMAT2 (Bernstein *et al.*, 2012), NTUA is likely to have entered into vesicles following reuptake in the current study. The fluorescence of NTUA and catecholamines (by glyoxylic acid) were also detected in intervaricose segments, but only very faintly. In the murine urogenital system, it was only in the presence of reserpine (VMAT2 inhibitor), where a more 'diffuse' and uniform appearance of neuronal NTUA fluorescence was seen (Parker *et al.*, 2010). Thus, it could be hypothesised that the NTUA fluorophore is primarily confined within the vesicular pool in mature sympathetic nerve terminals that innervate cardiovascular tissues.

In the current study, there was an accelerated loss of fluorescence during washout with the sympathomimetic amine, tyramine. Tyramine enters noradrenergic nerve terminals via NAT and rapidly displaces endogenous NAd by reverse transport of VMAT2 and NAT (Trendelenburg *et al.*, 1987, Pei *et al.*, 2016). Thus, it appears that the rapid loss of NTUA fluorescence in this study was mediated by a concerted release of NTUA from storage vesicles into the cytoplasm followed by its extrusion into the extracellular space by NAT reverse transport. These results are analogous to those observed with amphetamine, another NAT reverse transport agent (Parker *et al.*, 2010). To conclude, NTUA acts similarly to NAd, where it enters the sympathetic nerve via NAT and most likely becomes sequestered into the nerve terminal vesicular pool by VMAT2.

3.3.5.4. The use of NTUA to monitor NAT rate

As the accumulation of NTUA into the sympathetic nerve terminal depends on both the NAT and VMAT2, could the initial rise of NTUA fluorescence solely reflect NAT reuptake rate alone? Previous studies in the laboratory demonstrated no differences in NTUA reuptake rate in the reserpinised mouse vas deferens compared to its untreated control (Parker *et al.*, 2010), which is analogous to the finding that NAd uptake is initially determined by NAT and unaffected by VMAT2 (Lindmar and Muscholl, 1964, Iversen *et al.*, 1965). This suggests the dynamic observations made in this study of NTUA uptake rate is most likely to represent the initial phase of NAT-mediated uptake across the neuronal membrane.

Although images were acquired at the spatial resolution of one single sympathetic nerve terminal, does the measurement of NTUA fluorescence truly reflect sequestration through that one neuronal membrane? Parker *et al.* (2010) photobleached sympathetic nerve terminals containing NTUA *ex vivo* and saw a very slow recovery of fluorescence 1 hr later. This suggests that once NTUA is sequestered into neurotransmitter vesicles there is limited lateral movement between neighbouring nerve terminals, and therefore implies that NTUA accumulation rate of single nerve terminal can be taken as a single entity of measurement.

3.3.5.5. NAT rate and anaesthetics

Some anaesthetics have the potential to perturb NAT function. Exposing PC12 cells to volatile anaesthetics halothane, isoflurane, enflurane, and methoxyflurane in clinically relevant concentrations inhibited the NAT-mediated uptake of [^{3}H]-NAd (Tas *et al.*, 1987, Shahani *et al.*, 2002). Alphaxalone, a neurosteroid anaesthetic, and propofol have also

been reported to reduce NAT-mediated uptake of [^{3}H]-NAd in bovine adrenal medullary cells (Hara *et al.*, 2000, Horishita *et al.*, 2002). On the other hand, volatile anaesthetic seroflurane was reported to have no effect upon [^{3}H]-NAd uptake in human omental arteries and veins (Thorlacius *et al.*, 2003). The effect of anaesthetics on NAT are considered to be rapidly reversed upon its removal (Ko *et al.*, 2008). Therefore, in the current study, it was unlikely for isoflurane to have a profound effect upon NAT as there was at least a 20 min equilibration period with KHB prior to *ex vivo* studies, which could have been adequate to reverse any inhibitions of NAT. However, to omit the potential adverse effect of anaesthetics upon NAT function, future studies could adopt alternative methods of rodent sacrifice, such as cervical dislocation of the mouse, though these alternative methods are not in place for the rat.

Mesenteric periarterial NAT rate was reduced after chronic exposure to CO_2 compared to isoflurane sacrifice methods. However, it is not possible to draw a definitive conclusion as the MA group was underpowered (isoflurane: n=2, CO_2: n=4) due to low availabilities of tissue at the time of study. Nevertheless, the CO_2 sacrifice method consisted of near 10 min of chronic CO_2 exposure to the animal, and it is quite possible this procedure caused irreversible changes in NAT function due to severe perturbations in physiological pH. Thus, future studies should be mindful of the effect of rodent sacrifice methods on NAT transporter kinetics.

3.3.5.6. Summary

In summary, the neuronal structures labelled by NTUA in the rodent cardiovascular system are noradrenergic and the mechanism of entry is by the energy-dependent NAT. Demonstrated by previous colleagues from the laboratory, the tight sequestration of NTUA within vesicles with limited exchange between varicosities suggests that its

accumulation can be utilised as a single unit of measurement that represents an individual nerve terminal. Finally, researchers are to be mindful of the effects of anaesthesia agents upon NAT function, and that appropriate washout protocols may be required prior to functional studies.

3.3.6. Mechanisms of non-neuronal NTUA uptake (uptake$_2$)

3.3.6.1. Heart

In the current study, NTUA was consistently observed to accumulate into non-neuronal structures in the rodent heart. The extraneuronal mechanism of NAd uptake, termed 'uptake$_2$', is well established in the rat heart (Iversen, 1965), though it is yet to be characterised in the murine heart. As NTUA mimics NAd, uptake$_2$ is a likely route for non-neuronal cellular entry. Uptake$_2$ is distinguishable from uptake$_1$ by its differing transport mechanisms, substrate affinity (Iversen, 1965), and substrate selectivity (Grohmann and Trendelenburg, 1984).

The presence of uptake$_2$ in the murine heart is demonstrated by the persistent cardiac NAd uptake despite chemical sympathetic denervation with neurotoxin 6-hydroxydopamine (Wehrwein *et al.*, 2008) and in mice with NAT polymorphism knock in that reduces function (Shirey-Rice *et al.*, 2013). While it was not possible to characterise the murine cardiac non-neuronal NTUA kinetic profile in the current study, NTUA uptake by uptake$_2$ was implied by the maintained non-neuronal NTUA labelling in the presence of desipramine (Figure 3.11). Importantly, non-neuronal labelling was prevented by corticosterone, a known uptake$_2$ inhibitor (Iversen and Salt, 1970). It was concluded in this study that, at least in mice, the cardiac non-neuronal uptake of NTUA was mediated by uptake$_2$, with further confirmation required for the rat heart.

The rodent cardiac non-neuronal structures that accumulate NTUA are reminiscent of cardiomyocytes, identified by their size, cylindrical brick-like shape, and elongated nuclei (Bensley *et al.*, 2016). Confirmation of these structures can be achieved by co-labelling cardiomyocytes with styryl dyes (for example, di-4-ANEPPS, di-8-ANEPPS and RH-237) (Aguirre *et al.*, 2014).

Luckily, in the interest of measuring NAT reuptake rate, the presence of non-neuronal fluorescence did not profoundly affect quantification in single nerve terminals as 1) nerves were easily identifiable in areas of minimal overlap and 2) if the two structures happened to overlap slightly, the process of background subtraction would ensure minimal interference.

3.3.6.2. Physiological relevance of cardiac uptake$_2$

In studies where cardiac NAT-mediated uptake was ameliorated (e.g. by genetic NAT knockout, sympathetic denervation, or uptake$_1$ inhibition), the retention of NAd and NAd analogues were not significantly altered in the rat (Farnebo and Malmfors, 1969, Yu *et al.*, 2013, Higuchi *et al.*, 2013), dog (Chilian *et al.*, 1982, Dae *et al.*, 1992), and pig (Glowniak *et al.*, 1992), suggesting for a highly significant role of cardiac uptake$_2$ mechanisms in these three species. However, NAT inhibition significantly prevents total NAd uptake in rabbits, non-primate humans (Yu *et al.*, 2013), and humans (Dae *et al.*, 1992), thus demonstrating that, at least in these species, uptake$_1$ is the primary mechanism of NAd clearance. This is particularly in highlighted by the fact that, human patients with uptake$_2$ polymorphisms have no cardiovascular phenotype/malfunction (Roth *et al.*, 2012). While uptake$_2$ is indeed frequently discussed in the context of inactivating circulating catecholamines (Gasser and Lowry, 2018), the low reliance on

uptake$_2$ for NAd clearance in the healthy human heart questions the translational relevance in human cardiovascular physiology. However, in instances of chronic heart failure where NAT is defunct, there is a doubling of uptake$_2$-mediated transport of NAd into cardiomyocytes (Eisenhofer *et al.*, 1996) which some hypothesise as a mediator of disease progression via monoamine oxidase-dependent oxidative stress pathways in these cell types (Kaludercic *et al.*, 2014).

Interestingly, the highest expression of uptake$_2$ in murine tissues is located in the heart (Zwart *et al.*, 2001) where it could be functional even at low concentrations of NAd exposure, as demonstrated in the rat (Lightman and Iversen, 1969). Recently, a subpopulation of cardiomyocytes on the left side of the murine heart was reported to bear the NAd-to-adrenaline converting enzyme, phenylethanolamine-N-methyl transferase (PNMT), which was suggested to exert control of heart rhythm through localised adrenergic signalling (Wang *et al.*, 2017b). This prompted speculations of the source of NAd as these cardiomyocytes do not possess the machinery to synthesise catecholamines beyond embryonic development (Ignarro and Shideman, 1968).

Based on the current study, one is tempted to suggest that NAd released from sympathetic neuronal terminals enters murine cardiomyocytes through uptake$_2$ and is metabolised to adrenaline by PNMT. This is likely as the authors found that areas of PNMT$^+$ cardiomyocytes tended to overlap with dense innervations of sympathetic fibres (Wang *et al.*, 2017b, Fan *et al.*, 2019). Interestingly, rodent cardiac uptake$_2$ function is driven by the membrane potential (Bönisch *et al.*, 1985), where uptake$_2$ function is reduced (Ludwig *et al.*, 1986) or accentuated (Bryan-Lluka and Vuocolo, 1992) in depolarised or hyperpolarised states, respectively. This would suggest a multi-layered interplay system of neurotransmission between noradrenergic prejunctional signalling

and localised postjunctional adrenergic signalling dependent on their electrophysiological states. The current finding suggests NTUA could be used as a dual stain to measure for neuronal NAT reuptake rate as well as the uptake$_2$ mechanisms to elucidate the source of NAd for adrenaline synthesis.

3.3.6.3. Mesenteric artery

Here, non-neuronal uptake of NTUA into periarterial structures were not observed. This was unforeseen as ultrasensitive detection methods have demonstrated for uptake$_2$-mediated uptake into sympathetically-innervated vascular smooth muscle cells in various species, including rabbits (Nicol and Rae, 1972, Trendelenburg, 1987, Horvath *et al.*, 2001), rats, and mice (Doležel, 1966, Gillespie and Muir, 1970). Thus, a likely explanation for the current study is that the NTUA accumulation into smooth muscle cells was so low that fluorescence was undetectable in our recording conditions. The basis of this speculation is that one study had only demonstrated uptake$_2$-mediated NAd uptake into the rat femoral arterial wall after pharmacological inhibition of intracellular NAd inactivating enzymes [catechol-*O*-methyltransferase (COMT) and monoamine oxidase (MAO)] (Doležel, 1966). Moreover, the lack of vascular smooth muscle NAd uptake has been reported elsewhere in the rat tail artery (Stjärne *et al.*, 1994). Therefore, more experiments are warranted to elucidate the role of uptake$_2$ in the vasculature (if any); future experiments could also adopt COMT and MAO inhibitors, or utilise radiolabelled MPP^+ as an uptake$_2$ substrate as it is not affected by NAd metabolising enzymes (Russ *et al.*, 1992).

3.3.6.4. Summary

In summary, NTUA revealed cardiac $uptake_2$ in mice but not in the rodent MAs. The functional importance of cardiac $uptake_2$ is debatable and varies amongst species, including humans, though in mice it may be a source of NAd for adrenergic signalling in $PNMT^+$ cardiomyocytes. Further studies could utilise NTUA to further investigate the distribution of sympathetic nerve terminals and $PNMT^+$ cardiomyocytes. This would help to elucidate the interactions between $uptake_1$ and $uptake_2$ for adrenaline bioavailability in physiological conditions.

3.3.7. Neuronal NTUA labelling in other tissues

3.3.7.1. Other rat arterial vessels

Consistent with other immunohistochemistry studies, NTUA revealed the noradrenergic supply of the mesenteric vein is significantly sparser compared to their periarterial counterparts (Figure 3.4, 3.24). This pattern has been previously observed in the rat (Furness and Marshall, 1974, Park *et al.*, 2007) and guinea pig (Klemm *et al.*, 1993). Interestingly, the disparity of innervation density is reversed in humans mesenteric vessels (Birch *et al.*, 2008).

The splanchnic vascular bed itself receives about 20-25% of total CO in the unfed state (Matheson *et al.*, 2000), which is predominately located in the veins (Greenway, 1987) and readily mobilised by sympathetic activity in times of physical stress (Rowell, 1990). The significance of the splanchnic vascular bed in pathophysiology has been suggested in salt-sensitive hypertensive rat models (Kandlikar and Fink, 2011, Osborn *et al.*, 2011). Moreover, targeting the celiac ganglion has therapeutic potential for blood pressure control, either by ganglionectomy or plexus blockade (Lee *et al.*, 2016). Interestingly,

mesenteric veins are more sensitive to the constrictor effects of NAd compared to the arteries (Racchi *et al.*, 1997, Luo *et al.*, 2003, Park *et al.*, 2007), thus one may postulate a vessel-specific alteration in noradrenergic neurotransmission in disease states, too. Indeed, perivascular NAT function is reported to be exclusively higher in the MVs of DOCA-salt models of hypertension, but not in the MAs despite upregulation of NAT expression in both vessel types (Luo *et al.*, 2003). As the two vessel types are differently innervated by noradrenergic neuronal processes (Furness and Marshall, 1974) and vary in their neuroeffector- and prejunctional properties of transmission (Park *et al.*, 2007), further examinations are required to refine their contributions to disease states. Perhaps in the future, NTUA could be used to study the heterogeneity of NAT regulation and/or dysregulation between the MA and MV.

Rat femoral periarterial sympathetic nerve terminals were also labelled with NTUA amongst thick connective tissue, with morphologies consistent with previous studies (Long and Segal, 2009, Omar and Marshall, 2010). Interestingly, most studies of vascular sympathetic nerve function are centred upon medium-size or small resistance arteries, with limited information on the larger distributing arteries. With the use of sympathectomised rats, Mangoni *et al.* (1997) demonstrated sympathetic stimulation exerts a tonic, rather than exclusively phasic, restraint on the distensibility of large muscular arteries, which implies strong implications of noradrenergic-induced arterial impedance in large arteries in (patho)physiological states, such as ageing. As arterial stiffness is an indicator for vascular disease (Orr *et al.*, 2009), one could utilise NTUA in the future to not only study the noradrenergic effects on arteriolar tone, but on larger arteries that can affect cardiac load.

The sympathetic innervation of the inner carotid artery (ICA) has been previously described elsewhere in the rodent (Hill *et al.*, 1986, Maklad *et al.*, 2001). However, in the current study, there were no nerve-like structures labelled by NTUA. The lack of noradrenergic innervation could be explained by the tissue preparation method in the current study. The intact rat carotid bifurcation was collectively isolated by Dr Andrew Holmes (at the University of Birmingham), exposed to partial enzymatic digestions, and dissected to expose the carotid sinus nerve. It is quite possible that during this process the sparse neuronal fibres were damaged and subsequently appear as absent. However, the current study only investigated NTUA labelling in 1 ICA preparation, thus more samples are required in the future.

3.3.7.2. Rat carotid body

The oxygen-sensing carotid body (CB) type I glomus cells can release biogenic amines (dopamine, NAd, serotonin) to modulate chemoreception in response to hypoxia (Aldossary *et al.*, 2020). In the same context as neurotransmission termination by reuptake transporters, it was hypothesised that type I glomus cells might express biogenic amine transporters DAT, NAT, and SERT for signal termination.

In the current study, NTUA superfusion did not reveal any cell groups that are similar to the clustered morphology of type I glomus cells. This could be due to the intrinsic lack of biogenic amine transporters on the glomus cell plasma membrane. The observation of DAT in the CB is already conflicting; Jackson and Nurse (1998) demonstrated that inhibition of DAT in dissociated rat CB cultures with nomifensine increased extracellular dopamine concentration by 3-fold. However, Gonzalez *et al.* (1987) showed that [^{3}H]-DA uptake into the rabbit CB was of low-affinity and Na^{+}-independent, which contrasts

with the characteristics of Na^+/Cl^--dependent transporters. Moreover, *in situ* hybridisation and RT-PCR of murine CB slices did not detect for DAT mRNA (Toledo-Aral *et al.*, 2003). Finally, exposure of rat CB glomus cells to neurotoxin 6-hydroxydopamine (NAT and DAT substrate) at levels sufficient to denervate perivascular sympathetic nerve terminals resulted to no morphological effect on storage vesicles, thus suggesting the dual absence of DAT and NAT (Hansen and Ord, 1978), thus it could be that neurotransmitter diffusion and washout are the predominant dopaminergic transmission termination processes in this organ. Yet, glomus cells are immunoreactive for SERT (Yokoyama *et al.*, 2013) and may be a possible entry target for NTUA. However, I did not observe any uptake of NTUA into cell clusters reminiscent of CB type I cells. The study was underpowered (n=1), thus more experiments are required to investigate this further.

Interestingly, NTUA did reveal a dense supply of neuronal processes intertwined in and around the CB. It could be that these neurones are sympathetic in nature, as immunohistochemical data show innervation of the CB vasculature (Rees, 1967, Knoche and Kienecker, 1977) and directly upon type I/type II cell groups of the rat CB (Verna *et al.*, 1984). Previous retrograde labelling studies show sympathetic nerve processes that innervates the CB originates from the superior cervical ganglion (Claps and Torrealba, 1988). The functional relevance of CB perivascular noradrenergic innervation has been suggested to act as a modulator of chemosensitivity via regulation of blood flow into the CB (Kumar and Prabhakar, 2012).

However, in my hands I did not observe perivascular neuronal-like NTUA labelling in the CB (though this requires dual labelling of vascular smooth muscle cells to confirm), but rather a interwoven organisation of sympathetic nerve terminals in and around the CB

cell clusters as previously reported by Verna and colleagues (1984). There is some evidence to suggest for a direct sympathetic effect upon CB chemosensory activity. For example, the β-adrenoceptors present on rat CB type I cells (Alzahrani *et al.*, 2020) are hypothesised as target mediators for an increase in CO_2 chemosensitivity during exogenous adrenaline application (Thompson *et al.*, 2016). It is thought that the direct sympathetic activation may reset the chemoreflex sensitivity during physiological conditions that require enhanced sympathetic output, such as physical exercise, emotional stress, or during high altitude adaptation (Verna *et al.*, 1984).

3.3.7.3. Human mesenteric arteries

With the success of labelling noradrenergic neuronal fibres in rodent tissue, the use of NTUA was extended to the human mesenteric arteries with repeated attempts. However, no neuronal labelling was observed. What was prominent, however, was the abundance connective tissue fibres and fibrins that are reminiscent of elastin and collagen (Bloksgaard *et al.*, 2018), respectively.

One possible reason for the lack of NTUA labelling is very slow NAT kinetics in the human compared to the rodent. However, human tissues were incubated for 30 min with a near 1:1 dilution of NTUA, i.e., 100-fold higher than in the rodent, thus some labelling was expected. Next, confocal imaging was commenced within the first minute of NTUA superfusion, so even rapid NTUA uptake rate would have been captured. The next possibility is the damage of autonomic neurones during the dissection process. The artery/vein pairs were excised as a short preparation and it was not possible to determine which end of tissue was examined by pathologists for prognosis; therefore, it is possible autonomic neurones were damaged during this process. Furthermore, as the excess fat and connective tissue was more adherent onto the human vessels than

rodent vessels, the dissection process in the laboratory could have exacerbated the damage to the adventitial layer. Future experiments could request longer human artery/vein pairs as a complete dissection including the bowel wall (if possible), so that tissue furthest away from the lesion could be experimented on instead.

3.3.7.4. Summary

In summary, NTUA can also be used to label neuronal structures in the rodent MV and FA. NTUA-labelled sympathetic innervation was also observed in the rat CB, which could provide new insights into the autonomic innervation of the oxygen sensing organ (and its surroundings vasculature). However, despite the optimisation of NTUA for the rodent MAs, the fluorophore was not detectable in human mesenteric periarterial nerve terminals.

3.3.8. Limitations of NTUA

3.3.8.1. Photosensitivity

One fundamental caveat of quantitative imaging studies is that the photobleaching phenomenon prevents the direct correlation of the amount of fluorescence emitted with probe concentration. Here, it was demonstrated that illumination omission significantly preserved NTUA fluorescence. This raises questions to whether monitoring NTUA accumulation at each minute, rather than just the start- and endpoint, was necessary. However, the critical time period of the linear NAT-mediated uptake occurred within 10 minutes in the rodent tissues, thus it was not feasible to measure fast biological processes with infrequent protocols. Another approach to minimise exposure is to utilise a less phototoxic excitation laser line, such as 458 nm rather than 405 nm. The 458 nm line has been previously used effectively to excite NTUA in the laboratory

(Parker *et al.*, 2010) and was suggested in the present work to potentially have promising results.

3.3.8.2. Fate of NTUA

The intensity of the NTUA fluorescence is not only affected by the stability of the fluorophore, but also its retention within individual terminals. In pre-loaded varicosities with 1:100 NTUA, the fluorescence after the 6-min cooling period was significantly higher than their control counterparts (Figure 3.10). One is tempted to speculate that cooling also slowed down the enzymatic rate of temperature-dependent biological processes that would have otherwise inactivated the NTUA fluorophore, such as VMAT2 transport or MAO-mediated inactivation.

One potential biological process to inactivate NTUA fluorescence is the energy-dependent transport of cytoplasmic NTUA into vesicular stores by VMAT2 (Parker *et al.*, 2010, Bernstein *et al.*, 2012). Bernstein and colleagues (2012) postulated that the NTUA fluorophore is a pyridinium derivative, a compound type that has been previously suggested to become quenched in the vesicular polar environment (Karpowicz *et al.*, 2013). Thus, it is possible the cooling period slowed down the transport of NTUA into the vesicular pool and thus the quench of NTUA fluorescence.

Another biological process is the metabolism of NTUA by MAO. Based on other pyridinium dyes transported intracellularly by NAT (Schwartz *et al.*, 2005) and DAT (Karpowicz *et al.*, 2013), NTUA may become localised in the mitochondria and metabolised by MAO. However, this may be unlikely as tyramine, a sympathomimetic amine, depleted 100% of NTUA from vesicular stores within the terminals; if NTUA were

bound within mitochondria, some residual fluorescence might have been detected. Other sites of NTUA association may be the cisterns of smooth endoplasmic reticulum (Descarries *et al.*, 1977), for example.

3.3.8.3. Summary

In summary, I have demonstrated that once the NTUA fluorophore is transported across the prejunctional membrane, subcellular processes may affect the emitted fluorescence signal and interpretation of 'NTUA accumulation/concentration' and thus 'NAT reuptake rate'. As the investigation of this goes beyond the scope of my work, future work could take into account these mechanisms, through computational modelling, for example, and derive an accurate representation of the kinetic profile of the NAT transporter alone.

3.4. Overall conclusion

In this Chapter, the commercially available fluorescent NAT substrate, NTUA, was optimised to label noradrenergic terminals in the rodent heart and MAs and dynamically measure for NAT reuptake rate. While the retention of fluorescence may be confounded by phototoxicity and intracellular mechanisms governing the cellular fate of NTUA, the initial fast rise of NTUA uptake can adopted as an indicator of NAT reuptake rate. Varicose labelling was also confirmed in the MV, FA, and CB, though further works are required to elucidate the importance of NAT-mediated regulation in these tissues. Together, NTUA poses as an attractive optical tool to monitor single-terminal sympathetic neuronal function in rodent cardiovascular tissue, with further optimisation required for human tissues. Furthermore, NTUA accumulates in myocyte-like structures via $uptake_2$ in the murine heart and this could form the basis of exciting future work into

the mechanisms of localised adrenergic signalling in $PMNT^{+}$ cardiomyocytes in close relation to sympathetic neuronal activity.

CHAPTER IV. SINGLE-TERMINAL NORADRENALINE TRANSPORTER FUNCTION IN PHYSIOLOGY AND PATHOPHYSIOLOGY

4.1. Introduction

4.1.1. Overview

Up until now, the ability to measure dynamic changes in noradrenaline transporter (NAT) function had been limited by the low spatiotemporal resolutions of available methodologies. As the lifetime of noradrenaline (NAd) in a released quantum is estimated to be ~1.5-5 s (Gonon *et al.*, 1993, Stjärne, 2000), rapid and subtle changes in transporter kinetics could have been overlooked. In this Chapter, the optimised Neurotransmitter Transporter Uptake Assay (NTUA) is utilised to re-evaluate some pressing questions regarding the regulation of peripheral noradrenergic neurotransmission in the cardiovascular system; a few examples are highlighted below.

The heart is highly dependent on NAT for NAd clearance (Goldstein *et al.*, 1988), which implies heightened vulnerabilities to autonomic failure compared to other tissues. However, whether this is attributable to differences in intrinsic transporter rate *per se* or sympathetic nerve density is unclear. Likewise, while several studies have described chamber-specific alterations in NAT function in some cardiovascular diseases (CVDs) (Liang *et al.*, 1989, Jovanovic *et al.*, 2019), such findings could also be confounded by differences in noradrenergic innervation that are innately present between different

chambers/areas of the heart. Therefore, better understanding of the regional differences in single-terminal NAT regulation may elucidate tissue-specific therapeutic targets for CVDs. During this work, investigations into the inter-tissue differences in NAT function in disease was made possible by kind donations [heart and mesenteric arteries (MAs)] from the Birmingham Hypoxia and Arterial Chemoreceptor group; tissues were from a preclinical model of obstructive sleep apnoea (OSA) with cardiovascular phenotypes.

The prejunctional sympathetic membrane hosts both inhibitory and facilitatory receptors to modulate the net junctional availability of NAd. Previously, the laboratory demonstrated a muscarinic acetylcholine receptor (mAChR)-mediated suppression of NAT in the murine urogenital system. Whether or not the effect occurs in the heart is unknown, though sympathetic and parasympathetic nerve terminals are located closely together (Kawano *et al.*, 2003) and autonomic cross-over does occur (Herring *et al.*, 2012). Understanding these mechanisms would provide insight into the arrhythmogenic 'autonomic conflict' phenomenon, where the sympathetic and parasympathetic arms are concomitantly activated. Moreover, while accentuated sympathetic nerve activity (SNA) is often correlated with an increase in NAd release, its effect on NAT is conflicting in the literature (Gillis, 1963, Blakeley and Brown, 1964, Kirpekar and Wakade, 1968b, Chang and Chiueh, 1969), possibly due to tissue-, species- and methodological differences in these studies; understanding the effects is crucial to understand net noradrenergic transmission.

Finally, the rodent species are commonly used to experimentally assess the neural mechanisms of cardiovascular function and its modulation, for example by the cannabinoid type I receptors (Malinowska *et al.*, 2012) (Chapter V). The advent of genetic manipulations in mice has propelled this species to the forefront of biomedical

research. Rats are also preferred due to many strains that can mimic the complex nature of CVDs, such as spontaneously hypertensive rats (SHRs), as well as their larger size to facilitate surgical procedures (Bryda, 2013). However, to my knowledge, only one study has suggested for interspecies differences in NAT function between the two rodent species (Iversen *et al.*, 1971), though measurements may have been confounded by organ mass, perfusion flow, and density of sympathetic innervation. Further insight into species differences in NAT may provide insight into variations in sympathetic tone in rodent species, and considerations in the interpretation of neuro-cardiovascular regulation.

4.1.2. Objectives and aims

Therefore, I aim to address the following objectives:

1. Investigate inter-chamber differences in NAT function in the heart
2. Investigate tissue differences in cardiac and periarterial NAT function
3. Investigate inter-species differences in cardiac and periarterial NAT function
4. Assess if there is a mAChR-mediated modulation of cardiac NAT function
5. Investigate the effect of sympathetic neuronal activity on cardiac NAT function
6. Investigate changes in cardiac and periarterial NAT function in an experimental animal model of OSA

4.2. Results

4.2.1. Cardiac inter-chamber differences in NTUA uptake rate

To assess inter-cardiac differences in NAT rate, each murine cardiac chamber was dissected free and exposed to NTUA separately. Over the period of 6-min NTUA exposure, the linear NTUA uptake rates across the atria and ventricles on both the left- and right-hand side were not different [LA (left atrium): 12 (11, 13)%.min^{-1} (n=4, n_t=24) vs. RA (right atrium): 13 (10, 16)%.min^{-1} (n=4, n_t=24) vs. LV (left ventricle): 11 (9, 13)%.min^{-1} (n=4, n_t=24) vs. RV (right ventricle): 13 (9, 19)%.min^{-1} (n=4, n_t=24); p>0.05, Figure 4.1A-C].

However, looking closely at the minute-by-minute accumulation of NTUA in Figure 4.1A, NTUA fluorescence was observably greater in the first 3 min in the LA than RA, and jointly greater in the atria than in the ventricles. Thereafter, NTUA fluorescence was greater in the RV than LV (Figure 4.1A). These slight differences suggest for an asymmetrical pattern of uptake in the heart that would otherwise be overlooked by the linear fit model. In an attempt to detect for changes in NTUA accumulation that is not confined to a linear fit, the non-linear exponential one-phase association model was fit onto the data (Figure 4.1D). The model provides data for the maximum accumulation of NTUA fluorescence (Y_{max}) and the rate constant of the reaction (k).

In the unconstrained curve fit model, the Y_{max} was uniform in the heart [LA: 0.9 (0.7, 1.3) (n=3, n_t=13) vs. RAA: 0.8 (0.6, 1.2) (n=4, n_t=15) vs. LV: 1.1 (0.6, 1.4) (n=3, n_t=11) vs. RV: 1.1 (0.6, 1.5) (n=4, n_t=11), p>0.05, Figure 4.1E]. However, it is worth noting that 1) the unconstrained model eliminated many terminals due to limited time points, and 2) NTUA

accumulation had already tended towards a plateau in the atria, while the rise remained linear in the ventricles (Figure 4.1D).

To preserve the utility of all datapoints for *k*, the model for each cardiac chamber was constrained to its respective Y_{max} value. On both sides of the heart, the NTUA uptake rate constant was twice as high in the atrium than in the ventricle [LA: 0.3 (0.2, 0.9) min^{-1} (n=4, n_t=24) vs. LV: 0.1 (0.1, 1.2) min^{-1} (n=4, n_t=24), p<0.001; RA: 0.4 (0.2, 0.5) min^{-1} (n=4, n_t=24) vs. RV: 0.2 (0.1, 0.4) min^{-1} (n=4, n_t=24), p<0.001, Figure 4.1F]. Moreover, within each cardiac group, the NTUA uptake rate constants were similar within the atrial (LA vs. RA; p>0.05, Figure 4.1F) and ventricular groups (LV vs. RV; p>0.05, Figure 4.1F).

In summary, the linear fit method demonstrates for a homogenous NTUA uptake rate pattern in the heart; however, the non-linear curve fit model suggests for a higher uptake rate in the atria compared to the ventricles.

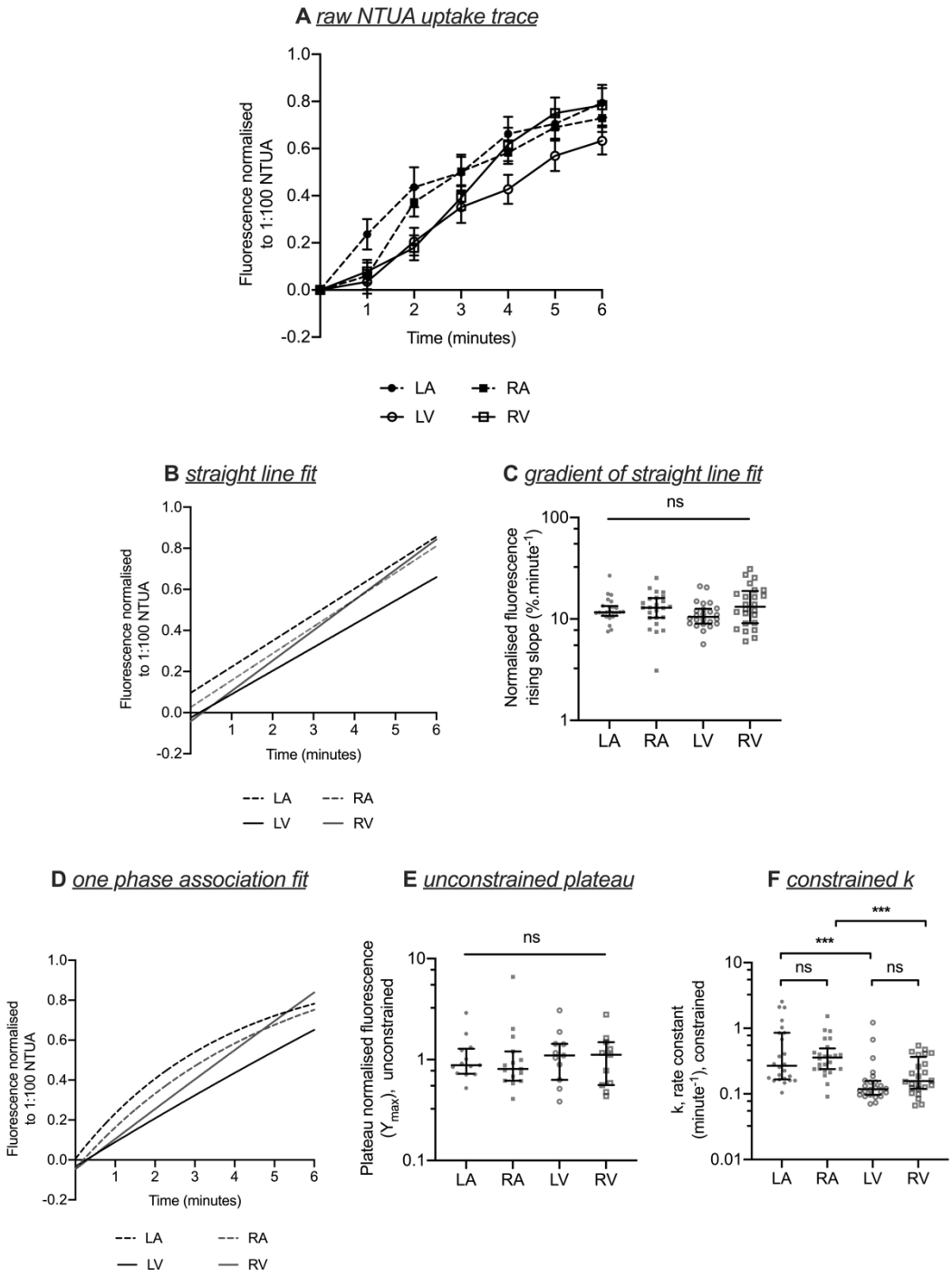


Figure 4.1: Pattern of neuronal NTUA uptake in each cardiac chamber across the murine heart

Please refer to the following page for the figure legend.

Description for figure on the preceding page.

Figure 4.1: Pattern of sympathetic NTUA uptake in each cardiac chamber across the murine heart

The inter-cardiac differences in NTUA uptake in the mouse heart by two analysis methods. **(A)** NTUA uptake trace in the left atrium (LA; •), right atrium (RA; ○), left ventricle (LV; ■) and right ventricle (RV; □). NTUA accumulation is similar within the atrial and ventricular groups, and faster in the former groups than the latter. NTUA uptake throughout the heart appears to approach a similar maximum fluorescence level.

(B, C) The linear analysis method did not reveal inter-cardiac differences in NTUA uptake rate between the cardiac chambers.

(D) The non-linear curve fit to the data demonstrates for a plateau of NTUA uptake in the atria but not the ventricle. **(E)** The maximal NTUA accumulation (Y_{max}) in a subset of n_t were not different between the cardiac chambers. However, the protocol eliminated many n_t. **(F)** The model was constrained to known Y_{max} values in (E) to encourage a higher retention of n_t to yield rate constant (*k*). This revealed a heterogeneous NTUA uptake pattern, where uptake rate is significantly faster in atria than ventricles on each side but did not differ within the atrial and ventricular groups.

Each individual datapoint in scatterplots corresponds to a single terminal. Data presented as **(A)** mean±SEM and **(C, E, F)** median (IQR).

Statistical analyses:
(C, F) Friedman test, followed by *post-hoc* Dunn's multiple comparison test
(E) Kruskal-Wallis test, followed by *post-hoc* Dunn's multiple comparison test
*** denotes $p<0.001$; ns denotes $p>0.05$

4.2.2. NTUA uptake rate is faster in the rodent heart than artery

4.2.2.1. Mice

To assess tissue differences in NAT uptake rate, the murine LA and MA were exposed to 1:20 NTUA for 6 min. At each time point of NTUA superfusion, the neuronal NTUA fluorescence was greater in the murine LA than the MA (Figure 4.2A, B). This corresponded to a 22% greater cardiac NTUA uptake rate compared to mesenteric periarterial terminals [LA: 12 (11, 27)%.min^{-1} (n=4, n_t=24) vs. MA: 10 (7, 11)%.min^{-1} (n=4, n_t=24), p<0.01, Figure 4.2B, C], thus demonstrating for a significantly faster cardiac neuronal NTUA clearance mechanism.

4.2.2.2. Rat

Neuronal NTUA accumulation into rat tissues began after an initial 2-min delay (Figure 4.3A). At each time point beyond t=4, NTUA fluorescence was consistently greater in the rat LA than MA (Figure 4.3A); thus, NTUA uptake rate was 50% faster in the former [LA: 6 (5, 7)%.min^{-1} (n=4, n_t=24) vs. MA: 4 (3, 5)%.min^{-1} (n=4, n_t=24), p<0.01, Figure 4.3C]. In addition to data from mice, this further suggests for faster cardiac NAT reuptake rate in single terminals than those supplying the MAs in the rodent.

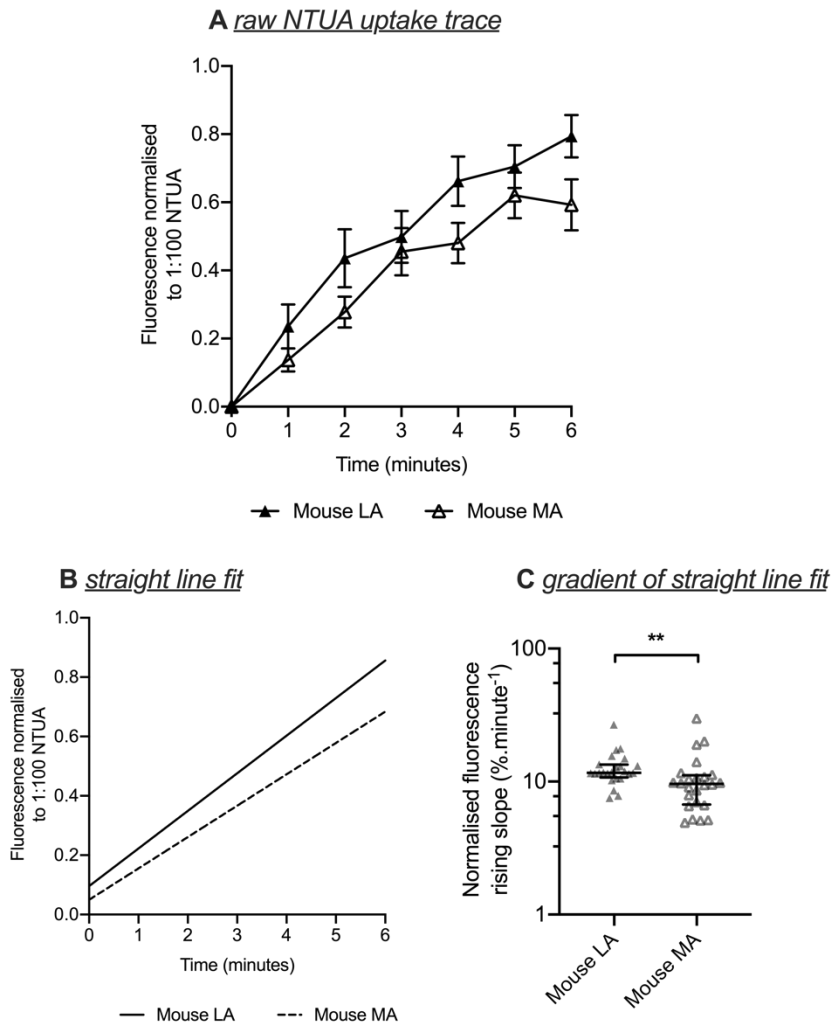


Figure 4.2: Faster sympathetic NTUA uptake rate in the murine heart than in the mesenteric arteries

Comparison of neuronal NTUA uptake between the murine LA and MAs. **(A, B)** Upon exposure, the cardiac- [left atrium (LA); ▲] and periarterial [mesenteric arteries (MAs); △] noradrenergic neurones accumulated NTUA in a linear fashion. At each timepoint, the fluorescence of accumulated NTUA was higher in the heart than vasculature. **(C)** The linear NTUA uptake rate was significantly greater in the LA than the MA.

Each individual datapoint in scatterplots corresponds to a single terminal. Data presented as **(A)** mean±SEM and **(C)** median (IQR).

Statistical analysis:
(C) Mann-Whitney test; ** denotes $p<0.01$.

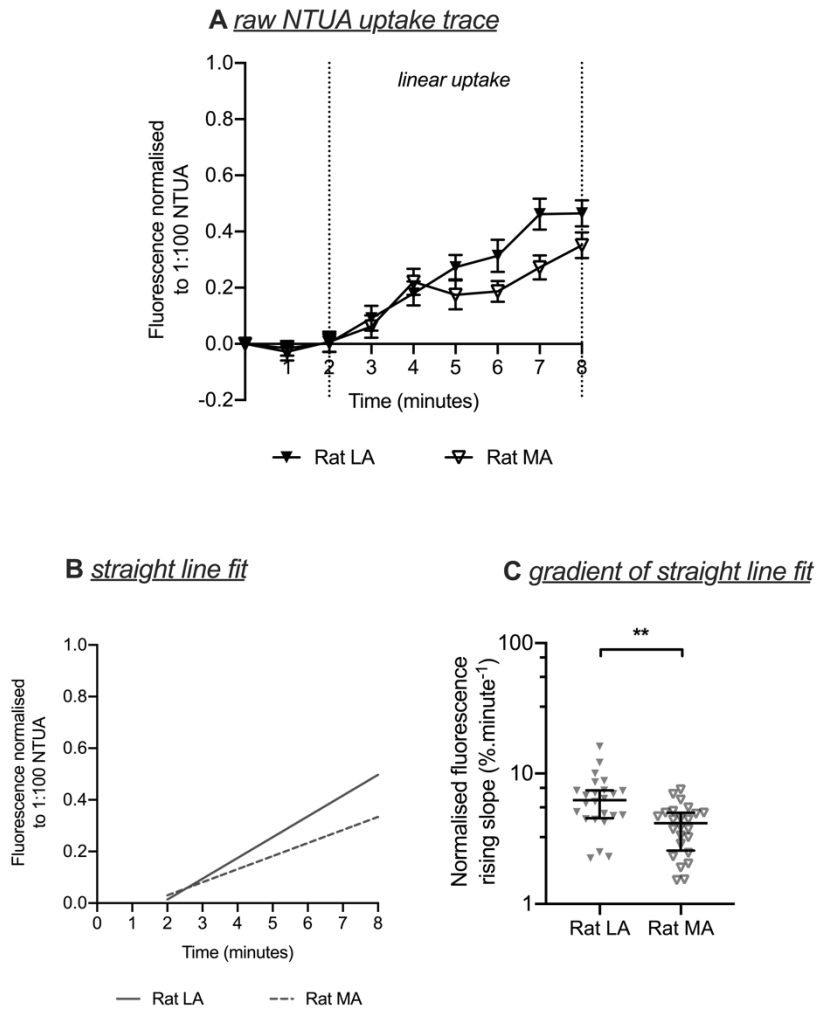


Figure 4.3: Faster sympathetic NTUA uptake rate in the rat heart than in the mesenteric arteries

Comparison of neuronal NTUA uptake between the rat LA and MAs. **(A, B)** NTUA accumulation into the cardiac- [left atrium (LA); ▼] and periarterial [mesenteric arteries (MAs); ▽] noradrenergic neurones began 2 min after 1:20 NTUA entry into the imaging chamber. The uptake was initially similar at t=2-4; thereafter, it was consistently greater in the LA than the MA. **(C)** NTUA uptake rate was significantly faster in the rat LA than the MA.

Each individual datapoint in scatterplots corresponds to a single terminal. Data presented as **(A)** mean±SEM and **(C)** median (IQR).

Statistical analysis:
(C) Mann-Whitney test. ** denotes $p<0.01$

4.2.3. NTUA uptake rate is faster in mice than in the rat

4.2.3.1. Heart

To assess interspecies differences in NAT uptake rate, the LA of mice and rats were exposed to 1:20 NTUA for 6 min. NTUA fluorescence in sympathetic nerve terminals of the murine LA was greater than in the rat LA at each time point of superfusion (Figure 4.4A); thus, the linear cardiac NTUA uptake rate was 140% greater in mice [mouse LA: 12 (11, 13)%.min^{-1} (n=4, n_t=24) vs. rat LA: 5 (3, 9)%.min^{-1} (n=4, n_t=24), p<0.001, Figure 4.4B, C].

4.2.3.2. Mesenteric artery

Similarly, NTUA fluorescence in periarterial noradrenergic neurones was greater in mice than the rat at each time point (Figure 4.5A). Consequently, the linear periarterial NTUA uptake rate was 233% faster in mice than the rat [mouse MA: 10 (7, 11)%.min^{-1} (n=4, n_t=24) vs. rat MA: 3 (2, 6)%.min^{-1} (n=4, n_t=24), p<0.0001, Figure 4.5B, C]. As with the heart, this suggests NAT reuptake rate is faster in in the murine species than in the rat.

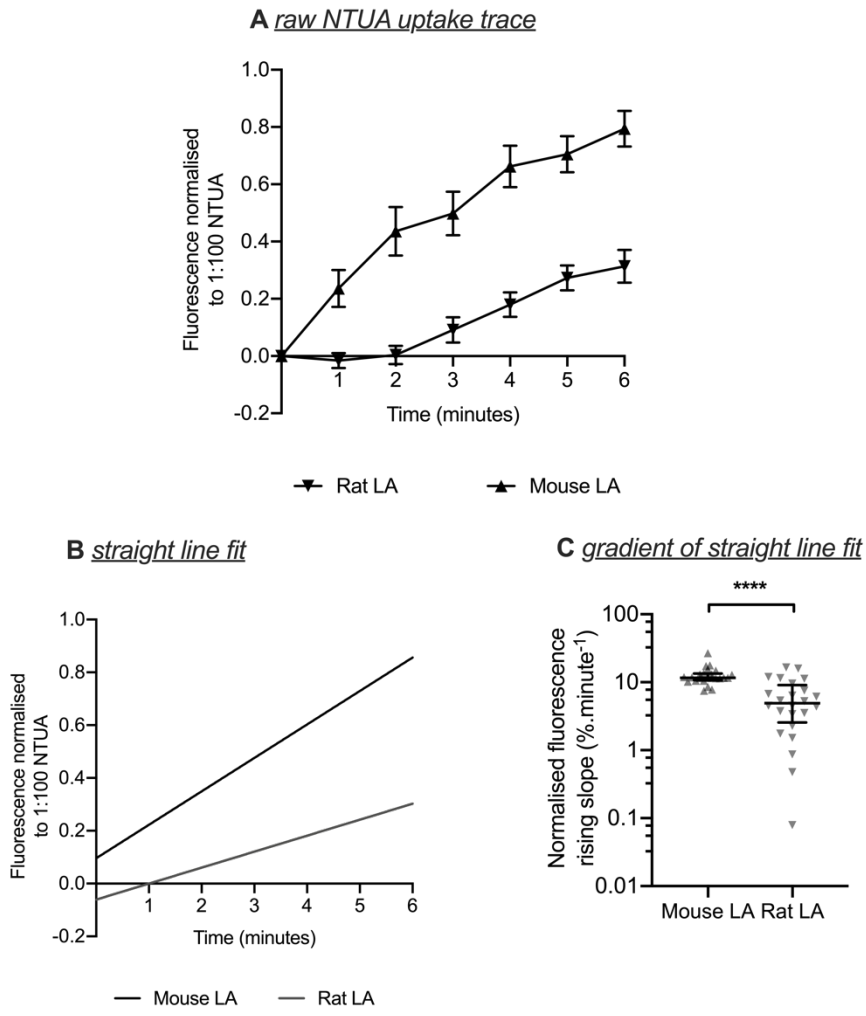


Figure 4.4: Faster cardiac sympathetic NTUA uptake in the mouse than in the rat
Comparison of cardiac neuronal NTUA uptake between the mouse and rat. **(A, B)** Uptake of NTUA fluorescence into the cardiac sympathetic nerve terminals in the mouse (▲) was greater than in the rat (▼) at each time point. **(C)** The linear NTUA uptake rate was significantly faster in the murine LA than the rat LA.

Each individual datapoint in the scatterplot corresponds to a single terminal. Data presented as **(A)** mean±SEM and **(C)** median (IQR).

Statistical analysis:
(C) Mann-Whitney test; **** denotes $p<0.0001$

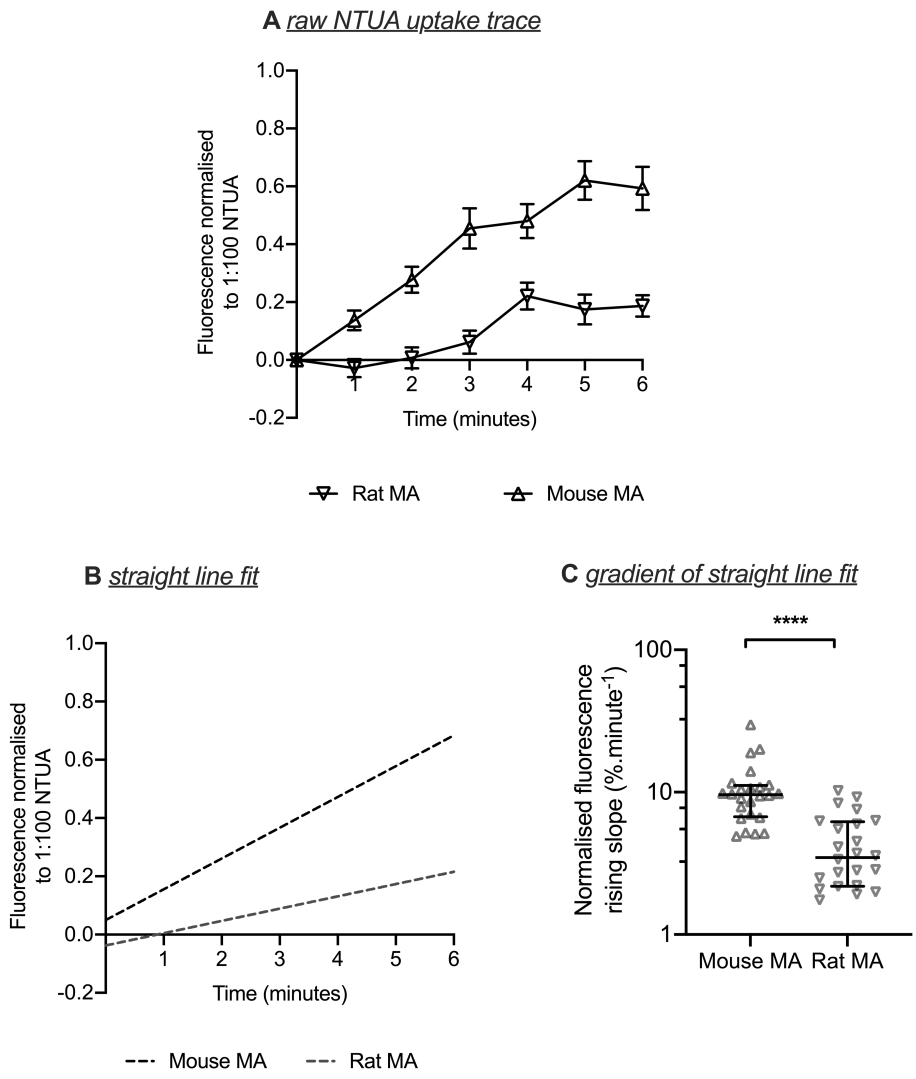


Figure 4.5: Faster mesenteric periarterial sympathetic NTUA uptake rate in the mouse than rat

Comparison of mesenteric periarterial neuronal NTUA uptake between the mouse and rat. **(A, B)** Uptake of NTUA fluorescence into periarterial sympathetic nerve terminals was greater in the mouse (△) than the rat (▽). **(C)** The linear NTUA uptake rate was significantly faster in the mouse MA than the rat MA.

Each individual datapoint in the scatterplot corresponds to a single terminal. Data presented as **(A)** mean±SEM and **(C)** median (IQR).

Statistical analysis:
(C) Mann-Whitney test; **** denotes $p<0.0001$.

4.2.4. Muscarinic receptor-mediated inhibition of cardiac NTUA uptake

Colleagues within the laboratory previously demonstrated a muscarinic acetylcholine receptor (mAChR)-mediated reduction in NAT reuptake rate in the murine urogenital system (Parker *et al.*, 2010). Here, the investigation was extended to the heart; briefly, the murine LA was pre-treated with mAChR agonist carbachol for 6 min [10 μM; Parker *et al.* (2010)] before the 1:20 NTUA+carbachol test period; mAChR specificity was tested with antagonist atropine [1 μM; (Nishimaru *et al.*, 2000)].

For the first 2 min, the accumulation of NTUA was similar between groups (Figure 4.6A). In control conditions, the rise in NTUA fluorescence was linear throughout the experiment. However, in carbachol-treated terminals, the rise in fluorescence was linear for the first 3 min, which then began to plateau to lower values compared to control (Figure 4.6A). Consequently, the linear NTUA uptake rate (t=0-6) in carbachol-treated terminals was significantly reduced by 35% from control values [control: 17 (14, 22)%.min^{-1} (n=4, n_t=24) vs. carbachol: 11.1 (9.9, 13.5)%.min^{-1} (n=4, n_t=24), p<0.001, Figure 4.6B, C]. This effect was prevented by atropine [control vs. carbachol+atropine: 15 (10, 21)%.min^{-1} (n=4, n_t=24), p>0.05, Figure 4.6B, C]. However, atropine did not completely restore the NTUA accumulation trace (Figure 4.6A).

As carbachol also led to an observably premature reduction in total NTUA accumulation in the designated timeframe, the non-linear curve fit model was fit onto the data (Figure 4.6D). Carbachol treatment significantly reduced the Y_{max} by 36% from control values [control: 1.4 (1.1, 2.3) (n=3, n_t=18) vs. carbachol: 0.9 (0.8, 1.0) (n=4, n_t=23), p<0.0001, Figure 4.6E], which was prevented by atropine [control vs. carbachol+atropine: 1.0 (0.9, 1.5) (n=4, n_t=17), p>0.05, Figure 4.6D, E]. There was no effect of carbachol upon the

NTUA uptake rate constant *k* [control: 0.2 (0.1, 0.4) min^{-1} (n=4, n_t=24) vs. carbachol: 0.4 (0.2, 0.6) min^{-1} (n=4, n_t=24), p>0.05, Figure 4.6D, F]. The alternative analysis method suggests the mAChR-mediated reduction of NAT function was due to an attenuation in total NTUA accumulation, without perturbing the initial enzymatic NTUA uptake phase.

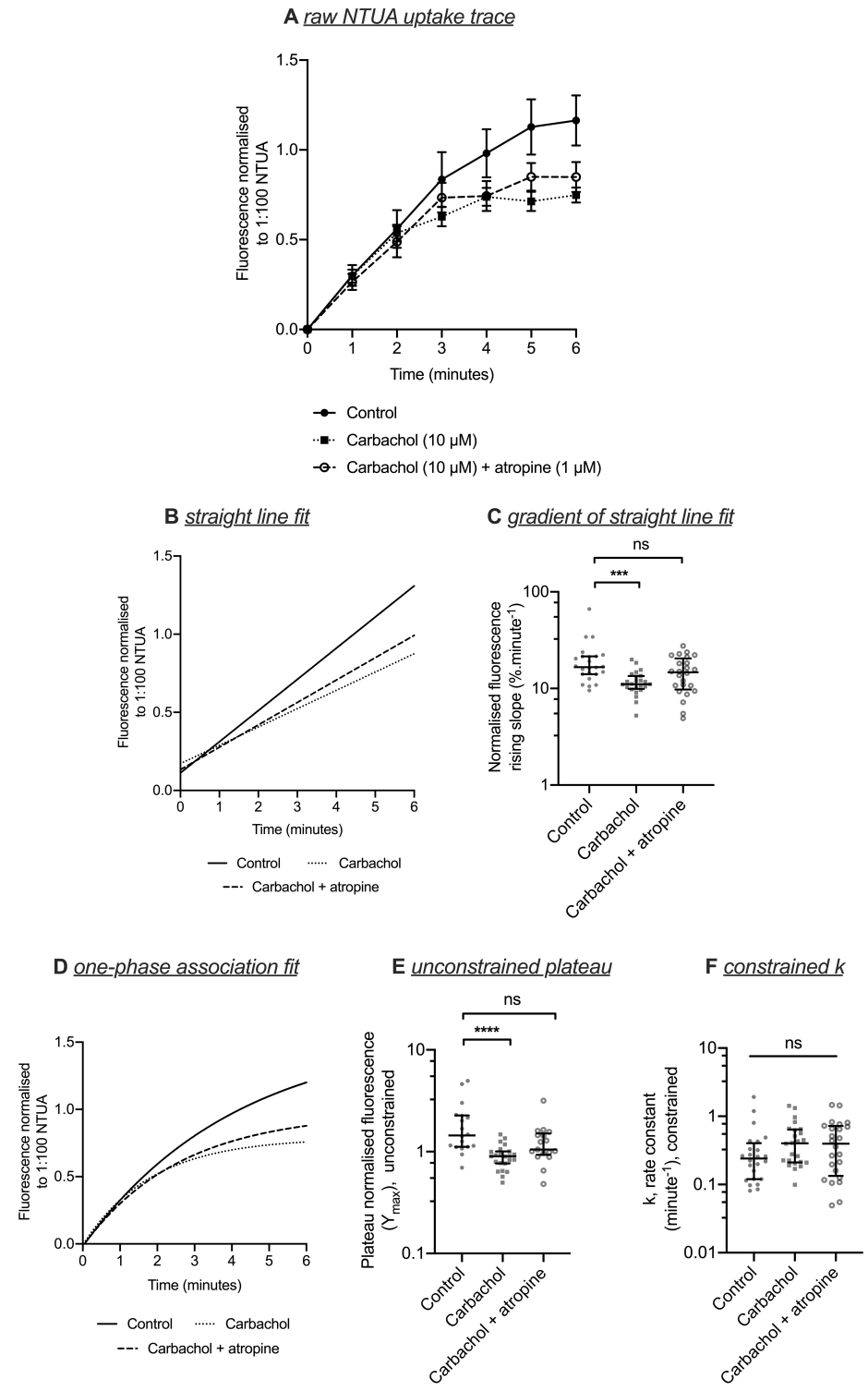


Figure 4.6: Muscarinic acetylcholine receptor activation reduces murine cardiac sympathetic NTUA uptake

Please refer to the following page for the figure legend.

Description for figure on the preceding page.

Figure 4.6: Muscarinic acetylcholine receptor activation reduces murine cardiac sympathetic NTUA uptake

The effect of muscarinic acetylcholine receptor (mAChR) activation upon murine cardiac NTUA uptake. **(A)** The NTUA fluorescence trace of murine cardiac sympathetic nerve terminals in control (●), carbachol-treated (○) and carbachol+atropine-treated conditions (■). From t=2 onwards, the trace became progressively blunted in carbachol groups compared to control. Pre-treatment with mAChR antagonist atropine prevented, but did not completely restore, this effect.

(B, C) The linear NTUA uptake rate was significantly reduced with carbachol pre-treatment, which was prevented by atropine pre-treatment.

(D) The non-linear curve fit to the data shows a premature plateau of NTUA fluorescence in carbachol group. **(E)** The Y_{max} values of noradrenergic terminals were significantly lower in the carbachol groups compared to control; this was prevented by atropine pre-treatment. **(F)** Rate constant values of NTUA uptake from all terminals were not different between groups.

Each individual datapoint in the scatterplot corresponds to a single terminal. Data presented as **(A)** mean±SEM and **(C, E, F)** median (IQR).

Statistical analysis:
(C, E, F) Kruskal-Wallis test, followed by *post-hoc* Dunn's multiple comparison test.
*** denotes $p<0.001$; **** denotes $p<0.0001$; ns denotes $p>0.05$

4.2.5. Electrical field stimulation rapidly reduces cardiac NTUA uptake

4.2.5.1. Frequency-dependent suppression of NTUA uptake

To assess the effect of SNA on NAT reuptake rate, NTUA uptake into cardiac sympathetic nerve terminals were measured simultaneously to action potential (AP) propagation elicited by electrical field stimulation (EFS). Briefly, the isolated mouse LA was stimulated at the point of 1:20 NTUA entry into the imaging chamber; EFS parameters were set at 80% of cardiomyocyte contraction threshold at frequencies 0.2, 0.5, 1, 2, 5, and 10 Hz.

In the absence of EFS [no stimulation (NS)], NTUA fluorescence rose in a linear fashion to NTUA superfusion (Figure 4.7A). In the presence of EFS, the NTUA uptake trace became progressively distorted in a frequency-dependent manner, where the initial rise in fluorescence became markedly shallower and thus the normal linearity of uptake was lost (Figure 4.7A). In the case of 10 Hz stimulation, the NTUA fluorescence fell below the starting fluorescence within 1 min, suggesting not only that uptake was perturbed but also that the initial 1:100 NTUA fluorescence was lost from the terminal. The disruption in NTUA uptake appeared to recover in the last few min of recording. For this reason, NTUA uptake rate was quantified in the first 3 min (termed 'early phase').

Between 0.2-1 Hz EFS, the NTUA uptake rates in the 'early phase' were not perturbed [NS: 16 (8, 23)%.min^{-1}; 0.2 Hz: 14 (9, 22)%.min^{-1} vs. NS: p>0.05; 0.5 Hz: 10 (3, 18)%.min^{-1} vs. NS: p>0.05; 1 Hz: 11 (5, 15)%.min^{-1} vs. NS: p>0.05]. However, NTUA reuptake rate became significantly reduced at higher AP frequencies: by 63% at 2 Hz [6 (1, 20)%.min^{-1} vs. NS: p<0.01], 69% at 5 Hz [5 (-2, 15)%.min^{-1} vs. NS: p<0.0001] and 75% at 10 Hz [4 (-5, 14)%.min^{-1} vs. NS: p<0.0001] (all EFS groups: n≥4, n_t≥60 per group;

Figure 4.7B). The inhibitory EF_{50} (EFS frequency inhibiting the half maximal reuptake effect) of the AP-induced suppression of NTUA uptake rate equated to 0.9 Hz (Figure 4.7C). Increasing the EFS voltage back to 100% of cardiomyocyte contraction threshold evoked contractions in all experiments, thus confirming consistent delivery of the EFS parameters intended.

Together, these results demonstrate there is a frequency-dependent suppression of single-terminal NTUA uptake kinetics in the murine LA in response to EFS. This suppression appears to affect the initial stages of NAT reuptake (first few min) and then recovers thereafter despite continued stimulation.

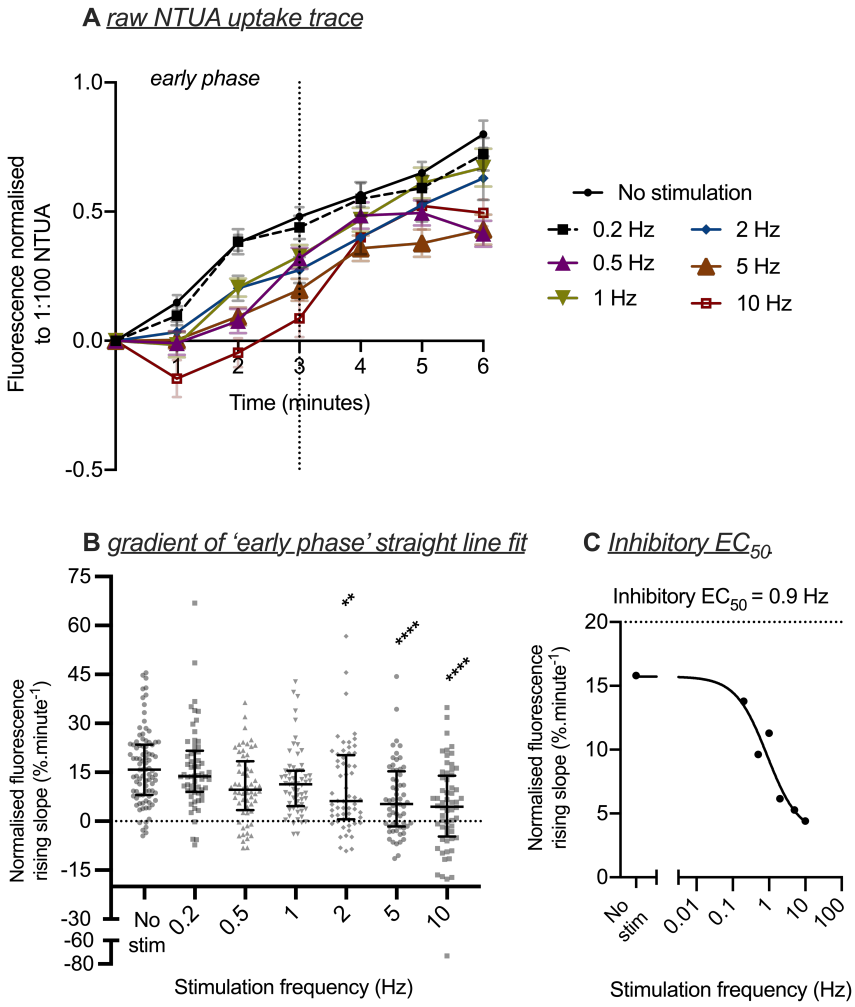


Figure 4.7: Cardiac NTUA uptake is transiently suppressed by sympathetic neuronal activity in a frequency-dependent manner

The murine left atria (LA) were stimulated at varying frequencies (non-stimulating ●; 0.2 Hz ■; 0.5 Hz ▲; 1 Hz ▼; 2 Hz ◆; 5 Hz ●; 10 Hz □) and exposed to NTUA. **(A)** Compared to non-stimulating conditions, the linearity of normalised NTUA accumulation became increasingly distorted in response to increases in EFS frequency in the first 3 min. **(B)** NTUA uptake rate was progressively suppressed by EFS in a frequency-dependent manner, where the effect was significant at 2, 5 and 10 Hz. **(C)** The stimulus-response effect mediated by EFS on NAT reuptake rate equated to an inhibitory EF_{50} of 0.9 Hz. Curve fit was conducted on median values previously seen in (C).

Each individual datapoint in the scatterplot corresponds to a single terminal. Data presented as **(A)** mean±SEM, **(B)** median (IQR) and **(C)** median only.

Statistical analysis:
(B) All statistical analyses were carried out between each EFS frequency and the non-stimulating condition. Kruskal-Wallis test followed by Dunn's multiple comparison *post-hoc* test. ** denotes $p<0.01$; **** denotes $p<0.0001$.

4.2.5.2. Local NAd release from the left atrium

To investigate whether the current EFS protocol (80% cardiomyocyte contraction) was sufficient to elicit sympathetic nerve depolarisation, the murine LA was pre-loaded with tritium labelled NAd ([^{3}H]-NAd) and stimulated with paralleled parameters to measure evoked liberation of the radiotracer. In the time control experiments, tissues were stimulated at 2 Hz at 100% cardiomyocyte contraction threshold at S_1 and S_2 for 6 min each (Figure 4.8A). In 80% EFS experiments, tissues were stimulated at 2 Hz with cardiomyocyte contraction (100% threshold) at S_1 and then without cardiomyocyte contraction (80% threshold) at S_2, for 6 min each (Figure 4.8B).

As shown in Figure 4.8, the radioactivity in the superfusate steadily decreased with time which suggests for a time-dependent loss of [^{3}H]-NAd from the tissue presumably due to the washout (analogous to NTUA; section 3.2.5.2.). However, there were random bouts of radioactive 'spikes', some coinciding with stimulation periods while others not. The majority of 'spikes' occurred at single time points rather than a sustained increase, as expected from the protocol of 6 min EFS. Moreover, there was a lack of radioactivity at some stimulation timepoints. For the reasons outlined, it is unlikely that that radioactivity directly correlated with nerve stimulation and that methodological refinements of the protocol are required.

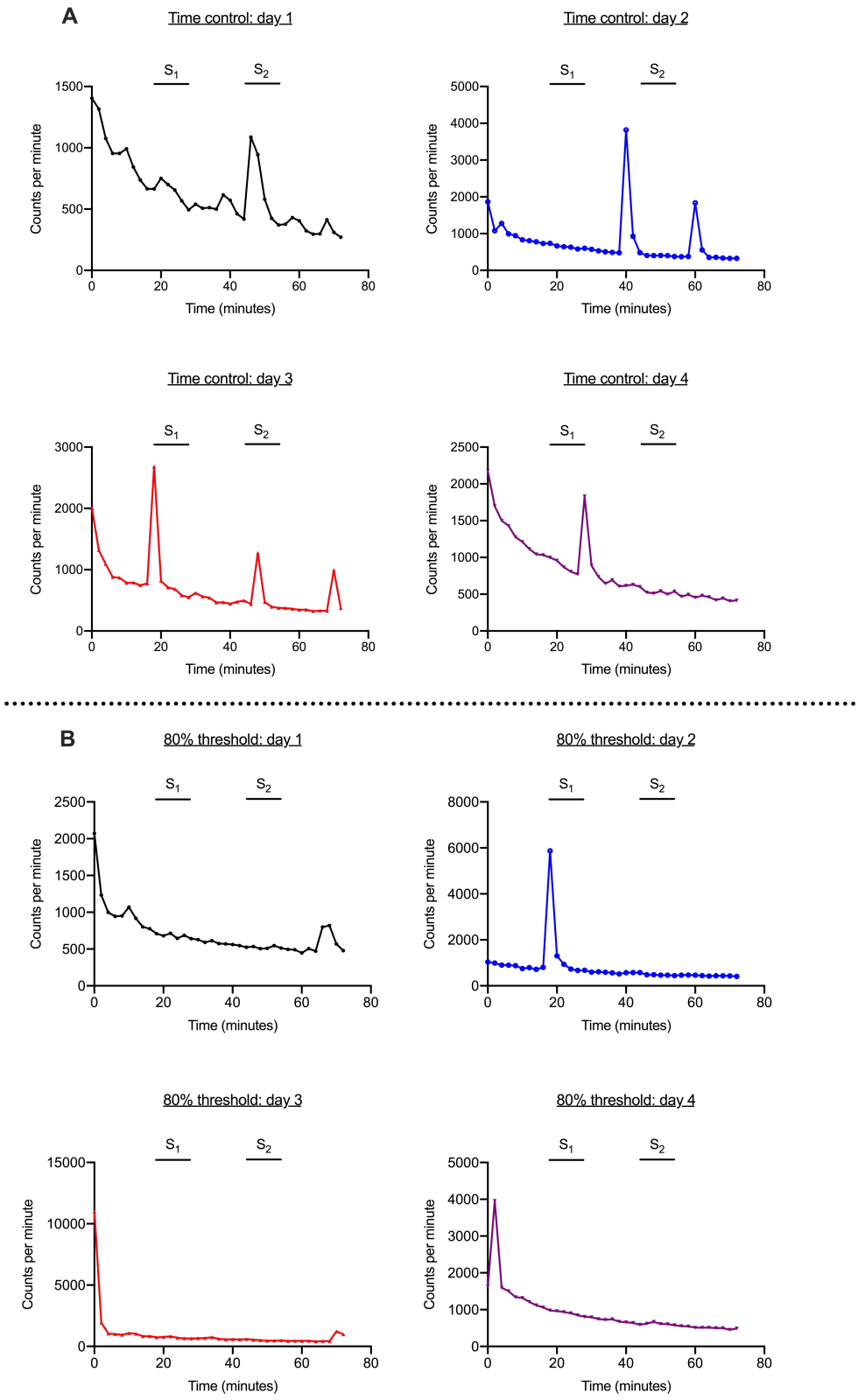


Figure 4.8: Measurements of evoked [^{3}H]-NAd release from the isolated murine atrium

Please refer to the following page for the figure legend.

Description for figure on the preceding page.

Figure 4.8: Measurements of evoked [^{3}H]-NAd release from the isolated murine atrium
The isolated murine left atria (LAs) were loaded with [^{3}H]-NAd and stimulated with matching EFS protocols as those in section 4.2.5.1 (6 min at 2 Hz). In all experiments, there was a steady decline in 'baseline' radioactivity, indicative of gradual loss of the radioisotope with time. **(A)** In time control experiments (S_1 and S_2 = 100% cardiomyocyte contraction threshold), there were random increases in detected radioactivity that coincided with stimulation periods, while others not. Those in the former consisted of single 'spikes' rather than a sustained level of radioactivity, as expected for continuous EFS. Furthermore, not all EFS protocols led to an increase in radioactivity. **(B)** In cardiomyocyte contraction subthreshold experiments (S_1=100% contraction threshold, S_2=80% contraction threshold), most stimulation periods did not correspond to any change in radioactivity. These results demonstrate the uncertainty of the evoked NAd release protocol, thus further experiments were not pursued further until successful troubleshooting.

Each colour represents a different day in which the experiment was carried out. On each 'day', fresh tissues were dissected from animals immediately prior to experimentation. No tissues were stored for any amount of time. Those experiments shown in the same colour occurred on the same day. Each line represents a single isolated mouse left atrium preparation. S_1 and S_2 denotes the 6 min stimulation period.

4.2.5.3. Role of sympathetic prejunctional receptors on NTUA uptake during EFS

Sympathetic nerve terminals are endowed with a plethora of autoreceptors and heteroreceptors that modulate neurotransmission. Thus, it is quite possible the release of neurotransmitters from sympathetic (NAd) and parasympathetic (acetylcholine) nerve terminals during EFS could modulate NAT function. Two potential prejunctional modulators of NAT function of interest was the α_2-adrenoceptor (α_2AR) and the mAChR. To investigate this, the murine LAs were pre-treated with modulatory receptor antagonists for 20 min prior the 1:20 NTUA+EFS test period. Although the inhibitory EF_{50} of EFS on NAT function was 0.9 Hz, at 1 Hz there were no significant changes in NTUA uptake rate compared to control (Figure 4.7). For this reason, tissues were stimulated with 2 Hz EFS in this study.

4.2.5.3.1. α_2-Adrenergic autoreceptor

Yohimbine [α_2AR inhibitor] pre-treatment significantly prevented the AP-induced suppression of NTUA rate during the 'early phase' (2 Hz only: 14±2%.min^{-1} vs. 2 Hz+yohimbine: 20±1%.min^{-1}; p<0.01; n=4, n_t=60 per group; Figure 4.9). However, the recovery of NTUA uptake was only transient that plateaued prematurely after 3 min of NTUA exposure; thus, yohimbine did not fully recover the accumulation of NTUA to that seen in non-stimulating conditions (linear throughout 6 min) (Figure 4.9A).

4.2.5.3.2. Muscarinic heteroreceptor

Within the lab, a mAChR-mediated reduction in NAT reuptake rate was observed in the murine vas deferens (Parker *et al.*, 2010) and heart (section 4.4). As the EFS conditions could have concomitantly depolarised parasympathetic nerve terminals, the action of evoked acetylcholine from local parasympathetic nerve terminals could have also acted

upon mAChR to reduce NAT uptake rate. Here, tissues were pre-treated with atropine (1 μM) in addition to yohimbine (1 μM) before the 1:20 NTUA test period.

Blockade of mAChRs did not elicit a further effect on NTUA accumulation compared to yohimbine alone in the 'early phase' [2 Hz+yohimbine: 20±1%.min^{-1} (n=4, n_t=60) vs. 2 Hz+yohimbine+atropine: 19±1%.min^{-1} (n=4, n_t=58), p>0.05; Figure 4.9]. As with α_2AR antagonism, there was a reduced plateau of the maximum NTUA fluorescence detected at the end of the 6-min NTUA superfusion period (Figure 4.9A).

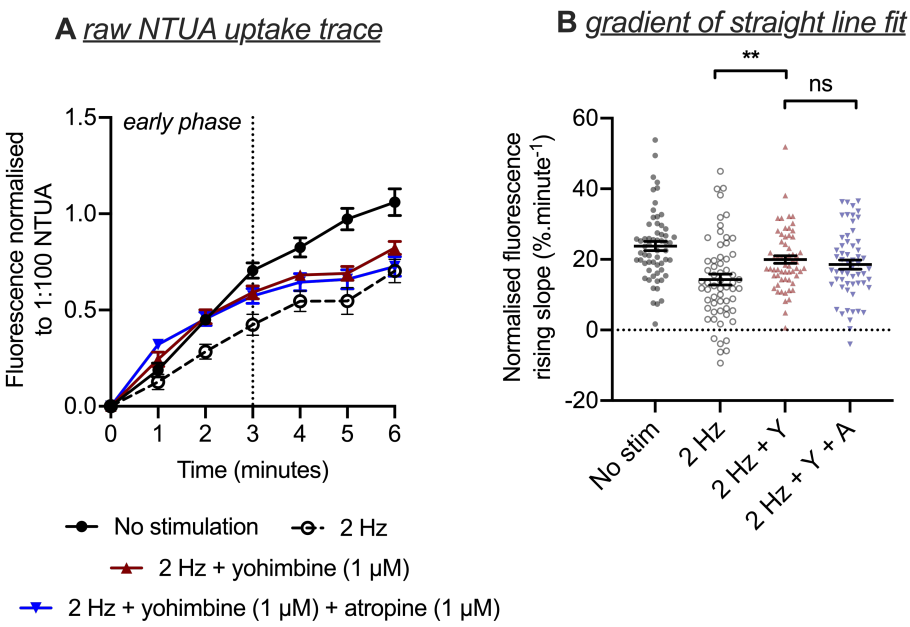


Figure 4.9: Inhibition of α_2-adrenoceptor, but not mAChR, prevents the transient stimulation-evoked NAT suppression in the murine heart

NTUA uptake into the murine left atria (LA) in non-stimulating conditions (●), in 2 Hz EFS conditions (○), in 2 Hz EFS conditions pre-treated with yohimbine (α_2-AR antagonist; Y; ▲), and in 2 Hz EFS conditions pre-treated with yohimbine+atropine (mAChR antagonist; Y+A; ▲) pre-treatment.

(A) Pre-treatment with Y recovered the initial accumulation of NTUA in the first 3 min of 2 Hz EFS. However, the recovery was transient where NTUA accumulation prematurely plateaued thereafter. No further effect was mediated by Y+A. **(B)** The reduction of NTUA uptake rate in the 'early phase' of EFS was recovered in the presence of Y with no further effect in the additional presence of atropine (Y+A).

Each individual datapoint in the scatterplot corresponds to a single terminal. Data presented as mean±SEM.

Statistical analysis:
(B) Welch's *t*-test between 2 Hz and 2 Hz + Y; unpaired *t*-test between 2 Hz + Y and 2 Hz + Y + A.
ns denotes $p>0.05$; ** denotes $p<0.01$.

4.2.5.4. Substrate competition: NAd and NTUA at NAT

4.2.5.4.1. NTUA competition with NAd during uptake

It is possible the EFS-induced suppression of cardiac NAT rate may be contributed by substrate competition between NTUA and the evoked release of endogenous NAd in the junctional cleft. To investigate this, the isolated murine LAs were exposed to NTUA and exogenously applied NAd in non-stimulating conditions. Initially, a very high concentration of NAd (100 µM) was chosen; however, NTUA competition with NAd was so great that the 1:100 NTUA fluorescence rapidly disappeared within 1 min (*observation only*). While this could have been overcome by continuous imaging protocols, the low concentration of 1:100 NTUA fluorescence could also have been compromised given the sensitivity of the NTUA fluorophore (section 3.2.1.7.).

Therefore, the isolated mouse LA was exposed to NAd at a concentration that elicits the maximum tension in the paced rodent left atrium (1 µM) (Williamson and Broadley, 1989, Oostendorp and Kaumann, 2000). The presence of 1 µM NAd abolished NTUA uptake in some, but not all, cardiac sympathetic nerve terminals (Figure 4.10); some terminals maintained an increase in uptake while others had begun to lose the pre-loaded 1:100 NTUA fluorescence (Figure 4.10C). Collectively, exogenous NAd reduced NTUA uptake by 104±7% [control: 10.5±0.7%.min^{-1} (n=4, n_t=60) vs. NAd: -0.4±0.7%.min^{-1} (n=4, n_t=60), p<0.0001, Figure 4.10C].

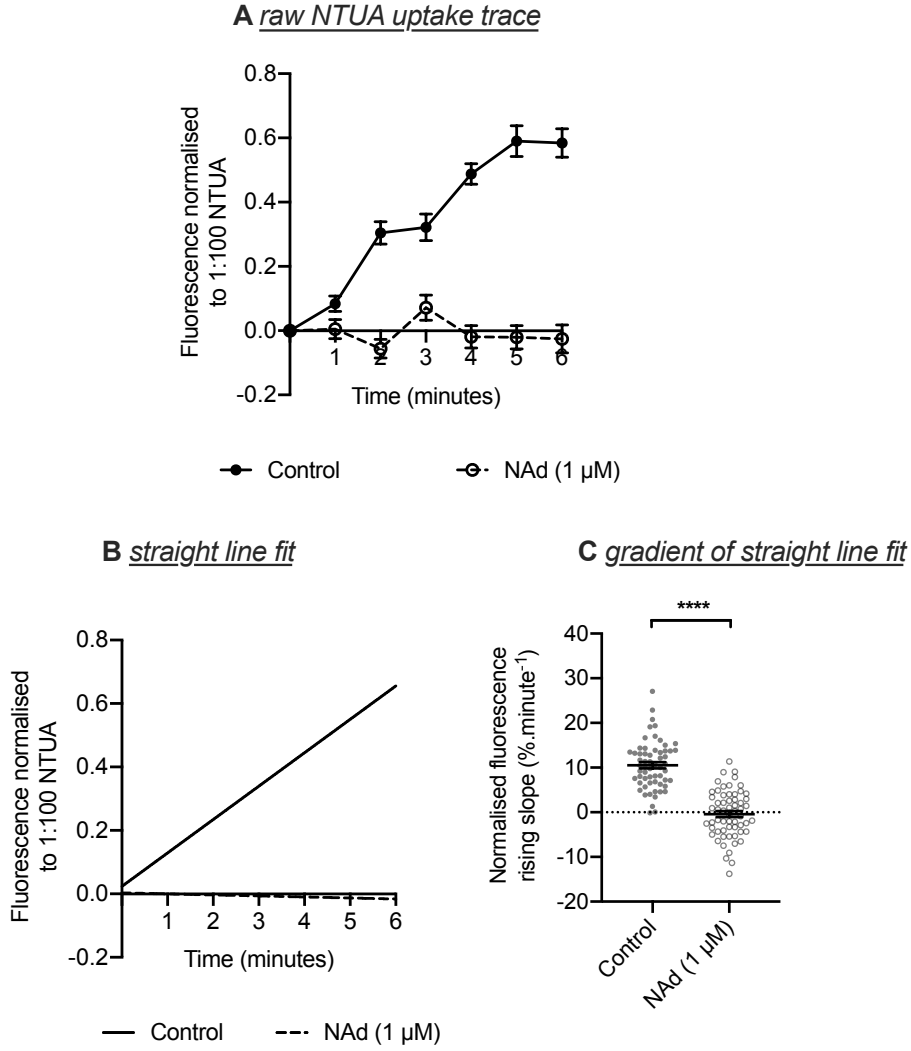


Figure 4.10: Competition of NTUA with NAd for murine cardiac NAT during uptake
The murine LA was exposed to NTUA and exogenous NAd in non-stimulating conditions. **(A)** The NTUA uptake trace in the absence (•) and presence of 1 µM NAd (○) during 1:20 NTUA superfusion. NTUA accumulation was collectively abolished when NAd was concomitantly superfused with NTUA. **(B)** The straight line fit of the data in the linear region. **(C)** Expressed as a percentage change from 1:100 NTUA, the linear NTUA uptake rate was preserved in some terminals but not all. In many cases, the pre-loaded 1:100 NTUA fluorescence was lost. This averaged to a subzero NTUA uptake rate in the presence of NAd during uptake.

Each individual datapoint in the scatterplot corresponds to a single terminal. Data presented as mean±SEM.

Statistical analysis:
(C) Unpaired *t*-test; **** denotes $p<0.0001$.

4.2.5.4.2. NTUA displacement by NAd during washout

Substrate displacement of NTUA from the sympathetic nerve terminals by NAd was also investigated during the washout phase with a concentration-response curve. Briefly, the mouse LA were superfused with 1:100 NTUA to identify noradrenergic nerve terminals followed by 1:20 NTUA for 6 min; the inflow line was then directed to a reservoir containing KHB ± 0.1-100 μM NAd.

Cardiac neuronal NTUA fluorescence was gradually washed out with KHB, which was accentuated in the presence of exogenously applied NAd in a concentration-dependent manner (Figure 4.11). At high NAd concentrations (10-100 μM), the loss of NTUA fluorescence tended towards -1.0 as the 1:100 NTUA starting fluorescence began to disappear. Thus, the traces were truncated between t=8-10 for rate analysis (Figure 4.11C).

The loss of NTUA fluorescence with KHB alone occurred at a rate of 7 (-6, 17)%.min^{-1} (n=4, n_t=60) in the first 2 min. The presence of exogenous NAd significantly accentuated the loss by 3-fold at 1 μM [control vs. 1 μM: 25 (17, 45)%.min^{-1} (n=4, n_t=60), p<0.0001], 5-fold at 10 μM [control vs. 10 μM: 34 (26, 45)%.min^{-1} (n=4, n_t=60), p<0.0001] and 6-fold at 100 μM [control vs. 100 μM: 40 (30-55)%.min^{-1} (n=4, n_t=60), p<0.0001], while no effect was observed with 0.1 μM NAd [control vs. 0.1 μM: 6 (-1, 14)%.min^{-1} (n=4, n_t=60), p>0.05] (Figure 4.11D). The concentration-dependent loss of NTUA fluorescence by exogenous NAd equated to an EC_{50} of 0.8 μM (Figure 4.11E).

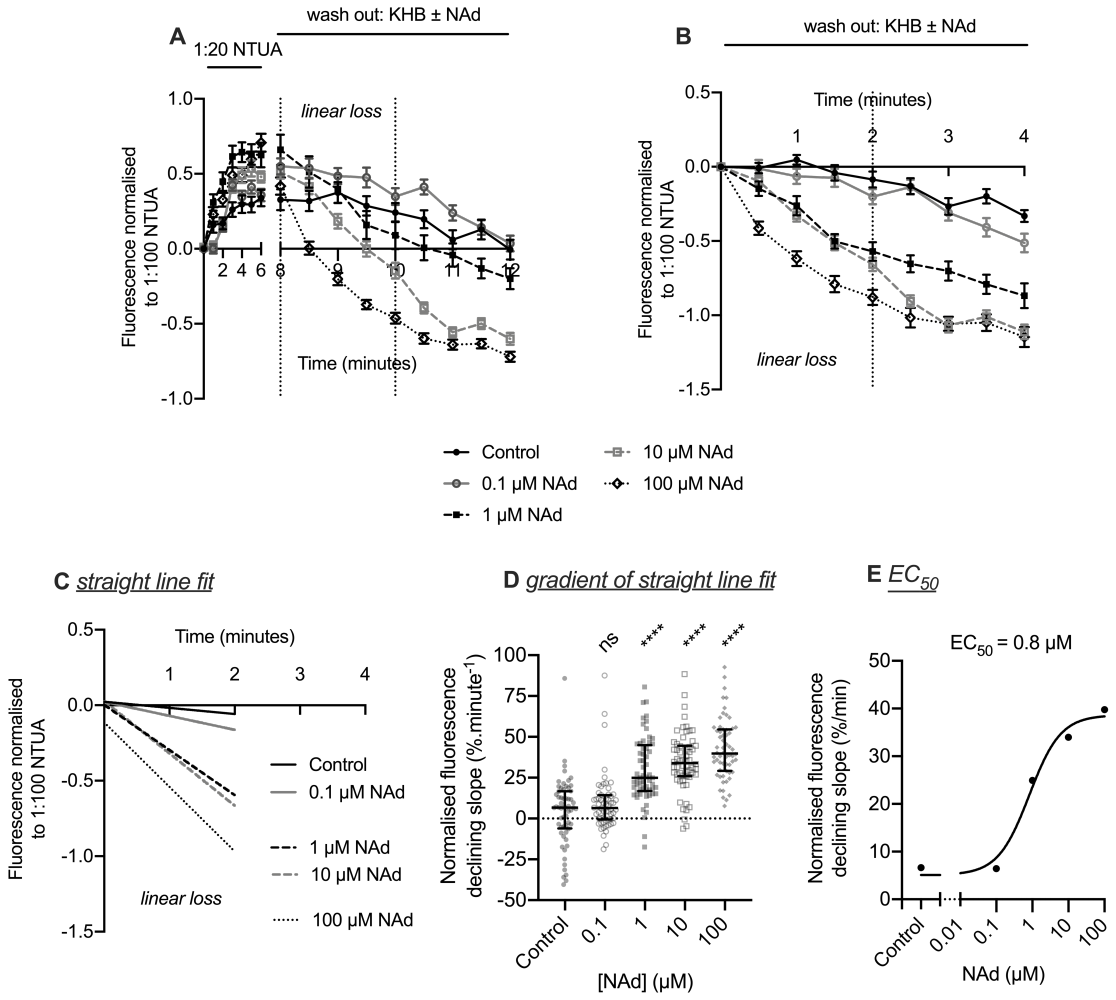


Figure 4.11: Displacement of NTUA from murine cardiac sympathetic nerve terminals by NAd during washout

The displacement of NTUA from murine cardiac sympathetic neurones by exogenously applied NAd. **(A)** The mouse left atrium (LA) was exposed to 1:100 NTUA followed by 1:20 NTUA for 6 min. 1:20 NTUA was then washed out with KHB with or without NAd (control ●; 0.1 µM ○; 1 µM ■; 10 µM □; 100 µM ◆). **(B)** Fluorescence during washout was normalised to t=8. **(C)** A straight-line fit through the datapoints in the linear region of NTUA loss. **(D)** The linear rate of NTUA loss was significantly accelerated in the presence of 1-100 µM NAd. **(E)** The EC_{50} of exogenous NAd for NTUA displacement is 0.8 µM. Curve fit was conducted on median values previously seen in (D).

Data presented as **(A, B)** mean±SEM, **(D)** median (IQR) and **(E)** median only.

Statistical analyses:
(D, F) All statistical analyses were carried out between each NAd concentration and the control condition. Kruskal-Wallis test followed by Dunn's multiple comparison *post-hoc* test. **** denotes $p<0.0001$, ns denotes $p>0.05$.

4.2.5.5. Inhibition of exocytosis mechanism

It was of particular interest to investigate the effect of membrane potential on NAT rate during EFS independently of evoked NAd. Colchicine, a microtubule destabilising agent, has been previously shown to significantly inhibit exocytosis in the rodent heart (Sorimachi *et al.*, 1973) and vas deferens (Thoa *et al.*, 1972). Thus, I was interested to use colchicine to inhibit exocytosis pharmacologically in a series of experiments. First and foremost, it was pertinent to investigate whether colchicine affects NAT function under non-stimulating conditions. Briefly, the murine LA was pre-treated with colchicine (1 mM) 20 min prior to and during 1:20 NTUA superfusion.

At each time point of NTUA accumulation, the NTUA fluorescence in colchicine-treated terminals were consistently less than in untreated terminals (Figure 4.12A). Thus, the linear increase in the former was reduced by 19% from control values [control: 16 (13, 21)%.min^{-1} (n=4, n_t=60) vs. colchicine: 13 (10-16)%.min^{-1} (n=4, n_t=60), p<0.001, Figure 4.12B, C]. As colchicine reduced NAT function in the absence of EFS, the investigation of its use during EFS to monitor dynamic changes in NAT function was not pursued further.

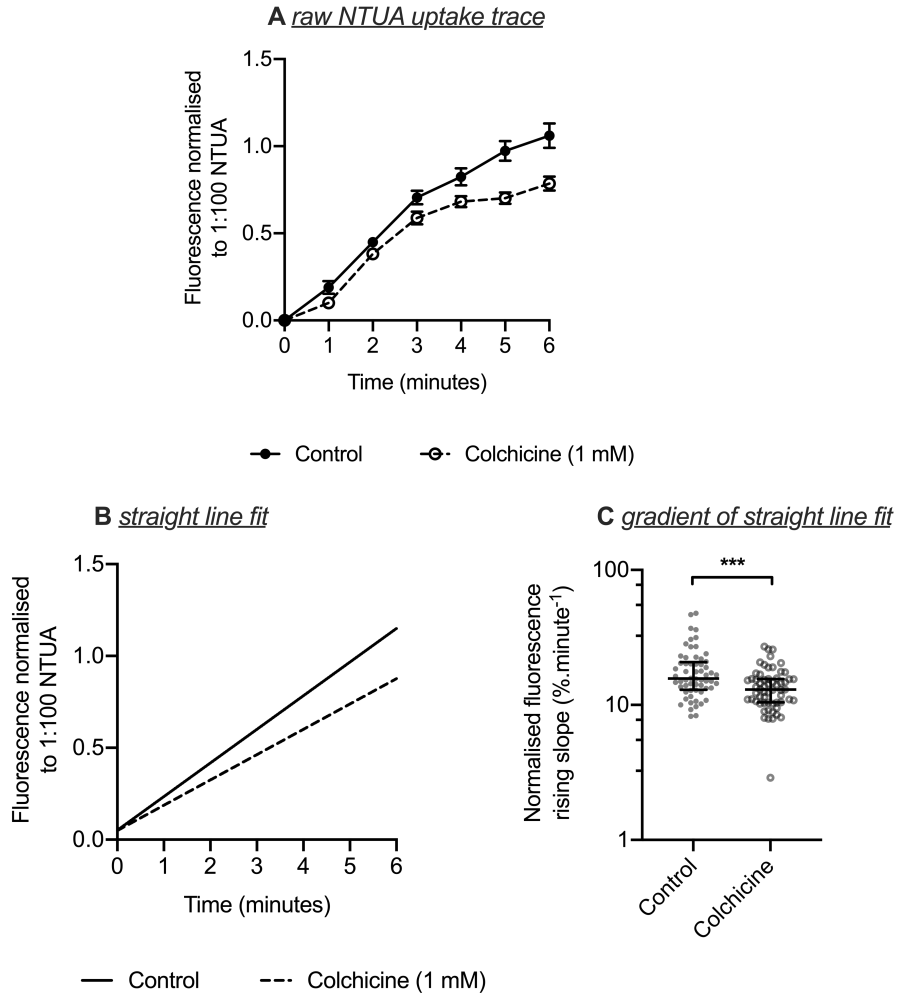


Figure 4.12: Microtubule destabilising agent, colchicine, reduces cardiac sympathetic NTUA uptake in non-stimulating conditions

The effect of colchicine upon cardiac NAT function in non-stimulating conditions. **(A)** The NTUA uptake trace in the absence (•) and presence of 1 mM colchicine (○) pre-treatment. NTUA fluorescence was consistently lower at each time point in colchicine treated terminals compared to control. **(B, C)** The linear NTUA uptake rate was significantly reduced by colchicine in cardiac sympathetic nerve terminals.

Each individual datapoint in the scatterplot corresponds to a single terminal. Data presented as **(A)** mean±SEM and **(C)** median (IQR).

Statistical analysis:
(C) Mann-Whitney test; *** denotes $p<0.001$.

4.2.6. Chronic intermittent hypoxia and NAT

Researchers elsewhere in the College (Birmingham Hypoxia and Arterial Chemoreceptor group) kindly provided tissues from their pre-clinical animal model of obstructive sleep apnoea (OSA) to investigate NAT function in the heart and MAs. In brief, Wistar rats were exposed to chronic intermittent hypoxia (CIH) for 21 consecutive days from 9 weeks of age. Some animals were pre-treated with nonselective β-adrenoceptor (βAR) antagonist, propranolol, for 10 days prior to and during the induction of CIH (CIHP), while animals in the control group (normoxia; N) were kept in their home cage during the entire duration. Detailed methodologies can be found in Alzahrani *et al.* (2020) and Appendix C.

4.2.6.1. CIH perturbs NTUA uptake in the heart

Following the initial 2-min delay in uptake, CIH cardiac noradrenergic terminals accumulated more NTUA at each time point of superfusion than N (Figure 4.13A). Furthermore, by 8 min, NTUA uptake in N began to plateau while the detected fluorescence in CIH continued to rise linearly to very high levels (Figure 4.13A). The linear NTUA uptake rate (t=2-8) in CIH was observably 52±29% higher than N animals, though it was not statistically significant (N: 8±1%.min^{-1} (n=4, n_t=24) vs. CIH: 12±2%.min^{-1} (n=4, n_t=24), p=0.057, Figure 4.13B, C).

A non-linear curve fit was applied to the data (Figure 4.13D). CIH induction significantly increased the Y_{max} by 134% from N values [N: 0.6 (0.4, 1.0) (n=3, n_t=22) vs. CIH: 1.4 (1.0, 2.6) (n=4, n_t=20), p<0.0001, Figure 4.13E]. Interestingly, in addition to this, the NTUA uptake rate constant in CIH was slower than N [N: 0.2 (0.1, 0.5).min^{-1} (n=4, n_t=24) vs. CIH: 0.1 (0.1, 0.3).min^{-1} (n=4, n_t=24), p<0.05, Figure 4.13F].

4.2.6.2. CIH does not affect NTUA uptake in the mesenteric arteries

The rise of NTUA fluorescence in mesenteric periarterial sympathetic nerve terminals were similar between the treatment groups at all time points (Figure 4.14A) of NTUA exposure. Consequently, the linear NTUA uptake rate (t=2-8) was not different in CIH compared to N (N: 5.1±0.4%.min^{-1} (n=4, n_t=24) vs. CIH: 5.0±0.7%.min^{-1} (n=4, n_t=24), p>0.05, Figure 4.14B, C).

4.2.6.3. β-adrenoceptor inhibition prevents CIH-induced vascular sympathetic hyperinnervation

At the end of the dynamic NTUA uptake studies, *Z*-stacks of MAs were acquired. In addition to the N and CIH groups, an additional CIHP group was present where animals were treated with propranolol 10 days before and during CIH induction. In CIH, there was an observably 23±8% greater surface density of mesenteric periarterial noradrenergic nerve fibres compared to N, though this was not statistically significant [N: 0.070±0.002 nerve intercepts/μm tissue (n=4) vs. CIH: 0.086±0.005 nerve intercepts/μm tissue (n=5), p=0.091; Figure 4.15A]. However, the total measured fluorescent area was significantly increased by 88±26% compared to N (control: 17±1% vs. CIH: 32±4%, p<0.05, Figure 4.15B). Interestingly, propranolol treatment significantly prevented the rise in surface density, as measured by total area occupied by noradrenergic terminals, to levels similar to N [N vs. CIHP: 18±2% (n=5), p>0.05; Figure 4.15B].

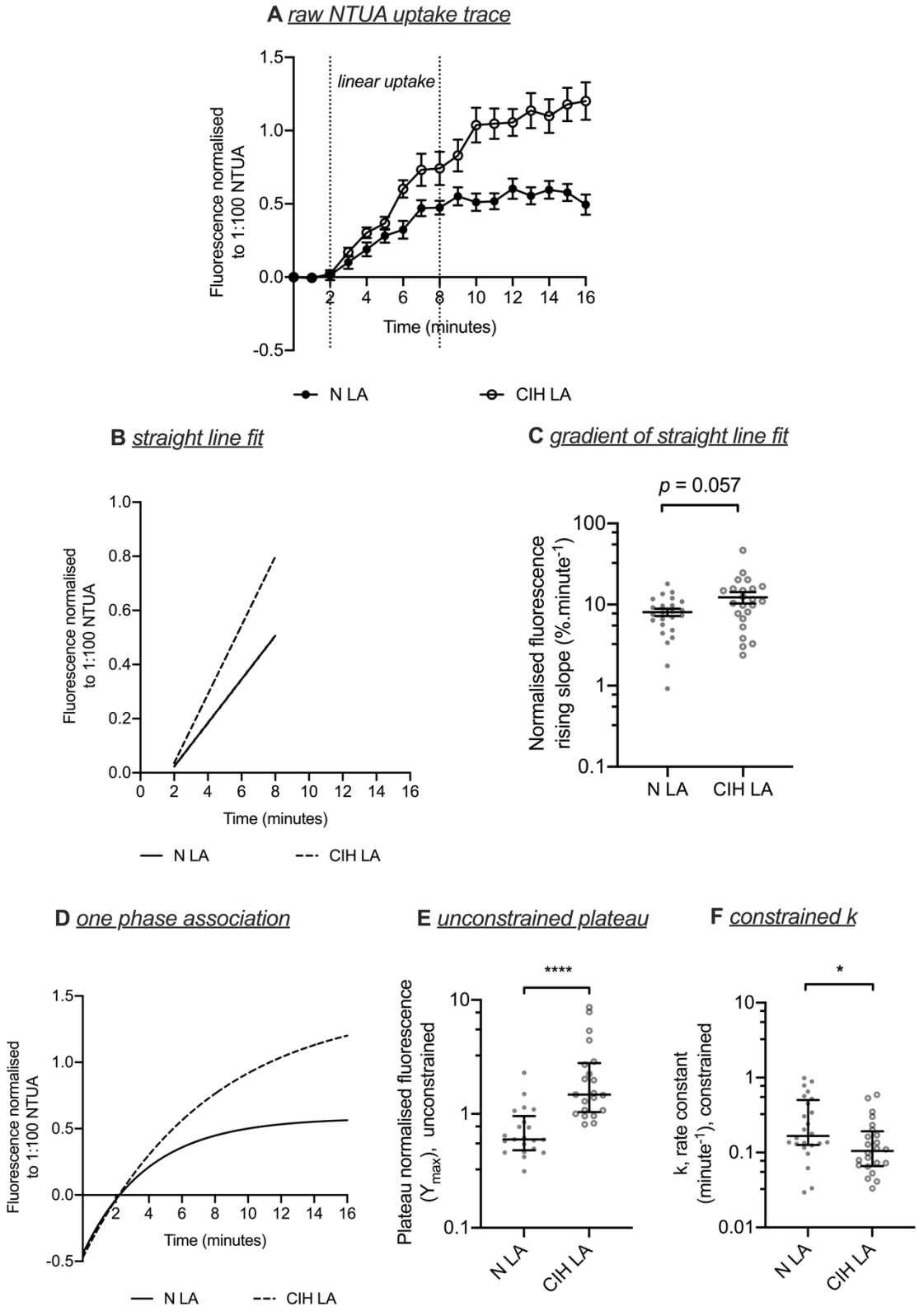


Figure 4.13: CIH accentuates cardiac sympathetic NTUA uptake

Please refer to the following page for the figure legend.

Description for figure on the preceding page.

Figure 4.13: CIH accentuates cardiac sympathetic NTUA uptake

The effect of CIH pathology upon NAT kinetics in the heart. **(A)** NTUA accumulation into cardiac sympathetic terminals in the isolated left atrium (LA) of rats exposed to ambient air (N, normoxia; ●) or CIH (○) for 21 days. Plateau levels were reached by 8 min in N LA while it continued to increase in CIH LA.

(B, C) The linear (t=2-8) NTUA uptake rate in CIH LA was higher, but not statistically different to control LA.

(D, E) An exponential one-phase association model fit to the data shows that Y_{max} values of each noradrenergic terminal were significantly higher in the CIH LA compared to N LA. **(F)** However, NTUA uptake rate constant was lower in the LA of CIH animals compared to N.

Each individual datapoint in the scatterplot corresponds to a single terminal. Data presented as **(A, C)** mean±SEM and **(E, F)** median (IQR).

Statistical analysis:
(C) Welch's *t*-test,
(E, F) Mann-Whitney test.
* denotes $p<0.05$; **** denotes $p<0.0001$

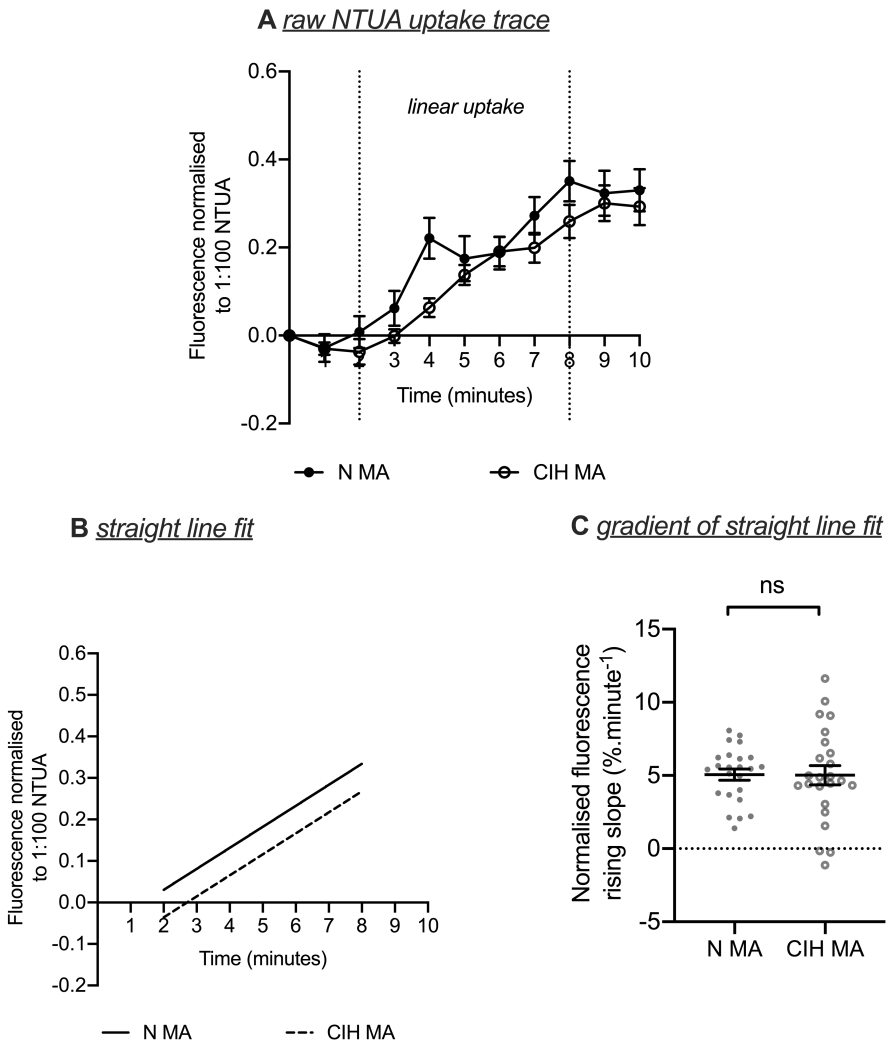


Figure 4.14: CIH does not affect mesenteric periarterial sympathetic NTUA uptake
The effect of CIH pathology upon NAT kinetics in the periarterial vasculature. **(A)** The NTUA uptake trace in isolated mesenteric arteries (MA) of rats exposed to ambient air (N, normoxia; ●) or CIH (○) for 21 days. **(B, C)** The linear NTUA uptake rate was not different between the N MA and CIH MA.

Each individual datapoint in the scatterplot corresponds to a single terminal in the scatterplot. Data presented as mean±SEM.

Statistical analysis:
(C) Welch's *t*-test
ns denotes $p>0.05$.

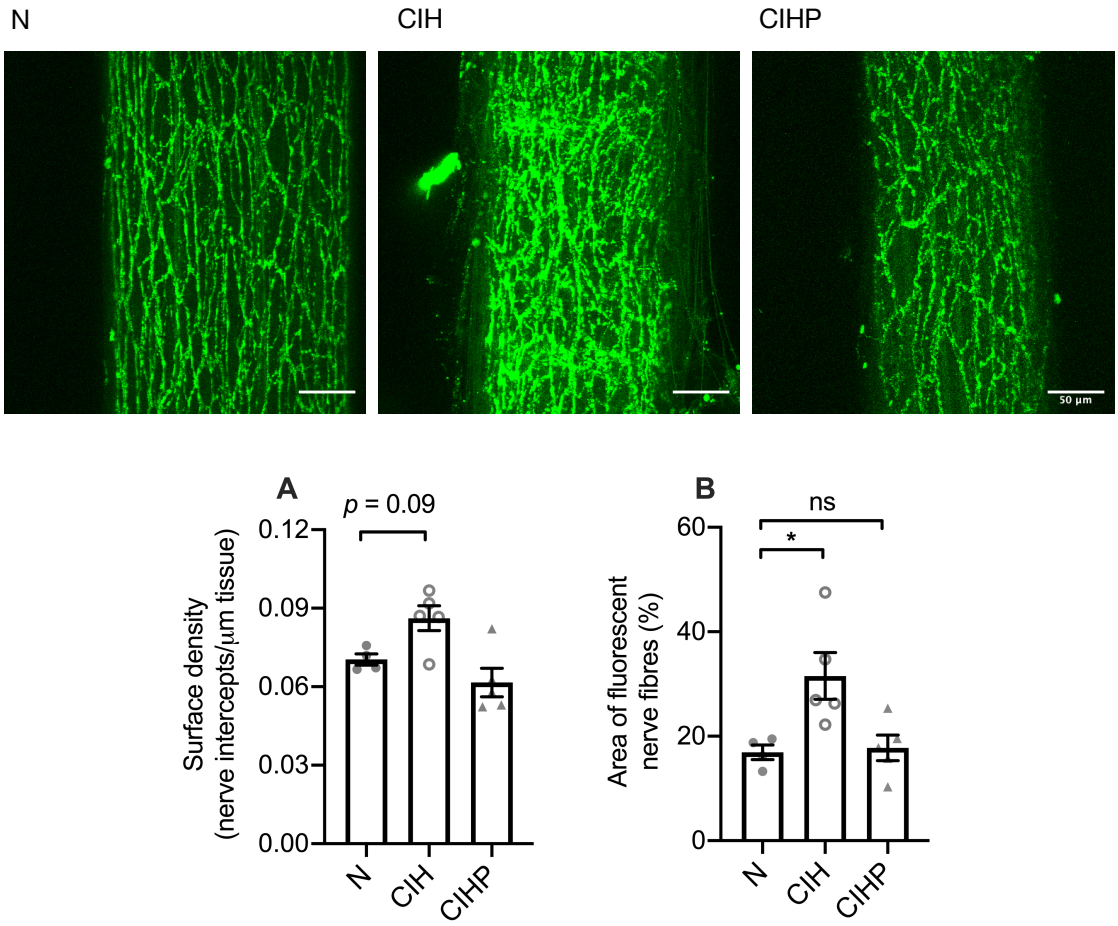


Figure 4.15: β-adrenoceptor inhibition prevents the CIH-induced increase in mesenteric periarterial sympathetic nerve density

Quantification of mesenteric periarterial sympathetic nerve density in a pre-clinical animal model of OSA. **(Top panel)** Representative images of periarterial mesenteric noradrenergic nerve fibres loaded with NTUA in rats exposed to N, CIH, and CIHP. CIH increased the density of surface sympathetic fibres, which was prevented with propranolol treatment. **(A)** Density, measured by the total number of nerve fibre intercepts/µm of tissue, was higher in CIH than N but it was not statistically significant. **(B)** CIH induction significantly increased the percentage of NTUA fluorescent area to total vascular area; this effect was prevented in CIHP.

Data presented as mean±SEM. Each datapoint in (A) corresponds to the mean surface density of 3 different areas of the same mesenteric artery, each counted on three separate days, and datapoint in (B) corresponds to the mean area of fluorescent fibres of 3 different areas of the same mesenteric artery, measured on one occasion. All micrographs: scale bar = 50 µm

Statistical analysis:
(A, B) Ordinary one-way ANOVA followed by Tukey's multiple comparisons test
* denotes $p<0.05$; ns denotes $p>0.05$

4.3. Discussion

4.3.1. Main findings

In this Chapter, the optimised NTUA technique was used to address several aspects of the physiology and pharmacology of single-terminal NAT regulation in the rodent cardiovascular system. I unveiled faster NAT reuptake rate in the rodent heart than in the MAs, and faster transporter function in mice compared to the rat, thus providing new insights into inter-tissue and inter-species differences in neuronal NAd clearance. I also discovered dynamic changes in NAT rate in response to sympathetic postganglionic nerve activity, in which the α_2AR appear to play suppressive role. Moreover, the possible autonomic crossover of NAT suppression from the parasympathetic arm was suggested by exogenous agonists but not in EFS conditions. These findings suggest the autonomic prejunctional regulation of NAT function is multifaceted and not as straightforward as one may think. Finally, CIH in the rat selectively accentuated cardiac NAT function and increased mesenteric periarterial innervation; the latter was reversed by βAR antagonism which identifies new mechanistic roles of disease progression.

4.3.2. NAT reuptake rate quantification method

4.3.2.1. Straight-line fit analysis

As demonstrated in Chapter III, the initial linear rise in NTUA fluorescence into sympathetic nerve terminals can be exploited as a measure of NAT function by straight-line fit analysis, analogous to previous work *in vitro* (Shanks *et al.*, 2013a) and *ex vivo* (Parker *et al.*, 2010). In the current work, the critical time points for linear uptake were empirically determined to restrict the duration of subsequent experiments, which ensured the economical use of NTUA.

However, some experimental manipulations had altered the linearity of NTUA accumulation compared to control conditions, for example to one that reached a premature plateau (example; Figure 4.6). Thus, forcing a straight-line fit through all the time points would underestimate NAT reuptake rate and/or oversee subtle changes in transporter regulation. Hence, I sought out to test a more sensitive method of analysis.

4.3.2.2. Non-linear curve fit analysis

The non-linear exponential one phase association curve fit method was chosen to analyse the NTUA uptake kinetic profile of each nerve terminal on an automated basis. This method provided two parameters: Y_{max} for the maximum NTUA fluorescence (plateau) and *k*, the rate constant. However, the strive for an economical use of NTUA came with a caveat with limited time points available in an experiment. Thus, the unconstrained curve fit of many terminals were unsuccessful (termed 'ambiguous' or 'interrupted' on GraphPad Prism), which led to its subsequent elimination from the analyses.

To maximise the utility of the total datapoints collected, the non-linear model was constrained to known Y_{max} values to help with the curve fit. However, it can be argued that each nerve terminal represents a single entity with a unique NAT reuptake profile, and that it cannot be assumed that all terminals would eventually plateau to the same Y_{max} value. While this is true, very high quantities of NTUA would otherwise be required identify the entire uptake profile of all terminals in all experiments of the current work. Future work is warranted to prolong the investigation of NTUA uptake beyond the initial linear phase, as this would also allow for optimum curve fit analysis of each terminal without constraining for variables.

If done correctly, the unconstrained curve fit method would be more sensitive than the straight-line fit to detect changes in NAT function; this would be helpful in cases where the linearity of uptake is compromised, and to provide insight into other uptake parameters, such as Y_{max}. In this work, the rate constant (*k*) was interpreted as the NAT rate of NTUA accumulation into the nerve terminal.

4.3.2.3. Summary

The straight-line method to quantify NAT reuptake rate is straightforward, though the results may be inaccurate in instances where the initial upslope is compromised by experimental conditions. The non-linear curve fit is a possible solution, though the caveat is that more time points are required for successful curve fits and as a result, significantly greater volumes of NTUA are required. In this Chapter, these analysis methods were utilised where deemed appropriate.

4.3.3. NAT rate is faster in the heart than the vasculature

4.3.3.1. Heart

4.3.3.1.1. Inter-chamber differences

Several studies have reported regional differences in cardiac NAd content, with the highest levels found in the atria and lowest levels in the ventricles in various species (Angelakos *et al.*, 1969, Novotny *et al.*, 2007, Wehrwein *et al.*, 2008). As NAT is the predominant method for junctional NAd clearance (Esler *et al.*, 1990), it may be that the transporter is more effective in the atria than the ventricles. Therefore, a heterogeneous single-terminal NAT reuptake rate pattern throughout the healthy heart was hypothesised.

Here, the non-linear curve fit revealed a two-fold faster single-terminal NAT reuptake rate in the atria than ventricles. To my knowledge, there is only one study that has investigated murine cardiac differences in NAT function, which reported analogous findings: "there was a 2-3 times higher retention of (NAT-mediated) [^{3}H]-NAd in the murine atria compared to the ventricles" [*personal communication with Dr Hahn, M. for Shirey-Rice et al. (2013)*]. However, the study investigated NAT reuptake on a macroscopic scale, which may have been confounded by differences in nerve density from the base of the heart towards the apex (Kimura *et al.*, 2012). Thus, the current study provides values for inter-chamber NAT rates at the spatial resolution of one single terminal independently of nerve density that had not been achieved elsewhere before.

One possible explanation for faster single-terminal atrial NAT rates than in the ventricles is the greater expression of NAT proteins per nerve terminal at the base of the heart than the apex. This is hypothesised on the basis that, sympathetic nerve density is highest in the former, particularly near the sinoatrial node which gradually declines towards the apex as it follows through the cardiac conduction system (Kimura *et al.*, 2012), thus a more efficient NAd clearance mechanism per terminal may be required for rhythm control. Surprisingly, binding studies with radiolabelled NAT antagonist, [^{3}H]-nisoxetine, demonstrated greater NAT density in the ventricles than atria (Wehrwein *et al.*, 2008). The negative correlation between nerve density and NAT density might therefore equate to a homogenous NAT surface expression per terminal within the heart. However, this is solely based on speculation and warrants further investigation.

The next hypothesis to explain for greater single-terminal NAT rates in the atrium is a faster intrinsic rate per transporter protein. However, to my knowledge, there are currently no studies that have directly addressed this question. Kinetics parameters of

'substrate molecules per transporter protein per second' or 'number of transport cycles per minute' are often reported in transfected cell culture studies (Apparsundaram *et al.*, 1998a, Paczkowski and Bryan-Lluka, 2002, Schwartz *et al.*, 2005) and membrane preparations from mammalian hearts (Raffel and Chen, 2004). Thus, future studies could investigate whether inter-chamber differences in single-terminal NAT rate originate from variations in intrinsic transporter kinetics.

4.3.3.1.2. Physiological relevance of cardiac heterogeneity

Several cardiac diseases exhibit chamber-specific NAT dysfunction phenotypes. For example, in animal models of left-sided or right-sided heart failure, the reductions in NAT density and/or NAT uptake of [^{3}H]-NAd in the affected chamber directly correlates with the regional-specific myocardial βAR downregulation (Liang *et al.*, 1989, Böhm *et al.*, 1998, Leineweber *et al.*, 2000). Importantly, myocardial βAR density remained unchanged in dogs with chronic infusion of NAd (Raum *et al.*, 1984), which suggest that the myocardial βAR density in heart failure is contributed vastly by localised NAT dysfunction (Beau and Saffitz, 1994). Interestingly, in socially isolated rats prone to stress-induced cardiovascular pathophysiology, there was an selective increase and decrease in NAT expression in the right- and left stellate ganglion, respectively (Jovanovic *et al.*, 2014); as the left sympathetic contributes vastly to LV pressure (Ng *et al.*, 2001), the regional reduction in NAT-mediated clearance may explain for the enhanced propensity for these rats to develop LV hypertrophy (Jovanovic *et al.*, 2019). Therefore, these studies highlight the importance of localised chamber heterogeneities in NAT function in pathological cardiac disease states; perhaps NTUA could be used as a tool to unveil further differences in neuroeffector function that may underlie chamber-specific disease progression.

Heterogeneities in NAT-mediated clearance in the left ventricular wall are also observed in human patients and experimental animal models of CVDs. For example, in human heart failure and idiopathic- and ischaemic cardiomyopathy, [^{3}H]-NAd uptake in the subendocardial layer was significantly less than in the subepicardial layer in non-infarct areas independently of nerve density, while the ratio was uniform in non-failing hearts (Beau and Saffitz, 1994). Moreover, analogous results were reported in Dahl salt-sensitive hypertensive rats corrected for ventricular distribution of [^{123}I]-MIBG (Nozawa *et al.*, 1998). The changes in transmural NAT function across the LV wall are thought to contribute to the electrical heterogeneities in malignant ventricular tachyarrhythmias seen in heart failure (Beau and Saffitz, 1994).

Ventricular fibrillation and sudden cardiac death with specific ECG abnormalities in the absence of cardiac structural defects are termed 'Brugada syndrome'. In a small study, 47% of those with Brugada syndrome exhibited regionally reduced [^{123}I]-MIBG in the inferior and septal LV wall, while no differences were observed in control patients (Wichter *et al.*, 2002). However, it is unclear whether this represents reduced intrinsic neuronal uptake or regional denervation. A murine model of Brugada Syndrome is currently available at the University of Birmingham (Kirchhof/Fabritz group), thus future investigations with NTUA would be helpful. NTUA could measure for differences in single-terminal NAT reuptake rate in areas of the LV wall in relation to changes in nerve density (after methodological refinement to overcome optical depth penetration). The resulting findings would be clinically relevant as Brugada syndrome patients are susceptible to sudden death, thus NTUA offers an opportunity to address important mechanistic questions.

4.3.3.1.3. Summary

Here, the first direct evidence of inter-chamber differences in single-terminal NAT reuptake rate is reported, where the atria possess faster NAT reuptake rates than the ventricles. Chamber-specific differences in NAT reuptake rate may be clinically relevant due to its role to drive localised disease progression. However, more time points are required to establish their full uptake profile to understand where these differences may lie, i.e., intrinsic transporter kinetics or NAT expression on the terminals.

4.3.3.2. Heart versus blood vessels

4.3.3.2.1. Cardiac dependence on NAT

The heart is regarded as the most reliant organ on the NAT for NAd clearance (Esler *et al.*, 1990). For example, NAT blockade by systemic administration of desipramine results in the greatest regional NAd spillover from the heart than forearm and kidneys, despite the suppressive central action of desipramine on sympathetic outflow (Esler *et al.*, 1990). Such tissue disparity may be explained by the width of the sympathetic neuroeffector junction; it is possible narrower clefts are present in the heart, so that there is less diffusion from the site of release and consequently greater reliance on NAT for reuptake. Indeed, ultrastructural studies demonstrate neuroeffector junctions in the rodent heart range from 10-30 nm, while the minimal distance in the arterioles and small arteries is 50-100 nm that increases with vessel diameter (Burnstock, 2008). Thus, it is likely the width of the junctional cleft contributes towards organ reliance on NAT to clear liberated NAd.

Here, I demonstrate a faster NAT reuptake rate in the heart compared to MAs in both rodent species with an exogenously applied NAT substrate. Analogous findings are

reported in humans with similar methodologies. For example, in the human, the NAT-mediated clearance of intravenously delivered [^{3}H]-NAd was predominately by the heart (69%) compared to the arm, leg, brain and lungs (35% total). Additionally, the concentration of the radioactive NAd metabolite, [^{3}H]-DHPG, in the great cardiac vein was significantly higher than in the respective arterial sample, while the pattern was reversed in other tissue beds (Goldstein *et al.*, 1988). This tissue asymmetry of neuronal NAd clearance may well be conserved across species, as analogous findings were also reported in the rat (Thackeray *et al.*, 2007, Barrett *et al.*, 2010) and non-human primate (Farde *et al.*, 1994). These findings suggest NAT function in the heart is important to remove both liberated NAd from sympathetic nerve terminals and circulating NAd.

Many studies, but not all, have controlled for confounding variables that could affect the quantification of NAT function in different tissues, such as organ mass and blood flow (Esler *et al.*, 1988). Here, the NTUA technique allows for NAT rate measurements independently of these factors at high spatial resolution. Similarly, in a study by Shanks and colleagues (2013a) the NTUA uptake rate into the rat isolated stellate postganglionic soma occurred at a rate of 3.8 arb.min^{-1}, while the celiac/superior mesenteric soma accumulated NTUA at a slower rate of 2.1 arb.min^{-1} (though statistical significance was not reported). The result, if significant, supports the current finding that sympathetic postganglionic neurones that innervate the heart has faster NAT-mediated clearance mechanisms than other tissues.

4.3.3.2.2. Physiological relevance of tissue heterogeneity

The high dependence of the heart on NAT for NAd removal indicates any abnormal changes to transporter function may result to catastrophic autonomic perturbations

more so in the heart compared to other organs. Indeed, in young pre-hypertensive rats there was a selective impairment of NAT function in the stellate sympathetic postganglionic soma compared to their counterpart controls, while no differences were found in ganglia innervating the abdominal organs (Shanks *et al.*, 2013a). Furthermore, in a clinical trial for atomoxetine (highly selective NAT inhibitor) to treat vasovagal syncope, the prevention from tilt-induced presyncope to syncope states were predominately due to the preservation of heart rate (HR), while systemic vascular resistance had remained unchanged (Sheldon *et al.*, 2019). Similarly, NAT reboxetine prevented entry into pre-syncope states in healthy subjects by sinus tachycardia (Schroeder *et al.*, 2006). These results suggest the NAT-mediated regulation of cardiac noradrenergic transmission is very important to preserve mean arterial blood pressure in those prone to syncope, and that NAT dysfunction in the heart may prevail in certain disease states compared to other organs.

4.3.3.3. Summary

Several *in vivo* studies have suggested the greater dependence of NAT-mediated NAd clearance in the heart compared to other organs, which have relied on macroscopic measurement techniques. Here, a similar conclusion was drawn at high spatiotemporal resolutions with the use of NTUA in the rodent heart and MAs. The great importance of NAT function in the heart may explain why any perturbations in autonomic function could lead to more catastrophic cardiac diseases compared to other tissues.

4.3.4. NAT kinetics is faster in mice than the rat

4.3.4.1. Faster NAT function in mice

In this study, single-terminal NAT reuptake rate was almost two-fold faster in murine tissues than in rat tissues. Interestingly, in rat tissues, there was a 2 min delay in NTUA accumulation from the time point of entry (Figure 3.12B, 3.23, 4.13). Although this could be explained by delays of NTUA penetration through a thicker pericardium in the rat heart, the delay also occurred in the MAs and may therefore be an inherent feature in the rat species compared to mice.

Currently, only one study demonstrates species differences in NAT-mediated uptake between rats and mice. In a study of perfused rodent hearts, Iversen and colleagues (1971) saw the uptake of [^{3}H]-NAd was 108.5 ng.ml^{-1}.g^{-1} into the murine heart compared to 53.8 ng.ml^{-1}.g^{-1} into the rat heart (though statistical significance was not reported). However, this study did not report differences in uptake in relation to time, thus any disparities in transporter rate in relation to exposure duration are unknown. While another group had investigated the stereospecificity of NAd uptake in these animals, the studies differed in their methodology thus the results could not be directly compared [rat: Krell and Patil (1972); mice: Garg *et al.* (1973)]. Nevertheless, the current study is the first to report species differences in NAT function at the spatiotemporal resolution of single sympathetic nerve terminals; the faster NAT reuptake rate in mice were present in both cardiac and vascular tissue.

4.3.4.2. Interspecies variation in NAT amino acid sequence

The interspecies differences in NAT rate could be explained by variations in intrinsic transporter kinetics. In cells transfected with species-specific NAT, the rate of substrate

translocation (V_{max}/B_{max} per unit time) was significantly greater by the rat NAT (rNAT) than the human NAT (hNAT), which was attributable to three non-conserved amino acid exchanges (from a total of 26), specifically at residues 7, 62 and 375 (Paczkowski and Bryan-Lluka, 2002). Similarly, significant differences in the transporter affinities for sodium ion and transporter substrates (NAd, cocaine) between rNAT, hNAT, and bovine NAT were attributed to slight differences in amino acid sequence (Paczkowski *et al.*, 1999). Finally, a 72-amino acid difference in the carboxyl end of another biogenic amine transporter, the dopamine transporter (DAT), has been hypothesised to explain functional differences between the hDAT and rDAT (Lee *et al.*, 1996). Thus, these studies suggest variations in the NAT amino acid sequence between rats and mice may explain for the observed faster NAT reuptake rate in the former species.

While there is a 90% amino acid homology between the rNAT and the murine NAT (Zerbino *et al.*, 2017), there are currently no studies that address the differences in their kinetic properties, such as ligand recognition, translocation, and ion dependence. Additionally, the current result could be contributed by interspecies differences in surface expression of NAT on each individual nerve terminal. To overcome this, future studies could investigate individual transporter function as 'substrate molecules per protein per second' or 'number of transport cycles per minute' as described in transfected cell lines (Apparsundaram *et al.*, 1998a, Paczkowski and Bryan-Lluka, 2002, Schwartz *et al.*, 2005).

4.3.4.3. Physiological relevance

Whether the interspecies variation in NAT function can contribute towards differences in autonomic control of cardiovascular function is unknown. However, it may relate to

species-specific mechanisms of autonomic cardiac control at rest. Sympathetic predominance of cardiac rhythmicity is well documented in the rodent; its influence to determine resting HR becomes less so in bigger rodents and other larger mammals [review on intrinsic HR, animal size and metabolic rate: Opthof (2000)]. For example, the resting HR in mice (600-720 BPM) is significantly higher than its intrinsic HR under combined autonomic blockade with mAChR and βAR inhibitors (~550 bpm) (Ishii *et al.*, 1996, Gehrmann *et al.*, 2000). The sympathetic predominance becomes less apparent in the rat where the spontaneous and intrinsic HR are similar, i.e. ~370 bpm and ~350 bpm, respectively (Carnevali *et al.*, 2013), and even less so in man where vagal predominance prevails (Jose and Collison, 1970).

Here, the assumption is that the extent of NAT function correlates with cardiac sympathetic predominance as an adaptive mechanism, i.e., the higher the sympathetic outflow at rest, the greater the NAT function. It is hypothesised that the sympathetic predominance to determine HR seen in rat>humans could correlate with the faster transporter cycle rates seen in the rNAT>hNAT transfected cells (Paczkowski and Bryan-Lluka, 2002) (section 4.3.4.2.). Therefore, it is tempting to also correlate the trend in NAT function seen in the current study (NTUA: mice>rat) with the species dependency of sympathetic predominance for resting HR (mice>rat). This leads to the speculation of whether the interspecies differences in NAT rate corresponds to a possible innate adaptive response to high sympathetic tone.

4.3.4.4. Summary

The interspecies differences in NAT reuptake rate have been rarely studied or reported in the literature. Here, I report consistently faster single-terminal NAT reuptake rate in murine tissues compared to the rat, which could be explained by variations in

transporter amino acid sequence, as seen with other species. The resulting differences in altered ligand recognition, translocation and ion dependence of transporter function may have implications upon the adaptive responses to sympathetic tone.

4.3.5. Prejunctional mAChR-mediated inhibition of cardiac NAT rate

4.3.5.1. Mechanism of mAChR-mediated reduction in NAT function

Sympathetic postganglionic nerve terminals are endowed with a repertoire of heteroreceptors that modulate neurotransmitter release, including the mAChRs. The mAChR-dependent cross inhibition of NAd release has been demonstrated by exogenous agonist application, in mAChR knockout animals (Trendelenburg *et al.*, 2003a, Bernhard *et al.*, 2004), and during dual autonomic nerve stimulation (Manabe *et al.*, 1991). In the current study, mAChR activation by exogenous agonists rapidly reduced NAT function in the murine heart in 6 min, paralleling previous reports from the laboratory in murine urogenital system (Parker *et al.*, 2010).

An analogous finding was reported in SK-N-SH (co-expressing NAT and mAChR) neuroblastoma cells; acute treatment with mAChR agonist methacholine (10 min) significantly reduced [^{3}H]-NAd uptake that was attributed to a reduction in [^{3}H]-nisoxetine binding sites (Apparsundaram *et al.*, 1998a). In the current study, there was a mAChR-mediated reduction in the maximum accumulation of NTUA (Y_{max}) with an unperturbed initial rate constant (*k*). Could these parameters provide insight into NAT expression and transporter intrinsic activity? Here, I speculate that mAChR agonists reduce NAT surface expression on the nerve terminal. This is based on the hypothesis that, as the NTUA concentration in the bath gradually transitions from 1:100 NTUA to 1:20 NTUA, only a subset of total NAT transporters facilitates the initial rise in

fluorescence. However, as the imaging bath becomes more concentrated with 1:20 NTUA, the downregulation of NAT prevents further accumulation of NTUA, thus resulting to a premature saturation of NAT transporters and a reduction in Y_{max}. If, however, mAChR activation suppressed the intrinsic transporter activity of all NAT, then a corresponding decline in the initial rate constant would be expected with an unperturbed Y_{max}, as eventually the available surface transporters would reach a similar level of saturation as in control conditions. However, the validity of this mechanism could be compromised by phototoxicity of NTUA during imaging (section 3.3.8.1.) and thus it is premature to conclude either mechanisms without conducting a Michaelis-Menten kinetics graph and/or radioligand binding studies.

In SK-N-SH cells, mAChR activation reduced [^{3}H]-nisoxetine binding sites without affecting membrane fractions of NAT, thus indicating transporter internalisation rather than protein degradation or reduced synthesis. The mAChR-induced NAT downregulation was predominately mediated by protein kinase C (PKC), with corroborated findings reported in SK-N-SH cells and NAT transfected HEK293 cells treated with PKC activator β-phorbol-12-myristate-13-acetate (β-PMA), in which the effect was prevented by PKC inhibitor staurosporine (Apparsundaram *et al.*, 1998a, 1998b). Moreover, in rat placental trophoblasts with endogenous NAT expression, surface expression of the transporter was significantly reduced by β-PMA in a time- and concentration-dependent manner, which corresponded to an attenuation in [^{3}H]-NAd uptake (Jayanthi *et al.*, 2004). Finally, transporter internalisation via a PKC-dependent pathway appears to be universal for biogenic amine transporters, as reported for HEK293-hSERT (Qian *et al.*, 1997) and PC12-hDAT (Loder and Melikian, 2003). Together, these studies demonstrate that the PKC-dependent NAT internalisation is a common native mechanism amongst biogenic amine transporters and may explain the

carbachol-mediated reduction in cardiac NAT reuptake function seen in the current study.

Which targets downstream of PKC signalling could lead to NAT surface downregulation? By mutating specific hNAT amino acids into those that cannot be phosphorylated (alanine), Jayanthi and colleagues (2006) identified that PKC specifically phosphorylates threonine 258 and serine 259 in rat placental trophoblast cells to internalise NAT. However, when the NAT transfected COS-7 cells were mutated at S259A, there were no changes in the β-PMA-mediated reduction in [^{3}H]-NAd uptake (Bönisch *et al.*, 1998). This difference could be explained by cell type, but also does point to other targets of NAT by PKC.

Another relevant target of PKC for NAT regulation is syntaxin1A, an essential SNARE protein present on the prejunctional membrane for excitation-secretion exocytosis. The surface expression of NAT is secured by its interactions with syntaxin 1A, which is thought to favour the synchrony between release and reuptake of the neurotransmitter. In both heterologous systems and native preparations, the methacholine-dependent PKC phosphorylation of the NAT N-terminus led to a dissociation between NAT and syntaxin1A which increased the propensity of redistribution of the transporter away from the surface membrane (Sung *et al.*, 2003). Given the similarities in NAT structure and function with other biogenic amine transporters, it is not surprising that transporter-syntaxin1A disruptions can also reduce surface expressions of DAT (Cervinski *et al.*, 2010) and SERT (Quick, 2002).

Together, these studies in the literature suggest that mAChR activation can induce a PKC-mediated NAT downregulation via several targets. However, to elucidate the exact

mechanism in the current study requires further investigations, particularly to answer the following questions: can PKC be sufficiently activated by endogenous acetylcholine in mature sympathetic nerve terminals to downregulate NAT expression?

4.3.5.2. mAChR subtype

In SK-N-SH cells, the methacholine-induced NAT internalisation was attributable to the M_3 mAChR subtype (Apparsundaram *et al.*, 1998a). However, the exact mAChR subtype in the current study is unknown. Some evidence suggests the prejunctional inhibitory mAChR for NAd release in the murine atria is of the M_2 and M_3 subtype (Trendelenburg *et al.*, 2005), thus the dual inhibitory effect of mAChR activation on NAd release and reuptake could be via similar receptor subtype and signalling pathways. Future experiments can incorporate selective mAChR antagonists in place of atropine, e.g., darifenacin (M_3), into the study to elucidate the mAChR subtype responsible for the suppressive effects upon NAT observed.

4.3.5.3. Physiological relevance of sympathetic-parasympathetic interplay

The physiological relevance for a mAChR-mediated reduction in NAT function is particularly important in the heart, where sympathetic and parasympathetic axons often run anatomically side-by-side (Kawano *et al.*, 2003, Hoard *et al.*, 2008). However, in addition to inhibitory mAChR subtypes (Trendelenburg *et al.*, 2005), there are also reports of facilitatory M_1-mAChR on sympathetic nerve terminals that will enhance NAd overflow when activated (Habermeier-Muth *et al.*, 1990, Costa and Majewski, 1991, Costa *et al.*, 1993). Thus, to determine the physiological net relevance of mAChR-mediated NAT suppression, it is important to elucidate the mAChR subtype responsible for the effect. If M_1 is activated, then the net result would be an accentuation in NAd

release, driven by a facilitation in release and reduction in NAd reuptake. On the other hand, the net effect of M_3 activation is unclear, as there would be concomitant reductions in release and reuptake.

Assuming the M_3 mode of activation, a simple interpretation would be that the inhibition of NAd uptake would partially negate or even reverse the cross-inhibition of release. The relative importance of the dual mechanism would depend on factors such as the spatiotemporal release of both ACh and NAd at once in the heart. For example, during periods of strong sympathetic and parasympathetic co-activation, termed 'autonomic conflict' [e.g. cold-water submersion (Paton *et al.*, 2005)], there is a higher tendency for arrhythmogenesis (Winter *et al.*, 2018). Therefore, the current study suggests a potential mechanism where autonomic co-activation would result in a cholinergic influence on sympathetic tone that might have implications upon cardiac electrical instability and vulnerability (Lavallée *et al.*, 1980).

4.3.5.4. Carbachol off-target effects

In the current study, the mAChR antagonist atropine did not completely reverse the effect of carbachol on the raw NTUA uptake trace to control conditions (Figure 4.6). One explanation is that atropine was used at inadequate concentrations to antagonise mAChRs. However, this is unlikely as the prepared atropine concentration was 500-5000 times greater than the K_i at rodent mAChRs (atropine: 1 μM vs. M_1-M_5: 0.0002-0.002 μM). This translates to a working concentration sufficient to occupy 99.9% of available mAChRs (Kashihara *et al.*, 1992, Armstrong *et al.*, 2019). Therefore, one would expect atropine to completely antagonise carbachol at the concentrations used.

Secondly, in addition to being a mAChR agonist, carbachol is also an agonist for the nicotinic acetylcholine receptors (nAChRs) (Armstrong *et al.*, 2019). Rapid application of the nAChR agonist, epibatidine, onto the murine vas deferens triggered action potential- and VGCC-independent excitatory junction potentials in smooth muscle cells indicative for neurotransmitter release (Williams *et al.*, 2011). Thus, it is possible the nAChR-triggered NAd release competed with NTUA to reduce its accumulation into sympathetic nerve terminals.

Thirdly, it is possible carbachol acts postjunctionally in the heart to release mediators for retrograde signalling back to nerve terminals to reduce NAT function. In the central nervous system, mAChR-induced retrograde signalling is important in the brain as it releases endocannabinoids to act upon presynaptic inhibitory cannabinoid receptors (Fukudome *et al.*, 2004, Thomsen *et al.*, 2018). However, such a role in the periphery, including the heart, has not yet been explored.

Finally, atropine was stored in its container for at least a few years with no clear indication of arrival date, thus a longer storage time is likely to have compromised chemical stability and explain for the incomplete reversal of NAT suppression in the current study.

4.3.5.5. Summary

In the current study, I demonstrated a mAChR-mediated suppression of cardiac NAT, which could have profound effects upon autonomic control of the heart. While it is unclear which mAChR subtype mediates NAT suppression, existing studies suggest for a M_3-mediated downregulation of NAT away from the surface membrane. Nevertheless,

elucidating the exact mAChR subtype is important to understand what the net physiological effect would be.

4.3.6. Suppression of NAT kinetics by sympathetic nerve activity

In this study, I demonstrate for the first time that acute SNA at physiological firing rates can rapidly suppresses cardiac NAT reuptake rate *ex vivo* at the spatiotemporal resolution of single noradrenergic nerve terminals. I also identified a modulator of NAT regulation: the sympathetic prejunctional α_2AR. Acting to rapidly suppress NAT rate during sympathetic APs concurrent to a reduction of NAd release, the α_2AR may induce a non-linear relationship between resting SNA and junctional NAd concentration. This finding suggests an additional layer of complexity and interconnectedness of multiple mechanisms that can govern release and reuptake and reminds us of the fact that sympathetic transmission seldomly relies upon the regulation of release alone. Finally, I demonstrate that at high concentrations, NAT substrates are likely to compete with and displace each other within the sympathetic nerve terminals, a factor which may have implications for the clinical interpretation of cardiac imaging studies.

4.3.6.1. Shortcomings of previous studies

Significant useful information regarding NAT function in response to membrane depolarisation have been obtained from *in vitro* systems, where an increase in transporter rate has been consistently observed (Savchenko *et al.*, 2003, Mandela and Ordway, 2006a, Habecker *et al.*, 2006, Sung *et al.*, 2017). However, most studies induced depolarisation with high [K^+] and it may not necessarily reflect transporter function during electrically evoked APs; this is because 1) sustained depolarisation over seconds or minutes does not adequately simulate the millisecond timescale of

sympathetic APs, and 2) the activation of protein kinases signalling pathways crucial for NAT regulation differs between phasic and chronic depolarising stimuli (Brosenitsch and Katz, 2001). Additionally, *in vitro* methodological settings may limit the translational aspect of transporter regulation in *in* ex/*vivo* systems, where paracrine- and retrograde signalling from other cell types may be significant (Mandela and Ordway, 2006b, Regehr *et al.*, 2009). Thus, it was pertinent to investigate transporter regulation in intact peripheral end organ preparations.

Unlike in *in vitro* systems, the observed effects of sympathetic neurone depolarisation on NAT function *ex/in vivo* has been unclear in the literature; some reported an accentuation (Gillis, 1963, Chang and Chiueh, 1969, Ungerer *et al.*, 1996), others a depression (Blakeley and Brown, 1964, Palaić and Panisset, 1969, Häggendal and Malmfors, 1969) and some found no effect (Kirpekar and Wakade, 1968a, Yamamoto and Kirpekar, 1972). These divergent results could be attributed to the variations in tissue-, species- and methodological choices employed. An example of the latter is stimulation span, whereby acute and chronic depolarisation has been shown to elicit distinct signalling pathways to regulate NAT, e.g., transporter membrane translocation and transcription, respectively (Savchenko *et al.*, 2003, Habecker *et al.*, 2006). As depolarising stimuli typically varied between 30 s to 1 h duration, differences in the activated intracellular pathways could add to the inconsistencies in the literature. Finally, traditional *ex/in vivo* studies of neuronal NAd clearance often relied on radiochemical or biochemical measurements that provide results with a significant delay after sample collection (hours to weeks). As the lifetime of NE in a released quantum is estimated to be 1.5-5 s (Gonon *et al.*, 1993, Stjärne, 2000), improved methods are required to capture the rapid change in transporter kinetics as acute events could be overlooked by end-point studies. Such techniques are available to detect NAT kinetics *in vitro* (Sung *et al.*,

2017) although inferences of transporter function in intact organs such as the heart is difficult to achieve due to the mixture of different peripheral neuronal types (Shivkumar and Ardell, 2016).

Here, I utilised the NTUA technique to dynamically measure NAT rate in single postganglionic sympathetic nerve terminals in response to electrically evoked AP propagation *ex vivo*. This optical technique suffices the requirement of high spatiotemporal resolution of single-terminal noradrenergic terminals and provides direct insights into the effect of SNA on NAT regulation. Most importantly, the current study also encompassed a broad range of firing frequencies that is typical of physiological activity, while most studies utilised those in the maximal range (5-30 Hz). I utilised 0.2-2 Hz, similar to the typical resting states in rodents [about 0.3-2.4 Hz (Häbler *et al.*, 1994)], rising to 5-10 Hz to represent maximal activity [about 6-8 Hz (Nilsson *et al.*, 1985)]. Encompassing a broad range of firing rates in one study should help elucidate NAT regulation in states from resting sympathetic tone to hyperactivation.

4.3.6.2. Sympathetic postganglionic nerve activity suppresses cardiac NAT kinetics ex vivo

In the current study, I demonstrate that EFS-induced sympathetic AP firing rates rapidly suppresses murine cardiac single-terminal NAT rate in a frequency-dependent manner. EFS delivered subthreshold for cardiomyocyte contraction (80% cardiomyocyte contraction threshold voltage; 0.1-0.2 ms pulse widths) was sufficient to elicit this effect. This further supports the greater excitability of neurones compared to cardiac muscle, as demonstrated by the approximate ten-fold briefer chronaxie (Struik, 2017) and the ten-fold lower rheobase (Reilly and Diamant, 2011). While I could not confirm AP

propagation simultaneously during imaging, I did observe sustained cardiomyocyte contraction in all tissue preparations when the EFS voltage was returned to 100%, thus suggesting EFS was delivered as intended during the protocol.

The finding differs to the observations of increased NAT-mediated inward currents in response to a 2 s depolarising step in single superior cervical ganglion (SCG) neurones (Sung *et al.*, 2017). In addition to the methodological limitations of *in vitro* studies, there is also evidence to suggest functional differences between the sympathetic SCG neurone somata and the nerve terminals in end-organs. Even within the SCG, there are subpopulation differences in AP mechanisms and modulatory responses to NAd between sympathetic secretomotor, pilomotor, and vasoconstrictor neurones (Li and Horn, 2008). More importantly, 1/3 of SCG neurone somata subpopulations lack the α_2AR-mediated inhibition of sympathetic neuronal excitability (Li and Horn, 2008) and 2/3 lack the expression of co-transmitter neuropeptide Y (NPY) (Gibbins, 1991). As these features are important well-established functional phenotypes of peripheral sympathetic postganglionic terminals in the heart (Wehrwein *et al.*, 2016), and that the (to my knowledge) *in vitro* SCG studies of NAT function did not distinguish between neuronal types, I believe such findings cannot be extrapolated with certainty beyond *in vitro* systems.

The current finding also differs with work by Shanks and colleagues (2013a), where there appeared to be a stimulation-evoked increase in NAT function in the rat sympathetic (cardiac) stellate ganglion (though statistical significance was not reported). This result could be due to intrinsic differences in NAT regulation between the somatic-dendritic sites and at the terminals. Firstly, [^{3}H]-DHPG is routinely measured in radiotracer dilution studies to detect for axoplasmic-specific uptake of [^{3}H]-NAd by

cardiac NAT *in vivo* (Eisenhofer *et al.*, 1991b); however, DHPG cannot be detected in the rat stellate with HPLC methods (Bayles *et al.*, 2019), thus suggesting for differences in uptake between ganglionic- and peripheral sites. Secondly, some sympathetic neurones in the SCG lack the α_2AR-mediated inhibition of sympathetic neuronal excitability (Li and Horn, 2008), thus if those in the stellate ganglia also lack α_2AR-mediated regulation, then it may explain why (the α_2AR-mediated) NAT suppression was not observed. Thirdly, it is also possible that AP-induced NAT regulation mechanisms are different between mice (current study) and rats [if present; Shanks *et al.* (2013a)]. At the time of this current thesis, whether a true difference in NAT function exists between the two sites still requires further work and statistical analyses. Thus, for now, while previous work on ganglia provides important functional implications for synaptic integration and ganglionic physiology; the current study at least adds new insight into AP-evoked modulation of neurotransmitter clearance at the end-organ where junctional NAd availability vastly determines the extent of neuromodulation.

4.3.6.3. Evoked [^{3}H]-NAd overflow experiments

To determine whether sympathetic nerve terminals were stimulated at 80% cardiomyocyte contraction threshold, evoked overflow of [^{3}H]-NAd was measured in analogous experimental conditions. The current results display a lack of correlation between stimulation and detected radioactivity, which is most likely explained by technical and methodological errors of the current experimental protocol.

Firstly, it is possible the heart preparations were not sufficiently loaded with tritium. Although the current study followed through established protocols for the isolated murine atrium (Trendelenburg *et al.*, 2003a, 2000, 2005, 2003b), some studies in other

tissues reported the requirement of a longer incubation period with tritium (Bernhard *et al.*, 2004). Furthermore, the current study utilised 2 Hz to deplete endogenous vesicular NAd and load [^{3}H]-NAd, which might not have been at a sufficient frequency to do so. In retrospect, the LA pieces should have been retained and solubilised at the end of the experiment to detect for tissue radioactivity to check whether loading was successful. Therefore, future studies could employ a longer tritium incubation period concomitantly to a higher stimulation protocol for maximum loading.

Secondly, it is possible the stimulation protocol did not elicit a detectable amount of the radioisotope that was collected in the superfusate. In a 2 mL superfusion bath in the current study, the evoked release of the radioisotope could have been diluted to undetectable amounts or the weak current within the bath could have prevented the wash off from the tissue into the superfusate. In the future, a methodological refinement could be to adopt a Langendorff perfusion set up, where the concentrated perfusate is collected instead.

Thirdly, the inconsistencies of radioactivity detected during the designated time points suggests for randomised stimulation events. However, this was not possible as close observations of cardiac contractile activity were made throughout the entire protocol, and that stimulation events occurred during the time points intended. Thus, there could not have been malfunctions of the EFS delivery from the isolated stimulation generator to the electrodes.

For the reasons outlined above, the results of the current study were not analysed, and the protocol was not taken further to investigate the effect of drug compounds on evoked NAd release. However, the fact that cardiomyocyte contraction was sustained

during fluorescence-based imaging when the voltage was returned to 100% threshold provides assurance that the EFS parameters were delivered as intended despite elimination of contraction artefacts.

Other methods to measure evoked release of NAd from sympathetic nerves include high performance liquid chromatography coupled to electrochemical detection [HPLC-ED; Ardell *et al.* (2019)], amperometry and cyclic voltammetry (Eisenhofer, 2001), all of which would require optimisation and validation for the experimental context required. Interestingly, to my knowledge, the use of enzyme-linked immunosorbent assay (ELISA) to detect for NAd overflow in superfusion set ups is yet to be established, though it would pose as an attractive alternative to tritium-based studies for health and safety and economic reasons.

4.3.6.4. α_2-adrenoceptor: a regulator of NAT kinetics?

The α_2AR are powerful autoreceptors that allow NAd to inhibit its own release from sympathetic terminals during neuronal activity (Starke, 2001); the murine α_{2A}AR and α_{2C}AR subtypes distinctly inhibit release at high- and low firing frequencies in the atria, respectively (Hein *et al.*, 1999). However, the effect of α_2AR on neuronal NAd clearance in the heart is unknown. The possibility that NAd autoreceptors can also regulate clearance is alluded by the fact that dopamine autoreceptors, D_2 and D_3 (also $G_{i/o}$-coupled), can rapidly regulate DAT function in rat striatal minces and *in vivo* (Meiergerd *et al.*, 1993). While α_2AR does not affect NAT in rat locus coeruleus (Callado and Stamford, 2000), transporter regulation by NAd autoreceptors may be different in the peripheral nervous system though there are currently no studies that have addressed this.

What is known, however, is that the activation of $G_{q/11}$- and $G_{i/o}$-coupled mAChRs on sympathetic nerve terminals can not only reduce neuronal excitability for autonomic cross-inhibition (Trendelenburg *et al.*, 2003a, Yang *et al.*, 2006), they can also suppress NAT rate [murine urogenital system: (Parker *et al.*, 2010); heart: section 4.3.5.]. Thus, it is possible that other $G_{q/11}$- or $G_{i/o}$-protein coupled receptors, α_2AR being an example of the latter, can also regulate NAT. This hypothesis was supported with the finding of an early reversal of EFS-mediated NAT suppression by the α_2AR antagonist yohimbine. 2 Hz was chosen because, even though the inhibitory EF_{50} of the stimulus-response effect on NAT was 0.9 Hz, the effect on NAT function at 1 Hz was not significant. Future studies could corroborate the present findings by exogenous application of α_2AR agonist, for example clonidine.

Although NAT is regulated by a plethora of protein kinase and phosphatases (Mandela and Ordway, 2006b), it is not clear by which mechanism(s) the $G_{i/o}$-protein coupled α_2AR acts to reduce NAT function. It may be that the reductions in the main $G_{i/o}$ secondary messengers, cyclic AMP and protein kinase A, exerts a direct effect on NAT, though its manipulations in either direction have produced contrasting observations in a strongly cell line- and species-dependent manner (Mandela and Ordway, 2006b).

An alternative mechanism is via the $G_{\beta\gamma}$ complex, which inhibits N-type VGCC open probability to reduce neuronal excitability [review: Starke (2001)]. The reduction in intracellular Ca^{2+} would in return lower the activities of Ca^{2+}-dependent kinases that can modify NAT regulation. Ca^{2+}/calmodulin-dependent kinases (CaMK) and p38 mitogen activated kinases are possible candidates for the effect observed, as activation of these kinases has been shown to increase NAT surface trafficking (Apparsundaram *et al.*, 2001, Sung *et al.*, 2017) (Figure 4.16). For example, the N-terminus of NAT can be

directly phosphorylated at threonine 30 by CaMKs to increase its surface expression (Sung *et al.*, 2017). The inhibitory effects on NAT are unlikely to be mediated by inwardly rectifying K^+ channels as they, unlike in the CNS, are not functional in native peripheral noradrenergic neurones (Ruiz-Velasco and Ikeda, 1998). Thus, changes in intracellular Ca^{2+} may be the most likely mechanism to suppress NAT. In addition to this, there is some evidence to suggest membrane potential can directly affect cardiac $uptake_2$, where cardiomyocyte $uptake_2$ is reduced (Ludwig *et al.*, 1986) or accentuated (Bryan-Lluka and Vuocolo, 1992, Bönisch *et al.*, 1985) in depolarised or hyperpolarised states, respectively. Therefore, there might be direct effects of ionic imbalances and membrane potential upon NAT kinetics. However, the exact downstream intracellular pathways of α_2AR were not investigated further, thus it could form the basis of future studies to elucidate the pathways for the effect observed.

4.3.6.5. Physiological relevance of α_2-adrenoceptor-mediated NAT inhibition

There are a host of regulatory mechanism for sympathetic junctional transmission, including feedback mechanisms mediated by NPY and other co-transmitters [for review, see Burnstock (2013)], but amongst these the α_2AR-mediated pathways are central (Stjärne, 1989). The α_2AR is an important suppressor of NAd release and their dysfunctions are often associated with sympathetic overactivity (Gilsbach and Hein, 2012), thus one would query the its suppressive role on NAT during AP propagation.

I suggest that α_2AR would be an important mediator to modulate and maintain appropriate junctional NAd concentrations crucial for cardiac function. At low resting SNA, single quanta are released randomly at very low probability, about 0.2-2% per varicosity (Åstrand and Stjärne, 1989), with highly efficient junctional clearance to

ensure that low levels of activity are virtually ignored (Stjärne *et al.*, 1993, Stjärne *et al.*, 1994). However, at very high frequencies where release probability increases due to frequency facilitation [a form of short-term junctional potentiation (Brain and Bennett, 1997)], junctional NAd clearance consequently becomes saturated (Stjärne *et al.*, 1993, Stjärne and Stjärne, 1995) which can lead to a non-linear relationship between SNA and junctional NAd concentration. This was demonstrated through the use of amperometry in the rat tail artery by Stjärne and colleagues (1993, 1995).

In the current study, it is demonstrated that even before transporter saturation occurs, prejunctional α_2AR could suppress NAT transporter rate, bringing the occurrence of non-linearity within the physiological range of sympathetic activity. This increase in junctional gain at physiological AP firing frequencies would in return increase the metabolic efficiency of junctional neurotransmission (Figure 4.16); by transiently suppressing uptake, fewer quanta are needed sustain sympathetic cardiac modulation. Otherwise, it would be metabolically inefficient for nerve terminals to release quanta great enough to sustain neurogenic contraction at each and every stimulus, only for it to be cleared away before the subsequent stimulus and repeat; it is plausible the α_2AR acts to set a level of NAd availability within the junctional cleft.

It is recognised the α_2AR antagonist, yohimbine, was not able to completely reverse the effects of nerve stimulation on transporter function (Figure 4.9A), though this could be explained that another mechanism, presumably substrate competition (section 4.3.6.7.), prevails to influence transporter kinetics during longer trains of stimuli.

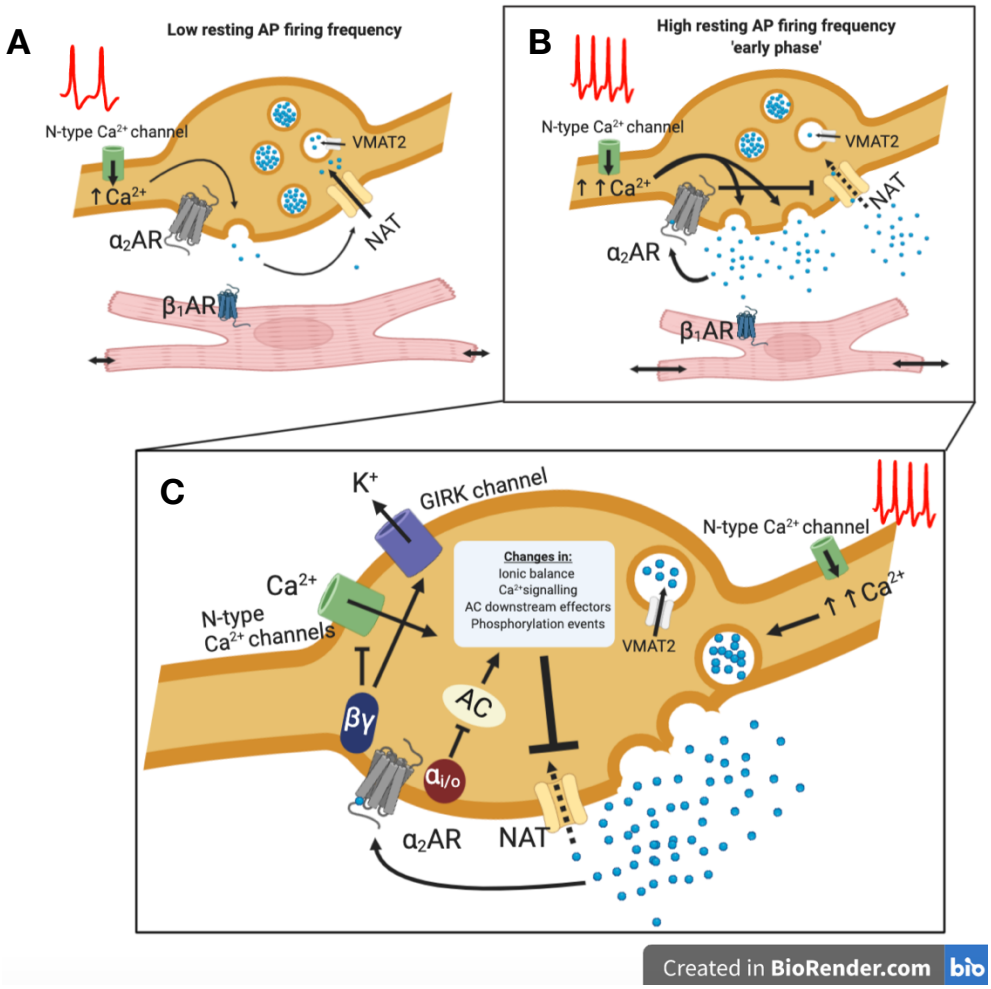


Figure 4.16: Simplistic schematic diagram of α_2-adrenoceptor-mediated NAT rate suppression during resting sympathetic neuronal activity

(A) At low resting sympathetic activity, single quanta of NAd are released at very low probability, and the efficient clearance by NAT means that low levels of activity are virtually ignored. **(B)** At high resting sympathetic firing frequencies where NAd release is high, but before NAT saturation occurs, the α_2-AR can suppress NAT rate thus producing a non-linear relationship between neuronal activity and junctional NAd availability. **(C)** α_2-adrenoceptor-mediated NAT rate suppression could occur via several mechanisms (but not restricted to): downstream effects of G_α-mediated inhibition of AC and downstream effects of $G_{\beta\gamma}$-mediated inhibition of N-type Ca^{2+} channels and activation of GIRK. This prompts further investigation.

Schematic was adapted with concepts from the following sources: Stjärne and colleagues (1993, 1994), Mandela and Ordway (2006b) and this current study.

Abbreviations: action potential, AP; α_2-adrenoceptor, α_2AR; noradrenaline transporter, NAT; β_1-adrenoceptor, β_1AR; G-protein coupled inwardly rectifying potassium channel, GIRK; vesicular monoamine transporter 2, VMAT2.

Note: the diagram is intended to demonstrate some of the possible EFS-induced downstream mechanisms to regulate NAT alone, rather than total noradrenergic transmission.

4.3.6.6. No mAChR-mediated effect on NAT during sympathetic nerve activity

It is likely the current EFS conditions also depolarised parasympathetic nerve terminals in the heart. However, while a mAChR-mediated reduction in NAT reuptake was demonstrated with an exogenous agonist in the murine vas deferens (Parker *et al.*, 2010) and the heart (section 4.2.4.), the current EFS conditions showed no evidence for autonomic interactions from parasympathetic to sympathetic nerve terminals via NAT inhibition, as atropine treatment during EFS had no additional effect on NAT rate (Figure 4.9).

Several reasons could explain for this. It is quite possible that within the fields of vision, sympathetic and parasympathetic nerve terminals did not run together in close enough proximity for the released ACh to diffuse across to the NAT on the surface of sympathetic nerve terminals. However, immunohistochemical studies have revealed that single nerve fibres of the two autonomic divisions often run parallel in the epicardium and myocardium side by side [mice heart: (Harden, 2009)] at such a close distance that would suggest some form of prejunctional communication ought to be present.

The next possible explanation is that the liberated ACh during EFS in the current conditions was not sufficient to activate inhibitory mAChRs. Even though a mAChR-mediated reduction in NAT was observed with 10 μM carbachol [Parker *et al.* (2010), section 4.2.4.], the concentration of ACh released into the junctional cleft evoked by the current EFS parameters (if any at 2 Hz) is unknown. In the context of a vagally-mediated inhibition of NAd release, however, its functional implications has been suggested to only be relevant when large amounts of ACh is released (Kimura *et al.*, 1985) during strong bouts parasympathetic activation. For example, a mAChR-mediated reduction

in NAd release in the mouse iris-ciliary body of was only detectable when cholinesterase inhibitors were included (Bernhard *et al.*, 2004). Thus, it is possible a muscarinic effect upon NAT function is likewise only detectable in conditions of high ACh concentrations, rather than at physiological conditions during sympathetic nerve stimulation as presented in the current study.

Finally, even if there was a muscarinic effect imposed upon NAT during EFS, it would be difficult to extrapolate such findings into a physiological context due to the experimental limitations of the study. Stimulation of the two autonomic arms *in vivo* occurs at discrete patterns of different frequencies (Fuder and Muscholl, 1995), where the inhibitory effect of ACh on NAd release in the rabbit only was only detected when the vagus nerve was stimulated at twice the frequency of the sympathetic chain (Löffelholz and Muscholl, 1970). However, in the current study, both autonomic arms were stimulated at set EFS parameters intended to mimic the physiological sympathetic firing frequencies. In the future, perhaps the best model to investigate prejunctional vagosympathetic interactions would be from *in vivo* experiments where the autonomic arms are activated by reflexes (Lavallée *et al.*, 1980) rather than artificial stimulation patterns.

In summary, the most likely explanation for an absence of the mAChR-mediated effect upon NAT is that the EFS parameters were not sufficient to release ACh in adequate concentrations to induce a response.

4.3.6.7. Substrate competition at NAT

NAd released by EFS is likely to compete with the NTUA fluorophore for transport; the current results with exogenously applied NAd supports this. Firstly, a complete abolition of NAT rate was demonstrated with exogenous NAd (1 μM) at a concentration that maximally increases rodent left atrial tension [pEC_{50}: 6.8 (Oostendorp and Kaumann, 2000)] (Figure 4.10). Furthermore, exogenous NAd only displaced NTUA at concentrations close to 1 μM (EC_{50}: 0.8 μM), while no effect was observed at NAd concentrations ten-fold lower (0.1 μM) (Figure 4.11). Additionally, when the inhibition of α_2AR was maintained after the initial 'early phase' of NAT uptake (and hence NAd release probability was high), the transporter-mediated uptake of the NTUA approached a premature plateau (Figure 4.9) where the peak accumulation of the fluorophore was poor. This suggests the gradual increase in junctional NAd attributed to α_2AR inhibition during EFS ultimately led to sufficient NAd concentrations to compete with the fluorophore at the transporter site. Together, these findings imply that, while α_2AR initially mediates NAT suppression during fluctuations in physiological firing frequencies, substrate competition comes to dominate suppression after several minutes of sustained stimulation (at least at 2 Hz when exocytosis is high in the presence of yohimbine), and at higher frequency stimulation frequencies (Stjärne *et al.*, 1993, 1994).

4.3.6.8. Clinical implications of activity-dependent NAT suppression

Hypertension, at least in SHRs, can be experimentally induced by either a loss of α_2AR-mediated negative feedback (Zugck *et al.*, 2003) or NAT impairment (Shanks *et al.*, 2013a, Shanks *et al.*, 2013b), thus implying that changes in both α_2AR and NAT function are clinically important for hypertension. Hence, it would be very interesting to determine whether the α_2AR-NAT coupling we demonstrate here in the healthy rodent is altered during the pathogenesis in SHRs. The current study demonstrated for an EFS-

induced, α_2AR-mediated NAT suppression at 2 Hz – a frequency representative of high resting states of sympathetic postganglionic firing. Whether the same effect is observed at 10 Hz (maximal activity recorded in the rodent) is unknown and requires further study. If so, the NAT suppression could add to the sympathetic hyperactive state seen in some cardiovascular diseases. It is important to note that sympathetic nerve firing can also liberate co-transmitter ATP and neuropeptides (NPY and galanin) that can jointly accentuate cardiac function (Herring, 2015). For example, the NPY receptor, Y_2, is localised on vagal neurones in the SA node that, when activated, reduces the heart rate response to vagal nerve stimulation (Herring *et al.*, 2008). Moreover, NPY receptor, Y_1, is present on cardiomyocytes and its activation can alter ionic handling, such as an increase in the size of intracellular calcium transients (Heredia Mdel *et al.*, 2005), which can contribute to the increase risk for ventricular fibrillation independently of βAR blockade (Kalla *et al.*, 2020). Like NPY, galanin can bind onto $GalR_1$ on vagal nerve endings to reduce ACh release and the subsequent bradycardia at the SA node via a PKC-dependent mechanism even in the presence of βAR blockade (Herring *et al.*, 2012). Thus, at high sympathetic firing frequencies, an increase in junctional availability of NAd due to α_2AR-mediated NAT suppression (if present) may only contribute to some effects seen in disease, but not all.

The current results drive the speculation that cardiac clinical imaging studies involving NAT tracer substrates, such as [^{123}I]-MIBG, under high sympathetic tone may be affected by both the α_2AR-mediated NAT inhibition and substrate competition. Interestingly, decreased NAT tracer uptake is often observed in patients with noradrenergic overactivation, such as myocardial infarction and stress-induced cardiomyopathies (Schroeder and Jordan, 2012). What is often unknown, however, is whether these patients have reduced NAT expression (due to terminal loss) or whether

NAT transporter activity had been transiently suppressed by the mechanisms we have described. The current findings suggest that NAT inhibition or substrate competition under high sympathetic tone could inhibit [^{123}I]-MIBG uptake, and so confounding the interpretation of clinical imaging studies.

4.3.6.9. Attempt to inhibit NAd release during sympathetic nerve activity

Due to the activation of a plethora of intracellular processes secondary to liberated NAd during EFS [i.e., α_2AR activation and NAd substrate competition], it was of particular interest to investigate NAT function independently from the neurotransmitter. Colchicine, a microtubule destabilising agent, has been reported to reduce the evoked release of [^{3}H]-NAd from the guinea pig atria by 50% (Sorimachi *et al.*, 1973), presumably by interfering with the excitation-secretion coupling step that modulates vesicular movement, fusion, and neurotransmitter exocytosis. Thus, colchicine posed as an attractive option to investigate the effect of AP propagation on NAT function in the absence of NAd release. However, the current study showed that colchicine had compromised NAT function even in non-stimulating conditions. Analogous findings were reported in the CNS and PNS, where the NAT-mediated uptakes of [^{3}H]-NAd into the rat brain synaptosomes and perfused heart were significantly attenuated by colchicine (Nicklas *et al.*, 1973, Hanbauer *et al.*, 1974), though which mechanism might colchicine be acting through?

There is interesting evidence that NAT trafficking and intrinsic transporter activity can be modulated by its interaction with SNARE proteins, such as syntaxin1A (Sung *et al.*, 2003), SNAP25, and synaptophysin (Schroeter *et al.*, 2000). It is thought that exocytotic membrane fusion events leading to neurotransmitter release will simultaneously insert NAT into the plasma membrane at the site of release for efficient reuptake (Mandela and

Ordway, 2006b), though NAT may also derive from non-exocytotic vesicles (Matthies *et al.*, 2009). Nevertheless, for rapid exocytotic events (occurring on the order of milliseconds), the cytoskeleton is pertinent for pre-fusion vesicular docking to the neuronal membrane (Porat-Shliom *et al.*, 2013); in particular, microtubules are essential for exocytotic organelles to reach the membrane over long distances for docking (Plattner *et al.*, 1982). Therefore, it is plausible that colchicine, a microtubule destabilising agent, prevented the trafficking of NAT-containing vesicles to the membrane for its stable interactions with syntaxin1A.

During the current study, the use of botulinum neurotoxin (BoNT) A to inhibit release was also considered. BoNTs are best known to cleave SNARE proteins to prevent the release of ACh into the neuromuscular junction (Montecucco and Molgó, 2005), though its use to inhibit noradrenergic neurotransmission has been reported in various isolated tissues (Rand and Whaler, 1965). However, BoNTs can also cleave syntaxin1A at the plasma membrane (Peng *et al.*, 2013), thus like colchicine, BoNT were also unsuitable to investigate NAT regulation.

It appears that NAT surface localisation and activity are readily regulated by intracellular processes and proteins involved in vesicular fusion. Therefore, investigating NAT regulation independently from evoked release of NAd during neuronal activity is not straightforward, and requires innovative ideas to isolate the effect of intrinsic NAT activity induced by AP independently of neurotransmitter release.

4.3.6.10. Summary

In summary, this study utilised an optical fluorescence-based technique to detect for a frequency-dependent suppression of NAT reuptake rate during physiological

sympathetic firing activity. The technique overcame the methodological limitations associated with previous studies of membrane depolarisation and NAT, provide new insights into the regulation of transporter function at the site of release. The study also uncovers a role for the prejunctional α_2AR to suppress NAd clearance during neuronal activity, which may evoke a non-linear relationship between resting sympathetic nerve activity and junctional NAd concentration. Finally, the current findings propose reasons for the reconsideration of clinical imaging interpretations with NAT tracer substrates. Finally, it would be of particular interest to investigate the effects of action potential propagation upon intrinsic NAT activity independent from the effects by NAd, though the decoupling of release and reuptake would not be straightforward.

4.3.7. NAT kinetics and sympathetic innervation in chronic intermittent hypoxia

4.3.7.1. Brief account of CIH-induced cardiovascular pathophysiology

In the current study, NAT function in the heart and MAs of a pre-clinical rodent model of OSA was measured with NTUA. Rats were exposed to CIH for 21 days to mimic the hypoxic events during sleep. Concurrent to this, researchers elsewhere in the College also investigated CIH-induced alterations in CB chemoreception and cardiorespiratory parameters. The results are summarised briefly in Table 4.1., and full details found in Alzahrani *et al.* (2020) (Appendix C). All data (with the exception of NTUA) were collected by the Birmingham Hypoxia and Arterial Chemoreceptor group.

OSA is the most common sleep-breathing disorder, and it is an independent risk factor for cardiac arrhythmias, tachycardia, and hypertension (Huang *et al.*, 2020). By exposing animal models to CIH to mimic the hypoxic events during sleep, the chemoreflex-mediated sympathetic overactivation and autonomic remodelling in CVDs

can be explored [see review: Huang *et al.* (2020)]. However, to date, there has been no indication to suggest cardiac NAd clearance mechanisms are perturbed in CIH.

Parameters	**Effect of CIH (compared to normoxia control animals)**		
Chemoafferent	**Baseline**	**Frequency (Hz)**	**↑***
	Evoked (*in vitro*)	Peak/sustained frequency (Hz)	-
		Nitrite sensitivity (ΔHz)	**↑***
		CO_2 sensitivity (ΔHz)	-
Respiratory	**Baseline**	Tidal volume ($mL.g^{-1}$)	-
		Respiratory frequency (min^{-1})	-
		Minute ventilation ($mL.g^{-1}.min^{-1}$)	**↑***
	Evoked (hypoxia, *in vivo*)	Tidal volume ($mL.g^{-1}$)	-
		Respiratory frequency (min^{-1})	-
		Minute ventilation ($mL.g^{-1}.min^{-1}$)	-
Cardiovascular	**Baseline**	**Mean arterial blood pressure (mmHg)**	**↑**
		Heart rate (bpm)	-
	Evoked (hypoxia, *in vivo*)	**Mean arterial blood pressure (mmHg)**	**↑**
		Heart rate (bpm)	-
Sympathetic (vasculature)		Area of nerve density (%)	-
		Intercepts of nerve density ($.\mu m^{-1}$)	**↑***
		NAT reuptake rate ($\%.min^{-1}$)	-

Table 4.1. Changes in chemoafferent sensory activity, cardiorespiratory parameters, and sympathetic nerve function in CIH

* denotes changes reversed by nonselective βAR antagonist, propranolol. Significant changes are marked in red. Data extracted from Alzahrani *et al.* (2020) and Appendix C.

4.3.7.2. CIH and NAT reuptake rate: heart

In the current study, CIH greatly accentuated cardiac single-terminal NAT function, which could be an adaptive response to a surge in sympathetic activation that occurs in the pathology (Huang *et al.*, 2020). There is a sympathetic predominance in OSA patients, as seen by an increase in the LF component of the LF/HF ratio from heart rate variability analysis (Zhong *et al.*, 2005), likely to be driven by the increased sensitisation and output from pre-sympathetic fibres located in the rostral ventrolateral medulla (Moraes *et al.*, 2013) and paraventricular nucleus (Li *et al.*, 2018). As a result, the persistent stimulation of sympathetic pre- and postganglionic neurones may induce changes in the termination mechanisms of noradrenergic neurotransmission at the end organ.

The upregulation of NAT function in response to prolonged, chronic stimulation has been demonstrated in various studies *in vitro*. Itoh and colleagues (2010) show that exposure of cultured bovine adrenal medullary cells to nicotine over the span of 1-5 days led an increase in NAT intrinsic activity. Similarly, chronic depolarisation elevates surface NAT expression (Habecker *et al.*, 2006). Interestingly, in addition to an upregulation of catecholamine biosynthesis in CIH/OSA human patients (Snow *et al.*, 2009, Zhao *et al.*, 2014), key mediators for NAd metabolism, such as monoamine oxidase A, is also significantly increased (Snow *et al.*, 2009). Therefore, it is possible the machinery for neuronal NAd clearance is also upregulated to increase the efficiency of reuptake for its subsequent catabolism in CIH. Upregulation of NAT function could also be attributable to changes in the modulators of the transporter. For example, nitric oxide (NO) can reduce NAT function by either direct nitrosylation of NAT (Kaye *et al.*, 2000) or (hypothetically) by the inhibition the Na^+/K^+ ATPase (Liang and Knox, 1999), which the latter could attenuate the sodium gradient that is required by NAT for its secondary

active process. Interestingly, intermittent hypoxia reduces neuronal NOS (nNOS) activity in the RA of guinea pigs (Mohan *et al.*, 2001). Could the reduction in NO availability attenuate the inhibitory effect on NAT, and therefore explain for the heightened function seen in this study?

The upregulation of NAT function suggests NAd clearance is higher in CIH animals compared to those kept in normoxia. Could this observation suggest why HR was not augmented by CIH in this joint study (Table 4.1)? Perhaps the increase in cardiac NAT function in CIH was able to prevent deleterious effects of liberated NAd on cardiac function. However, net sympathetic transmission rarely relies upon NAd clearance alone; rather it is a combined effect of junctional NAd (and other transmitters; NPY, galanin, etc.) availability, sensitivity of the postjunctional effector organ, amongst other factors. For example, a decrease availability of nNOS in sympathetic nerve terminals can also enhance neurotransmitter release by elevations in N-type Ca^{2+} channel Ca^{2+} conductance, and thus may contribute to increased firing rate and spike amplitude observed in disease (Bardsley and Paterson, 2020). As discussed previously, an increase in sympathetic nerve firing frequency can also liberate neuropeptides NPY and galanin, in which the former is pro-arrhythmic by its pre- and postjunctional targets (Kalla *et al.*, 2020), and both can reduce the vagally-mediated bradycardia by their actions on parasympathetic nerve terminals (Herring, 2015). An interesting future prospect of where the current work could lead to is whether CIH may increase the risk of atrial fibrillation (AF), an index that was not investigated in the present study due to blood pressure recordings to derive HR.

Pilot data from the Birmingham Hypoxia and Arterial Chemoreceptor group have revealed that the CIH-induced pro-arrhythmic changes in left atrial electrophysiology

are reminiscent of excessive sympathetic nerve stimulation (*Holmes, A.P., unpublished data*). Furthermore, cardiac sympathetic denervation by resection of the stellate ganglion prevents AF vulnerabilities in CIH-induced rats (Yang *et al.*, 2019). Therefore, it could be that CIH animals in the current study were susceptible to AF due to sympathetic overactivity. However, it is unknown how (or if) the increase in NAT function in this study could contribute to the induction of electrical heterogeneities. Therefore, more in-depth analysis and investigations of cardiac innervation, sympathetic outflow to the heart, plasma NAd overflow, etc., is required to build a more comprehensive view of how the balance between release and reuptake is implicated in CIH-induced cardiac pathologies.

4.3.7.3. Propranolol prevents CIH-induced elevated vascular sympathetic nerve density

In contrast to the findings in the heart, there were no aberrations in single-terminal periarterial NAT function induced by CIH on the surface of mesenteric arteries. What was profound, however, was the increase in periarterial sympathetic nerve density in these animals, which is analogous to previous findings of arterial hyperinnervation in the tibial and sural arteries following CIH-induction in adult rats (Lucking *et al.*, 2014) and young rats exposed to chronic hypoxia in utero (Rook *et al.*, 2014). This, and an accentuation in cardiac sympathetic innervation reported in other studies (Zhao *et al.*, 2014, Sun *et al.*, 2017, Yang *et al.*, 2019), suggest a universal CIH-mediated peripheral nerve growth phenomenon in the cardiovascular system. However, changes in cardiac innervation in response to CIH were not investigated here, though it forms the foundation for future studies.

The functional implications of arterial hyperinnervation are unclear. In the current joint study, the CIH-induced vascular hyperinnervation could have contributed towards to the increase in mean arterial blood pressure (Table 4.1) by the means of raising total peripheral resistance. As a result, this would lead to an increase in hypertensive states as observed in adult OSA patients and experimental animal models (Beaudin *et al.*, 2017). However, Lucking and colleagues (2014) (who also noted vascular hyperinnervation) and Silva and Schreihofer (2011) repudiate this by reporting significant blunting in vascular sensitivity to stimulation in CIH animals, while others reported no significant differences of vessel reactivity in the mesenteric bed (Lefebvre *et al.*, 2006). Therefore, for now, the contribution of vascular hyperinnervation (if any) towards the hypertensive state of CIH in this current study is unclear and requires further study.

Interestingly, the increase in vascular sympathetic nerve density was significantly prevented by propranolol thereby suggesting a βAR-mediated mechanism of nerve growth. The downstream βAR pathway for sympathetic hyperinnervation is unclear, though a previous study suggests that the βAR-dependent cardiac (atria) sympathetic remodelling in CIH could be attributable to activation of myocardial energy metabolism pathways (Sun *et al.*, 2017). In addition, as the Birmingham Hypoxia group detected for βAR in CB type I glomus cells, it is also possible the arterial hyperinnervation is secondary to an increase in chemoreceptor sensitivity in CIH (Alzahrani *et al.*, 2020), (Table 4.1).

Another mechanism for CIH-induced vascular hyperinnervation is the direct effect of transient ischemia on nerve growth. In CIH, the pro-oxidant hypoxia inducible factor 1α (HIF-1α) can trigger the activation of numerous mediators of sympathetic nerve growth, such as endothelin-1 and neurotrophic growth factors (Ieda *et al.*, 2004). HIF-1α also

downregulates the chemorepellent of axonal outgrowth, semaphoring 3A, to further encourage sympathetic nerve sprouting (Hu *et al.*, 2016). Therefore, it is also likely that the global hypoxic effects directly at the end organ led to its hyperinnervation. Interestingly, the HIF-1α-mediated sympathetic nerve hyperinnervation in the heart can be elicited by a paracrine effect. Following localised tissue hypoxia in the heart induced by myocardial infarction, HIF-1α are produced by epicardial cells near the site of damage to promote nerve growth in and around the area (Ge *et al.*, 2020). Therefore, future studies could identify whether cardiac hyperinnervation in CIH is driven by global release of HIF-1α by epicardial cells or by a βAR-dependent mechanism, as seen with the mesenteric arteries.

4.3.7.4. Summary

In summary, this study reveals that CIH substantially increases single terminal NAT function in the heart. While there were with no perturbations in NAT function on the periarterial surface of mesenteric arteries, CIH induced periarterial sympathetic hyperinnervation via a βAR pathway. These findings coupled with the chemosensory activities and cardiorespiratory parameters may reveal possible mechanisms of the disease phenotype. However, with respect to the autonomic mechanisms that may govern this, the current results on NAT function remain preliminary with plentiful of future experiments required to consolidate such findings.

4.3.8. Limitations

4.3.8.1. Analysis methods of NAT reuptake rate

A limitation of the current work is the restricted number of time points for NTUA accumulation in all studies. This led to shortcomings associated with the analysis

methods, which could have been overcome by longer NTUA superfusion protocols. For example, the non-linear curve fit was often unsuccessful due to the failure to establish the full timeline of NTUA accumulation. In the current work, this was overcome by constraining the model to known values, i.e., Y_{max}, to maximise the number of rate constant values extracted.

However, in the interest of the current study, it was important to maintain the economical use of NTUA as large volumes were used for the present experiments. To put into context, if the n=4 count was maintained in an experiment set of 3 groups, then by doubling the volume of NTUA required for one experiment to gain 6 more time points would mean 1 order from Molecular Devices would only facilitate 2 experimental sets. As this body of work focused on the initial kinetics of NAT function, NTUA accumulation was captured in the first few min to reduce the volume of the assay required.

4.3.8.2. Sympathetic nerve activity and NAT function

There was great variability of single-terminal NAT reuptake rate in response to EFS, where NAT function appears suppressed in some terminals but not in others. This could be explained by the low intrinsic probability of neurotransmitter release in response to neuronal depolarisation (Brain *et al.*, 2002), meaning that not every nerve terminal stimulus would result in the stimulus-secretion coupling, despite no failure of AP propagation. Alternatively, it may be that some sympathetic terminals fail to respond to EFS under the stimulus conditions used, a feature incidentally noted during experiments in Ca^{2+}-indicator-loaded terminals in the vas deferens (Brain and Bennett, 1997).

Another limitation of the current study is whether the EFS conditions *ex vivo* truly represents resting and maximal sympathetic nerve activity *in vivo*. Here, EFS was held

constant throughout NTUA exposure to measure NAT reuptake rate. It is suggested that, while compound APs of sympathetic nerve activity show asynchronous firing of neurones that appear in bursts (Nilsson *et al.*, 1985), single fibre analysis show that individual axons rarely fire doublets (Rook *et al.*, 2014, Macefield and Wallin, 2018). Hence, EFS at a regular frequency to some extent replicates the synchronous activation of noradrenergic terminals (driven by the cardiac cycle), with predominately singlet firing at the level of individual axons (where imaging resides).

4.4. Overall conclusion

In this Chapter, the established NTUA assay was utilised to re-evaluate various aspects of NAT function in the cardiovascular system in physiological- and pathophysiological settings. In the heart, NAT-mediated clearance was significantly faster than in the vasculature. Cardiac NAT kinetics was reduced by sympathetic nerve depolarisations in physiological firing frequencies in a α_2AR-dependent manner, while substrate competition may prevail at higher frequencies. While there is a mAChR-mediated suppression of NAT, it may only occur in exceptional circumstances of intense sympathetic-parasympathetic co-activation. NAT function is also consistently faster in the murine species than in the rat, thus unveiling interspecies differences in noradrenergic regulation. Finally, it is shown that cardiac NAT function and periarterial innervation becomes perturbed in repetitive CIH exposure states, which could predispose OSA patients to autonomic imbalance.

CHAPTER V. (ENDO)CANNABINOIDS AND NORADRENALINE TRANSPORTER FUNCTION IN THE RODENT CARDIOVASCULAR SYSTEM

5.1. Introduction

5.1.1. Overview

The peripheral sympathetic postganglionic neurones possess an array of prejunctional receptors that can modulate neurotransmitter release. The activation of the α_2-adrenoceptors (α_2AR) by noradrenaline (NAd) liberated from the same nerve terminal are classically known to inhibit its own release, and are termed 'autoreceptors' (Starke, 2001). Those prejunctional receptors that can be activated by ligands other than the neurotransmitter liberated from the parent nerve terminal are termed 'heteroreceptors', which includes the muscarinic acetylcholine receptors (mAChR) (Ritter *et al.*, 2020) and cannabinoid type I receptor (CB_1R) (Malinowska *et al.*, 2012), amongst others. These prejunctional receptors can either induce, enhance, or inhibit ongoing neurotransmitter release [full review found in Fuder and Muscholl (1995)].

The 'cannabinoids' refer to the endogenous and exogenous ligands that can activate the endocannabinoid system (ECS) in a functionally similar manner as the main psychoactive component of *Cannabis sativa*, Δ^9-tetrahydrocannabinol (Δ^9-THC) (Mechoulam *et al.*, 2014). Cannabinoids are known to exert complex cardiovascular effects (O'Sullivan, 2015) that involve both peripheral and central sites. Of the efferent

sympathetic nervous system (SNS) out in the periphery, cannabinoids predominately suppress cardiac- and vascular function by the activation of the prejunctional CB_1R to reduce NAd release, though its receptor presence is yet to be morphologically determined. Interestingly, despite the repertoire of evidence for release-inhibiting CB_1R in experimental pithed animals and *ex vivo* tissues, there is currently no evidence whether CB_1R has a neuromodulatory role upon the noradrenaline transporter (NAT) in the cardiovascular system.

Pathological activation of the ECS has been implicated in several cardiovascular conditions, such as hypotension associated with shock as well as hypertension (Haspula and Clark, 2020). As these pathologies could also be induced by NAT dysfunction (Schroeder and Jordan, 2012, Sheldon *et al.*, 2019), it was of particular interest to investigate whether CB_1R activation also affects NAd clearance in the neuroeffector junction. The current laboratory has previously demonstrated for a CB_1R-mediated reduction in NAT rate in the murine urogenital system, thus supporting for a neuromodulatory role of cannabinoids upon NAd clearance (Kennard, 2015). Therefore, to build a comprehensive picture of the role of CB_1R upon sympathetic transmission in the cardiovascular system, I sought to explore the CB_1R-NAT interaction in rodent cardiac and vascular tissues with the use of NTUA.

5.1.2. Objectives and aims

In this Chapter, I aim to address the following objectives with nonselective CBR agonist WIN 55,212-2, CB_1R selective agonist ACEA, and CB_1R inverse agonist, SR141716:

1. Investigate the effect of exogenous CB_1R agonists on NAT function in the murine and rat heart

2. Investigate the effect of exogenous CB_1R agonists on NAT function in the murine and rat arterial vasculature
3. Morphologically determine the localisation of CB_1R in the heart and vasculature of mice and rats
4. Investigate the role of ECS in the murine heart *ex vivo*

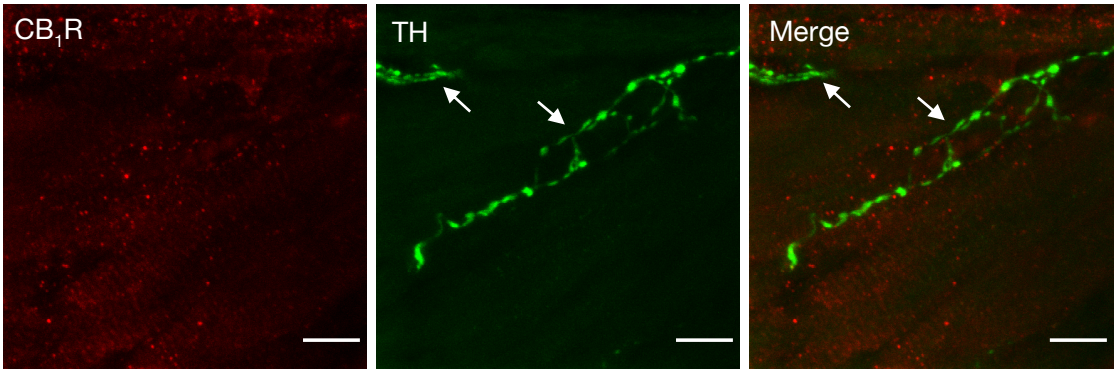
5.2. Results: rodent heart

5.2.1. Mice

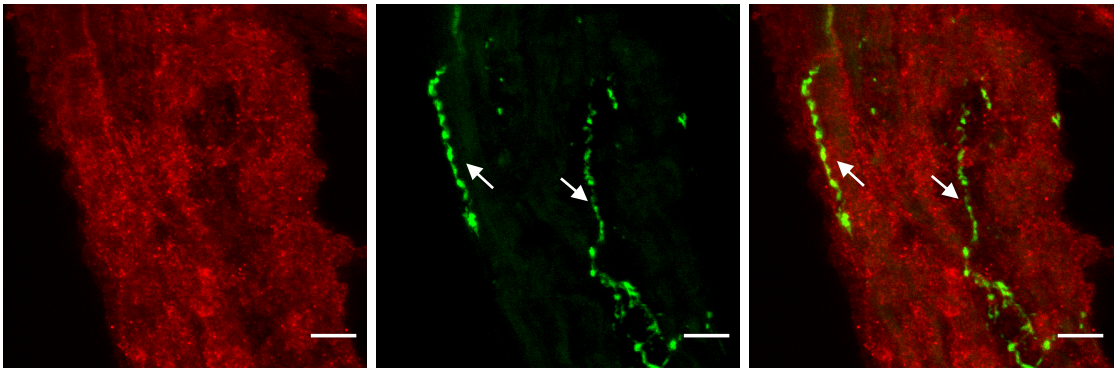
5.2.1.1. Localisation of CB_1R and TH in the murine heart

Immunohistochemistry (IHC) experiments were carried out to identify the presence of prejunctional CB_1R on cardiac sympathetic nerve terminals. In the murine heart, positive identification of CB_1R (red) were seen in non-neuronal structures in a 'clustered' manner throughout (Figure 5.1; leftmost columns). However, there were no co-localisations of CB_1R staining with the positive marker for sympathetic nerve terminals (tyrosine hydroxylase; green), thus suggesting for an absence of prejunctional CB_1R on noradrenergic nerves in the current study (Figure 5.1; middle and rightmost columns). The lack of co-localisation was consistent throughout the four chambers of the murine heart (Figure 5.1; LA: A, RAA: B, LV: C, RV: D) across 3 animals. Sections stained with secondary antibodies in the absence of primary antibodies produced negligible fluorescence signals for CB_1R and TH, demonstrating for low levels of non-selective binding (Figure 5.1E).

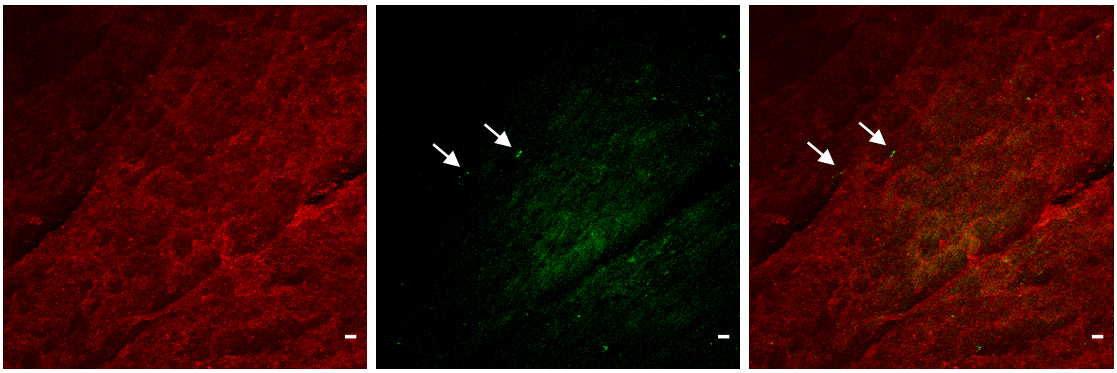
A: Mouse LA: 1:250 anti-CB_1R, 1:500 anti-TH



B: Mouse RA: 1:250 anti-CB_1R, 1:500 anti-TH



C: Mouse LV: 1:250 anti-CB_1R, 1:500 anti-TH



D: Mouse RV: 1:250 anti-CB_1R, 1:500 anti-TH

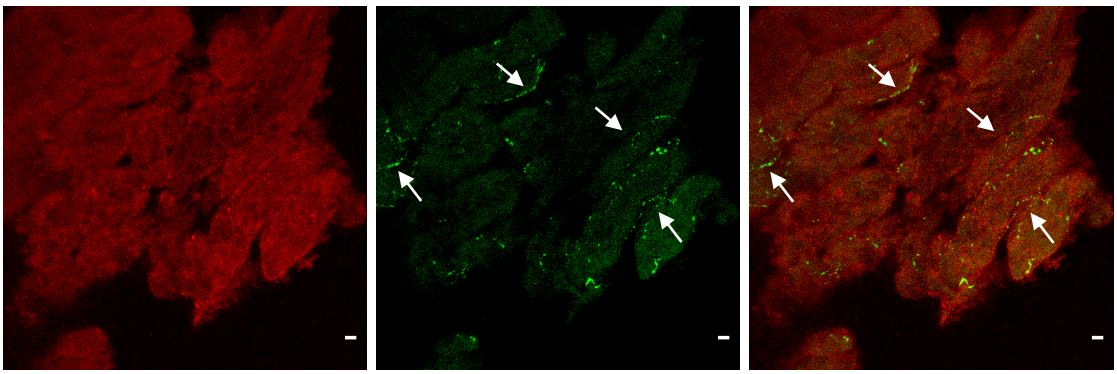
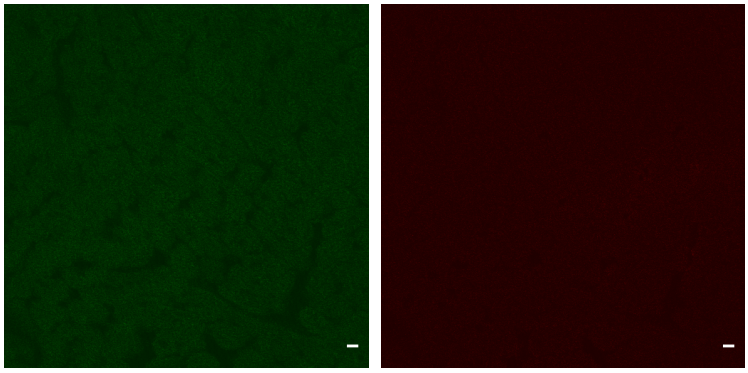


Figure 5.1: Prejunctional CB_1R are not present on murine cardiac sympathetic nerve terminals

Please refer to the following page for the figure legend. All micrographs, bars = 10 µm.

E: mouse LA, omission of anti-CB_1R and anti-TH 1° Ab



Description for figure on the present and preceding page.

Figure 5.1: Prejunctional CB_1R are not present on murine cardiac sympathetic nerve terminals

IHC labelling of cardiac sections (8-10 µm) for CB_1R and TH showed no co-localisation in all four chambers of the murine heart (**A**, LA; **B**, RAA; **C**, LV; **D**, RV). The leftmost columns **(A-D)** demonstrate CB_1R (rabbit host, 1:250) positive fluorescent staining (red) appearing in non-neuronal structures. Sympathetic nerve terminals labelled with tyrosine hydroxylase (TH; sheep host, 1:500) are demonstrated the middle columns **(A-D)** and exhibits the typical morphology of 'beads on a string' (green). The rightmost columns **(A-D)** contain the merged sections from CB_1R and TH staining (red and green); however, no co-localisations were detected suggesting for a lack of prejunctional CB_1R on sympathetic nerve terminals in the murine heart. Staining was repeated for 3 different animals. **(E)** In the absence of primary antibodies there was minimal fluorescence detected, demonstrating for low levels of non-selective binding (Alexa Fluor 488 and Alexa Fluor 647, 1:250 each). All micrographs: bars = 10 µm

Abbreviations: LA, left atrium; RAA, right atrium; LV, left ventricle; RV, right ventricle

5.2.1.2. CB_1R-mediated reduction in murine cardiac NTUA uptake

To investigate whether a CB_1R-mediated reduction in NAT rate occurs beyond the murine urogenital system (Kennard, 2015), the isolated mouse LA was incubated in nonselective CBR agonist WIN 55,212-2 (1 μM) during a 40 min pre-treatment time prior to NTUA studies; specificity was tested with CB_1R reverse agonist SR141716A (30 nM). The effect of the highly selective CB_1R agonist, ACEA (100 nM), on NAT rate was also tested. CBR agonist exposure took place in non-stimulating conditions.

5.2.1.2.1. WIN 55,212-2

In vehicle control conditions (0.01% DMSO), the rise of NTUA fluorescence in cardiac sympathetic nerve terminals was linear for the first 4 min and began to plateau towards a fluorescence intensity of 1.0 thereafter (Figure 5.2A). While a similar time course of uptake occurred in the WIN 55,212-2 treated terminals, the fluorescence reached at the end of the experiment was approximately 0.6 (Figure 5.2A). As a result, WIN 55,212-2 significantly reduced the linear NTUA uptake rate at t=0-4 by 35±7% from vehicle control conditions [control: 22±1%.min^{-1} (n=4, n_t=60) vs. WIN 55,212-2: 14±1.0%.min^{-1} (n=4, n_t=60), p<0.0001, Figure 5.1B, C]. Pre-treating the heart with CB_1R inverse agonist, SR141716A, prevented the effect [WIN 55,212-2: 22±1%.min^{-1} (n=4, n_t=60) vs. control, p>0.05, Figure 5.1B, C), which suggests for a CB_1R-mediated NAT rate suppression in the mouse heart.

As discussed previously (section 4.3.1.), forcing a straight-line fit through data points that do not follow a linear trend may mask important changes in transporter function. Thus, a non-linear one-phase association curve was fit onto the data to detect for changes in Y_{max} for the maximum NTUA fluorescence (plateau), and k, the rate constant. The analysis method is analogous to that reported in Chapter IV (section 4.3.2.).

In WIN 55,212-2 treated cardiac nerve terminals, there was a 43% reduction in Y_{max} [control: 1.18 (0.85-1.83) (n=4, n_t=52) vs. WIN 55,212-2: 0.67 (0.46-0.96) (n=4, n_t=53), p<0.0001, Figure 5.2E], which was prevented by SR141716A [1.04 (0.69-1.56) (n=4, n_t=57) vs. vehicle control, p>0.05, Figure 5.2E]. This suggests for a CB_1R-mediated attenuation of maximal NTUA fluorescence accumulated by NAT. Interestingly, WIN 55,212-2 increased the rate constants by 56% [control: 0.27 (0.15-0.44).min^{-1} (n=4, n_t=60) vs. WIN 55,212-2: 0.42 (0.23-0.89).min^{-1} (n=4, n_t=60), p<0.05, Figure 5.2F] via CB_1R activation [SR141716A: [0.38 (0.20-0.57).min^{-1} (n=4, n_t=59) vs. control, p>0.05, Figure 5.2F]. These results therefore suggest that the CB_1R-mediated reduction of NAT function by WIN 55-212,2 was primarily due to the attenuation in maximum fluorescence detected of NTUA.

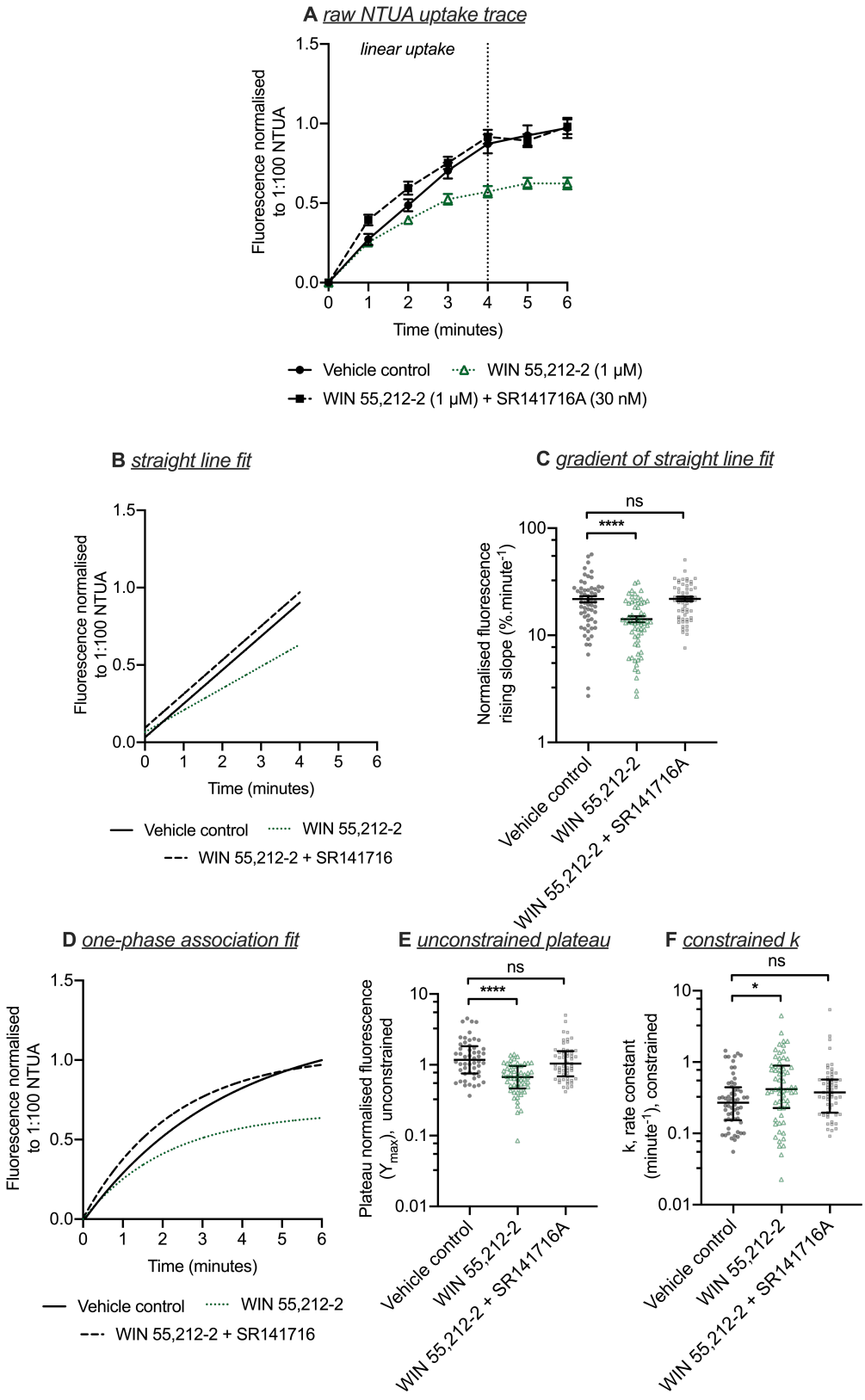


Figure 5.2: Nonselective CBR agonist WIN 55,212-2 reduces murine cardiac sympathetic NTUA uptake function via a CB_1R-dependent pathway

Please refer to the following page for the figure legend.

Description for figure on the preceding page.

Figure 5.2: Nonselective CBR agonist WIN 55,212-2 reduces murine cardiac sympathetic NTUA uptake function via a CB_1R-dependent pathway

The effects of nonselective CBR agonist WIN 55,212-2 on murine cardiac NTUA uptake function into sympathetic nerve terminals. **(A)** The murine left atria (LA) were exposed to 1:20 NTUA in three conditions: vehicle control (0.01% DMSO) (●), WIN 55,212-2 treated- (△) and WIN 55,212-2+SR141716A (CB_1R inverse agonist) treated conditions (■). Tissues exposed to WIN 55,212-2 for 40 min accumulated less NTUA, which was prevented by SR141716A pre-treatment.

(B, C) WIN 55-212,2 significantly reduced the linear NTUA uptake rate, which was prevented by SR141716A pre-treatment.

(D, E) A non-linear curve fit to the data demonstrates a CB_1R-mediated premature plateau of NTUA accumulation (Y_{max}) in terminals pre-treated with WIN 55,212-2 compared to vehicle control. **(F)** The curve fit model constrained to Y_{max} values seen in (E) revealed a faster rate constant of NTUA accumulation in WIN 55,212-2 treated cardiac nerve terminals in a CB_1R-dependent fashion.

Each individual datapoint in the scatterplot corresponds to a single terminal. Data presented as **(A, C)** mean±SEM and **(E, F)** median (IQR).

Statistical analysis:
(C) Ordinary one-way ANOVA followed by *post-hoc* Tukey's multiple comparison test.
(E, F) Kruskal-Wallis test, followed by *post-hoc* Dunn's multiple comparison test.
* denotes $p<0.05$; **** denotes $p<0.0001$; ns denotes $p>0.05$

5.2.1.2.2. ACEA

To further demonstrate a CB_1R-mediated NTUA uptake suppression, the murine LA was pre-treated with the highly selective CB_1R agonist ACEA (100 nM) for 40 min prior to the 1:20 NTUA test period. At each time point, the accumulation of NTUA fluorescence was consistently lower in the ACEA group than control (Figure 5.3A). As a consequence, there was a significant reduction in the linear NTUA uptake rate (t=0-4) by 30±7% in the ACEA group [control: 25±2%.min^{-1} (n=4, n_t=60) vs. ACEA: 18±1%.min^{-1} (n=4, n_t=60), p<0.001, Figure 5.3B, C].

Analysis of NTUA uptake by the non-linear curve fit (Figure 5.3D) demonstrate that the Y_{max} was not different between groups [control: 1.17 (0.80-1.77) (n=4, n_t=57) vs. ACEA: 1.07 (0.76-1.46) (n=4, n_t=42), p>0.05, Figure 5.3E), presumably because NTUA accumulation had not fully approached a full plateau by the end of the experiment. The rate constant, on the other hand, was significantly slower in the ACEA groups by 38% [control: 0.37 (0.19-0.73).min^{-1} (n=4, n_t=59) vs. ACEA: 0.23 (0.13-0.49).min^{-1} (n=4, n_t=60), p<0.05, Figure 5.3F]. These results therefore suggest the ACEA-mediated reduction in NTUA uptake function was due to an attenuation in reaction rate.

With the use of two CB_1R agonists, WIN 55,212-2 and ACEA, the current study suggests for a prejunctional CB_1R-mediated suppression of NTUA uptake function; however, the target receptors were not detected by the present IHC method.

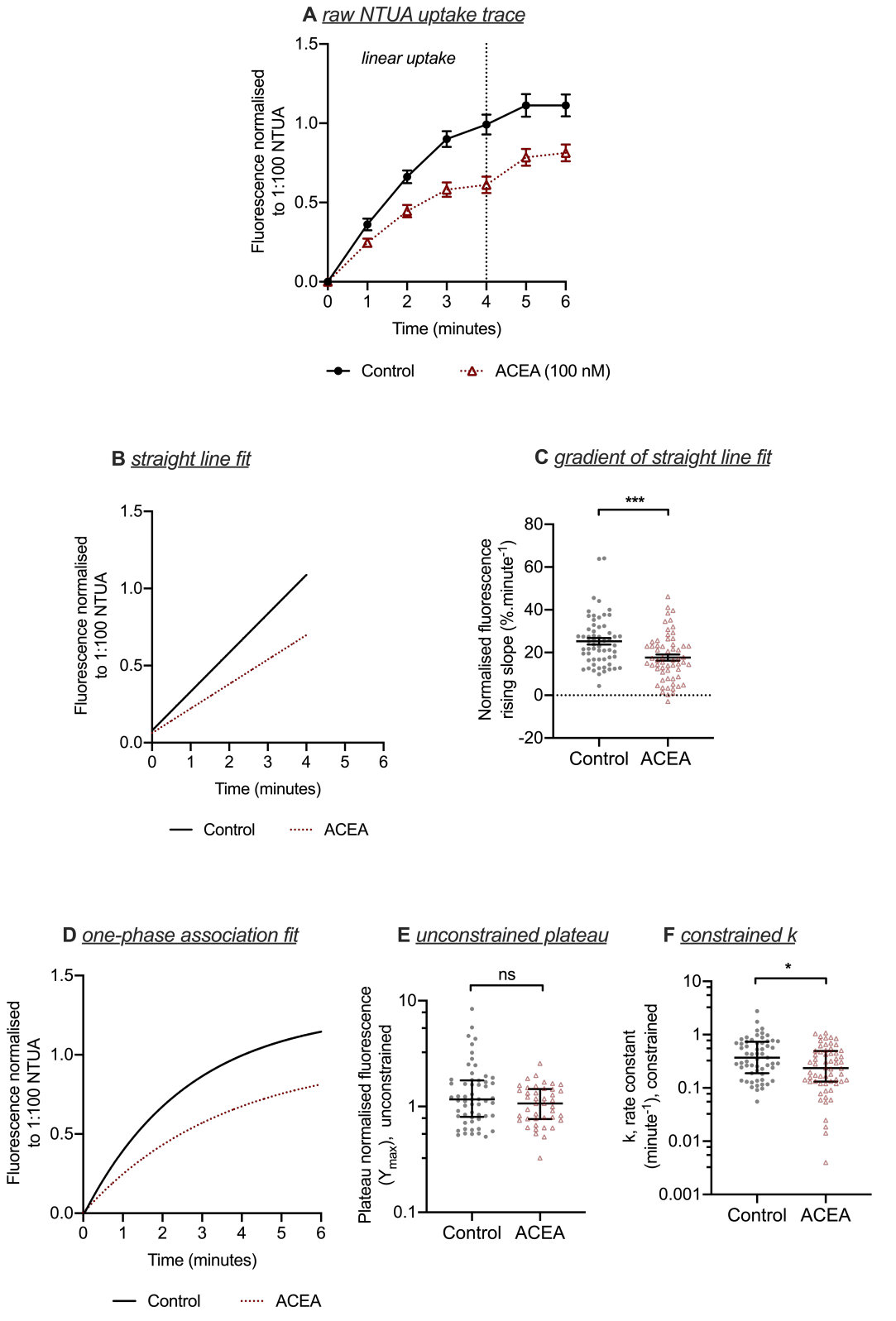


Figure 5.3: Highly selective CB_1R agonist ACEA suppresses murine cardiac sympathetic NTUA uptake rate

Please refer to the following page for the figure legend.

Description for figure on the preceding page.

Figure 5.3: Highly selective CB_1R agonist, ACEA, suppresses NAT reuptake rate in the mouse heart

The effects of CB_1R-specific agonist ACEA on murine cardiac NTUA uptake into sympathetic nerve terminals. **(A)** Neuronal NTUA accumulation into the murine left atrium (LA) was reduced at each time points following pre-treatment with ACEA (△) compared to control conditions (●).

(B, C) The linear NTUA uptake rate was significantly reduced with ACEA pre-treatment from control values.

(D, E) A non-linear curve fit model demonstrates similar Y_{max} values of NTUA fluorescence between groups. **(F)** NTUA uptake rate constant values from all terminals constrained to the corresponding Y_{max} in (E). ACEA pre-treatment decreased the rate constant of NTUA accumulation into sympathetic nerve terminals compared to control conditions.

Each individual datapoint in the scatterplot corresponds to a single terminal. Data presented as **(A, C)** mean±SEM and **(E, F)** median (IQR).

Statistical analysis:
(C) Welch's *t*-test
(E, F) Mann-Whitney test
* denotes $p<0.05$; *** denotes $p<0.001$; ns denotes $p>0.05$

5.2.1.3. Sympathetic nerve activity reduces murine cardiac NTUA uptake via a CB_1R-dependent mechanism

Within the central nervous system (CNS), the eCBs are synthesised de novo by depolarised postsynaptic cells to retrogradely act upon presynaptic CB_1R for neuromodulation (Cadas *et al.*, 1996). To investigate whether the CB_1R-mediated suppression of cardiac NAT might be tonically present during neuronal activity, the sympathetic nerve terminals of the mouse LA were stimulated in the presence of CB_1R inverse agonist, SR141716A (S; 30 nM). Tissues were also pre-treated with yohimbine and atropine to prevent confounding neuromodulatory factors induced by EFS (Figure 4.6, 4.9).

In the absence of EFS, SR141716A did not affect NTUA uptake into cardiac nerve terminals (Figure 5.4G-I). In both 2 Hz and 10 Hz EFS, SR141716A treatment appeared to accentuate the maximum NTUA accumulation within the nerve terminals (Figure 5.4A, D). To analyse this aspect, the non-linear curve fit was adopted to yield the Y_{max}. However, the effect was only statistically significant at 10 Hz, where there was a 18% increase in Y_{max} with SR141716A [Y+A: 1.06 (0.82, 1.29) (n=4, n_t=52) vs. Y+A+S: 1.25 (1.11, 1.71) (n=4, n_t=55), p<0.001, Figure 5.4E] but not at 2 Hz [Y+A: 1.15 (0.92, 1.48) (n=4, n_t=49) vs. Y+A+S: 1.30 (1.06, 1.52) (n=4, n_t=58), p>0.05, Figure 5.4B]. This result suggests that, at the high end of resting stimulation frequencies, there is a CB_1R-dependent suppression of NTUA uptake.

In the presence of yohimbine, the gradual increase in junctional NAd could interfere with NTUA uptake kinetics due to substrate competition (Figure 4.9). Thus, NAT rate was investigated by linear line fit through the 'early phase' (t=0-3). At 2 Hz, SR141716A increased the NTUA uptake rate by 21±16% [Y+A: 29±2%.min^{-1} (n=4, n_t=60) vs. Y+A+S:

35±1%.min^{-1} (n=4, n_t=60), p<0.05, Figure 5.4C], whereas the effect at 10 Hz was not statistically significant [Y+A: 31 (26, 40)%.min^{-1} (n=4, n_t=60) vs. Y+A+S: 35 (29, 40)%.min^{-1} (n=4, n_t=60), p>0.05, Figure 5.4F].

These results suggest that, at both resting and maximal sympathetic nerve activity there is a CB_1R-mediated tonic reduction in NAT function. The effect is stimulation-dependent as SR141716A did not perturb parameters of NTUA uptake in non-stimulating conditions (Figure 5.4G-I). One possibility is that EFS induces the liberation of endocannabinoid ligands that tonically suppresses NAT function via a CB_1R-dependent mechanism. However, the source of CB_1R ligands is unclear as the cardiomyocytes were not contracting in the current EFS conditions to allow for dynamic monitoring of single terminals.

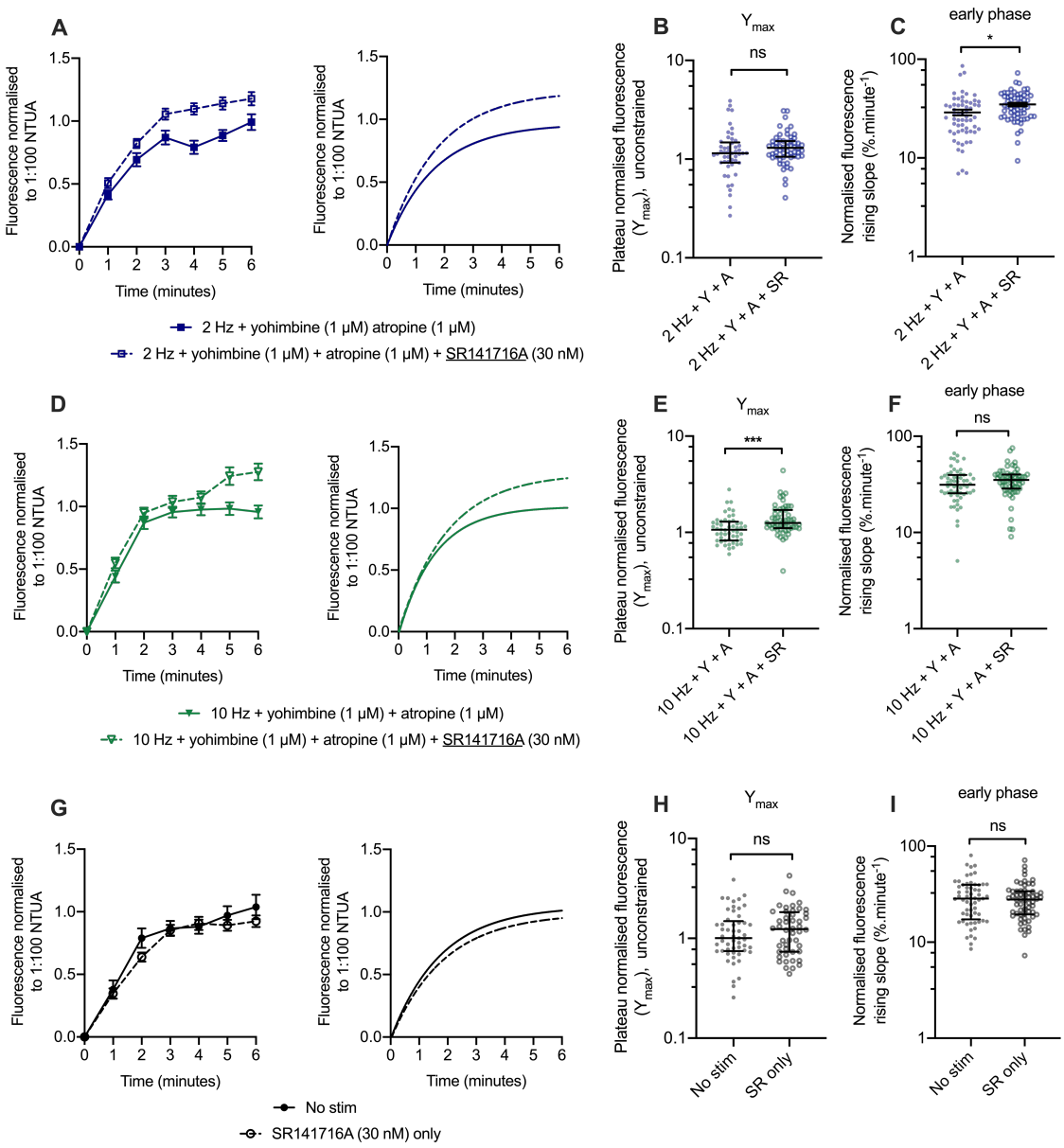


Figure 5.4: Sympathetic neuronal activity reduces murine cardiac noradrenergic NTUA uptake via an endogenous CB_1R-dependent pathway

The effect of CB_1R antagonism on murine cardiac sympathetic NTUA uptake during neuronal activity (2 Hz). **(A-F)** The accumulation of NTUA into sympathetic nerve terminals were observably greater in the presence of SR141716A at 2 Hz (□) and 10 Hz (▽). **(G-I)** SR141716A did not perturb NTUA uptake in non-stimulating conditions (☐), suggesting the CB_1R-mediated effect was induced in EFS conditions.

Each individual datapoint in the scatterplot corresponds to a single terminal. Data presented as **(A, C, D, G)** mean±SEM and **(B, E, F, H, I)** median (IQR).

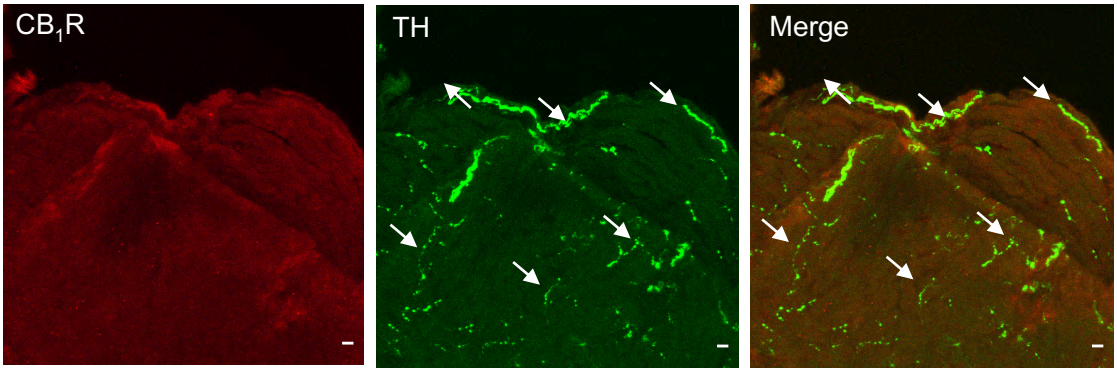
Statistical analysis:
(C) Welch's *t*-test; **(B, E, F, H, I)** Mann-Whitney test
* denotes $p<0.05$; *** denotes $p<0.001$; ns denotes $p>0.05$

5.2.2. Rat

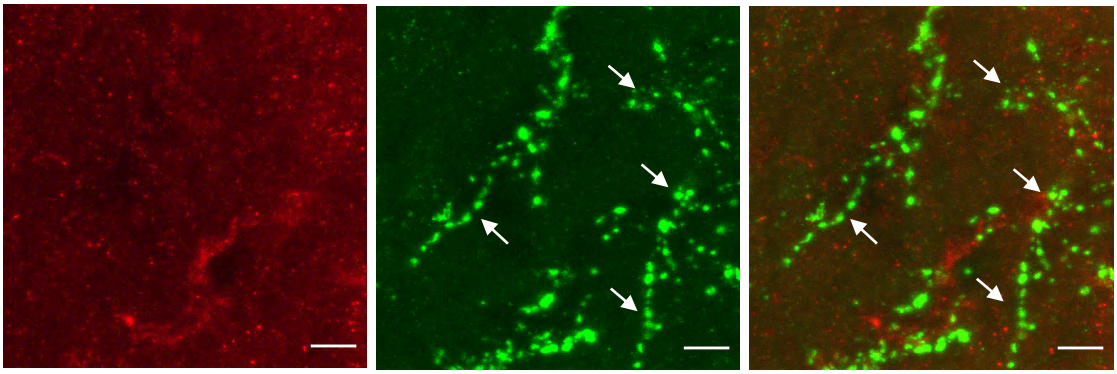
5.2.2.1. Localisation of CB_1R and TH in the rat heart

Similar to the murine heart, IHC experiments did not reveal prejunctional CB_1R on rat cardiac sympathetic nerve terminals. CB_1R staining (red) can be seen as 'clustered' labelling throughout the LA, though no co-localisations with TH (green) were observed at low- (Figure 5.5A) or high magnifications (Figure 5.5B). The lack of co-localisation was consistent across multiple heart sections from 3 animals. Sections stained with secondary antibodies in the absence of primary antibodies produced negligible fluorescence signals for CB_1R and tyrosine hydroxylase, demonstrating for low levels of non-selective binding (Figure 5.5C).

A: Rat LA: 1:250 anti-CB_1R, 1:500 anti-TH



B: Rat LA: 1:250 anti-CB_1R, 1:500 anti-TH



C: Rat LA: omission of anti-CB_1R and anti-TH 1° Ab

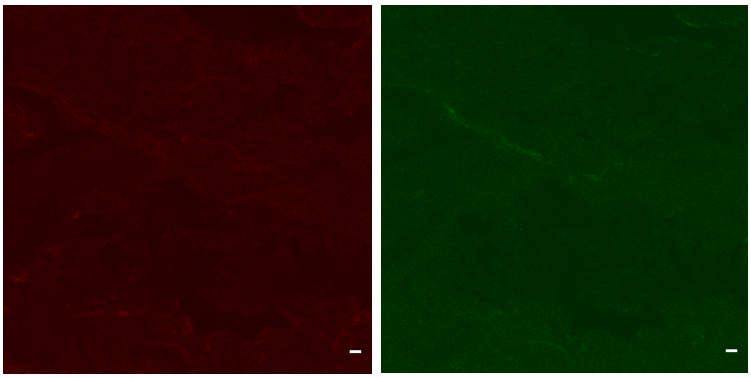


Figure 5.5: Prejunctional CB_1R are not present on rat cardiac sympathetic nerve terminals

IHC labelling of rat cardiac sections (8-10 µm) for CB_1R and TH expression. No co-localisations were detected at **(A)** low- and **(B)** high magnifications. The leftmost columns in each row demonstrate CB_1R (rabbit host, 1:250) positive fluorescent staining (red). Sympathetic nerve terminals stained with tyrosine hydroxylase (TH; sheep host, 1:500) are demonstrated the middle columns and exhibits the typical morphology of 'beads on a string' (green). The rightmost columns contain the merged sections from CB_1R and TH staining (red and green). Staining was repeated for 3 different animals. **(C)** In the absence of primary antibodies, there was minimal fluorescence detected, demonstrating low levels of non-selective binding (Alexa Fluor 488 and Alexa Fluor 647, 1:250 each). All micrographs: bars = 10 µm.

5.2.2.2. CB_1R activation does not affect rat cardiac NTUA uptake

To investigate whether CB_1R activation affects cardiac NTUA uptake in the rat, the isolated rat LA was exposed to WIN 55,212-2 (1 μM) and ACEA (100 nM) for 40 min before and during the 10-min 1:20 NTUA test period in non-stimulating conditions.

5.2.2.2.1. WIN 55,212-2

In both vehicle control (0.01% DMSO) and WIN 55,212-2 treated nerve terminals, the accumulation of NTUA into rat cardiac sympathetic nerve terminals occurred linearly for 6 min before reaching a plateau by the end of the experiment (Figure 5.6A). At each time point the NTUA uptake trace in the WIN 55,212-2 group directly overlapped with vehicle control. Hence, NTUA uptake rate was not perturbed by WIN 55,212-2 [vehicle control: 10±1%.min^{-1} (n=4, n_t=60) vs. WIN 55,212-2: 10±1%.min^{-1} (n=4, n_t=60), p>0.05, Figure 5.6B, C], suggesting CBR activation does not affect cardiac NTUA uptake in the rat.

5.2.2.2.2. ACEA

Similarly, ACEA did not affect NTUA accumulation into cardiac noradrenergic terminals compared to the control group (Figure 5.7A). The linear NTUA uptake rate was not affected by ACEA [control: 10 (8-13)%.min^{-1} (n=4, n_t=60) vs. ACEA: 10 (8-12)%.min^{-1} (n=4, n_t=60), p>0.05, Figure 5.7B, C]. These results further suggest CB_1R activation does not affect NTUA uptake in the rat heart.

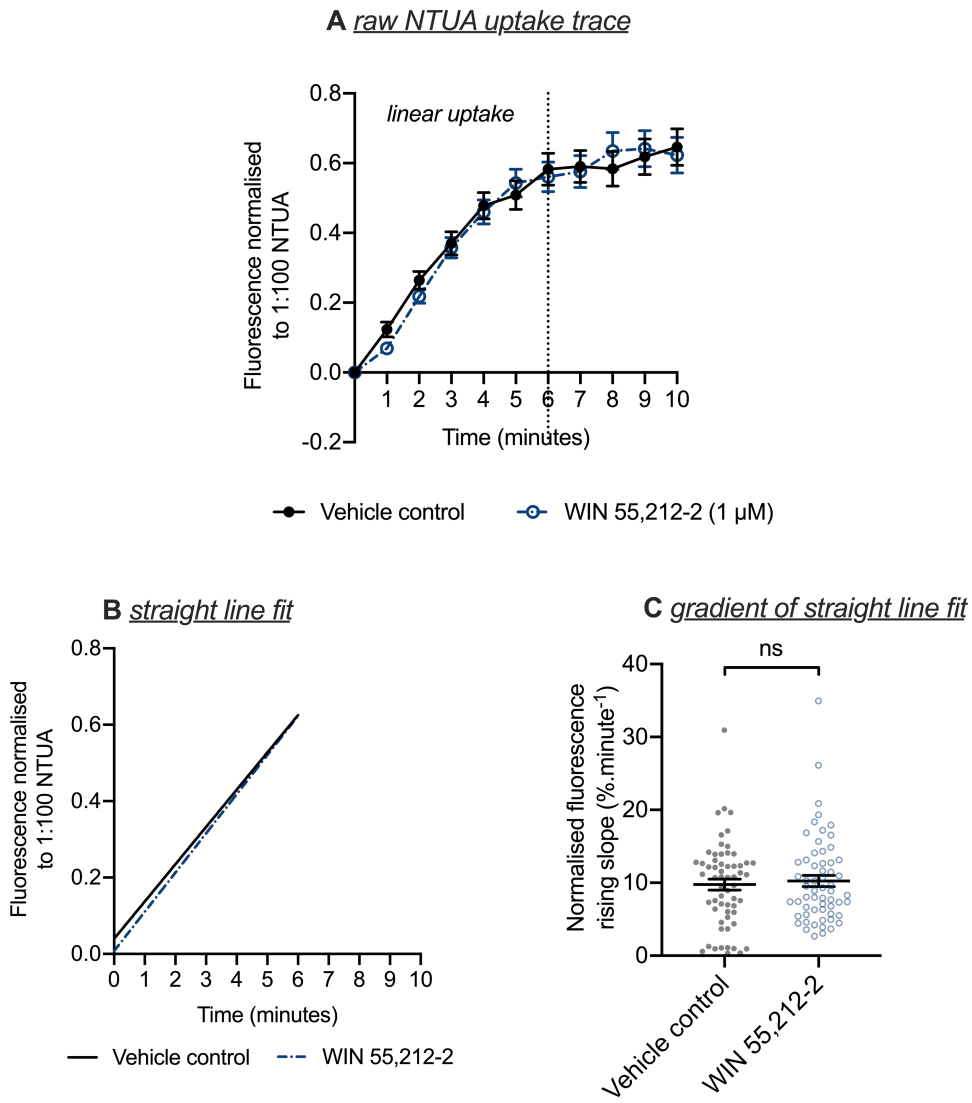


Figure 5.6: Nonselective CBR agonist WIN 55,212-2 does not affect rat cardiac sympathetic NTUA uptake function

The effect of nonselective CBR agonist WIN 55,212-2 on rat cardiac sympathetic NTUA uptake into nerve terminals. **(A)** The NTUA uptake trace of the rat left atrium (LA) in vehicle control- (●) and WIN 55,212-2 treated conditions (○) overlapped one another. **(B, C)** The linear NTUA uptake rate did not different between groups.

Each individual datapoint in scatterplots corresponds to a single terminal. Data presented as **(A, C)** mean±SEM.

Statistical analysis:
(C) Unpaired *t*-test; ns denotes $p>0.05$.

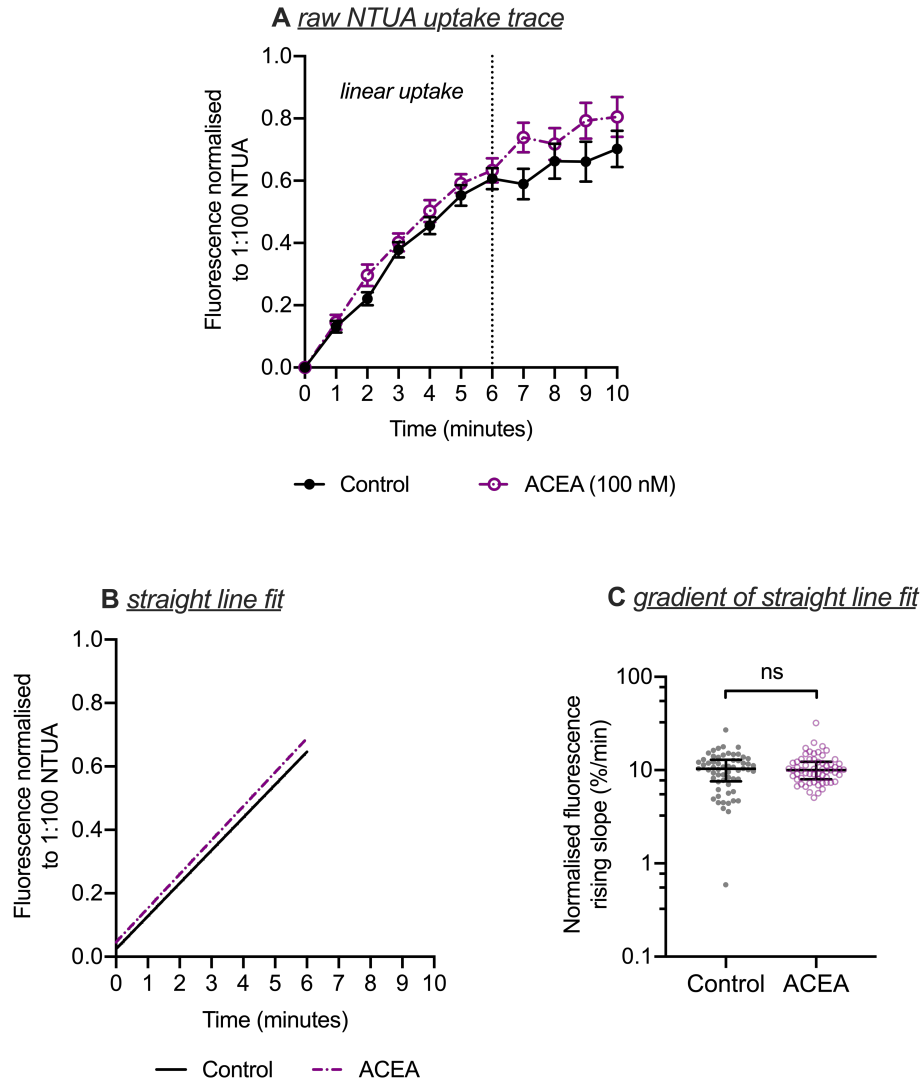


Figure 5.7: Highly selective CB_1R agonist ACEA does not affect rat cardiac sympathetic NTUA uptake function

The effect of highly selective CB_1R agonist ACEA on rat cardiac sympathetic NTUA uptake into nerve terminals. **(A)** The NTUA uptake trace of the rat left atrium in vehicle control- (●) and WIN 55,212-2 treated conditions (○) overlapped at each time point. **(B, C)** The linear NTUA uptake rates were not different between groups.

Each individual datapoint in scatterplots corresponds to a single terminal. Data presented as **(A)** mean±SEM and **(C)** median (IQR).

Statistical analysis:
(C) Mann-Whitney test; ns denotes $p>0.05$.

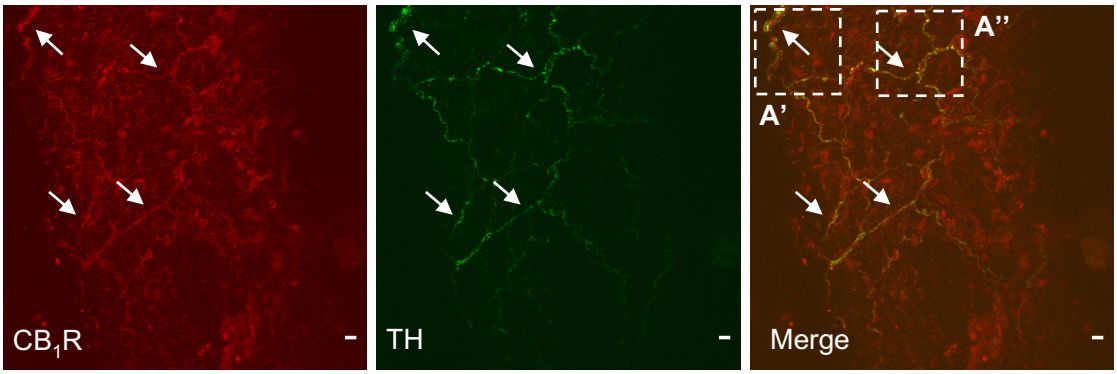
5.3. Results: rodent mesenteric artery

5.3.1. Mice

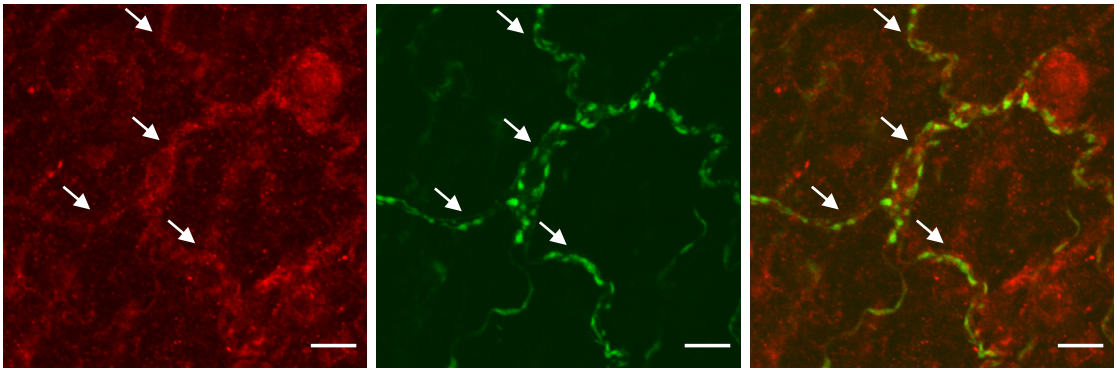
5.3.1.1. Localisation of CB_1R and TH in the murine mesenteric artery

IHC staining of the murine mesenteric artery with TH revealed noradrenergic innervation (green) that surrounds the arterial vessel surface (Figure 5.8A-B, middle columns) and axonal bundles nearby (Figure 5.9). CB_1R staining (red) were observed in abundance in non-neuronal tissues as 'clustered' appearances and on 'round' structures suggesting for multiple CB_1R-positive vascular cell types (Figure 5.8, 5.9). Interestingly, CB_1R staining was also observed overlapping with sympathetic nerve fibres (Figure 5.8A-B) and noradrenergic axonal bundles surrounded by cell nuclei (DAPI, blue) (Figure 5.9). However, the 'neuronal' distribution of CB_1R was diffuse and appeared 'shadow-like', rather than punctate (as with TH). Furthermore, CB_1R labelling overlapped with TH positive structures in some regions, but not in others. Thus, it is not entirely clear whether the CB_1R staining were indeed on sympathetic nerve terminals. Nevertheless, sections stained with secondary antibodies in the absence of primary antibodies produced negligible fluorescence signals for CB_1R and TH, demonstrating for low levels of non-selective binding (Figure 5.8C). The observations were consistent across multiple mesenteric artery preparations from 3 animals and 2 animals for single noradrenergic fibres and axonal bundles, respectively.

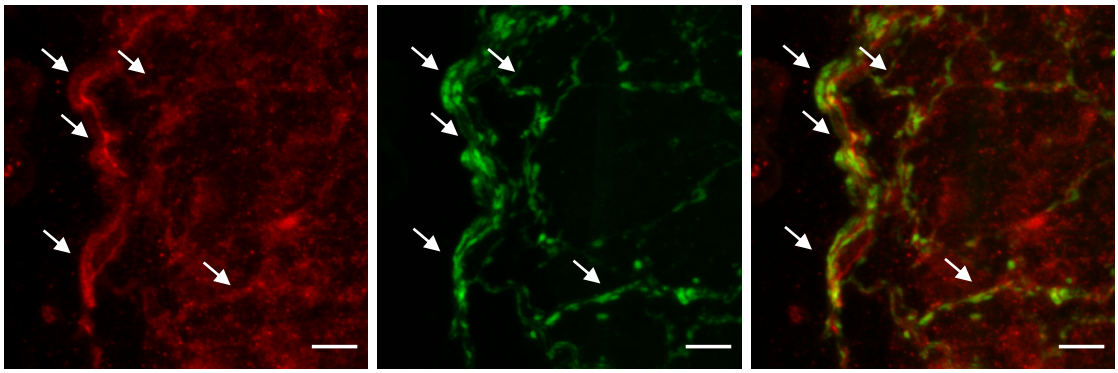
A: Mouse MA; 1:250 anti-CB_1R, 1:500 anti-TH



A': Mouse MA; 1:250 anti-CB_1R, 1:500 anti-TH



A'': MA; *single slice*; 1:250 anti-CB_1R, 1:500 anti-TH



B: Mouse MA; 1:250 anti-CB_1R, 1:500 anti-TH

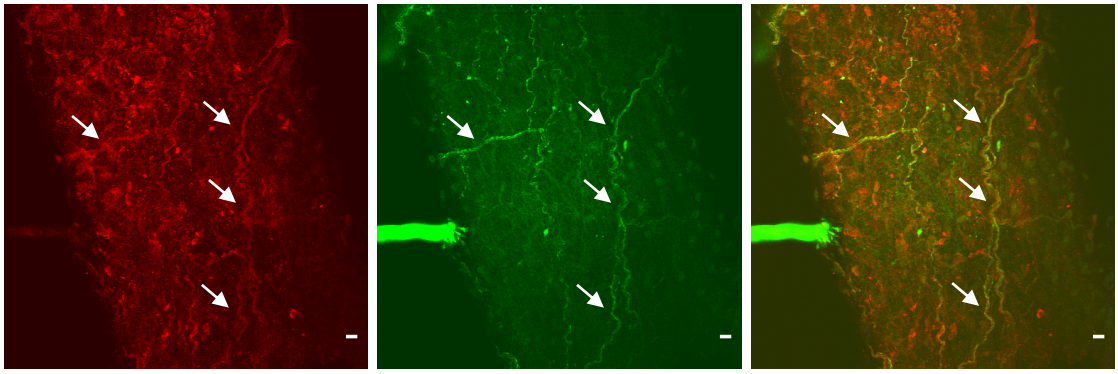
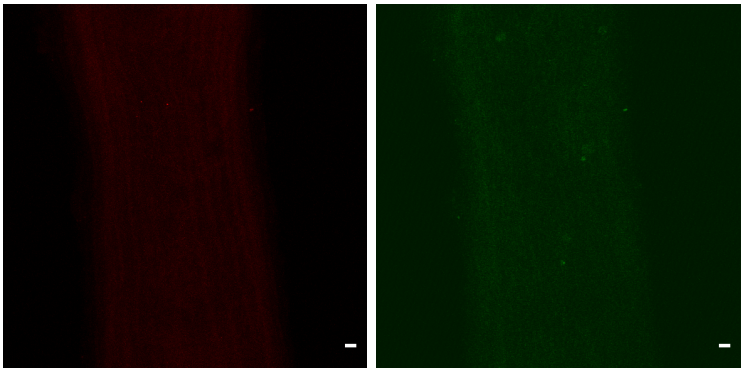


Figure 5.8: Localisation of CB_1R and TH in the murine mesenteric artery
Corresponding figure legend on the following page. All micrographs: bars = 10 µm

C: MA, 40x, omission of anti-CB_1R and anti-TH 1º Ab



Description for figure on the preceding and present page.

Figure 5.8: Localisation of CB_1R and TH in the murine mesenteric artery
IHC labelling of whole preparations of murine mesenteric arteries for CB_1R and TH expression. CB_1R staining (red; leftmost columns, arrows) were present in abundance in non-neuronal tissue and in very close proximity with sympathetic nerve fibres (green; middle columns, arrows), but not in other regions. However, CB_1R and TH does not appear to co-localise when merged (rightmost columns, arrows). CB_1R were labelled with 1:250 1º Ab dilution (rabbit host) and TH with 1:500 1:250 1º Ab dilution (sheep host). Images were taken at low magnifications **(A, B)** and high magnifications **(A', A'')**, with merged *z*-stacks **(A', A'')** and individual slices displayed **(A, B)**. **(C)** In the absence of primary antibodies, there was minimal fluorescence detected, demonstrating low levels of non-selective binding (Alexa Fluor 488 and Alexa Fluor 647, 1:250 each). Images are representative of n=3. All micrographs: bars = 10 µm.

Description for figure on the following page.

Figure 5.9: Localisation CB_1R with sympathetic single fibre processes and axonal bundles in the murine mesenteric artery
IHC labelling of murine mesenteric arteries for CB_1R (red), TH (green) and cell nuclei (blue). Noradrenergic axonal bundles (arrowheads) displayed strong labelling for CB_1R and TH, though in some areas a lack of nearby localisation was seen. Surrounding the axonal bundles were a different population of cell types, as demonstrated by an abundance of cell nuclei. CB_1R labelling are close to single sympathetic nerve fibres (arrows), though it does not appear to have the same morphology as varicose nerve terminals. CB_1R staining are also present in non-neuronal regions. CB_1R were labelled with 1:250 1º Ab dilution (rabbit host) and tyrosine hydroxylase with 1:500 1:250 1º Ab dilution (sheep host). Images are representative of n=2. All micrographs: bars = 10 µm.

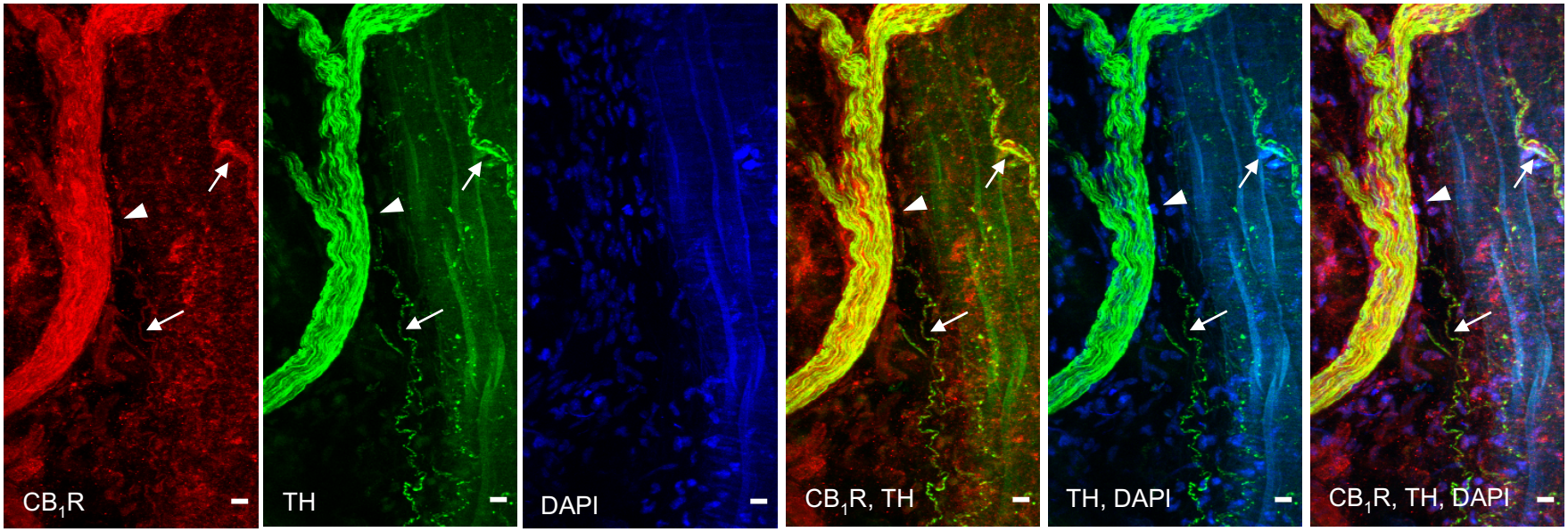


Figure 5.9A: Localisation CB_1R amongst sympathetic single fibre processes and axonal bundles in the mouse mesenteric artery

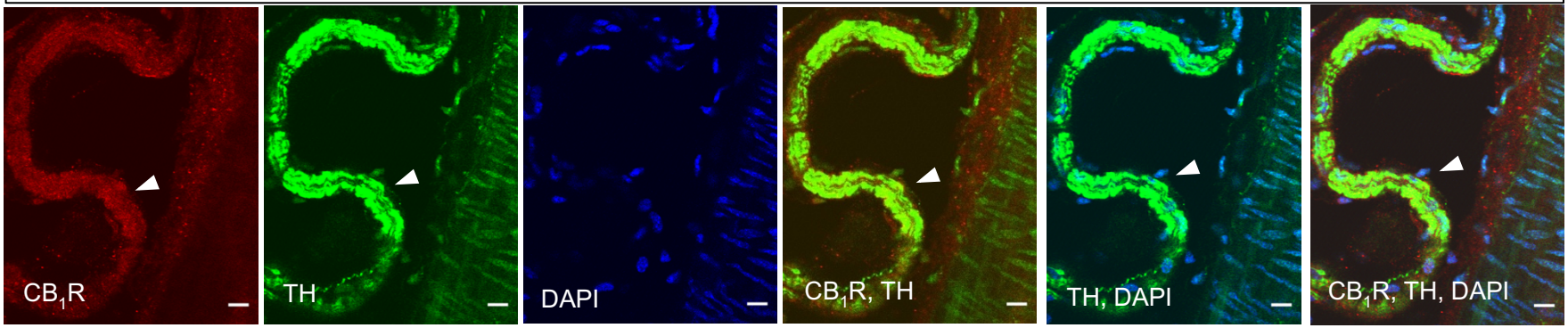


Figure 5.9B: Localisation CB_1R amongst sympathetic single fibre processes and axonal bundles in the mouse mesenteric artery
Corresponding figure legend on the preceding page.

5.3.1.2. CB_1R activation does not affect murine periarterial NTUA uptake

Having demonstrated for a CB_1R-dependent reduction in murine cardiac NTUA uptake function, the investigation was extended to the mesenteric arteries. Briefly, the isolated mouse MAs were incubated in a nonselective CBR agonist and CB_1R selective agonist, WIN 55,212-2 (1 μM) and ACEA (100 nM), respectively, during a 40 min pre-treatment time in non-stimulating conditions.

5.3.1.2.1. WIN 55,212-2

At each time point, NTUA fluorescence was similar between the vehicle control (0.01% DMSO) and WIN 55,212-2 treated nerve terminals (Figure 5.10A). There were no differences in the linear NTUA uptake rate between groups [control: 13 (8-20)%.min^{-1} (n=4, n_t=60) vs. WIN 55,212-2: 13 (10-18)%.min^{-1} (n=4, n_t=60), p>0.05, Figure 5.10B, C], suggesting for a lack of a CBR-mediated effect upon murine periarterial NTUA uptake function.

5.3.1.2.2. ACEA

As with WIN 55,212-2, the linear NTUA uptake rates in ACEA-treated periarterial nerve terminals were not statistically different to control values [control: 18±1%.min^{-1} (n=4, n_t=60) vs. ACEA: 23±3%.min^{-1} (n=4, n_t=60), p>0.05, Figure 5.11). This result further supports for the absence of a CB_1R-mediated effect upon NTUA uptake function in murine mesenteric periarterial nerve terminals.

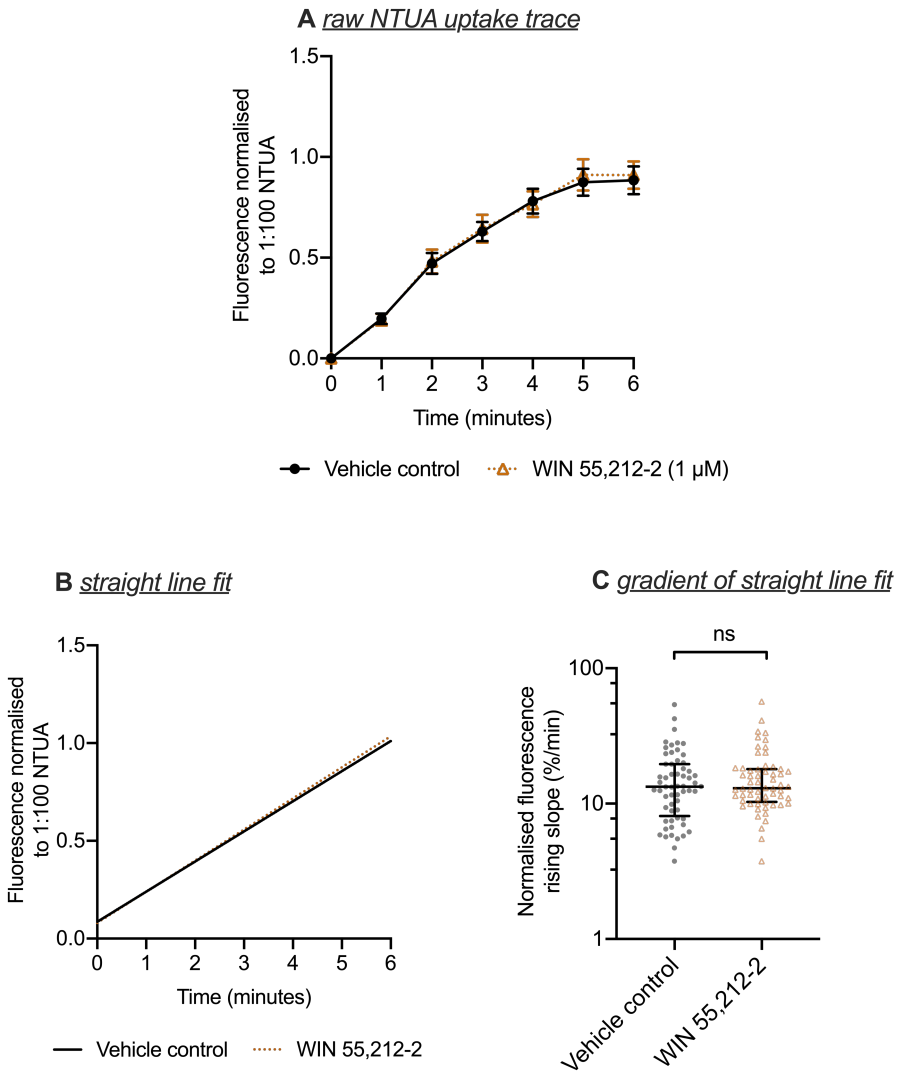


Figure 5.10: Nonselective CBR agonist WIN 55,212-2 does not affect murine periarterial sympathetic NTUA uptake function

The effect of nonselective CBR agonist WIN 55,212-2 on periarterial sympathetic NTUA uptake into nerve terminals. **(A)** The NTUA uptake trace of the murine MA in vehicle control- (●) and WIN 55,212-2 treated conditions (△) overlapped at each time point. **(B, C)** The linear NTUA uptake rate did not differ different between groups.

Each individual datapoint in scatterplots corresponds to a single terminal. Data presented as **(A)** mean±SEM and **(C)** median (IQR).

Statistical analysis:
(C) Mann-Whitney test; ns denotes $p>0.05$.

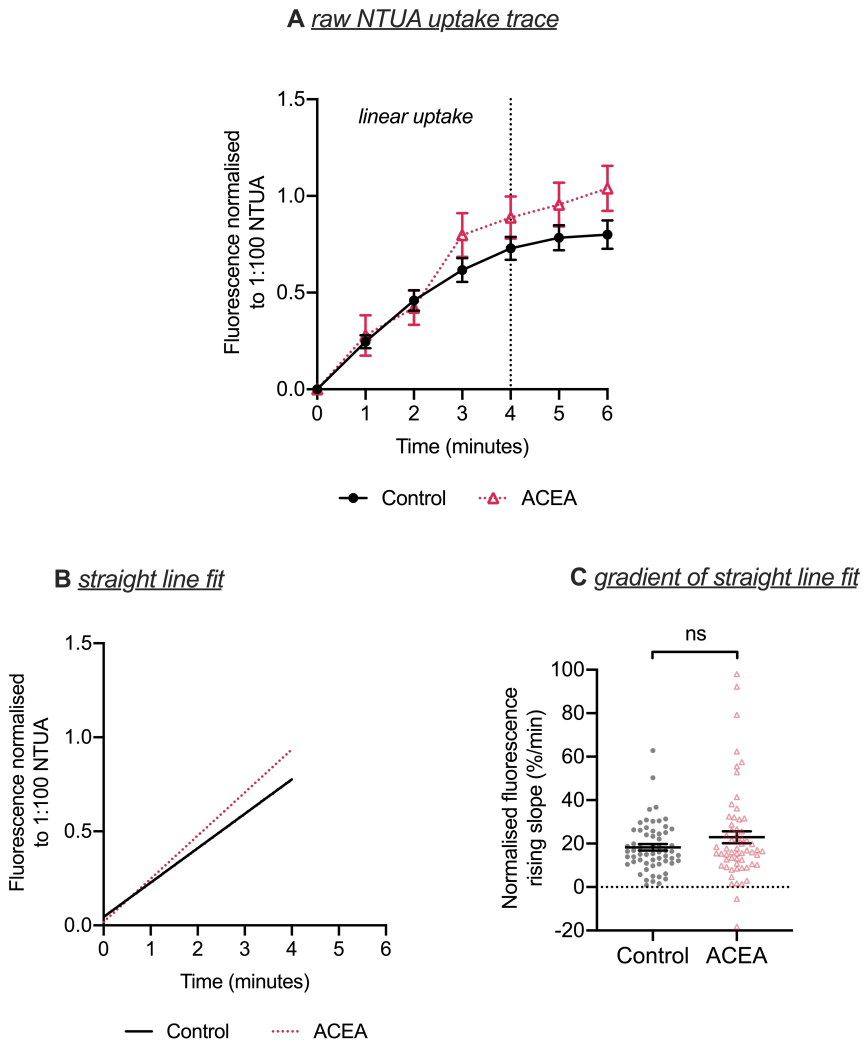


Figure 5.11: Highly selective CB_1R agonist ACEA does not affect murine periarterial sympathetic NTUA uptake function

The effect of selective CB_1R agonist ACEA on periarterial sympathetic NTUA uptake into nerve terminals. **(A)** The NTUA uptake trace of the murine MA in vehicle control- (●) and WIN 55,212-2 treated conditions (△) almost consistently overlapped at each time point of the linear phase. **(B, C)** The linear NTUA uptake rate was not different between groups.

Each individual datapoint in scatterplots corresponds to a single terminal. Data presented as **(A, C)** mean±SEM.

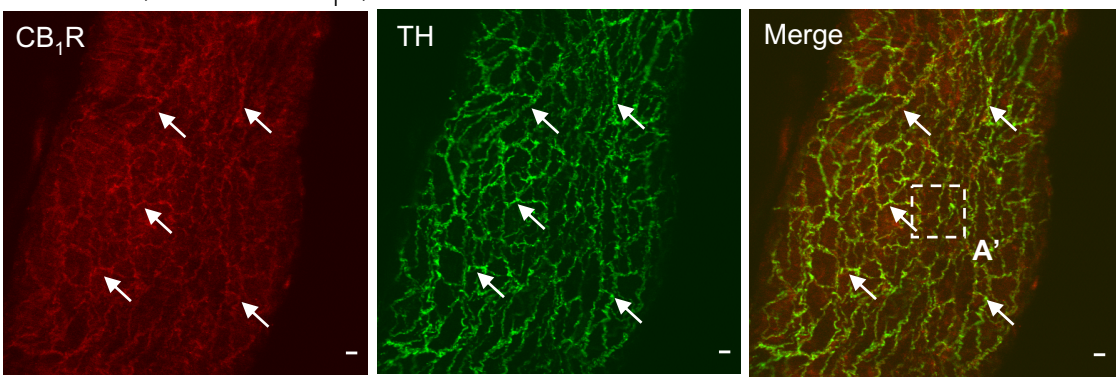
Statistical analysis:
(C) Welch's *t*-test; ns denotes $p>0.05$.

5.3.2. Rat

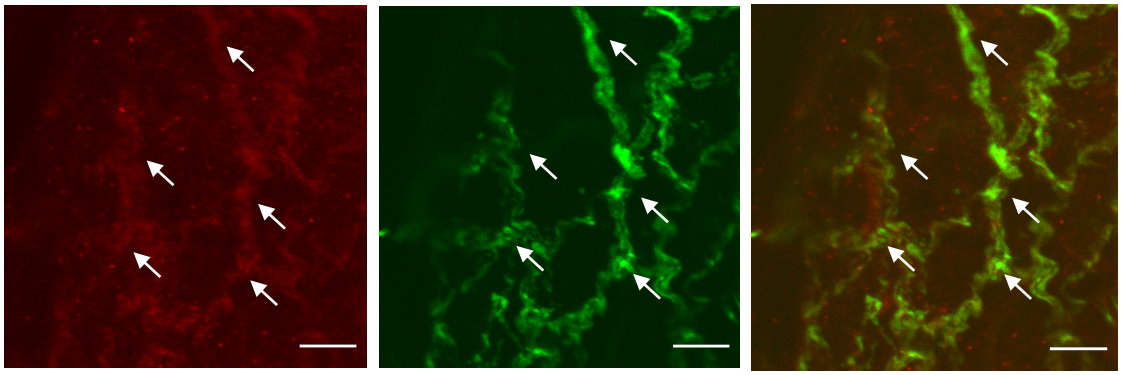
5.3.2.1. Localisation of CB_1R and TH in the rat mesenteric artery

IHC labelling of the rat MA demonstrated dense noradrenergic fibres innervation (TH, green) that surrounds the arterial vessel surface (Figure 5.10, middle columns). CB_1R staining (red) were observed in abundance in non-neuronal tissues as 'clustered appearances' (Figure 5.10B, leftmost columns). Like in the murine MA, very faint CB_1R labelling was observed overlapping with TH in a dispersed manner that is not completely localised to the nerve terminal, but rather throughout the length of the nerve fibre, including intervaricose segments (Figure 5.10A-C). Likewise, it was not entirely clear whether the CB_1R stainings were prejunctional receptors present on the nerve terminals or other structures that surroundings the length of the nerve fibre. Nevertheless, sections stained with secondary antibodies in the absence of primary antibodies produced negligible fluorescence signals for CB_1R and TH, demonstrating for low levels of non-selective binding of the antibody in the current protocol (Figure 5.10D). The observations were consistent across multiple mesenteric artery preparations from 3 animals.

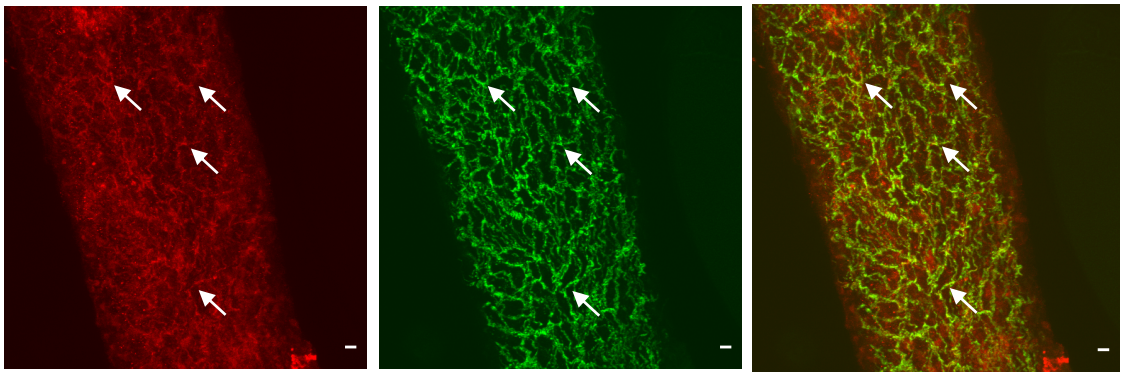
A: Rat MA; 1:250 anti-CB_1R, 1:500 anti-TH



A': Rat MA; 1:250 anti-CB_1R, 1:500 anti-TH



B: Rat MA; 1:250 anti-CB_1R, 1:500 anti-TH



C: Rat MA; 1:250 anti-CB_1R, 1:500 anti-TH

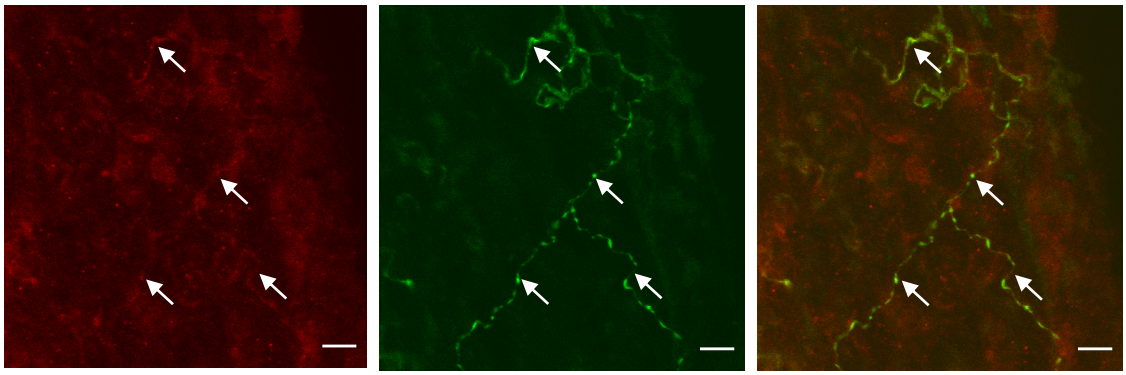
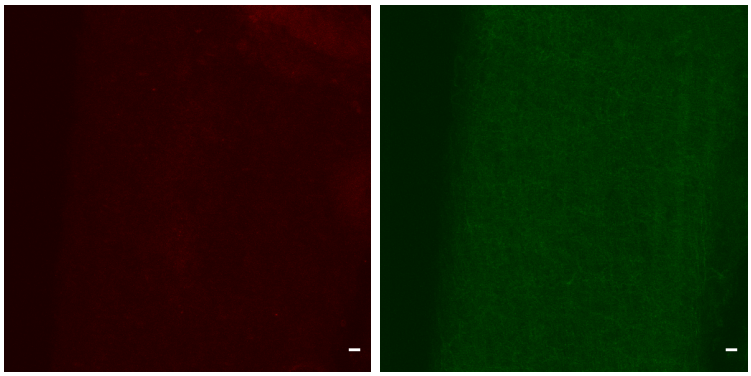


Figure 5.12: Localisation of CB_1R and TH in the rat mesenteric artery

Please refer to the following page for the figure legend. All micrographs, bars = 10 µm.

D: Rat MA: omission of anti-CB_1R and anti-TH 1º Ab



Description for figure on the preceding and present page.

Figure 5.12: Localisation of CB_1R and TH in the rat mesenteric artery

IHC labelling of whole preparations of rat MAs for CB_1R and TH expression. CB_1R labelling (red; leftmost columns, arrows) were present in abundance in non-neuronal tissue and overlaps with sympathetic nerve fibres (green; middle columns, arrows) without co-localisation when merged (rightmost columns, arrows). CB_1R were labelled with 1:250 1º Ab dilution (rabbit host) and TH with 1:500 1:250 1º Ab dilution (sheep host). Images were taken at low magnifications **(A, B)** and high magnifications **(A', C)**. **(D)** In the absence of primary antibodies, there was minimal fluorescence detected, demonstrating low levels of non-selective binding (Alexa Fluor 488 and Alexa Fluor 647, 1:250 each). Images are representative of n=3. All micrographs: bars = 10 µm.

5.3.2.2. CB_1R activation does not affect rat periarterial NTUA uptake

To detect whether CB_1R activation affects NTUA uptake in rat mesenteric periarterial sympathetic nerve terminals, the isolated MAs were exposed to WIN 55,212-2 (1 μM) and ACEA (100 nM) for 40 min before and during the 10 min 1:20 NTUA test period in non-stimulating conditions.

5.3.2.2.1. WIN 55,212-2

The accumulation of NTUA into periarterial noradrenergic neurones were similar between WIN 55,212-2-treated MAs and their vehicle control counterparts (0.01% DMSO) (Figure 5.13A). Thus, the linear NTUA uptake rate were not different between groups [control: 7.0 (2.9, 12.7)%.min^{-1} (n=4, n_t=60) vs. WIN 55,212-2: 8.6 (6.3, 11.4)%.min^{-1} (n=4, n_t=60), p>0.05, Figure 5.13B, C], which suggests CBR activation does not affect NTUA uptake function in the rat MAs.

5.3.2.2.2. ACEA

Relative to the control group, ACEA-treated terminals accumulated more NTUA at each time point during the linear phase (Figure 5.13A). However, the linear NTUA uptake rate was not statistically different between groups [control: 10.8 (7.7, 13.5)%.min^{-1} (n=4, n_t=60) vs. ACEA: 10.0 (8.3, 12.8)%.min^{-1} (n=4, n_t=60), p>0.05, Figure 5.14B, C]. This result further supports the lack of a CB_1R-mediated effect upon NTUA uptake function in rat mesenteric periarterial sympathetic nerve terminals.

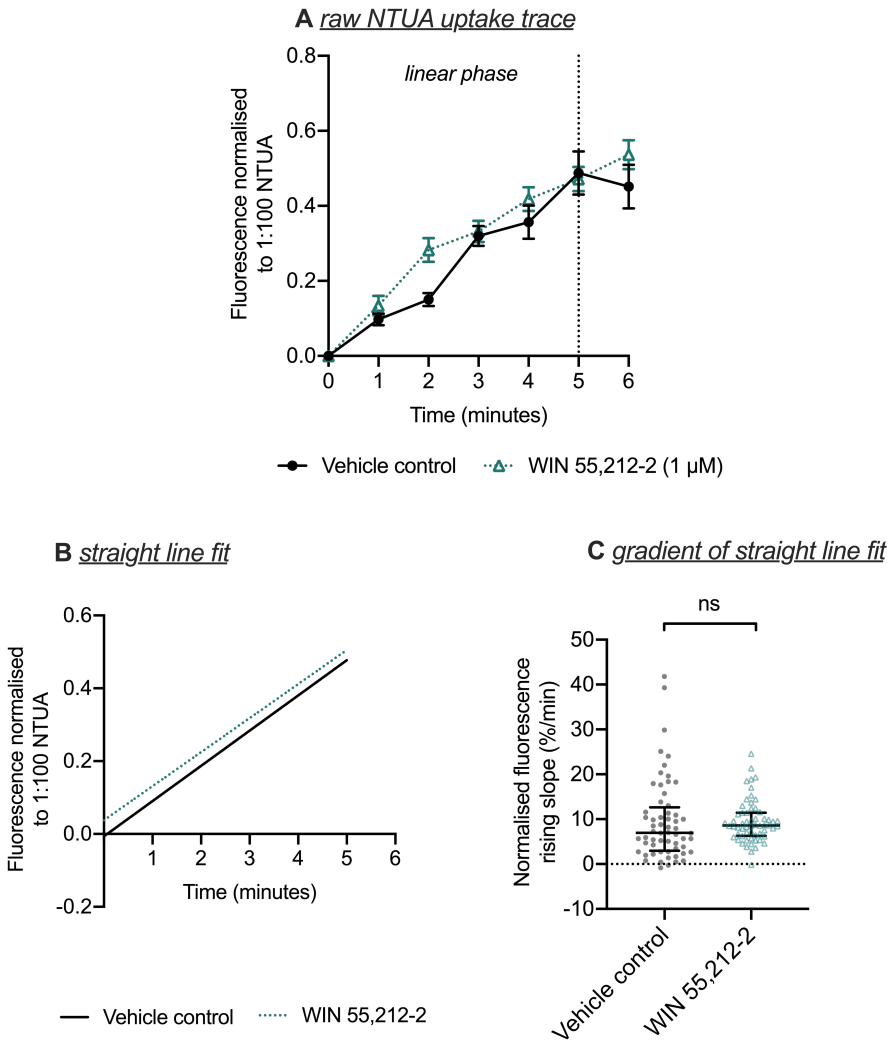


Figure 5.13: Nonselective CBR agonist WIN 55,212-2 does not affect rat periarterial sympathetic NTUA uptake function

The effect of nonselective CBR agonist WIN 55,212-2 on periarterial sympathetic NTUA uptake into nerve terminals. **(A)** The NTUA uptake trace of the rat MA in vehicle control- (●) and WIN 55,212-2 treated conditions (△) were similar, though fluorescence in the latter groups were observably greater at some time points. **(B, C)** However, there no differences in the linear NTUA uptake rate between WIN 55,212-2- and vehicle control groups.

Each individual datapoint in scatterplots corresponds to a single terminal. Data presented as **(A)** mean±SEM and **(C)** median (IQR).

Statistical analysis:
(C) Mann-Whitney test; ns denotes $p>0.05$.

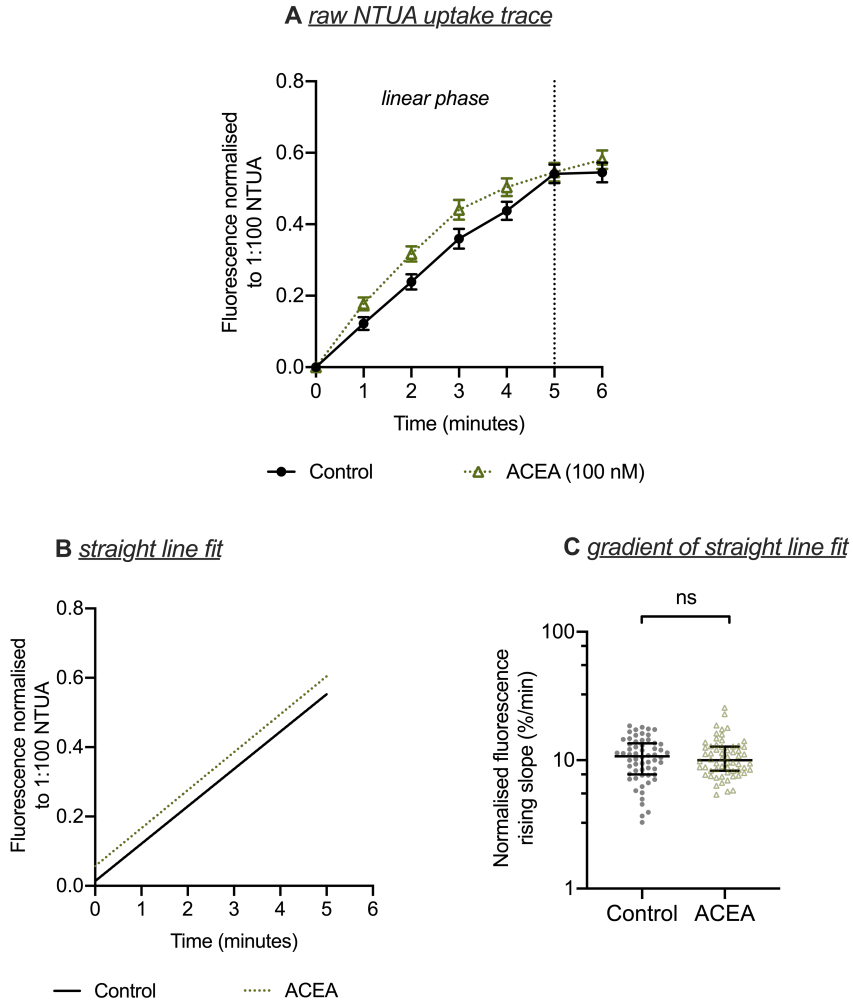


Figure 5.14: Highly selective CB_1R agonist ACEA does not affect rat periarterial sympathetic NTUA uptake function

The effect of selective CB_1R agonist ACEA on periarterial sympathetic NTUA uptake into nerve terminals. **(A)** The NTUA uptake trace of the rat MA in control- (●) and ACEA treated conditions (△) where the fluorescence in the latter group were greater than control at each time point. **(B, C)** However, the linear NTUA uptake rate between ACEA-treated and untreated terminals were not different.

Each individual datapoint in scatterplots corresponds to a single terminal. Data presented as **(A)** mean±SEM and **(C)** median (IQR).

Statistical analysis:
(C) Mann-Whitney test; ns denotes $p>0.05$.

5.4. Discussion

5.4.1. Main findings

In this Chapter, the optimised NTUA technique was used to measure cannabinoid regulation of NAT rate in rodent cardiovascular tissue, namely the heart and mesenteric arterial vasculature. This is the first study to demonstrate for a CB_1R-mediated reduction in single-terminal NAT rate in the murine (but not rat) heart, which may be tonically active during sympathetic neuronal activity. However, an effect of CB_1R activation on mesenteric periarterial NAT function was not observed in either species. Despite these findings, immunolabelling studies did not reveal CB_1R expression on cardiac noradrenergic terminals but might be present on the MAs. Thus, while this study unveils a suppressive role of CB_1R cardiac NAT, the location of the receptor in both tissues requires further investigation.

5.4.2. CB_1R activation suppresses cardiac NAT kinetics

5.4.2.1. Location of neuromodulatory cardiac CB_1R

Within the SNS, mRNA for CB_1R has been detected in the rat sympathetic ganglia (Ishac *et al.*, 1996) with a plethora of functional evidence at the prejunctional level to inhibit NAd release (Szabo and Schlicker, 2005). However, to my knowledge at the time of this thesis, the subcellular localisation of CB_1R on sympathetic nerve terminals in the cardiovascular system is yet to be morphologically demonstrated. Interestingly in the CNS, CB_1R are localised closely with NAT on noradrenergic terminals in the rat frontal cortex, and that CB_1R activation can significantly reduce NAT expression levels as a method of neuromodulation (Reyes *et al.*, 2009). However, whether or not a similar pattern of regulation occurs in sympathetic postganglionic neurones in the periphery is largely unknown. The laboratory previously demonstrated a CB_1R-mediated

suppression of NAT function in the murine urogenital system (Kennard, 2015), thus the current study sought out to extend the investigation to the rodent cardiovascular system.

5.4.2.1.1. CB_1R: prejunctional localisation

Rat

The current study did not provide evidence for cardiac prejunctional CB_1R immunolabelling in the rat. However, there is a body of functional literature from isolated tissues and pithed rats that strongly indicates for its presence. For example, Δ^9-THC (Ishac *et al.*, 1996) and AEA (Kurihara *et al.*, 2001) reduces the electrically evoked release of [^{3}H]-NAd from the isolated rat atrium in a CB_1R- and concentration-dependent manner. In the pithed rat, CBR agonists WIN 55,212-2 and CP 55,940 reduced the nicotine-induced tachycardia in a CB_1R-specific manner but had no effect upon isoprenaline-induced tachycardia; this strongly indicates a prejunctional, rather than postjunctional, effect (Malinowska *et al.*, 2001). Furthermore, the release of eCB induced by myocardial infarction reduced the electrically-mediated (but not isoprenaline-mediated) tachycardia via a CB_1R-dependent pathway in pithed rats (Rudź *et al.*, 2012).

These results from the literature strongly imply that the neuromodulatory CB_1R in the rat heart are located on the noradrenergic nerve terminal itself to directly reduce NAd release. However, prejunctional CB_1R were not optically detectable in the current study, which leads to the hypothesis that the IHC protocol may not have been sufficient for detection (discussion: section 5.4.2.1.3).

Mice

Most functional evidence of release-inhibiting CB_1R in mice are reported in the CNS and vas deferens (Ralevic, 2003, van Diepen *et al.*, 2008), while those in the heart generally yielded negative outcomes. WIN 55,212-2 (0.1 nM-1 μM) does not affect the evoked overflow of [^{3}H]-NAd from the murine heart (Trendelenburg *et al.*, 2000, Schlicker *et al.*, 2003), and Δ^9-THC, CP 55,940, and AEA (≥1 mM) does not functionally affect the electrically-evoked tachycardia (Lay *et al.*, 2000). Moreover, RT-PCR revealed the lack of CB_1R mRNA in the murine atria (Ishac *et al.*, 1996). Although transcription could occur in the sympathetic nerve soma, there is currently no genetic evidence for CB_1R expression in the mice stellate ganglia either. Thus, the lack of functional evidence in the murine heart suggests against cardiac sympathetic prejunctional CB_1R, and thus unveils species differences to the rat. Furthermore, although the prejunctional inhibitory CB_1R in the murine vas deferens is well established (Burnstock and Verkhratsky, 2010), tissue heterogeneity of CB_1R expression in the heart has been hypothesised prior in the murine species (Lay *et al.*, 2000).

However, the present study did demonstrate for a CB_1R-mediated suppression of NAT in the murine heart at the site of exocytotic release, which then suggests for its presence and thus warrants further investigation. It could be possible that the activation of CB_1R, if present, has no effect upon NAd release but rather exclusively upon clearance in the murine heart. Future studies could adopt sensitive RT-PCR methods to locate mRNA in the stellate ganglia and refine immunolabelling techniques at the site of release, for example. Thus, this remains an incomplete area of study and all assumptions discussed here are based on speculation only.

5.4.2.1.2. CB_1R: non-neuronal localisation

The current IHC study revealed localisation of CB_1R in non-neuronal structures of the rodent heart, presumably cardiomyocytes as it was dispersed throughout. This supports previous reports of CB_1R mRNA found in rat cardiomyocytes and positive immunoreactivity in the rodent- (Bátkai *et al.*, 2004, Mukhopadhyay *et al.*, 2007) and human heart (Bonz *et al.*, 2003). Functionally, activation of cardiomyocyte CB_1R can elicits direct negative chronotropic effects in the presence of hexamethonium (Krylatov *et al.*, 2007).

These studies suggest CB_1R are located postjunctionally in the heart (in some species at least), though final confirmation could be reached by co-staining cardiomyocytes with sacromeric actin with phalloidin in future studies. If the current IHC protocol was sufficient to detect for CB_1R in the rat heart, why weren't the prejunctional CB_1R also immunolabelled?

5.4.2.1.3. Immunohistochemistry protocol

If CB_1R were in fact expressed prejunctionally, then the lack of immunolabelling could be explained by methodological discrepancies of the current IHC protocol compared to others, namely related to the sample fixation process. In the 2 studies that utilised the same anti-CB_1R primary Ab as the current protocol, live cells were immunolabelled prior to fixation (Leonti *et al.*, 2010, Kleyer *et al.*, 2012) rather than after (current study). The current protocol could have abrogated immunoreactivity due to changes in the three-dimensional structure of the antigen during the protein cross-linking process (Kumar *et al.*, 2015). Future studies could adopt antigen retrieval techniques, such as with the use

of heat (Yamashita and Katsumata, 2017) or formaldehyde scavengers (Vollert *et al.*, 2015) following cryosectioning as a method of protocol refinement.

However, the hypothesis of fixation-induced abolition of immunoreactivity is disputed by the positive labelling of CB_1R in cardiac non-neuronal structures of both species. While the lack of neuronal CB_1R immunoreactivity could be attributed to cell type-dependent differences in the epitope due to, for example, polymorphisms, splice variants, and heterogeneities of receptor glycosylation, the anti-CB_1R antibody in the current study was polyclonal in nature, and so should have a high affinity to detect for multiple epitopes of the same protein. Nevertheless, future experiments could build upon neuronal-specific protocols that had previously demonstrated for CB_1R-positive co-localisation with noradrenergic axons within the CNS (Oropeza *et al.*, 2007).

Moreover, the anti-CB_1R antibody is later shown to be sufficient to detect for neuronal-like structures in the vasculature (further discussed in 5.4.3.1.). Thus, it is possible the additional cryopreservation step for cardiac tissue preparation abrogated immunoreactivity. As antibody specificity and selectivity can be difficult to predict and is highly dependent upon assay type and conditions, more experiments are required to troubleshoot the current IHC protocol to determine whether it was insufficient to detect prejunctional CB_1R or that the receptor is not intrinsically present.

5.4.2.1.4. Summary

Due to the wealth of functional data alluding to the presence of rat cardiac prejunctional CB_1R, the lack of its immunolabelling was surprising. While the absence might be explained by a methodological fault rather than a biological absence, future studies should first focus on protocol refinement. A refined protocol could then explore the

expression of prejunctional CB_1R in the murine heart. Until then, it would be premature to draw conclusions of its expression in either species.

5.4.2.2. Murine NAT suppression with CB_1R agonists: mechanism of action

The current study is the first to demonstrate for a CB_1R-mediated reduction in murine cardiac NAT function. However, the uncertainties of the IHC protocol complicates the localisation of CB_1R that could have elicited the observed effects. Moreover, an attempt to elucidate the target mechanism that governed the murine cardiac CB_1R-NAT interaction is complicated by promiscuous G protein coupling bias of the cannabinoid receptor. Thus, the following sections discusses the mechanism of action in hypothetical scenarios of CB_1R localisation.

5.4.2.2.1. Prejunctional CB_1R upon NAT

5.4.2.2.1.1. CB_1R-$G_{i/o}$ signalling

The murine sympathetic CB_1R is $G_{i/o}$-coupled (Göbel *et al.*, 2000) and the downstream effect of receptor activation in central- and peripheral neurones to inhibit neurotransmitter release is via the suppression of P/Q- and N-type voltage gated Ca^{2+} channels (Mackie and Hille, 1992, Twitchell *et al.*, 1997). In the previous Chapter I have already discussed potential mechanisms of another $G_{i/o}$-coupled prejunctional receptor, the α_2AR, to suppress NAT. Thus, analogous speculations of the mechanism can be found in section 4.3.6.4.

Interestingly, CB_1R activation of $G_{i/o}$ can also enhance neuronal nitric oxide (NO) synthase (NOS) activity to release NO (Carney *et al.*, 2009), which can have important implications upon NAT function. NOS-I can co-localises with tyrosine hydroxylase

positive neurones in the isolated rat heart (Schwarz *et al.*, 1995), and the incubations of cultured PC12 cells and superior cervical ganglion neurones with a NO donor significantly reduced desipramine-sensitive [^{3}H]-NAd uptake in a concentration-dependent manner (Kaye *et al.*, 1997). This effect was later attributed to a direct nitrosylation of the transporter (Kaye *et al.*, 2000). Therefore, this suggests that CBR agonists in the current study may have activated a neuronal CB_1R-$G_{i/o}$-NOS-NO pathway to reduce NAT rate in cardiac sympathetic nerve terminals.

5.4.2.2.1.2. CB_1R-G_s signalling

CB_1R can also be G_s-coupled in some settings, as observed by increases in cyclic adenosine monophosphate (cAMP) following receptor activation. In CHO cells transfected with CB_1R and cultured rat striatal neurones, CBR activation led to a CB_1R- and dose-dependent increase in cAMP (Glass and Felder, 1997, Calandra *et al.*, 1999). However, Mukhopadhyay and Howlett (2005) could not immunoprecipitate G proteins other than $G_{i/o}$ with CB_1R from N18TG2 cells, and that Eldeeb *et al.* (2016) demonstrated an increase in cAMP does not necessarily correlate to G_s activation, but in fact correlates with an attenuation of the tonic inhibitory influence of $G_{i/o}$ upon adenylyl cyclase (AC). Such differences may be attributable to ligand- and/or cell type differences. Nonetheless, there is currently no general consensus of the effect of AC, cAMP, or protein kinase A (PKA) signalling on NAT function, as the observed effects upon transporter function are strongly cell line- and species-dependent *in vitro* [reviews: Mandela and Ordway (2006b) and Bermingham and Blakely (2016)].

5.4.2.2.1.3. CB_1R-$G_{q/11}$ signalling

CB_1R can also be $G_{q/11}$-coupled; Lauckner and colleagues (2005) reported that in stably transfected HEK293 cells and hippocampal neurones treated with high concentrations of WIN 55,212-2 (5 μM), the CB_1R-mediated increase in $[Ca^{2+}]_i$ was significantly reduced with dominant-negative $G_{q/11}$ or phospholipase C inhibitors but was maintained in pertussis toxin-treated cells. As previously discussed in section 4.3.5.1., protein kinase C (PKC) activation (downstream of $G_{q/11}$) can reduce NAT surface expression (Apparsundaram *et al.*, 1998a, Sung *et al.*, 2003). Therefore, it is possible NAT suppression in the current study was attributed to a CB_1R-$G_{q/11}$-PKC-mediated reduction in NAT surface bioavailability. This would also support for the CB_1R-mediated reduction of maximum fluorescence in cardiac nerve terminals (Y_{max}; Figure 5.2) without affecting the initial rate constant of the reaction. However, CB_1R-$G_{q/11}$ coupling is highly ligand specific to WIN 55,212-2 [review: Laprairie *et al.* (2017) and Wouters *et al.* (2019)]. Therefore, while CB_1R-$G_{q/11}$ coupling could explain for the WIN 55,212-2-NAT effect in the current study, it is unknown whether ACEA activates the same downstream mechanisms.

In order to fully understand the mechanisms of NAT suppression if CB_1R were located prejunctionally, further experiments are required to elucidate the G protein- and ligand-specificity of signalling pathways activated by CB_1R in the current experimental context. This would help to decipher cannabinoid regulation of sympathetic volume neurotransmission, as prejunctional CB_1R activation also modulates NAd release.

5.4.2.2.2. Retrograde effect upon NAT by postjunctional CB_1R activation

The uniform expression of non-neuronal CB_1R in the current study suggests an alternative mechanism for NAT suppression: retrograde signalling induced by

postjunctional CB_1R activation. A likewise mechanism is present in the brain, where postjunctional mAChR activation induces eCB release to act upon presynaptic CB_1R to modulate neurotransmission (Thomsen *et al.*, 2018). A hypothesis here would therefore be: WIN 55,212-2 and ACEA acts upon CB_1R located postjunctionally in the murine heart to release mediators for retrograde signalling back onto the nerve terminals to suppress NAT function. However, this would assume an uncharacterised signalling pathway between an unknown liberated ligand and prejunctional receptor, and thus would require further study.

5.4.2.2.3. Other cannabinoid-sensitive receptors

Other than CB_1R, there are also the CB_2R and non-cannabinoid receptors that are sensitive to cannabinoid agonists, such as the transient receptor potential vanilloid type I ($TRPV_1$), orphan GPCR, non-CB_1R, non-CB_2, and non-$TRPV_1$ receptors (Pertwee, 2005). Thus, the possibility of these cannabinoid ligand targets to evoke cardiac NAT suppression is discussed below.

While CB_2R on sympathetic nerve terminals has been suggested to be present in the murine vas deferens (Griffin *et al.*, 1997), CB_2 activation was unlikely to suppress cardiac NAT in the current study. This is because the CB_1R-specific inverse agonist, SR141716A, was able to completely reverse cardiac NAT suppression. Furthermore, ACEA, a compound that is >1400-fold more selective for CB_1R (K_i=1.4 nM; Tocris Bioscience; *datasheet*) than for CB_2R induced a similar effect on NAT as WIN 55,212-2.

Next, the cardiac cannabinoid-sensitive GRP55 and $TRPV_1$ receptors do not interact with WIN 55,212-2 (Pertwee, 2005, Henstridge *et al.*, 2016) and most importantly, there is currently no evidence that either targets are expressed on cardiac sympathetic nerve

terminals. Therefore, these cannabinoid-sensitive targets also cannot explain the findings with WIN 55,212-2 (and ACEA) in the current study.

In the CNS, clonidine can activate prejunctional α_2AR and (α_2AR-like) imidazoline receptors to modulate noradrenergic transmission (Bousquet *et al.*, 2020). Interestingly, a non-I_1R/non-I_2 imidazoline receptor subtype that is CB_1R-like is present in the human atria (Molderings *et al.*, 1999) and has been shown to inhibit veratridine-evoked [^{3}H]-NAd release from PC12 cells (devoid of α_2-AR and CB_1R) in a CB_1R-dependent manner (Molderings *et al.*, 2002). While it is possible the putative cannabinoid-sensitive imidazoline receptor subtype (also $G_{i/o}$-coupled) may also affect NAT function, there is evidence to show that the receptor type does not become activated by WIN 55,212-2 at 1 μM (Molderings *et al.*, 2002), a concentration used in the current study.

5.4.2.2.4. Summary

To briefly summarise, the cannabinoid-mediated suppression of NAT in the murine heart is most likely attributed to CB_1R, though the precise mechanisms downstream of CB_1R is complicated by the promiscuous G protein coupling and ligand specificity. The effect could be attributed to the same signalling pathways to reduce NAd release, i.e., via $G_{i/o}$, or via undiscovered pathway(s) of neuromodulation. At present, more experiments and investigations are required to decipher the inhibitory effects of CB_1R upon NAT-mediated clearance.

5.4.2.3. CB_1R-mediated tonic suppression of NAT: endocannabinoid source

The eCBs, including 2-AG and AEA, are enzymatically biosynthesised ‘on demand’ from membrane phospholipids and are released locally or bound onto serum albumin into

the circulation (Di Marzo, 2008). Triggered by depolarisation-induced increases in $[Ca^{2+}]_i$ or $G_{q/11}$-mediated Ca^{2+} mobilisation in postsynaptic neurones (Cadas *et al.*, 1996), the immediate synthesis and liberation for retrograde action in the CNS is often termed 'depolarisation-induced suppression of inhibition/excitation' (Szabo and Schlicker, 2005, Di Marzo, 2008).

In the current study, a stimulation-evoked, CB_1R-dependent suppression of murine cardiac NAT function suggests for an activity-dependent liberation of eCB for transporter regulation. The lack of an effect in non-stimulating conditions supports this notion (Figure 5.4). Thus far, indirect evidence has suggested for eCB production in the heart; high levels of AEA synthesising enzyme are found in rodent heart microsomes (Moesgaard *et al.*, 2002) and that elevated levels of eCB were observed in $FAAH^{-/-}$ (fatty acid amide hydroxylase, crucial enzyme for eCB degradation) murine hearts (Pacher *et al.*, 2005c).

However, the exact cellular source of liberated eCB to mediate NAT suppression in the heart is unknown. It could be from cardiomyocytes, neurones, or resident immune cells in the tissue. It has been suggested that mesenteric sensory nerve endings are a source of AEA to drive vasorelaxation in pre-contracted vessels (Ishioka and Bukoski, 1999). As the heart is also innervated by sensory nerve terminals (Shivkumar and Ardell, 2016), it is quite possible the current EFS protocol also depolarised sensory nerves for eCB production to act on NAT on nearby sympathetic nerve terminals. To rule out a neuronal source of eCB, which is interestingly a prominent source in cirrhotic cardiomyopathy (Gaskari *et al.*, 2005), future studies could adopt the use of tetrodotoxin to selectively inhibit neuronal voltage-gated Na^+ channels (Honerjäger, 1982). However, this would in return intervene with the EFS dependency of the study. Immune cells are also capable

to synthesise eCB; for example, enhanced Ca^{2+} currents in macrophages increase eCB production (Di Marzo *et al.*, 1999), and platelets and neutrophils possess eCB metabolism machinery (Edgemond *et al.*, 1998). However, immune cells are activated by cytokines and only exhibit CB_1R-mediated effects in pro-inflammatory conditions; therefore, immune cells are an unlikely source of eCB for sympathetic neuromodulation in the current study.

Another source of neuromodulatory eCB liberation is from cardiomyocytes, as the extent of postjunctional activation would consequently determine subsequent stimulatory release events from the prejunctional terminal. However, whether or not cardiomyocytes qualify as a source of eCB in the current study is complicated by the deliberate lack of electrically evoked contraction to favour undisrupted monitoring of noradrenergic terminals. However, it is possible that subthreshold depolarisations of cardiomyocytes are sufficient to trigger acute synthesis and release of eCB to act upon NAT, this is based on speculation only and it is currently premature to speculate the origin of eCB for the current study.

5.4.2.4. (Patho)physiological relevance in the heart

Chronic application of exogenous cannabinoids is generally considered to depress cardiovascular function via some action on prejunctional release-inhibiting CB_1R on sympathetic nerve terminals in experimental animals (Malinowska *et al.*, 2012). However, low or moderate doses of CB_1R agonists in man immediately leads to a tachycardic and hypertensive response that can last up to 1 hr, collectively referred to as a 'cannabis-induced hyperadrenergic state', which can manifest into increased incidences of cardiovascular fatalities, such as atrial fibrillation and dysrhythmia (Richards *et al.*, 2020). As cannabis-induced tachycardia is preventable by propranolol pre-treatment (Gash *et*

al., 1978), cardiac dysrhythmias are suggested to precipitate as a result of sympathetic overactivation (Malinowska *et al.*, 2012, Oliveira *et al.*, 2018). The current results suggest the CB_1R-mediated NAT suppression may be a mechanism to potentiate junctional availability in NAd and increase the effect of the monoamine. As there is evidence to show that cannabidiol (main non-psychotropic constituent of *Cannabis sativa*) can inhibit NAd reuptake in rat hypothalamic synaptosomes (Poddar and Dewey, 1980), and elicit a carrier-mediated increase in heart rate (HR) in pithed and adrenalectomized rats (Kossakowski *et al.*, 2019), the current finding suggests Δ^9-THC in cannabis may also contribute to the pathology during exposure. However, although the reduction in NAT function in response to WIN 55,212-2 and ACEA were demonstrated with NTUA exposure in the 6 min timeframe, the murine heart had already been exposed to CB_1R agonists for 40 min prior to the introduction of the NTUA test period. Thus, the CB_1R-mediated NAT suppression may be more applicable to the phase III cardiovascular response (bradycardia/hypotensive) to cannabinoids. Perhaps a way to investigate this in the future is to expose tissues to CB_1R agonists concomitantly with NTUA during imaging. Until then, it is difficult to determine which phase of the haemodynamic response to cannabinoids could NAT suppression coincide with. It is important to note others have suggested the tachycardiac response in humans may be attributed to inhibitory CB_1R present on cardiac parasympathetic nerve terminals (Pacher *et al.*, 2005b).

Interestingly, cannabinoids have been shown to suppress reuptake activities of other biogenic amines, such as dopamine (Poddar and Dewey, 1980, Sakurai-Yamashita *et al.*, 1989) which has been implicated in high dopaminergic states in schizophrenia (Sekiguchi *et al.*, 2019). However, the effect of cannabinoids on the NAT had not yet been reported. Although the CB_1R-mediated suppression of NAT function may

counteract the reduction in NAd release (phase III), the extent of potentiating junctional NAd concentrations and the net target end-organ effect is unclear.

During my study, I wondered whether an endogenous eCB tone may exist to modulate sympathetic transmission function at rest. The current result of an activity-dependent, CB_1R-mediated cardiac NAT suppression seems to suggest so. However, previous studies have disputed this hypothesis; for example, the evoked release of [^{3}H]-NAd from the isolated atria and haemodynamic parameters *in vivo* did not differ between $CB_1R^{-/-}$ and $CB_1R^{+/+}$ mice (Schlicker *et al.*, 2003, Rajesh *et al.*, 2012). Although this may relate back to an innate lack of an inhibitory CB_1R for NAd release in the murine heart (Trendelenburg *et al.*, 2000, Schlicker *et al.*, 2003, Lay *et al.*, 2000), it cannot be definitively concluded that CB_1R activation does not affect NAT function. However, it is unlikely that the current result would amount to significant physiological relevance in the heart, as the effect (very small) was only uncovered by α_2AR antagonism during EFS.

In order to fully investigate the contribution of NAT function to cannabinoid-induced cardiac effects, improved techniques are required to study NAT exclusively. Overflow studies have been pivotal to study CB_1R-mediated effects upon NAd release, but almost all protocols of overflow utilise the NAT inhibitor desipramine (or equivalent) to block the transporter, thus the role of NAT has been unintentionally overlooked. Additionally, insight into NAT function by CB_1R activation *in vivo* can be further complicated by the great variabilities in cardiac responses in animals (anaesthetised versus conscious) and the multitude of cannabinoid targets and activated modulation pathways (Pacher *et al.*, 2005c). The latter includes the effect of cannabinoids centrally, via the parasympathetic pathway (Varga *et al.*, 1995, Niederhoffer *et al.*, 2003, Pacher *et al.*, 2004), and non-neuronal targets of cannabinoids capable to induce bradycardia and vasodepression

(Ledent *et al.*, 1999, Bátkai *et al.*, 2004). Thus, the effect of eCB upon junctional clearance of neurotransmitters is a new field of study that requires technical methodologies that can exclusively investigate NAT, such as the current NTUA technique.

5.4.2.5. Species-specific effect of CB_1R-mediated cardiac NAT suppression

In the present study, the CB_1R-mediated cardiac NAT suppression was only observed in the murine species but not in the rat. This was surprising because it directly contrasts with the observations of functional inhibitory CB_1R in the heart in these species. However, it may be that CB_1R activation selectively inhibits NAT without affecting NAd release in mice, and vice versa in the rat.

Despite the species differences in the CB_1R-mediated suppression of NAT, it appears that in both species there is a lack of eCB tone that regulates cardiac sympathetic function *in vivo* at rest. For example, $CB_1R^{-/-}$ and $FAAH^{-/-}$ mice do not have strong cardiac phenotypes, and no haemodynamic changes were observed in pithed rats exposed to systemic CB_1R antagonist SR141716A (Pfitzer *et al.*, 2005). Therefore, even if cannabinoids were to exert an effect on NAT function via CB_1R activation *in vivo*, it is unlikely to affect overall cardiac and haemodynamic function in non-pathological conditions, but probably more so in pathological- or drug-induced states.

5.4.2.6. Summary

The current study demonstrates for a CB_1R-mediated NAT suppression in the murine heart that is not present in the rat. However, the localisation of CB_1R remains elusive due to the uncertainties of the IHC protocol. Also unveiled in the murine heart was the

slight activity-dependent CB_1R-mediated suppression of NAT, likely by the liberation of eCB during neuronal activity. Further experiments are required to identify the candidate G proteins, signalling pathways, and effector molecules coupled to CB_1R to mediate such response to better understand whether the ECS may offer novel therapeutic approaches in a variety of cardiovascular disorders.

5.4.3. CB_1R activation does not affect periarterial NAT kinetics

5.4.3.1. Vascular CB_1R localisation

5.4.3.1.1. CB_1R: prejunctional localisation

Similar to the heart, previous studies have suggested for the presence of prejunctionally located CB_1R on rat resistance arteries to modulate sympathetic neurotransmission. CB_1R-mediated reductions in [^{3}H]-NAd release and the associated vasoconstriction have been reported in the rat tail arteries (Malinowska *et al.*, 1997), perfused mesenteric bed (Ralevic and Kendall, 2002, Pakdeechote *et al.*, 2007), and renal arteries (Deutsch *et al.*, 1997). In mice, on the other hand, there is very little evidence, with the exception of a negative outcome in the aorta (Schultheiss *et al.*, 2005), of an effect in arteries. Most importantly, to date, there are currently no morphological studies that have identified or disputed CB_1R on rodent perivascular sympathetic nerve terminals.

In the current study, immunolabelling revealed faint CB_1R expression on structures very close (almost overlapping) to rodent periarterial sympathetic nerve terminals in a diffused manner, rather than distinctly punctate with varicose terminals. The lack of the classic 'beads on a string' morphology of CB_1R staining suggests they are not present on the nerve terminals or intervaricose segments themselves. Furthermore, CB_1R were strongly localised with rat sympathetic nerve axons, though it may have represented

intracellular CB_1R being transported away from soma to the site of release [CB_1R mRNA has been identified in the sympathetic ganglia; (Ishac *et al.*, 1996, Buckley *et al.*, 1998)]. However, there were several TH-positive areas that were not CB_1R positive. Thus, this prompted the question whether CB_1R were in fact present on non-neuronal structures, an example being Schwann cells (see below).

5.4.3.1.2. CB_1R: non-neuronal localisation

The rat mesenteric arterial adventitial layer also contains Schwann cells (SC), which could be in very close apposition with the sympathetic nerve terminals for continuous and dynamic communication (Hansen *et al.*, 2019). Perivascular SC investment around the sympathetic nerve terminals may explain why the nerve 'swellings' were lost in CB_1R immunolabelling. However, most varicosities lose their SC investment as they form neuroeffector junctions with postjunctional target cells (Jänig, 2006b), though to my knowledge, there is currently no anatomical/morphological evidence of perivascular mesenteric SC-sympathetic interactions right down at the nerve varicosity level, and this may be the first study to do so. Future studies could immunolabel for glial fibrillary acidic protein (peripheral glial cell marker) in addition to anti-CB_1R to confirm for cannabinoid receptor expression on SC. In the noradrenergic axon bundles, CB_1R-positive structures were also in very close contact with noradrenergic fibres where cell nuclei were interweaved throughout (Figure 5.9B), might the nuclei belong to SC?

Finally, in both species, CB_1R were also prominently localised in non-neuronal vascular tissue. One cell type may be vascular smooth muscle cells in the media where CB_1R are widely distributed; mRNA has been detected in these cell types in the human aorta (Sugiura *et al.*, 1998) and feline cerebral vessels (Gebremedhin *et al.*, 1999), with positive CB_1R immunoreactivity identified in rat mesenteric vessels (Darker *et al.*, 1998).

Thorough cell-type analysis is required, as some non-neuronal CB_1R-positive cells have been shown to play a direct role in the vasodepressive effects (Malinowska *et al.*, 2012).

5.4.3.2. Physiological relevance

As the location of neuronal-like CB_1R labelling cannot be conclusively determined (nerve terminal versus SC), the functional relevance of CB_1R is discussed in hypothetical scenarios of localisation.

Prejunctional sympathetic CB_1R

Cannabinoids elicits a CB_1R-mediated vasorelaxant effect in the mesenteric vasculature by the release-inhibiting action at the prejunctional site. However, in the current study CBR agonist WIN 55,212-2 and CB_1R selective agonist ACEA did not alter NAT rate in perivascular sympathetic nerve terminals in either species. This would therefore suggest that, at least on periarterial sympathetic postganglionic neurones, cannabinoids may exclusively modulate NAd release rather than reuptake for sympathoinhibition.

However, interestingly, the NAT has been implicated in the rapid, transient pressor response of cannabinoids in phase II; the increase in hindlimb perfusion pressure in response to Δ^9-THC administration in anaesthetised rats was counteracted by phentolamine and reserpine thus indicating a CB_1R-mediated tyramine-like effect of NAd displacement for sympathoexcitation (Adams *et al.*, 1976). Could it be possible that NAT engages in reverse transport mode under CB_1R activation? However, in the current study, the levels of (pre-loaded) NTUA in WIN 55-212,2 and ACEA treated terminals did not differ to control conditions. Likewise, the tyramine-like effect of CB_1R activation could not be replicated by other researchers (Ilayan *et al.*, 2013).

Non-prejunctional CB_1R

The exclusive contribution of inhibitory prejunctional CB_1R to mediate vasorelaxation has been challenged. For example, Ralevic and Kendall (2009) identified cannabinoids can act via $TRPV_1$ on sensory nerve fibres for sensory neurogenic relaxation. Furthermore, Gebremedhin and colleagues (1999) reported eCB can act directly upon CB_1R on feline cerebral vascular smooth muscle cells to reduce Ca^{2+} currents for vasorelaxation. Moreover, Wagner and colleagues (2001) observed a persistent hypotensive effect to HU-210 even after ganglionic block with hexamethonium. Therefore, the CB_1R-positive labelling in non-neuronal tissue in the current study may support for targets of cannabinoids for vasorelaxation other than modulation of sympathetic neurotransmission [comprehensive reviews: O'Sullivan (2015) and Ho and Kelly (2017)].

The current study also postulates the presence of CB_1R-expressing SC that surrounds noradrenergic nerve terminals. Within the CNS, CB_1R expression has been reported in glial cells, such as astrocytes, oligodendrocytes, and microglia (Zou and Kumar, 2018). Interestingly, the expression of CB_1R on SC that myelinates sensory nerve fibres has been implicated in the neuromodulation of nociceptive processing (Milligan *et al.*, 2020). Therefore, it may be possible that cannabinoids also act upon CB_1R on Schwann cells to modulate sympathetic excitability in terminals nearby for a vasodepressive effect. However, to my knowledge, the CB_1R-mediated modulation of SC surrounding peripheral sympathetic neurones is an entirely new field of study.

5.4.3.3. Summary

In summary, the current study demonstrates for CB_1R-positive labelling in neuronal-like structures that surroundings perivascular sympathetic nerve terminals in both rodent

species, though further study is required to conclude whether CB_1R are present prejunctionally at the site of release or on SC that may encapsulates the nerve terminal. Neither CB_1R agonists elicited an effect upon NAT kinetics, suggesting that vasorelaxation effects by cannabinoids occurs independently of NAd clearance from the junctional cleft, for example via neurotransmitter release inhibition or directly at the postjunctional site on vascular smooth muscle.

5.4.4. Therapeutic potential of cannabinoids to treat cardiovascular disease?

Interestingly, cannabinoids can induce both detrimental and beneficial effects outcomes for cardiovascular pathology. For example, the mass release of eCB from macrophages can elicit extreme pathological hypotension in the form of shock (Mendizábal and Adler-Graschinsky, 2007). On the other hand, ECS overactivation at multiple targets in hypertension is considered beneficial by limiting the elevation in blood pressure (BP) triggered by sympathetic augmentation (Haspula and Clark, 2020). The possibility to utilise cannabinoid receptor ligands as antihypertensive agents was first considered in the 1970s and resumed from the 1990s onwards following the molecular cloning of the CBR and the discovery of endogenous eCB ligands (Haspula and Clark, 2020).

There is a body of evidence to demonstrate for the beneficial effects of ECS overactivation in hypertension. Systemic administration of CB_1R agonists AEA (Bátkai *et al.*, 2004) and THC (Kosersky, 1978) elicited a greater and longer lasting hypotension in spontaneously hypertensive rats (SHR), angiotensin II-induced, and Dahl salt-sensitive hypertensive rats (Bátkai *et al.*, 2004) compared to their normotensive counterparts. Likewise, inhalation of THC led to a more profound decrease in arterial

BP in hypertensive patients compared to normotensive individuals (Crawford and Merritt, 1979). In DOCA-salt sensitive hypertensive rats treated with AM251 alone, there was an accentuation in the neurogenic vasopressor response to EFS, which was absent in normotensive rats (Toczek *et al.*, 2015). Interestingly, haemodynamic variables in hypertensive animals were restored to normotensive values by enhancement of AEA bioavailability through preventions of degradation and reuptake (Bátkai *et al.*, 2004). The most likely explanation for these findings is an exaggerated ECS 'tone' that limits the increase in BP and cardiac contractility, hence why it is of particular interest to target the ECS for therapeutic purposes.

The mechanism of ECS hyperactivation to elicit a cardioprotective depressor effect in hypertensive states is multifaceted. While the central mechanisms of ECS in hypertension is unclear (Haspula and Clark, 2020), studies have suggested for several peripheral-based mechanisms of the protective effects of ECS overactivation. Bátkai and colleagues (2004) suggest for a direct CB_1R-mediated cardio/vasodepressive effect in the myocardium and aortic endothelium, while Wang and colleagues (2005) attribute a partial effect to $TRPV_1$ presumably on perivascular sensory nerve terminals (Mendizábal *et al.*, 2001). Moreover, Toczek and colleagues (2015) demonstrate the presence of CB_1R on periarterial sympathetic nerve terminals can tonically inhibit NAd release in hypertensive rats.

The current study provides an additional mechanism of cannabinoids in the cardiovascular system: CB_1R-mediated suppression of NAT function in cardiac sympathetic nerve terminals. However, whether or not this mechanism contributes towards cardiovascular regulation in normal states or hypertensive states *in vivo* is unknown and requires further research. More importantly, if true, then the effect on NAT

function may reverse or even counteract the well-characterised and well-desired suppression cardiovascular function, thus highlighting the complexity of effects exerted by cannabinoids. Nevertheless, while the therapeutic potential of enhancing the ECS in hypertensive states is of great interest (Toczek and Malinowska, 2018), it currently remains complicated and uncertain, particularly due to recent observations of side effects associated with FAAH inhibition in experimental animal studies (Baranowska-Kuczko *et al.*, 2016, Pędzińska-Betiuk *et al.*, 2017).

5.5. Overall conclusion

This is the first study to investigate the action of CB_1R activation upon NAT function in the rodent heart and mesenteric arteries. While there was no detectable expression of prejunctional CB_1R in the rodent heart, CB_1R activation by exogenous agonists and neuronal activity led to a reduction in NAT function in the murine heart. The CB_1R-mediated cardiac NAT suppression is unlikely to alter cardiac physiology at rest, though it could contribute towards the transient tachycardic response to cannabinoid exposure in human heart, which has important implications upon arrhythmogenesis. On the other hand, perivascular NAT were not affected by CB_1R agonists, suggesting modulation of neurogenic contraction occurs independently of neuronal NAd clearance. In both species, there were CB_1R expressions in non-neuronal cell types, one of which possibly being Schwann cells, that could modulate perivascular sympathetic nerve activity. Together, these results demonstrate for the first time for tissue- and species-differences in CB_1R expression and modulation of NAd clearance. Further investigations are now required to explore the mechanistic pathways of cardiac NAT suppression by CB_1R, and whether novel therapeutic approaches could be developed to reduce the incidences of CB_1R-mediated tachycardia and associated pathologies.

CHAPTER VI. DISCUSSIONS AND CONCLUSIONS

General conclusions

In the current study, the regulation of the noradrenaline transporter (NAT) in rodent cardiovascular tissues was investigated with the use of a fluorescence-based assay. This tool is able to label individual sympathetic nerve terminals and concomitantly monitor for real-time changes in NAT-mediated substrate clearance at discrete neuroeffector sites in the heart and mesenteric periarterial vessels. To meet the objectives and aims, firstly the specificity of the assay (NTUA; Neurotransmitter Transporter Uptake Assay) for NAT was validated with the use of a NAT-specific inhibitor and reverse transport substrate, desipramine and tyramine, respectively. Secondly, this work has unveiled several possible negative modulators of NAT function in the heart, such as the muscarinic acetylcholine receptor (mAChR), α_2-adrenoceptor (α_2AR), and cannabinoid type I receptor (CB_1R). Interestingly, the neuromodulatory roles of α_2AR and CB_1R were also uncovered in bouts of sympathetic neuronal activity. Thirdly, the investigations into single-terminal NAT function between species and tissues also revealed distinct differences, namely faster NAT function in the murine species than the rat, as well as in the heart than mesenteric vessels. The tissue selectivity of NAT function was further demonstrated in a pre-clinical animal model of obstructive sleep apnoea (OSA), a disease with complex cardiovascular implications. Finally, an immunolabelling approach revealed postjunctional localisation of CB_1R in the heart and vessels, while a prejunctional presence was suspected exclusively in the periarterial vessels.

Challenges and limitations

The current NTUA protocol to measure single-terminal NAT rate was time restricted to the critical period of linear uptake. However, it was only during the progression of this work when I began to appreciate the value that a full timeline of uptake would bring, particularly when certain treatments were observed to alter the linearity of fluorophore accumulation. As dynamic changes in NTUA uptake can result from modifications of NAT surface expression, intrinsic transporter rate, fluorophore metabolism/quenching, and as I demonstrate here, vulnerabilities from phototoxicity, more sophisticated methods are required to give accurate readings of transporter rate. I had attempted to analyse NTUA uptake with a non-linear curve fit method to provide additional results and interpretations of NAT function, though regrettably it was limited by the low number of time-points available. Thus, while the quantification of the initial linear uptake slope is a straightforward methodology, it would be ideal to extend the time of NTUA exposure in order to build a more comprehensive profile of NAT kinetics and investigate parameters beyond the initial rise. Future work could focus upon identifying key influencers of single-terminal NTUA uptake and retention, and factor them into thorough computational models for transporter function analysis.

In the heart, the effects of sympathetic neuronal activity on NAT function were most likely contributed by the joint actions of evoked NAd at the α_2AR and as a competitive substrate with NTUA at the NAT. However, the direct effect of changes in neuronal membrane potential upon NAT function was overlooked. While changes in membrane potential is pertinent for exocytotic events, it may also have important implications for reuptake as demonstrated *in vitro* (Sung *et al.*, 2017). In this thesis, the attempt to uncouple exocytotic events from depolarising stimuli in order to measure intrinsic NAT

function failed on the basis that colchicine directly interfered with NAT kinetics in non-stimulating conditions, suggesting for the complex interconnectedness between the intracellular machinery responsible for release and reuptake. Thus, future experiments are required to isolate the depolarisation-dependent and exocytosis-independent modes of NAT regulation. A starting point would be to investigate the effect of exogenous α_2AR agonist, e.g., clonidine, on cardiac NAT function in non-stimulating conditions, for example.

Another limitation of the current work is the narrow focus on sympathetic noradrenergic signalling. In addition to the main neurotransmitter NAd, sympathetic postganglionic neurones also contain the co-transmitters ATP, neuropeptide Y (NPY), galanin (Herring *et al.*, 2012), and tissue plasminogen activator (Jiang *et al.*, 2002), which are released in a highly stimulus-dependent manner. Importantly, prejunctional regulatory mechanisms are also in place for these co-transmitters, with some being inhibitory and others facilitatory (Schlicker and Feuerstein, 2017). Therefore, it is possible these modulatory pathways might have also affected NAT function during nerve stimulation, though they were not investigated in the current work. Future studies could utilise NTUA to investigate the prejunctional regulation of NAT kinetics by sympathetic co-transmitters, particularly during prolonged nerve stimulation protocols, to study a more representative profile of NAT regulation that could occur at high sympathetic nerve activity.

Future work

Future applications of the NTUA assay

Although I have optimised the NTUA assay to measure single-terminal NAT rate *ex vivo*, the fluorescence-based technique would also be useful for visualisations of sympathetic innervation density concomitant to measurements of transporter function in living tissue. The ability to do so was demonstrated with mesenteric arteries from a rodent model of cardiovascular pathology, though it would be technically challenging in the heart due to uneven tissue surfaces and limited depth penetration of the dye/optical laser. Although the technical issues associated with quantifying cardiac nerve density could be overcome by traditional techniques of tissue sectioning (De la Torre, 1980) and advanced tissue clearing methods (Yokoyama *et al.*, 2017), the added advantage of the NTUA tool is the preservation of physiologically relevant data. Therefore, future studies could optimise the multi-photon parameters to study cardiac nerve density distribution in the three-dimensional space simultaneously to measuring for NAT rate in deeper structures with the incorporation of uptake$_2$ inhibitors, such as corticosterone, to minimise non-neuronal uptake of NTUA, a feature noted in both species.

While the current study was focused on the mechanisms that govern NAT regulation, one weakness is the lack of functional data to measure how changes in NAT-mediated clearance could correlate with physiological changes in an integrative system. Thus, NTUA could serve as an *in vivo* intravital label for future work that can be used to correlate changes in sympathetic nerve density and NAT function to net sympathetic transmission and disease progression in experimental animals, for example. Moreover, *in vivo* imaging of NTUA in cardiovascular tissue would allow the study of NAT function in response to local paracrine signalling (from, for example, the vascular endothelium),

hormones, and drugs (such as cannabinoids) in an integrated system to understand the relative merits and risks of modifying the junctional transmission in the cardiovascular system.

What are the interactions between sympathetic neurotransmitter release and reuptake to determine net transmission?

The NAT is often described as a neurotransmitter 'reuptake' system that tightly operates in harmony with release, and that disease often occurs when there is a mismatch between the two. Such coupling is demonstrated by colocalisations of NAT with SNAREs at the site of release, which presumes NAT membrane insertion occurs during vesicular shuttling (Sung *et al.*, 2003, Mandela and Ordway, 2006b). However, an interesting observation of the current study is that some well-characterised release-inhibiting prejunctional modulators, i.e., mAChR, α_2AR, and CB_1R, were consistently shown to suppress NAT-mediated clearance, thus extending the instances of mismatch as an intrinsic feature of transmission. Moreover, others demonstrate that NAT can also enter reverse transport mode to mediate a Ca^{2+}-independent, non-exocytotic 'release' of NAd into the heart (Kurz *et al.*, 1995, Lameris *et al.*, 2000). This introduces a thought-provoking concept that the dynamic features of the transporter in relation to release may not be as clear-cut as one may think. Given the current progression of utilising fluorescence-based tools to monitor transmission at discrete synapses, future investigations could probe the interactions between release and reuptake in healthy and diseased states in more detail.

Do cannabinoids have the therapeutic potential to treat hypertension?

The upregulation of the endocannabinoid system (ECS) in hypertension is thought to serve as an autoprotective mechanism to prevent further disease progression (Toczek and Malinowska, 2018). The inhibitory mechanisms of the ECS on the cardiovascular system include direct effects on the myocardium and vasculature, but also suppressions of sympathetic outflow to target end-organs (Malinowska *et al.*, 2012). In the current study, I unveiled a CB_1R-mediated reduction of NAT function in the murine heart. The implication of this finding may be that the reduced NAd release post-exposure to cannabinoids may be a result of intraneuronal catecholaminergic store depletion. However, more importantly, it should not be ignored that NAT suppression may also counteract or even reverse the mechanism of sympathoinhibition. While this new finding adds to the plethora of effects imposed by cannabinoids on the cardiovascular system, it is pertinent to investigate whether NAT suppression would manifest into alterations in cardiovascular regulation in *in vivo* settings. This is because, there is currently a great therapeutic interest to enhance the ECS pharmacologically by the inhibitions of endocannabinoid degradation and reuptake (Toczek and Malinowska, 2018), thus it is important to investigate the net effect of NAT suppression in ECS upregulated states to ensure the inhibitory effects on the cardiovascular system are preserved. This could form the basis of future studies with NTUA, particularly in animal models of hypertension. Once the application of NTUA in *in vivo* systems has been optimised, the tool would prove invaluable to investigate the endocannabinoid regulation of NAT-mediated clearance in the periphery, and how this may be altered in pathology- and drug-induced states.

Concluding remarks

In summary, this thesis has provided a new fluorescence-based tool to monitor NAT function in cardiovascular tissue at the spatiotemporal resolution of a single sympathetic nerve terminal. This technique will help strengthen the literature on the mechanisms that govern NAT function at the end-organ, provide new interpretations of junctional NAd availability, and form the foundation for future work in *in vivo* settings. The current study also revealed important negative modulators of NAT function, including the mAChR, α_2AR, and CB_1R, which can have important implications upon cardiovascular physiology in both health and disease. Future investigations will no doubt determine whether these neuromodulations manifest as physiological changes and, if so, be able to investigate in detail whether they can be exploited as therapeutic targets in pathological conditions.

APPENDICES

Appendix A: Cao *et al.* (2020) Dynamic monitoring of single-terminal norepinephrine transporter rate in the rodent cardiovascular system: A novel fluorescence imaging method.

Autonomic Neuroscience: Basic and Clinical 223 (2020) 102611

Contents lists available at ScienceDirect

Autonomic Neuroscience: Basic and Clinical

journal homepage: www.elsevier.com/locate/autneu

Dynamic monitoring of single-terminal norepinephrine transporter rate in the rodent cardiovascular system: A novel fluorescence imaging method

Lily L. Cao[a], Andrew P. Holmes[a], Janice M. Marshall[a], Larissa Fabritz[b,c], Keith L. Brain[a,*]

[a] School of Biomedical Science, Institute of Clinical Sciences, College of Medical and Dental Sciences, University of Birmingham, B15 2TT, United Kingdom
[b] Institute of Cardiovascular Science, College of Medical and Dental Sciences, University of Birmingham, B15 2TT, United Kingdom
[c] Department of Cardiology, University Hospitals Birmingham NHS Foundation Trust, Birmingham, United Kingdom

ARTICLE INFO

Keywords:
Norepinephrine transporter kinetics
Fluorescence imaging
Sympathetic
Rodent
Cardiovascular system

ABSTRACT

Here, we validate the use of a novel fluorescent norepinephrine transporter (NET) substrate for dynamic measurements of transporter function in rodent cardiovascular tissue; this technique avoids the use of radiotracers and provides single-terminal resolution.

Rodent (Wistar rats and C57BL/6 mice) hearts and mesenteric arteries (MA) were isolated, loaded with NET substrate Neurotransmitter Transporter Uptake Assay (NTUA) ex vivo and imaged with confocal microscopy.

NTUA labelled noradrenergic nerve terminals in all four chambers of the heart and on the surface of MA. In all tissues, a temperature-dependent, stable linear increase in intra-terminal fluorescence upon NTUA exposure was observed; this was abolished by NET inhibitor desipramine (1 μM) and reversed by indirectly-acting sympathomimetic amine tyramine (10 μM). NET reuptake rates were similar across the mouse cardiac chambers. In both species, cardiac NET activity was significantly greater than in MA (by 62 ± 29% (mouse) and 21 ± 16% (rat)). We also show that mouse NET reuptake rate was twice as fast as that in the rat (for example, in the heart, by 94 ± 30%). Finally, NET reuptake rate in the mouse heart was attenuated with muscarinic agonist carbachol (10 μM) thus demonstrating the potential for parasympathetic regulation of norepinephrine clearance.

Our data provide the first demonstration of monitoring intra-terminal NET function in rodent cardiovascular tissue. This straightforward method allows dynamic measurements of transporter rate in response to varying physiological conditions and drug treatments; this offers the potential to study new mechanisms of sympathetic dysfunction associated with cardiovascular disease.

1. Introduction

Noradrenergic volume transmission depends on the interplay between norepinephrine (NE) release and its subsequent reuptake by the norepinephrine transporter (NET). The presynaptically located NET terminates the action of NE through a Na^+/Cl^--dependent secondary active transport process, which transports NE back into nerve terminals (Iversen, 1963; Esler et al., 1990), and hence represents an important determinant of NE availability in the extracellular space. However, inferences of dynamic changes in NET reuptake rate in mature sympathetic nerve terminals are difficult to achieve, relying on indirect measurements such as NE overflow (with and without NET inhibition) (Esler et al., 1988; Grassi and Esler, 1999) or tissue reuptake of radioactive substrates on a macroscopic scale (Pandit-Taskar and Modak, 2017; Chen et al., 2019).

Tools to directly study NET kinetics in mature sympathetic nerve terminals are needed in order to better understand transporter regulation, which has been shown to be impaired in several cardiovascular diseases (Schroeder and Jordan, 2011, 2012), and is frequently used as a target for pharmacotherapeutics (Zhou, 2004). Fluorescence imaging has proved useful in discerning individual synapses microscopically at high temporal resolutions and, indeed, our group demonstrated the use of a fluorescent NET substrate to measure NET function in sympathetic terminals of the mouse vas deferens (Parker et al., 2010). An additional benefit of this technique is the ability to identify such terminals amongst a mix of peripheral neuronal types; for example, in addition to

Abbreviations: NET, norepinephrine transporter; NE, norepinephrine; NTUA, neurotransmitter transporter uptake assay; LAA, left atrial appendage; MA, mesenteric artery

* Corresponding author at: School of Biomedical Sciences, Institute of Clinical Science, University of Birmingham, Edgbaston, Birmingham B15 2TT, United Kingdom.
E-mail addresses: LXC319@student.bham.ac.uk (L.L. Cao), A.P.Holmes@bham.ac.uk (A.P. Holmes), j.m.marshall@bham.ac.uk (J.M. Marshall), L.Fabritz@bham.ac.uk (L. Fabritz), k.l.brain@bham.ac.uk (K.L. Brain).

https://doi.org/10.1016/j.autneu.2019.102611
Received 17 September 2019; Received in revised form 29 November 2019; Accepted 14 December 2019
1566-0702/ © 2019 The Authors. Published by Elsevier B.V. This is an open access article under the CC BY license (http://creativecommons.org/licenses/BY/4.0/).

Appendix B: Cao *et al.* (2021) Resting cardiac sympathetic firing frequencies suppress terminal norepinephrine transporter uptake.

Autonomic Neuroscience: Basic and Clinical 232 (2021) 102794

Contents lists available at ScienceDirect

Autonomic Neuroscience: Basic and Clinical

journal homepage: www.elsevier.com/locate/autneu

Resting cardiac sympathetic firing frequencies suppress terminal norepinephrine transporter uptake

Lily L. Cao [a], Janice M. Marshall [a], Larissa Fabritz [b,c], Keith L. Brain [a,*]

[a] School of Biomedical Science, Institute of Clinical Science, College of Medical and Dental Sciences, University of Birmingham, B15 2TT, UK
[b] Institute of Cardiovascular Science, College of Medical and Dental Sciences, University of Birmingham, B15 2TT, UK
[c] Department of Cardiology, University Hospitals Birmingham NHS Foundation Trust, Birmingham, UK

ARTICLE INFO

Keywords:
Electrical field stimulation
Norepinephrine transporter
Left atrium
Murine
Sympathetic
α_2-adrenoceptors

ABSTRACT

The prejunctional norepinephrine transporter (NET) is responsible for the clearance of released norepinephrine (NE) back into the sympathetic nerve terminal. NET regulation must be tightly controlled as variations could have important implications for neurotransmission. Thus far, the effects of sympathetic neuronal activity on NET function have been unclear. Here, we optically monitor single-terminal cardiac NET activity *ex vivo* in response to a broad range of sympathetic postganglionic action potential (AP) firing frequencies.

Isolated murine left atrial appendages were loaded with a fluorescent NET substrate [Neurotransmitter Transporter Uptake Assay (NTUA)] and imaged with confocal microscopy. Sympathetic APs were induced with electrical field stimulation at 0.2–10 Hz (0.1–0.2 ms pulse width). Exogenous NE was applied during the NTUA uptake- and washout phases to investigate substrate competition and displacement, respectively, on transport.

Single-terminal NET reuptake rate was rapidly suppressed in a frequency-dependent manner with an inhibitory EF_{50} of 0.9 Hz. At 2 Hz, the effect was reversed by the α_2-adrenoceptor antagonist yohimbine (1 μM) ($p < 0.01$) with no further effect imposed by the muscarinic receptor antagonist atropine (1 μM). Additionally, high exogenous NE concentrations abolished NET reuptake (1 μM NE; $p < 0.0001$) and displaced terminal specific NTUA during washout (1–100 μM NE; $p < 0.0001$). We have also identified α_2-adrenoceptor-induced suppression of NET reuptake rate during resting stimulation frequencies, which could oppose the effect of autoinhibition-mediated suppression of exocytosis and thus amplify the effects of sympathetic drive on cardiac function.

1. Introduction

The Na^+/Cl^--dependent norepinephrine transporter (NET), located on the presynaptic membrane of sympathetic nerve terminals, is responsible for the high-affinity reuptake of released norepinephrine (NE) back into the nerve ending [termed $uptake_1$; Iversen, 1963]. In the periphery, prejunctional NET is crucial for cardiovascular homeostasis as it represents up to 90% of neurotransmitter clearance in the heart (Goldstein et al., 1988; Esler et al., 1990) and is therefore an important determinant of noradrenergic volume transmission. Unsurprisingly, disruptions in NET function are often associated with sympathetic overactivity observed in cardiovascular pathologies such as hypertension, tachycardia, orthostatic intolerance (Schroeder and Jordan, 2012) and heart failure (Kaludercic et al., 2010; Liang et al., 1989).

Many factors influence NET function, including endogenous hormones (Apparsundaram et al., 1998; Mandela and Ordway, 2006b) and psychotropic drugs (Zhou, 2004; Weinshenker and Schroeder, 2007). Governed by kinases and phosphatases, they elicit changes in transporter trafficking, activity and/or expression either independently or in combination (Mandela and Ordway, 2006b). However, the effect of sympathetic nerve activity upon NET in intact tissue preparations remains unclear.

While the increase in NET function induced by membrane depolarisation is well established in *in vitro* systems (Savchenko et al., 2003; Mandela and Ordway, 2006a; Habecker et al., 2006; Sung et al., 2017), the findings *ex/in vivo* remains uncertain. Gillis (1963) demonstrated

Abbreviations: NET, norepinephrine transporter; NE, norepinephrine; NTUA, neurotransmitter transporter uptake assay; AP, action potential; EFS, electrical field stimulation; LAA, left atrial appendage.

* Corresponding author at: School of Biomedical Sciences, Institute of Clinical Science, University of Birmingham, Edgbaston, Birmingham, B15 2TT, UK.
E-mail addresses: LXC319@student.bham.ac.uk (L.L. Cao), janice.m.marshall@bham.ac.uk (J.M. Marshall), l.fabritz@bham.ac.uk (L. Fabritz), k.l.brain@bham.ac.uk (K.L. Brain).

https://doi.org/10.1016/j.autneu.2021.102794
Received 19 January 2021; Received in revised form 23 February 2021; Accepted 25 February 2021
Available online 27 February 2021
1566-0702/© 2021 Elsevier B.V. All rights reserved.

Appendix C: Alzahrani *et al.* (2020) β-Adrenoceptor blockade prevents carotid body hyperactivity and elevated vascular sympathetic nerve density induced by chronic intermittent hypoxia.

Pflügers Archiv - European Journal of Physiology
https://doi.org/10.1007/s00424-020-02492-0

INTEGRATIVE PHYSIOLOGY

β-Adrenoceptor blockade prevents carotid body hyperactivity and elevated vascular sympathetic nerve density induced by chronic intermittent hypoxia

Abdulaziz A. Alzahrani[1,2] · Lily L. Cao[1,3] · Hayyaf S. Aldossary[1,4] · Demitris Nathanael[1] · Jiarong Fu[1] · Clare J. Ray[1] · Keith L. Brain[1,3] · Prem Kumar[1] · Andrew M. Coney[1] · Andrew P. Holmes[1,3]

Received: 24 August 2020 / Revised: 26 October 2020 / Accepted: 6 November 2020
© The Author(s) 2020

Abstract
Carotid body (CB) hyperactivity promotes hypertension in response to chronic intermittent hypoxia (CIH). The plasma concentration of adrenaline is reported to be elevated in CIH and our previous work suggests that adrenaline directly activates the CB. However, a role for chronic adrenergic stimulation in mediating CB hyperactivity is currently unknown. This study evaluated whether beta-blocker treatment with propranolol (Prop) prevented the development of CB hyperactivity, vascular sympathetic nerve growth and hypertension caused by CIH. Adult male Wistar rats were assigned into 1 of 4 groups: Control (N), N + Prop, CIH and CIH + Prop. The CIH paradigm consisted of 8 cycles h^{-1}, 8 h day^{-1}, for 3 weeks. Propranolol was administered via drinking water to achieve a dose of 40 mg kg^{-1} day^{-1}. Immunohistochemistry revealed the presence of both β_1 and β_2-adrenoceptor subtypes on the CB type I cell. CIH caused a 2–3-fold elevation in basal CB single-fibre chemoafferent activity and this was prevented by chronic propranolol treatment. Chemoafferent responses to hypoxia and mitochondrial inhibitors were attenuated by propranolol, an effect that was greater in CIH animals. Propranolol decreased respiratory frequency in normoxia and hypoxia in N and CIH. Propranolol also abolished the CIH mediated increase in vascular sympathetic nerve density. Arterial blood pressure was reduced in propranolol groups during hypoxia. Propranolol exaggerated the fall in blood pressure in most (6/7) CIH animals during hypoxia, suggestive of reduced sympathetic tone. These findings therefore identify new roles for β-adrenergic stimulation in evoking CB hyperactivity, sympathetic vascular hyperinnervation and altered blood pressure control in response to CIH.

Keywords Carotid body · Hypoxia · Adrenaline · β-Adrenoceptors · Chronic intermittent hypoxia · Hypertension · Beta-blockers · Vascular sympathetic nerves

Abbreviations

CB	Carotid body
MABP	Mean arterial blood pressure
HR	Heart rate
V_E	Minute ventilation
V_t	Tidal volume
R_f	Respiratory frequency
HVR	Hypoxic ventilatory response
CIH	Chronic intermittent hypoxia
OSA	Obstructive sleep apnoea
MA	Mesenteric artery

✉ Andrew M. Coney
a.m.coney@bham.ac.uk

✉ Andrew P. Holmes
a.p.holmes@bham.ac.uk

[1] Institute of Clinical Sciences, University of Birmingham, Edgbaston, Birmingham B15 2TT, UK

[2] Respiratory Care Department, Faculty of Applied Medical Sciences, Umm Al-Qura University, Makkah, Saudi Arabia

[3] Institute of Cardiovascular Sciences, University of Birmingham, Edgbaston, Birmingham B15 2TT, UK

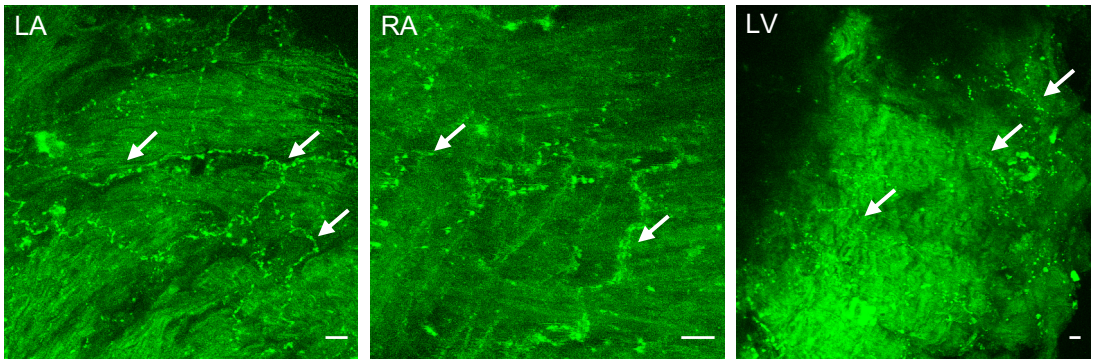
[4] College of Medicine, Basic Medical Sciences, King Saud bin Abdulaziz University for Health Sciences, Riyadh, Saudi Arabia

Introduction

The carotid body (CB) is the major sensory organ in the human body that responds to acute hypoxic stress [30, 50]. When stimulated the CB activates vital protective reflexes including hyperventilation, systemic vasoconstriction and elevated heart rate [29, 30]. CB activation in hypoxia is critical

Published online: 19 November 2020

Appendix 3.1: NTUA labelling of murine cardiac nerve structures by Langendorff retrograde perfusion



The mouse heart was retrogradely perfused with NTUA with a Langendorff perfusion apparatus. NTUA administration through a bolus port above the cannulated heart at a final concentration of 1:80 NTUA for 5 min labelled neuronal structures reminiscent of autonomic nerves in the left atrium (LA), right atrium (RAA) and left ventricle (LV). Images of the right ventricle were not captured.

All micrographs, bars = 10 µm

REFERENCES

Adams, M. D., Earnhardt, J. T., Dewey, W. L. & Harris, L. S. (1976) Vasoconstrictor actions of Δ^8- and Δ^9-tetrahydrocannabinol in the rat. *J Pharmacol Exp Ther,* **196,** 649-56.

Adderley, N. J., Ryan, R., Nirantharakumar, K. & Marshall, T. (2019) Prevalence and treatment of atrial fibrillation in UK general practice from 2000 to 2016. *Heart,* **105,** 27-33.

Aguirre, A. D., Vinegoni, C., Sebas, M. & Weissleder, R. (2014) Intravital imaging of cardiac function at the single-cell level. *Proc Natl Acad Sci U S A,* **111,** 11257-62.

Aldossary, H. S., Alzahrani, A. A., Nathanael, D., Alhuthail, E. A., Ray, C. J., Batis, N., . . . Holmes, A. P. (2020) G-protein-coupled receptor (GPCR) signaling in the carotid body: roles in hypoxia and cardiovascular and respiratory disease. *Int J Mol Sci,* **21,** 6012.

Allen, E., Coote, J. H., Grubb, B. D., Batten, T. F. C., Pauza, D. H., Ng, G. A. & Brack, K. E. (2018) Electrophysiological effects of nicotinic and electrical stimulation of intrinsic cardiac ganglia in the absence of extrinsic autonomic nerves in the rabbit heart. *Heart Rhythm,* **15,** 1698-707.

Alzahrani, A. A., Cao, L. L., Aldossary, H. S., Nathanael, D., Fu, J., Ray, C. J., . . . Holmes, A. P. (2020) β-Adrenoceptor blockade prevents carotid body hyperactivity and elevated vascular sympathetic nerve density induced by chronic intermittent hypoxia. *Pflugers Arch,* **473,** 37-51.

Amenta, F. & Ferrante, F. (1983) Detection of neuronal uptake of [^{3}H]dopamine in the rabbit celiac artery. *Eur J Pharmacol,* **88,** 251-54.

Amos, R. J. (2007) Neurotransmission in the rodent anococcygeus: high resolution studies of autonomic neuroeffector mechanisms. University of Oxford, Oxford: Pharmacology. 271.

Angelakos, E. T., King, M. P. & Millard, R. W. (1969) Regional distribution of catecholamines in the hearts of various species. *Ann N Y Acad Sci,* **156,** 219-40.

Apparsundaram, S., Galli, A., DeFelice, L. J., Hartzell, H. C. & Blakely, R. D. (1998a) Acute regulation of norepinephrine transport: I. protein kinase C-linked muscarinic receptors influence transport capacity and transporter density in SK-N-SH cells. *J Pharmacol Exp Ther,* **287,** 733-43.

Apparsundaram, S., Schroeter, S., Giovanetti, E. & Blakely, R. D. (1998b) Acute regulation of norepinephrine transport: II. PKC-modulated surface expression of human norepinephrine transporter proteins. *J Pharmacol Exp Ther,* **287,** 744-51.

Apparsundaram, S., Sung, U., Price, R. D. & Blakely, R. D. (2001) Trafficking-dependent and -independent pathways of neurotransmitter transporter regulation differentially involving p38 mitogen-

activated protein kinase revealed in studies of insulin modulation of norepinephrine transport in SK-N-SH cells. *J Pharmacol Exp Ther,* **299,** 666-77.

Ardell, J. L., Foreman, R. D., Armour, J. A. & Shivkumar, K. (2019) Cardiac sympathectomy and spinal cord stimulation attenuate reflex-mediated norepinephrine release during ischemia preventing ventricular fibrillation. *JCI Insight,* **4,** e131648.

Armour, J. A. (2008) Potential clinical relevance of the 'little brain' on the mammalian heart. *Exp Physiol,* **93,** 165-76.

Armour, J. A., Murphy, D. A., Yuan, B. X., Macdonald, S. & Hopkins, D. A. (1997) Gross and microscopic anatomy of the human intrinsic cardiac nervous system. *Anat Rec,* **247,** 289-98.

Armstrong, J. F., Faccenda, E., Harding, S. D., Pawson, A. J., Southan, C., Sharman, J. L., . . . Nc, I. (2019) The IUPHAR/BPS Guide to PHARMACOLOGY in 2020: extending immunopharmacology content and introducing the IUPHAR/MMV Guide to MALARIA PHARMACOLOGY. *Nucleic Acids Res,* **48,** D1006-21.

Åstrand, P. & Stjärne, L. (1989) On the secretory activity of single varicosities in the sympathetic nerves innervating the rat tail artery. *J Physiol,* **409,** 207-20.

Aviado, D. M. & Guevara Aviado, D. (2001) The Bezold-Jarisch reflex. A historical perspective of cardiopulmonary reflexes. *Ann N Y Acad Sci,* **940,** 48-58.

Axelrod, J. (1998) Julius Axelrod. *In:* Squire, L. R. *The History of Neuroscience in Autobiography.* Academic Press. **1,** 50-78.

Backs, J., Bresch, E., Lutz, M., Kristen, A. V. & Haass, M. (2005) Endothelin-1 inhibits the neuronal norepinephrine transporter in hearts of male rats. *Cardiovasc Res,* **67,** 283-90.

Backs, J., Haunstetter, A., Gerber, S. H., Metz, J., Borst, M. M., Strasser, R. H., . . . Haass, M. (2001) The neuronal norepinephrine transporter in experimental heart failure: evidence for a posttranscriptional downregulation. *J Mol Cell Cardiol,* **33,** 461-72.

Bao, J. X., Gonon, F. & Stjärne, L. (1993) Frequency- and train length-dependent variation in the roles of postjunctional alpha$_1$- and alpha$_2$ -adrenoceptors for the field stimulation-induced neurogenic contraction of rat tail artery. *Naunyn Schmiedebergs Arch Pharmacol,* **347,** 601-16.

Baranowska-Kuczko, M., Kozłowska, H., Kloza, M., Karpińska, O., Toczek, M., Harasim, E., . . . Malinowska, B. (2016) Protective role of cannabinoid CB$_1$ receptors and vascular effects of chronic administration of FAAH inhibitor URB597 in DOCA-salt hypertensive rats. *Life Sci,* **151,** 288-99.

Bardsley, E. N. & Paterson, D. J. (2020) Neurocardiac regulation: from cardiac mechanisms to novel therapeutic approaches. *J Physiol,* **598,** 2957-76.

Barrett, J. A., Joyal, J. L., Hillier, S. M., Maresca, K. P., Femia, F. J., Kronauge, J. F., . . . Babich, J. W. (2010) Comparison of high-specific-activity ultratrace $^{123/131}$I-MIBG and carrier-added $^{123/131}$I-MIBG on efficacy, pharmacokinetics, and tissue distribution. *Cancer Biother Radiopharm,* **25,** 299-308.

Bátkai, S., Pacher, P., Osei-Hyiaman, D., Radaeva, S., Liu, J., Harvey-White, J., . . . Kunos, G. (2004) Endocannabinoids acting at cannabinoid-1 receptors regulate cardiovascular function in hypertension. *Circulation,* **110,** 1996-2002.

Bayles, R. G., Tran, J., Olivas, A., Woodward, W. R., Fei, S. S., Gao, L. & Habecker, B. A. (2019) Sex differences in sympathetic gene expression and cardiac neurochemistry in Wistar Kyoto rats. *PLoS One,* **14,** e0218133.

Beau, S. L. & Saffitz, J. E. (1994) Transmural heterogeneity of norepinephrine uptake in failing human hearts. *J Am Coll Cardiol,* **23,** 579-85.

Beaudin, A. E., Waltz, X., Hanly, P. J. & Poulin, M. J. (2017) Impact of obstructive sleep apnoea and intermittent hypoxia on cardiovascular and cerebrovascular regulation. *Exp Physiol,* **102,** 743-63.

Bencivenga, L., Liccardo, D., Napolitano, C., Visaggi, L., Rengo, G. & Leosco, D. (2019) β-Adrenergic receptor signaling and heart failure: from bench to bedside. *Heart Fail Clin,* **15,** 409-19.

Bennett, M. R. (1993) Quantal secretion at visualized sympathetic nerve varicosities. *Physiology,* **8,** 199-201.

Bensley, J. G., De Matteo, R., Harding, R. & Black, M. J. (2016) Three-dimensional direct measurement of cardiomyocyte volume, nuclearity, and ploidy in thick histological sections. *Sci Rep,* **6,** 23756.

Bermingham, D. P. & Blakely, R. D. (2016) Kinase-dependent regulation of monoamine neurotransmitter transporters. *Pharmacol Rev,* **68,** 888-953.

Bernhard, M., Takeda, K., Keller, C., Haslebacher, M., Lambrou, G. N. & Trendelenburg, A. U. (2004) ^{3}H-Noradrenaline release from mouse iris-ciliary body: role of presynaptic muscarinic heteroreceptors. *Naunyn Schmiedebergs Arch Pharmakol,* **370,** 305-13.

Bernstein, A. I., Stout, K. A. & Miller, G. W. (2012) A fluorescent-based assay for live cell, spatially resolved assessment of vesicular monoamine transporter 2-mediated neurotransmitter transport. *J Neurosci Methods,* **209,** 357-66.

Birch, D. J., Turmaine, M., Boulos, P. B. & Burnstock, G. (2008) Sympathetic innervation of human mesenteric artery and vein. *J Vasc Res,* **45,** 323-32.

Blakeley, A. G. & Cunnane, T. C. (1979a) The packeted release of transmitter from the sympathetic nerves of the guinea-pig vas deferens: an electrophysiological study. *J Physiol,* **296,** 85-96.

Blakeley, A. G. & Cunnane, T. C. (1979b) Packeted transmitter release in the mouse vas deferens; an electrophysiological study *J Physiol,* **295,** 44-45.

Blakeley, A. G. H. & Brown, G. L. (1964) The effect of nerve stimulation on the uptake of infused noradrenaline by the perfused spleen, In: Proceedings of the Physiological Society. University College London Meeting. **172 (Suppl),** 19-21.

Blanco-Rivero, J., Couto, G. K., Paula, S. M., Fontes, M. T. & Rossoni, L. V. (2021) Enhanced sympathetic neurotransduction in the superior mesenteric artery in a rat model of heart failure: role of noradrenaline and ATP. *Am J Physiol Heart Circ Physiol,* **320,** H563-74.

Bloksgaard, M., Thorsted, B., Brewer, J. R. & De Mey, J. G. R. (2018) Assessing collagen and elastin pressure-dependent microarchitectures in live, human resistance arteries by label-free fluorescence microscopy. *J Vis Exp* [Online].

Böhm, M., Castellano, M., Flesch, M., Maack, C., Moll, M., Paul, M., . . . Zolk, O. (1998) Chamber-specific alterations of norepinephrine uptake sites in cardiac hypertrophy. *Hypertension,* **32,** 831-37.

Bondarenko, A. I. (2014) Endothelial atypical cannabinoid receptor: do we have enough evidence? *Br J Pharmacol,* **171,** 5573-88.

Bonica, J. J. (1968) Autonomic innervation of the viscera in relation to nerve block. *Anesthesiology,* **29,** 793-813.

Bönisch, H., Bryan, L. J., Henseling, M., O'Donnell, S. R., Stockmann, P. & Trendelenburg, U. (1985) The effect of various ions on uptake$_2$ of catecholamines. *Naunyn Schmiedebergs Arch Pharmacol,* **328,** 407-16.

Bönisch, H., Hammermann, R. & Brüss, M. (1998) Role of protein kinase C and second messengers in regulation of the norepinephrine transporter. *Adv Pharmacol,* **42,** 183-86.

Bonz, A., Laser, M., Küllmer, S., Kniesch, S., Babin-Ebell, J., Popp, V., . . . Wagner, J. A. (2003) Cannabinoids acting on CB_1 receptors decrease contractile performance in human atrial muscle. *J Cardiovasc Pharmacol,* **41,** 657-64.

Borovac, J. A., D'Amario, D., Bozic, J. & Glavas, D. (2020) Sympathetic nervous system activation and heart failure: Current state of evidence and the pathophysiology in the light of novel biomarkers. *World J Cardiol,* **12,** 373-408.

Bousquet, P., Hudson, A., García-Sevilla, J. A. & Li, J. X. (2020) Imidazoline receptor system: the past, the present, and the future. *Pharmacol Rev,* **72,** 50-79.

Brain, K. L. & Bennett, M. R. (1997) Calcium in sympathetic varicosities of mouse vas deferens during facilitation, augmentation and autoinhibition. *J Physiol,* **502,** 521-36.

Brain, K. L., Cottee, L. J. & Bennett, M. R. (1997) Varicosities of single sympathetic nerve terminals possess syntaxin zones and different synaptotagmin N-terminus labelling following stimulation. *J Neurocytol,* **26,** 491-500.

Brain, K. L. & Cunnane, T. C. (2008) Bretylium abolishes neurotransmitter release without necessarily abolishing the nerve terminal action potential in sympathetic terminals. *Br J Pharmacol,* **153,** 831-39.

Brain, K. L., Jackson, V. M., Trout, S. J. & Cunnane, T. C. (2002) Intermittent ATP release from nerve terminals elicits focal smooth muscle Ca^{2+} transients in mouse vas deferens. *J Physiol,* **541,** 849-62.

Braunschweig, F., Cowie, M. R. & Auricchio, A. (2011) What are the costs of heart failure? *Europace,* **13,** 13-17.

Brock, J. A. & Cunnane, T. C. (1993) Neurotransmitter release mechanisms at the sympathetic neuroeffector junction. *Exp Physiol,* **78,** 591-614.

Bröer, S. & Gether, U. (2012) The solute carrier 6 family of transporters. *Br J Pharmacol,* **167,** 256-78.

Brosenitsch, T. A. & Katz, D. M. (2001) Physiological patterns of electrical stimulation can induce neuronal gene expression by activating N-type calcium channels. *J Neurosci,* **21,** 2571-79.

Brown, G. L. & Gillespie, J. S. (1957) The output of sympathetic transmitter from the spleen of the cat. *J Physiol,* **138,** 81-102.

Bryan-Lluka, L. J. & Vuocolo, H. E. (1992) Evidence from guinea-pig trachealis that uptake$_2$ of isoprenaline is enhanced by hyperpolarization of the smooth muscle. *Naunyn Schmiedebergs Arch Pharmacol,* **346,** 399-404.

Bryda, E. C. (2013) The mighty mouse: the impact of rodents on advances in biomedical research. *Mo Med,* **110,** 207-11.

Buckley, N. E., Hansson, S., Harta, G. & Mezey, E. (1998) Expression of the CB_1 and CB_2 receptor messenger RNAs during embryonic development in the rat. *Neuroscience,* **82,** 1131-49.

Burdett, P. & Lip, G. Y. H. (2020) Atrial fibrillation in the United Kingdom: predicting costs of an emerging epidemic recognising and forecasting the cost drivers of atrial fibrillation-related costs. *Eur Heart J Qual Care Clin Outcomes***,** [Online ahead of print].

Burnette, W. B., Bailey, M. D., Kukoyi, S., Blakely, R. D., Trowbridge, C. G. & Justice, J. B. (1996) Human norepinephrine transporter kinetics using rotating disk electrode voltammetry. *Anal Chem,* **68,** 2932-38.

Burnstock, G. (2008) Non-synaptic transmission at autonomic neuroeffector junctions. *Neurochem Int,* **52,** 14-25.

Burnstock, G. (2009) Autonomic neurotransmission: 60 years since Sir Henry Dale. *Annu Rev Pharmacol Toxicol,* **49,** 1-30.

Burnstock, G. (2013) Cotransmission in the autonomic nervous system. *Handb Clin Neurol,* **117,** 23-35.

Burnstock, G. & Verkhratsky, A. (2010) Vas deferens--a model used to establish sympathetic cotransmission. *Trends Pharmacol Sci,* **31,** 131-39.

Buss, S. J., Backs, J., Kreusser, M. M., Hardt, S. E., Maser-Gluth, C., Katus, H. A. & Haass, M. (2006) Spironolactone preserves cardiac norepinephrine reuptake in salt-sensitive Dahl rats. *Endocrinology,* **147,** 2526-34.

Buttgereit, J., Shanks, J., Li, D., Hao, G., Athwal, A., Langenickel, T. H., . . . Herring, N. (2016) C-type natriuretic peptide and natriuretic peptide receptor B signalling inhibits cardiac sympathetic neurotransmission and autonomic function. *Cardiovasc Res,* **112,** 637-44.

Cadas, H., Gaillet, S., Beltramo, M., Venance, L. & Piomelli, D. (1996) Biosynthesis of an endogenous cannabinoid precursor in neurons and its control by calcium and cAMP. *J Neurosci,* **16,** 3934-42.

Calandra, B., Portier, M., Kernéis, A., Delpech, M., Carillon, C., Le Fur, G., . . . Shire, D. (1999) Dual intracellular signaling pathways mediated by the human cannabinoid CB_1 receptor. *Eur J Pharmacol,* **374,** 445-55.

Callado, L. F. & Stamford, J. A. (2000) Spatiotemporal interaction of α_2 autoreceptors and noradrenaline transporters in the rat locus coeruleus. *J Neurochem,* **74,** 2350-58.

Carlson, J. T., Hedner, J., Elam, M., Ejnell, H., Sellgren, J. & Wallin, B. G. (1993) Augmented resting sympathetic activity in awake patients with obstructive sleep apnea. *CHEST,* **103,** 1763-68.

Carnevali, L., Trombini, M., Porta, A., Montano, N., de Boer, S. F. & Sgoifo, A. (2013) Vagal withdrawal and susceptibility to cardiac arrhythmias in rats with high trait aggressiveness. *PLoS One,* **8,** e68316.

Carney, S. T., Lloyd, M. L., MacKinnon, S. E., Newton, D. C., Jones, J. D., Howlett, A. C. & Norford, D. C. (2009) Cannabinoid regulation of nitric oxide synthase I (nNOS) in neuronal cells. *J Neuroimmune Pharmacol,* **4,** 338-49.

Celsus, A. C. & Spencer, W. G. (1935) *De Medicina (On Medicine),* Cambridge, MA, USA/W. Heinemann, Ltd, London., Harvard University Press.

Cervinski, M. A., Foster, J. D. & Vaughan, R. A. (2010) Syntaxin 1A regulates dopamine transporter activity, phosphorylation and surface expression. *Neuroscience,* **170,** 408-16.

Chang, C. C. & Chiueh, C. C. (1969) Modulation of noradrenaline incorporation by nerve activities in the rat submaxillary gland. *J Physiol,* **203,** 145-57.

Chen, Y. A. & Scheller, R. H. (2001) SNARE-mediated membrane fusion. *Nat Rev Mol Cell Biol,* **2,** 98-106.

Chilian, W. M., Boatwright, R. B., Shoji, T. & Griggs, D. M., Jr. (1982) Regional uptake of [^{3}H]norepinephrine by the canine left ventricle *Proc Soc Exp Biol Med,* **171,** 158-63.

Chow, L. T., Chow, S. S., Anderson, R. H. & Gosling, J. A. (2001) Autonomic innervation of the human cardiac conduction system: changes from infancy to senility - an immunohistochemical and histochemical analysis. *Anat Rec,* **264,** 169-82.

Christensen, K. L. & Mulvany, M. J. (1993) Mesenteric arcade arteries contribute substantially to vascular resistance in conscious rats. *J Vasc Res,* **30,** 73-79.

Claps, A. & Torrealba, F. (1988) The carotid body connections: a WGA-HRP study in the cat. *Brain Res,* **455,** 123-33.

Coote, J. H. (2010) Recovery of heart rate following intense dynamic exercise. *Exp Physiol,* **95,** 431-40.

Coote, J. H. & Chauhan, R. A. (2016) The sympathetic innervation of the heart: Important new insights. *Auton Neurosci,* **199,** 17-23.

Costa, M., Barrington, M. & Majewski, H. (1993) Evidence that M_1 muscarinic receptors enhance noradrenaline release in mouse atria by activating protein kinase C. *Br J Pharmacol,* **110,** 910-16.

Costa, M. & Majewski, H. (1991) Evidence for facilitatory and inhibitory muscarinic receptors on postganglionic sympathetic nerves in mouse isolated atria. *Br J Pharmacol,* **102,** 855-60.

Crawford, W. J. & Merritt, J. C. (1979) Effects of tetrahydrocannabinol on arterial and intraocular hypertension. *Int J Clin Pharmacol Biopharm,* **17,** 191-96.

Cunnane, T. C. & Stjärne, L. (1984) Transmitter secretion from individual varicosities of guinea-pig and mouse vas deferens: Highly intermittent and monoquantal. *Neuroscience,* **13,** 1-20.

Dae, M. W., De Marco, T., Botvinick, E. H., O'Connell, J. W., Hattner, R. S., Huberty, J. P. & Yuen-Green, M. S. (1992) Scintigraphic assessment of MIBG uptake in globally denervated human and canine hearts--implications for clinical studies. *J Nucl Med,* **33,** 1444-50.

Dahlström, A., Fuxe, K., Mya-Tu, M. & Zetterström, B. E. M. (1965) Observations on adrenergic innervation of dog heart. *AJP-Legacy,* **209,** 689-92.

Dahlström, A., Häggendal, J. & Hökfelt, T. (1966) The noradrenaline content of the varicosities of sympathetic adrenergic nerve terminals in the rat. *Acta Physiol Scand,* **67,** 289-94.

Darker, I. Y., Millns, P. J., Selbie, L., Randall, M. S., S-Baxter, G. & Kendall, D. A. (1998) Cannabinoid (CB_1) receptor expression is associated with mesenteric resistance vessels but not thoracic aorta in the rat. *Br J Pharmacol,* **125,** 95.

De la Torre, J. C. (1980) An improved approach to histofluorescence using the SPG method for tissue monoamines. *J Neurosci Methods,* **3,** 1-5.

Degenhardt, L. & Hall, W. (2012) Extent of illicit drug use and dependence, and their contribution to the global burden of disease. *Lancet,* **379,** 55-70.

Deng, M., Tufan, T., Raza, M. U., Jones, T. C. & Zhu, M. Y. (2016) MicroRNAs 29b and 181a down-regulate the expression of the norepinephrine transporter and glucocorticoid receptors in PC12 cells. *J Neurochem,* **139,** 197-207.

Descarries, L., Watkins, K. C. & Lapierre, Y. (1977) Noradrenergic axon terminals in the cerebral cortex of rat. III. Topometric ultrastructural analysis. *Brain Res,* **133,** 197-222.

Deutsch, D. G., Goligorsky, M. S., Schmid, P. C., Krebsbach, R. J., Schmid, H. H., Das, S. K., . . . Moore, L. C. (1997) Production and physiological actions of anandamide in the vasculature of the rat kidney. *J Clin Invest,* **100,** 1538-46.

Dewan, N. A., Nieto, F. J. & Somers, V. K. (2015) Intermittent hypoxemia and OSA: implications for comorbidities. *Chest,* **147,** 266-74.

Di Marzo, V. (2008) Endocannabinoids: synthesis and degradation. *Rev Physiol Biochem Pharmacol,* **160,** 1-24.

Di Marzo, V., Bisogno, T., De Petrocellis, L., Melck, D., Orlando, P., Wagner, J. A. & Kunos, G. (1999) Biosynthesis and inactivation of the endocannabinoid 2-arachidonoylglycerol in circulating and tumoral macrophages. *Eur J Biochem,* **264,** 258-67.

Djonlagic, I., Saboisky, J., Carusona, A., Stickgold, R. & Malhotra, A. (2012) Increased sleep fragmentation leads to impaired off-line consolidation of motor memories in humans. *PLoS One,* **7,** e34106.

Doležel, S. (1966) Histochemical identification of monoamine in the arterial wall. *Experientia,* **22,** 307.

Dunn, M., Henke, A., Clark, S., Kovalyova, Y., Kempadoo, K. A., Karpowicz, R. J., Jr., . . . Sames, D. (2018) Designing a norepinephrine optical tracer for imaging individual noradrenergic synapses and their activity in vivo. *Nat Commun,* **9,** 2838.

Edgemond, W. S., Hillard, C. J., Falck, J. R., Kearn, C. S. & Campbell, W. B. (1998) Human platelets and polymorphonuclear leukocytes synthesize oxygenated derivatives of arachidonylethanolamide (anandamide): their affinities for cannabinoid receptors and pathways of inactivation. *Mol Pharmacol,* **54,** 180-88.

Eikelis, N., Marques, F. Z., Hering, D., Marusic, P., Head, G. A., Walton, A. S., . . . Lambert, G. W. (2018) A polymorphism in the noradrenaline transporter gene is associated with increased blood pressure in patients with resistant hypertension. *J Hypertens,* **36,** 1571-77.

Eisenhofer, G. (2001) The role of neuronal and extraneuronal plasma membrane transporters in the inactivation of peripheral catecholamines. *Pharmacol Ther,* **91,** 35-62.

Eisenhofer, G., Esler, M. D., Goldstein, D. S. & Kopin, I. J. (1991a) Neuronal uptake, metabolism, and release of tritium-labeled norepinephrine during assessment of its plasma kinetics. *Am J Physiol,* **261,** E505-15.

Eisenhofer, G., Friberg, P., Rundqvist, B., Quyyumi, A. A., Lambert, G., Kaye, D. M., . . . Esler, M. D. (1996) Cardiac sympathetic nerve function in congestive heart failure. *Circulation,* **93,** 1667-76.

Eisenhofer, G., Kopin, I. J. & Goldstein, D. S. (2004) Catecholamine metabolism: a contemporary view with implications for physiology and medicine. *Pharmacol Rev,* **56,** 331-49.

Eisenhofer, G., Smolich, J. J., Cox, H. S. & Esler, M. D. (1991b) Neuronal reuptake of norepinephrine and production of dihydroxyphenylglycol by cardiac sympathetic nerves in the anesthetized dog. *Circulation,* **84,** 1354-63.

Eldeeb, K., Leone-Kabler, S. & Howlett, A. C. (2016) CB_1 cannabinoid receptor-mediated increases in cyclic AMP accumulation are correlated with reduced $G_{i/o}$ function. *J Basic Clin Physiol Pharmacol,* **27,** 311-22.

Emmenlauer, M., Ronneberger, O., Ponti, A., Schwarb, P., Griffa, A., Filippi, A., . . . Burkhardt, H. (2009) XuvTools: free, fast and reliable stitching of large 3D datasets. *J Microsc,* **233,** 42-60.

Engelman, K. (1988) Side effects of sympatholytic antihypertensive drugs. *Hypertension,* **11,** 30-33.

Esler, M., Jennings, G., Korner, P., Blombery, P., Sacharias, N. & Leonard, P. (1984) Measurement of total and organ-specific norepinephrine kinetics in humans. *Am J Physiol Endocrinol Metab,* **247,** E21-28.

Esler, M., Jennings, G., Korner, P., Willett, I., Dudley, F., Hasking, G., . . . Lambert, G. (1988) Assessment of human sympathetic nervous system activity from measurements of norepinephrine turnover. *Hypertension,* **11,** 3-20.

Esler, M., Jennings, G., Lambert, G., Meredith, I., Horne, M. & Eisenhofer, G. (1990) Overflow of catecholamine neurotransmitters to the circulation: source, fate, and functions. *Physiol Rev,* **70,** 963-85.

Espinosa-Medina, I., Saha, O., Boismoreau, F., Chettouh, Z., Rossi, F., Richardson, W. D. & Brunet, J. F. (2016) The sacral autonomic outflow is sympathetic. *Science,* **354,** 893-97.

Fadl Elmula, F. E., Jin, Y., Yang, W. Y., Thijs, L., Lu, Y. C., Larstorp, A. C., . . . Staessen, J. A. (2015) Meta-analysis of randomized controlled trials of renal denervation in treatment-resistant hypertension. *Blood Press,* **24,** 263-74.

Fan, X., Sun, T., Crawford, W., Tan, X., Ou, X., Terrar, D. A., . . . Lei, M. (2019) Pnmt-derived cardiomyocytes: anatomical localization, function and future perspectives. *Front Physiol,* **10,** 713.

Farde, L., Halldin, C., Nagren, K., Suhara, T., Karlsson, P., Schoeps, K. O., . . . Bone, D. (1994) Positron emission tomography shows high specific uptake of racemic carbon-11 labelled norepinephrine in the primate heart. *Eur J Nucl Med,* **21,** 345-47.

Farnebo, L.-O. & Malmfors, T. (1969) Histochemical studies on the uptake of noradrenaline and α-methyl-noradrenaline in the perfused rat heart. *Eur J Pharmacol,* **5,** 313-20.

Fehér, E., Csányi, K. & Vajda, J. (1980) Intrinsic innervation of the urinary bladder. *Acta Anat (Basel),* **106,** 335-44.

Feng, J., Zhang, C., Lischinsky, J. E., Jing, M., Zhou, J., Wang, H., . . . Li, Y. (2019) A genetically encoded fluorescent sensor for rapid and specific in vivo detection of norepinephrine. *Neuron,* **102,** 745-61.

Florea, V. G. & Cohn, J. N. (2014) The autonomic nervous system and heart failure. *Circ Res,* **114,** 1815-26.

Freeman, K., Tao, W., Sun, H., Soonpaa, M. H. & Rubart, M. (2014) In situ three-dimensional reconstruction of mouse heart sympathetic innervation by two-photon excitation fluorescence imaging. *J Neurosci Methods,* **221,** 48-61.

Friberg, J., Buch, P., Scharling, H., Gadsbphioll, N. & Jensen, G. B. (2003) Rising rates of hospital admissions for atrial fibrillation. *Epidemiology,* **14,** 666-72.

Fuchs, F. & Smith, S. H. (2001) Calcium, cross-bridges, and the Frank-Starling relationship. *News Physiol Sci,* **16,** 5-10.

Fuder, H. & Muscholl, E. (1995) Heteroreceptor-mediated modulation of noradrenaline and acetylcholine release from peripheral nerves. *Reviews of Physiology, Biochemistry and Pharmacology.* Berlin, Heidelberg: Springer Berlin Heidelberg. **126,** 265-412.

Fukudome, Y., Ohno-Shosaku, T., Matsui, M., Omori, Y., Fukaya, M., Tsubokawa, H., . . . Kano, M. (2004) Two distinct classes of muscarinic action on hippocampal inhibitory synapses: M_2-mediated direct suppression and $M_{1/3}$ mediated indirect suppression through endocannabinoid signalling. *Eur J Neurosci,* **19,** 2682-92.

Furness, J. B. (1973) Arrangement of blood vessels and their relation with adrenergic nerves in the rat mesentery. *J Anat,* **115,** 347-64.

Furness, J. B. & Costa, M. (1975) The use of glyoxylic acid for the fluorescence histochemical demonstration of peripheral stores of noradrenaline and 5-hydroxytryptamine in whole mounts. *Histochemistry,* **41,** 335-52.

Furness, J. B., Heath, J. W. & Costa, M. (1978) Aqueous aldehyde (Faglu) methods for the fluorescence histochemical localization of catecholamines and for ultrastructural studies of central nervous tissue. *Histochemistry,* **57,** 285-95.

Furness, J. B. & Marshall, J. M. (1974) Correlation of the directly observed responses of mesenteric vessles of the rat to nerve stimulation and noradrenaline with the distribution of adrenergic nerves. *J Physiol,* **239,** 75-88.

Gabella, G. (1992) Fine structure of post-ganglionic nerve fibres and autonomic neuroeffector junctions. *In:* Burnstock, G. & Hoyle, C. H. V. *Autonomic Neuroeffector Mechanisms.* UK: Harwood Academic Publishers.

Gaoni, Y. & Mechoulam, R. (1964) Isolation, structure, and partial synthesis of an active constituent of hashish. *J Am Chem Soc,* **86,** 1646-47.

Garbarino, S., Guglielmi, O., Sanna, A., Mancardi, G. L. & Magnavita, N. (2016) Risk of occupational accidents in workers with obstructive sleep apnea: systematic review and meta-analysis. *Sleep,* **39,** 1211-18.

Garg, B. D., Krell, R. D., Sokoloski, T. & Patil, P. N. (1973) Steric aspects of adrenergic drugs. XXII. Retention of (+)- and (-)-^{14}C-norepinephrine by mouse heart. *J Pharm Sci,* **62,** 1126-29.

Gash, A., Karliner, J. S., Janowsky, D. & Lake, C. R. (1978) Effects of smoking marihuana on left ventricular performance and plasma norepinephrine: studies in normal men. *Ann Intern Med,* **89,** 448-52.

Gaskari, S. A., Liu, H., Moezi, L., Li, Y., Baik, S. K. & Lee, S. S. (2005) Role of endocannabinoids in the pathogenesis of cirrhotic cardiomyopathy in bile duct-ligated rats. *Br J Pharmacol,* **146,** 315-23.

Gasser, P. J. & Lowry, C. A. (2018) Organic cation transporter 3: A cellular mechanism underlying rapid, non-genomic glucocorticoid regulation of monoaminergic neurotransmission, physiology, and behavior. *Horm Behav,* **104,** 173-82.

Ge, Y., Smits, A. M., van Munsteren, J. C., Gittenberger-de Groot, A. C., Poelmann, R. E., van Brakel, T. J., . . . Jongbloed, M. R. M. (2020) Human epicardium-derived cells reinforce cardiac sympathetic innervation. *J Mol Cell,* **143,** 26-37.

Gebremedhin, D., Lange, A. R., Campbell, W. B., Hillard, C. J. & Harder, D. R. (1999) Cannabinoid CB_1 receptor of cat cerebral arterial muscle functions to inhibit L-type Ca^{2+} channel current. *Am J Physiol,* **276,** H2085-93.

Gehrmann, J., Hammer, P. E., Maguire, C. T., Wakimoto, H., Triedman, J. K. & Berul, C. I. (2000) Phenotypic screening for heart rate variability in the mouse. *Am J Physiol Heart Circ Physiol,* **279,** H733-40.

Gerhardt, G. A. & Burmeister, J. J. (2000) Voltammetry in vivo for chemical analysis of the nervous system. *In:* Meyers, R. A. *Encyclopedia of Analytical Chemistry.* Chichester: John Wiley & Sons Ltd. **710**.

Gibbins, I. L. (1991) Vasomotor, pilomotor and secretomotor neurons distinguished by size and neuropeptide content in superior cervical ganglia of mice. *J Auton Nerv Syst,* **34,** 171-83.

Gillespie, J. S. & Muir, T. C. (1970) Species and tissue variation in extraneuronal and neuronal accumulation of noradrenaline. *J Physiol,* **206,** 591-604.

Gillis, C. N. (1963) Increased retention of exogenous norepinephrine by cat atria after electrical stimulation of the cardioaccelerator nerves. *Biochem Pharmacol,* **12,** 593-95.

Gilsbach, R. & Hein, L. (2012) Are the pharmacology and physiology of α_2 adrenoceptors determined by α_2-heteroreceptors and autoreceptors respectively? *Br J Pharmacol,* **165,** 90-102.

Glass, M. & Felder, C. C. (1997) Concurrent stimulation of cannabinoid CB_1 and dopamine D_2 receptors augments cAMP accumulation in striatal neurons: evidence for a G_s linkage to the CB_1 receptor. *J Neurosci,* **17,** 5327-33.

Glowniak, J. V., Wilson, R. A., Joyce, M. E. & Turner, F. E. (1992) Evaluation of metaiodobenzylguanidine heart and lung extraction fraction by first-pass analysis in pigs. *J Nucl Med,* **33,** 716-23.

Göbel, I., Trendelenburg, A. U., Cox, S. L., Meyer, A. & Starke, K. (2000) Electrically evoked release of [^{3}H]noradrenaline from mouse cultured sympathetic neurons: release-modulating heteroreceptors. *J Neurochem,* **75,** 2087-94.

Goldstein, D. S. (2010) Adrenaline and noradrenaline. *Encyclopedia of Life Sciences.* Chichester: John Wiley & Sons, Ltd.

Goldstein, D. S., Brush, J. E., Jr., Eisenhofer, G., Stull, R. & Esler, M. (1988) In vivo measurement of neuronal uptake of norepinephrine in the human heart. *Circulation,* **78,** 41-48.

Gonon, F., Bao, J. X., Msghina, M., Suaud-Chagny, M. F. & Stjärne, L. (1993) Fast and local electrochemical monitoring of noradrenaline release from sympathetic terminals in isolated rat tail artery. *J Neurochem,* **60,** 1251-57.

Gonzalez, C., Almaraz, L., Obeso, A. & Rigual, R. (1994) Carotid body chemoreceptors: from natural stimuli to sensory discharges. *Physiol Rev,* **74,** 829-98.

Gonzalez, E., Rigual, R., Fidone, S. J. & Gonzalez, C. (1987) Mechanisms for termination of the action of dopamine in carotid body chemoreceptors. *J Auton Nerv Syst,* **18,** 249-59.

Gordan, R., Gwathmey, J. K. & Xie, L.-H. (2015) Autonomic and endocrine control of cardiovascular function. *World J Cardiol,* **7,** 204-14.

Gorenek, B. & Kudaiberdieva, G. (2012) Atrial fibrillation in acute ST-elevation myocardial infarction: clinical and prognostic features. *Curr Cardiol Rev,* **8,** 281-89.

Grassi, G. & Ram, V. S. (2016) Evidence for a critical role of the sympathetic nervous system in hypertension. *J Am Soc Hypertens,* **10,** 457-66.

Grassi, G., Seravalle, G. & Mancia, G. (2015) Sympathetic activation in cardiovascular disease: evidence, clinical impact and therapeutic implications. *Eur J Clin Invest,* **45,** 1367-75.

Greenway, C. V. (1987) Role of a changing venous capacitance in cardiovascular homeostasis. *In:* Ter Keurs, H. E. D. J. & Tyberg, J. V. *Mechanics of the Circulation. Developments in Cardiovascular Medicine* Dordrecht: Springer. **69**.

Griffin, G., Fernando, S. R., Ross, R. A., McKay, N. G., Ashford, M. L., Shire, D., . . . Pertwee, R. G. (1997) Evidence for the presence of CB_2-like cannabinoid receptors on peripheral nerve terminals. *Eur J Pharmacol,* **339,** 53-61.

Grohmann, M. & Trendelenburg, U. (1984) The substrate specificity of uptake$_2$ in the rat heart. *Naunyn Schmiedebergs Arch Pharmacol,* **328,** 164-73.

Gubernator, N., G., Zhang, H., Staal, R. G. W., Mosharov, E. V., Pereira, D. B., Yue, M., . . . Sames, D. (2009) Fluorescent false neurotransmitters visualize dopamine release from individual presynaptic terminals. *Science,* **324,** 1441-44.

Guyton, A. C. & Hall, J. E. (2010) *Guyton and Hall Textbook of Medical Physiology,* Philadelphia Saunders, Elsevier.

Habecker, B. A., Willison, B. D., Shi, X. & Woodward, W. R. (2006) Chronic depolarization stimulates norepinephrine transporter expression via catecholamines. *J Neurochem,* **97,** 1044-51.

Habermeier-Muth, A., Altes, U., Forsyth, K. M. & Muscholl, E. (1990) A presynaptic excitatory M_1 muscarine receptor at postganglionic cardiac noradrenergic nerve fibres that is activated by endogenous acetylcholine. *Naunyn Schmiedebergs Arch Pharmacol,* **342,** 483-89.

Häbler, H. J., Jänig, W., Krummel, M. & Peters, O. A. (1994) Reflex patterns in postganglionic neurons supplying skin and skeletal muscle of the rat hindlimb. *J Neurophysiol,* **72,** 2222-36.

Hagan, C. E., Neumaier, J. F. & Schenk, J. O. (2010) Rotating disk electrode voltammetric measurements of serotonin transporter kinetics in synaptosomes. *J Neurosci Methods,* **193,** 29-38.

Häggendal, J. & Malmfors, T. (1969) The effect of nerve stimulation on the uptake of noradrenaline into the adrenergic nerve terminals. *Acta Physiol Scand,* **75,** 28-32.

Hanbauer, I., Jacobowitz, D. M. & Kopin, I. J. (1974) Effects of vinblastine on noradrenergic axons. *Br J Pharmacol,* **50,** 219-25.

Hansen, J. & Ord, T. (1978) Effects of 6-hydroxydopamine on rat carotid body chief cells. *Experientia,* **34,** 1357-58.

Hansen, T., Tarasova, O. S., Khammy, M. M., Ferreira, A., Kennard, J. A., Andresen, J., . . . Aalkjær, C. (2019) [Ca^{2+}] changes in sympathetic varicosities and Schwann cells in rat mesenteric arteries—Relation to noradrenaline release and contraction. *Acta Physiologica,* **226,** e13279.

Hara, K., Yanagihara, N., Minami, K., Hirano, H., Sata, T., Shigematsu, A. & Izumi, F. (2000) Dual effects of intravenous anesthetics on the function of norepinephrine transporters. *Anesthesiology,* **93,** 1329-35.

Harden, S. (2009) *Microscopic analysis of sympathetic and parasympathetic distribution, terminal morphology, and interaction in whole-mount atria.* PhD thesis, University of Central Florida.

Harvey, W. (1929) *Exercitatio anatomica de motu cordis et sanguinis in animalibus* Springfield, IL., Charles C Thomas.

Hasenhuetl, P. S., Bhat, S., Freissmuth, M. & Sandtner, W. (2019) Functional selectivity and partial efficacy at the monoamine transporters: a unified model of allosteric modulation and amphetamine-induced substrate release. *Mol Pharmacol,* **95,** 303-12.

Haspula, D. & Clark, M. A. (2020) Cannabinoid receptors: an update on cell signaling, pathophysiological roles and therapeutic opportunities in neurological, cardiovascular, and inflammatory diseases. *Int J Mol Sci,* **21,** 7693.

Haunsø, A. & Buchanan, D. (2007) Pharmacological characterization of a fluorescent uptake assay for the noradrenaline transporter. *J Biomol Screen,* **12,** 378-84.

Hein, L., Altman, J. D. & Kobilka, B. K. (1999) Two functionally distinct α_2-adrenergic receptors regulate sympathetic neurotransmission. *Nature,* **402,** 181-84.

Henstridge, C. M., Brown, A. J. & Waldhoer, M. (2016) GPR55: metabolic help or hindrance? *Trends Endrocrinol Metab,* **27,** 606-08.

Heredia Mdel, P., Delgado, C., Pereira, L., Perrier, R., Richard, S., Vassort, G., . . . Gómez, A. M. (2005) Neuropeptide Y rapidly enhances $[Ca^{2+}]_i$ transients and Ca^{2+} sparks in adult rat ventricular myocytes through Y_1 receptor and PLC activation. *J Mol Cell Cardiol,* **38,** 205-12.

Herring, N. (2015) Autonomic control of the heart: going beyond the classical neurotransmitters. *Exp Physiol,* **100,** 354-8.

Herring, N., Cranley, J., Lokale, M. N., Li, D., Shanks, J., Alston, E. N., . . . Paterson, D. J. (2012) The cardiac sympathetic co-transmitter galanin reduces acetylcholine release and vagal bradycardia: Implications for neural control of cardiac excitability. *J Mol Cell Cardiol,* **52,** 667-76.

Herring, N., Lokale, M. N., Danson, E. J., Heaton, D. A. & Paterson, D. J. (2008) Neuropeptide Y reduces acetylcholine release and vagal bradycardia via a Y2 receptor-mediated, protein kinase C-dependent pathway. *J Mol Cell Cardiol,* **44,** 477-85.

Herring, N. & Paterson, D. J. (2021) The heart's little brain. *Circ Res,* **128,** 1297-99.

Hertting, G. & Axelrod, J. (1961) Fate of tritiated noradrenaline at the sympathetic nerve-endings. *Nature,* **192,** 172-73.

Hertting, G., Axelrod, J., Kopin, I. J. & Whitby, L. G. (1961) Lack of uptake of catecholamines after chronic denervation of sympathetic nerves. *Nature,* **189,** 66.

Higuchi, T., Yousefi, B. H., Kaiser, F., Gärtner, F., Rischpler, C., Reder, S., . . . Nekolla, S. G. (2013) Assessment of the ^{18}F-labeled PET tracer LMI1195 for imaging norepinephrine handling in rat hearts. *J Nucl Med,* **54,** 1142-46.

Hill, A. J. & Iaizzo, P. A. (2015) Comparative cardiac anatomy. *In:* Iaizzo, P. A. *Handbook of Cardiac Anatomy, Physiology, and Devices.* Cham: Springer. 89-114.

Hill, C. E., Hirst, G. D., Silverberg, G. D. & van Helden, D. F. (1986) Sympathetic innervation and excitability of arterioles originating from the rat middle cerebral artery. *J Physiol,* **371,** 305-16.

Ho, W. S. V. & Kelly, M. E. M. (2017) Cannabinoids in the cardiovascular system. *Adv Pharmacol,* **80,** 329-66.

Hoard, J. L., Hoover, D. B., Mabe, A. M., Blakely, R. D., Feng, N. & Paolocci, N. (2008) Cholinergic neurons of mouse intrinsic cardiac ganglia contain noradrenergic enzymes, norepinephrine transporters, and the neurotrophin receptors tropomyosin-related kinase A and p75. *Neuroscience,* **156,** 129-42.

Holmes, A. P., Ray, C. J., Thompson, E. L., Alshehri, Z., Coney, A. M. & Kumar, P. (2019) Adrenaline activation of the carotid body: Key to CO_2 and pH homeostasis in hypoglycaemia and potential pathological implications in cardiovascular disease. *Respir Physiol Neurobiol,* **265,** 92-99.

Holmes, A. P., Yu, T. Y., Tull, S., Syeda, F., Kuhlmann, S. M., O'Brien, S. M., . . . Kirchhof, P. (2016) A regional reduction in Ito and IKACh in the murine posterior left atrial myocardium is associated with action potential prolongation and increased ectopic activity. *PLoS One,* **11,** e0154077.

Honerjäger, P. (1982) Cardioactive substances that prolong the open state of sodium channels. *In:* Adrian, R. H., zur Hausen, H., Helmreich, E., Holzer, H., Jung, R., Krayer, O., . . . Weber, A. *Reviews of Physiology, Biochemistry and Pharmacology.* Berlin, Heidelberg: Springer Berlin Heidelberg. **92,** 1-74.

Horishita, T., Minami, K., Yanagihara, N., Shiraishi, M., Okamoto, T., Shiga, Y., . . . Shigematsu, A. (2002) Alphaxalone, a neurosteroid anesthetic, inhibits norepinephrine transporter function in cultured bovine adrenal medullary cells. *Anesth Analg,* **95,** 1661-66.

Horvath, G., Lieb, T., Conner, G. E., Salathe, M. & Wanner, A. (2001) Steroid sensitivity of norepinephrine uptake by human bronchial arterial and rabbit aortic smooth muscle cells. *Am J Respir Cell Mol Biol,* **25,** 500-06.

Hu, H., Xuan, Y., Xue, M., Cheng, W., Wang, Y., Li, X., . . . Yan, S. (2016) Semaphorin 3A attenuates cardiac autonomic disorders and reduces inducible ventricular arrhythmias in rats with experimental myocardial infarction. *BMC Cardiovasc Disord,* **16,** 16.

Huang, B., Liu, H., Scherlag, B. J., Sun, L., Xing, S., Xu, J., . . . Jiang, H. (2020) Atrial fibrillation in obstructive sleep apnea: Neural mechanisms and emerging therapies. *Trends Cardiovasc Med,* **31,** 127-32.

Ieda, M., Fukuda, K., Hisaka, Y., Kimura, K., Kawaguchi, H., Fujita, J., . . . Ogawa, S. (2004) Endothelin-1 regulates cardiac sympathetic innervation in the rodent heart by controlling nerve growth factor expression. *J Clin Invest,* **113,** 876-84.

Ignarro, L. J. & Shideman, F. E. (1968) The requirement of sympathetic innervation for the active transport of norepinephrine by the heart. *J Pharmacol Exp Ther,* **159,** 59-65.

Ilayan, E., Feliszek, M., Malinowska, B. & Schlicker, E. (2013) Do cannabinoids exhibit a tyramine-like effect? *Naunyn Schmiedebergs Arch Pharmacol,* **386,** 1041-46.

Imamura, Y., Fukuyama, T., Mochizuki, T., Miyagawa, M. & Watanabe, K. (2001) Prognostic value of iodine-123-metaiodobenzylguanidine imaging and cardiac natriuretic peptide levels in patients with left ventricular dysfunction resulting from cardiomyopathy. *Jpn Circ J,* **65,** 155-60.

Inazu, M., Takeda, H. & Matsumiya, T. (2003) Functional expression of the norepinephrine transporter in cultured rat astrocytes. *J Neurochem,* **84,** 136-44.

ISAN. **(2017)** *ISAN Symposium 11: Redefining the sacral autonomic outflow* [Online]. Available: https://autonomicneuroscience.info/ISAN/Debate2017.html [Accessed 23/02/2021].

Ishac, E. J., Jiang, L., Lake, K. D., Varga, K., Abood, M. E. & Kunos, G. (1996) Inhibition of exocytotic noradrenaline release by presynaptic cannabinoid CB_1 receptors on peripheral sympathetic nerves. *Br J Pharmacol,* **118,** 2023-8.

Ishii, K., Kuwahara, M., Tsubone, H. & Sugano, S. (1996) Autonomic nervous function in mice and voles (Microtus arvalis): investigation by power spectral analysis of heart rate variability. *Lab Anim,* **30,** 359-64.

Ishioka, N. & Bukoski, R. D. (1999) A role for N-arachidonylethanolamine (anandamide) as the mediator of sensory nerve-dependent Ca^{2+}-induced relaxation. *J Pharmacol Exp Ther,* **289,** 245-50.

Itoh, H., Toyohira, Y., Ueno, S., Saeki, S., Zhang, H., Furuno, Y., . . . Yanagihara, N. (2010) Upregulation of norepinephrine transporter function by prolonged exposure to nicotine in cultured bovine adrenal medullary cells. *Naunyn Schmiedebergs Arch Pharmacol,* **382,** 235-43.

Iversen, L. (2006) Neurotransmitter transporters and their impact on the development of psychopharmacology. *Br J Pharmacol,* **147,** 82-88.

Iversen, L. L. (1963) The uptake of noradrenaline by the isolated perfused rat heart *Br J Pharmacol Chemother,* **21,** 523-37.

Iversen, L. L. (1965) The uptake of catechol amines at high perfusion concentrations in the rat isolated heart: A novel catechol amine uptake process. *Br J Pharmacol,* **25,** 18-33.

Iversen, L. L. (1967) *The Uptake and Storage of Noradrenaline in Sympathetic Nerves,* Cambridge, Cambridge University Press.

Iversen, L. L., Glowinski, J. & Axelrod, J. (1965) The uptake and storage of H^3-norepinephrine in the reserpine-pretreated rat heart. *J Pharmacol Exp Ther,* **150,** 173-83.

Iversen, L. L., Jarrott, B. & Simmonds, M. A. (1971) Differences in the uptake, storage and metabolism of (+)- and (-)-noradrenaline. *Br J Pharmacol,* **43,** 845-55.

Iversen, L. L. & Salt, P. J. (1970) Inhibition of catecholamine uptake-$_2$ by steroids in the isolated rat heart. *Br J Pharmacol,* **40,** 528-30.

Jackson, A. & Nurse, C. A. (1998) Role of acetylcholine receptors and dopamine transporter in regulation of extracellular dopamine in rat carotid body cultures grown in chronic hypoxia or nicotine. *J Neurochem,* **70,** 653-62.

Jackson, V. M., Trout, S. J., Brain, K. L. & Cunnane, T. C. (2001) Characterization of action potential-evoked calcium transients in mouse postganglionic sympathetic axon bundles. *J Physiol,* **537,** 3-16.

Jänig, W. (2006a) Chapter 6.5: Different types of autonomic ganglia and their functions in vivo. *Integrative Action of the Autonomic Nervous System: Neurobiology of Homeostasis.* Cambridge: Cambridge University Press. 231.

Jänig, W. (2006b) *Integrative Action of the Autonomic Nervous System: Neurobiology of Homeostasis,* Cambridge, Cambridge University Press.

Jänig, W., Keast, J. R., McLachlan, E. M., Neuhuber, W. L. & Southard-Smith, M. (2017) Renaming all spinal autonomic outflows as sympathetic is a mistake. *Auton Neurosci,* **206,** 60-62.

Jänig, W., McLachlan, E. M. & Neuhuber, W. L. (2018) The sacral autonomic outflow: against premature oversimplification. *Clin Auton Res,* **28,** 5-6.

Jansen, H. J. & Rose, R. A. (2019) Isolation of atrial myocytes from adult mice. *J Vis Exp***,** e59588.

Jayanthi, L. D., Annamalai, B., Samuvel, D. J., Gether, U. & Ramamoorthy, S. (2006) Phosphorylation of the norepinephrine transporter at threonine 258 and serine 259 is linked to protein kinase C-mediated transporter internalization. *J Biol Chem,* **281,** 23326-40.

Jayanthi, L. D., Samuvel, D. J. & Ramamoorthy, S. (2004) Regulated internalization and phosphorylation of the native norepinephrine transporter in response to phorbol esters. Evidence for localization in lipid rafts and lipid raft-mediated internalization. *J Biol Chem,* **279,** 19315-26.

Jehan, S., Zizi, F., Pandi-Perumal, S. R., McFarlane, S. I., Jean-Louis, G. & Myers, A. K. (2020) Obstructive sleep apnea, hypertension, resistant hypertension and cardiovascular disease. *Sleep Med Disord,* **4,** 67-76.

Jiang, X., Wang, Y., Hand, A. R., Gillies, C., Cone, R. E., Kirk, J. & O'Rourke, J. (2002) Storage and release of tissue plasminogen activator by sympathetic axons in resistance vessel walls. *Microvasc Res,* **64,** 438-47.

Jing, M., Zhang, Y., Wang, H. & Li, Y. (2019) G-protein-coupled receptor-based sensors for imaging neurochemicals with high sensitivity and specificity. *J Neurochem,* **151,** 279-88.

Johnson, J. O. (2019) Chapter 13 - Autonomic Nervous System: Physiology. *In:* Hemmings, H. C. & Egan, T. D. *Pharmacology and Physiology for Anesthesia.* 2nd ed. Philadelphia: Elsevier. 270-81.

Jordan, J. & Grassi, G. (2018) The norepinephrine transporter deserves more attention. *J Hypertens,* **36,** 1472-74.

Jørgensen, S., Nielsen, E., Peters, D. & Dyhring, T. (2008) Validation of a fluorescence-based high-throughput assay for the measurement of neurotransmitter transporter uptake activity. *J Neurosci Methods,* **169,** 168-76.

Jose, A. D. & Collison, D. (1970) The normal range and determinants of the intrinsic heart rate in man. *Cardiovasc Res,* **4,** 160-67.

Jovanovic, P., Spasojevic, N., Puskas, N., Stefanovic, B. & Dronjak, S. (2019) Oxytocin modulates the expression of norepinephrine transporter, β_3-adrenoceptors and muscarinic M_2 receptors in the hearts of socially isolated rats. *Peptides,* **111,** 132-41.

Jovanovic, P., Spasojevic, N., Stefanovic, B. & Dronjak, S. (2014) Differential expression of tyrosine hydroxylase and transporters in the right and left stellate ganglion of socially isolated rats. *Auton Neurosci,* **181,** 85-89.

Kalant, H. (2001) Medicinal use of cannabis: history and current status. *Pain Res Manag,* **6,** 80-91.

Kalla, M., Hao, G., Tapoulal, N., Tomek, J., Liu, K., Woodward, L., . . . Herring, N. (2020) The cardiac sympathetic co-transmitter neuropeptide Y is pro-arrhythmic following ST-elevation myocardial infarction despite beta-blockade. *Eur Heart J,* **41,** 2168-79.

Kaludercic, N., Mialet-Perez, J., Paolocci, N., Parini, A. & Di Lisa, F. (2014) Monoamine oxidases as sources of oxidants in the heart. *J Mol Cell Cardiol,* **73,** 34-42.

Kaludercic, N., Takimoto, E., Nagayama, T., Feng, N., Lai, E. W., Bedja, D., . . . Paolocci, N. (2010) Monoamine oxidase A-mediated enhanced catabolism of norepinephrine contributes to adverse remodeling and pump failure in hearts with pressure overload. *Circ Res,* **106,** 193-202.

Kandlikar, S. S. & Fink, G. D. (2011) Splanchnic sympathetic nerves in the development of mild DOCA-salt hypertension. *Am J Physiol Heart Circ,* **301,** H1965-73.

Karpowicz, R. J., Jr., Dunn, M., Sulzer, D. & Sames, D. (2013) APP^+, a fluorescent analogue of the neurotoxin MPP^+, is a marker of catecholamine neurons in brain tissue, but not a fluorescent false neurotransmitter. *ACS Chem Neurosci,* **4,** 858-69.

Kashihara, K., Varga, E. V., Waite, S. L., Roeske, W. R. & Yamamura, H. I. (1992) Cloning of the rat M_3, M_4 and M_5 muscarinic acetylcholine receptor genes by the polymerase chain reaction (PCR) and the pharmacological characterization of the expressed genes. *Life Sci,* **51,** 955-71.

Kavanaugh, M. P. (1998) Neurotransmitter transport: models in flux. *Proc Natl Acad Sci U S A,* **95,** 12737-38.

Kawano, H., Okada, R. & Yano, K. (2003) Histological study on the distribution of autonomic nerves in the human heart. *Heart and Vessels,* **18,** 32-39.

Kawashima, T. (2005) The autonomic nervous system of the human heart with special reference to its origin, course, and peripheral distribution. *Anat Embryol (Berl),* **209,** 425-38.

Kaye, D. M., Gruskin, S., Smith, A. I. & Esler, M. D. (2000) Nitric oxide mediated modulation of norepinephrine transport: identification of a potential target for S-nitrosylation. *Br J Pharmacol,* **130,** 1060-64.

Kaye, D. M., Wiviott, S. D., Kobzik, L., Kelly, R. A. & Smith, T. W. (1997) S-nitrosothiols inhibit neuronal norepinephrine transport. *Am J Physiol,* **272,** H875-83.

Kazanietz, M. G. & Enero, M. A. (1989) Modulation of noradrenaline release by presynaptic alpha$_2$ and β adrenoceptors in rat atria. Effect of pretreatment with clenbuter. *Naunyn Schmiedebergs Arch Pharmacol,* **340,** 274-78.

Kennard, J. (2015) *Junctional modulation of sympathetic transmission.* PhD thesis, University of Oxford.

Kimura, K., Ieda, M. & Fukuda, K. (2012) Development, maturation, and transdifferentiation of cardiac sympathetic nerves. *Circ Res,* **110,** 325-36.

Kimura, T., Uchida, W. & Satoh, S. (1985) Predominance of postsynaptic mechanism in vagal suppression of sympathetic tachycardia in the dog. *J Pharmacol Exp Ther,* **235,** 793-97.

Kirpekar, S. M. & Wakade, A. R. (1968a) Factors influencing noradrenaline uptake by the perfused spleen of the cat. *J Physiol,* **194,** 609-26.

Kirpekar, S. M. & Wakade, A. R. (1968b) Factors influencing noradrenaline uptake by the perfused spleen of the cat. *J Physiol,* **194,** 609-26.

Klabunde, R. E. (2012) *Cardiovascular Physiology Concepts*, Lippincott Williams & Wilkins.

Klein, R. L. & Lagercrantz, H. (1981) Noradrenergic vesicles: composition and function. *In:* Stjärne, L., Hedqvist, P., Lagercrantz, H. & Wennmalm, Å. *Chemical Neurotransmission 75 Years.* London: Academic Press. 69-83.

Klemm, M. F., Van Helden, D. F. & Luff, S. E. (1993) Ultrastructural analysis of sympathetic neuromuscular junctions on mesenteric veins of the guinea pig. *J Comp Neurol,* **334,** 159-67.

Kleyer, J., Nicolussi, S., Taylor, P., Simonelli, D., Furger, E., Anderle, P. & Gertsch, J. (2012) Cannabinoid receptor trafficking in peripheral cells is dynamically regulated by a binary biochemical switch. *Biochem Pharmacol,* **83,** 1393-412.

Knight, W. D., Saxena, A., Shell, B., Nedungadi, T. P., Mifflin, S. W. & Cunningham, J. T. (2013) Central losartan attenuates increases in arterial pressure and expression of FosB/ΔFosB along the autonomic axis associated with chronic intermittent hypoxia. *Am J Physiol Regul Integr Comp Physiol,* **305,** R1051-58.

Knoche, H. & Kienecker, E. W. (1977) Sympathetic innervation of the carotid bifurcation in the rabbit and cat: Blood vessels, carotid body and carotid sinus. *Cell Tissue Res,* **184,** 103-12.

Ko, B. H., Paik, J. Y., Jung, K. H., Bae, J. S., Lee, E. J., Choe, Y. S., . . . Lee, K. H. (2008) Effects of anesthetic agents on cellular ^{123}I-MIBG transport and in vivo ^{123}I-MIBG biodistribution. *Eur J Nucl Med Mol Imaging,* **35,** 554-61.

Kopin, I. J., Rundqvist, B., Friberg, P., Lenders, J., Goldstein, D. S. & Eisenhofer, G. (1998) Different relationships of spillover to release of norepinephrine in human heart, kidneys, and forearm. *Am J Physiol,* **275,** R165-73.

Kosersky, D. S. (1978) Antihypertensive effects of delta9-tetrahydrocannabinol. *Arch Int Pharmacodyn Ther,* **233,** 76-81.

Kossakowski, R., Schlicker, E., Toczek, M., Weresa, J. & Malinowska, B. (2019) Cannabidiol affects the Bezold-Jarisch reflex via $TRPV_1$ and 5-HT_3 receptors and has peripheral sympathomimetic effects in spontaneously hypertensive and normotensive rats. *Front Pharmacol,* **10,** 500.

Krell, R. D. & Patil, P. N. (1972) Steric aspects of adrenergic drugs. XX. Accumulation of (-)- and (+)-norepinephrine- ^{14}C by peripheral tissues of the rat. *J Pharmacol Exp Ther,* **182,** 273-83.

Kreusser, M. M., Buss, S. J., Krebs, J., Kinscherf, R., Metz, J., Katus, H. A., . . . Backs, J. (2008) Differential expression of cardiac neurotrophic factors and sympathetic nerve ending abnormalities within the failing heart. *J Mol Cell Cardiol,* **44,** 380-87.

Kreusser, M. M., Lehmann, L. H., Haass, M., Buss, S. J., Katus, H. A. & Lossnitzer, D. (2017) Depletion of cardiac catecholamine stores impairs cardiac norepinephrine re-uptake by downregulation of the norepinephrine transporter. *PLoS One,* **12,** e0172070.

Kristen, A. V., Kreusser, M. M., Lehmann, L., Kinscherf, R., Katus, H. A., Haass, M. & Backs, J. (2006) Preserved norepinephrine reuptake but reduced sympathetic nerve endings in hypertrophic volume-overloaded rat hearts. *J Card Fail,* **12,** 577-83.

Krylatov, A. V., Maslov, L. N., Ermakov, S., Lasukova, O. V., Barzakh, E. I., Crawford, D. & Pertwee, R. G. (2007) Significance of cardiac cannabinoid receptors in regulation of cardiac rhythm, myocardial contractility, and electrophysiologic processes in heart. *Izv Akad Nauk Ser Biol***,** 35-44.

Kubista, H., Kosenburger, K., Mahlknecht, P., Drobny, H. & Boehm, S. (2009) Inhibition of transmitter release from rat sympathetic neurons via presynaptic M_1 muscarinic acetylcholine receptors. *Br J Pharmacol,* **156,** 1342-52.

Kumar, A., Accorsi, A., Rhee, Y. & Girgenrath, M. (2015) Do's and don'ts in the preparation of muscle cryosections for histological analysis. *J Vis Exp***,** e52793.

Kumar, P. & Prabhakar, N. R. (2012) Peripheral chemoreceptors: function and plasticity of the carotid body. *Compr Physiol,* **2,** 141-219.

Kurihara, J., Nishigaki, M., Suzuki, S., Okubo, Y., Takata, Y., Nakane, S., . . . Kato, H. (2001) 2-Arachidonoylglycerol and anandamide oppositely modulate norepinephrine release from the rat heart sympathetic nerves. *Jpn J Pharmacol,* **87,** 93-96.

Kurz, T., Richardt, G., Hagl, S., Seyfarth, M. & Schömig, A. (1995) Two different mechanisms of noradrenaline release during normoxia and simulated ischemia in human cardiac tissue. *J Mol Cell Cardiol,* **27,** 1161-72.

Lake, K. D., Compton, D. R., Varga, K., Martin, B. R. & Kunos, G. (1997) Cannabinoid-induced hypotension and bradycardia in rats mediated by CB_1-like cannabinoid receptors. *J Pharmacol Exp Ther,* **281,** 1030-37.

Lameris, T. W., de Zeeuw, S., Alberts, G., Boomsma, F., Duncker, D. J., Verdouw, P. D., . . . van Den Meiracker, A. H. (2000) Time course and mechanism of myocardial catecholamine release during transient ischemia in vivo. *Circulation,* **101,** 2645-50.

Langley, J. N. (1901) Observations on the physiological action of extracts of the supra-renal bodies. *J Physiol,* **27,** 237-56.

Langley, J. N. (1905) On the reaction of cells and of nerve-endings to certain poisons, chiefly as regards the reaction of striated muscle to nicotine and to curari. *J Physiol,* **33,** 374-413.

Langley, J. N. (1921) *The Autonomic Nervous System,* Cambridge, W. Heffer & Sons.

Laprairie, R. B., Bagher, A. M. & Denovan-Wright, E. M. (2017) Cannabinoid receptor ligand bias: implications in the central nervous system. *Curr Opin Pharmacol,* **32,** 32-43.

Lashford, L. S., Hancock, J. P. & Kemshead, J. T. (1991) Meta-iodobenzylguanidine (mIBG) uptake and storage in the human neuroblastoma cell line SK-N-BE(2C). *Int J Cancer,* **47,** 105-09.

Lauckner, J. E., Hille, B. & Mackie, K. (2005) The cannabinoid agonist WIN55,212-2 increases intracellular calcium via CB_1 receptor coupling to $G_{q/11}$ G proteins. *Proc Natl Acad Sci U S A,* **102,** 19144-49.

Lavallée, M., de Champlain, J. & Nadeau, R. A. (1980) Reflexly induced inhibition of catecholamine release through a peripheral muscarinic mechanism. *Can J Physiol Pharmacol,* **58,** 1334-41.

Lay, L., Angus, J. A. & Wright, C. E. (2000) Pharmacological characterisation of cannabinoid CB_1 receptors in the rat and mouse. *Eur J Pharmacol,* **391,** 151-61.

Ledent, C., Valverde, O., Cossu, G., Petitet, F., Aubert, J. F., Beslot, F., . . . Parmentier, M. (1999) Unresponsiveness to cannabinoids and reduced addictive effects of opiates in CB_1 receptor knockout mice. *Science,* **283,** 401-04.

Lee, S. H., Lim, D. H., Lee, J. H., Chang, K., Koo, J. M. & Park, H. J. (2016) Long-term blood pressure control effect of celiac plexus block with botulinum toxin. *Toxins,* **8,** 51.

Lee, S. H., Rhee, J., Koh, J. K. & Lee, Y. S. (1996) Species differences in functions of dopamine transporter: paucity of MPP^+ uptake and cocaine binding in bovine dopamine transporter. *Neurosci Lett,* **214,** 199-201.

Lefebvre, B., Godin-Ribuot, D., Joyeux-Faure, M., Caron, F., Bessard, G., Lévy, P. & Stanke-Labesque, F. (2006) Functional assessment of vascular reactivity after chronic intermittent hypoxia in the rat. *Respir Physiol Neurobiol,* **150,** 278-86.

Leineweber, K., Seyfarth, T. & Brodde, O. (2000) Chamber-specific alterations of noradrenaline uptake ($uptake_1$) in right ventricles of monocrotaline-treated rats. *Br J Pharmacol,* **131,** 1438-44.

Lenders, J. W., Duh, Q. Y., Eisenhofer, G., Gimenez-Roqueplo, A. P., Grebe, S. K., Murad, M. H., . . . Young, W. F., Jr. (2014) Pheochromocytoma and paraganglioma: an endocrine society clinical practice guideline. *J Clin Endocrinol Metab,* **99,** 1915-42.

Leonti, M., Casu, L., Raduner, S., Cottiglia, F., Floris, C., Altmann, K. H. & Gertsch, J. (2010) Falcarinol is a covalent cannabinoid CB1 receptor antagonist and induces pro-allergic effects in skin. *Biochem Pharmacol,* **79,** 1815-26.

Leopold, A. V., Shcherbakova, D. M. & Verkhusha, V. V. (2019) Fluorescent biosensors for neurotransmission and neuromodulation: engineering and applications. *Front Cell Neurosci,* **13**.

Leuenberger, U., Gleeson, K., Wroblewski, K., Prophet, S., Zelis, R., Zwillich, C. & Sinoway, L. (1991) Norepinephrine clearance is increased during acute hypoxemia in humans. *Am J Physiol,* **261,** H1659-64.

Li, C. & Horn, J. P. (2008) Differential inhibition of Ca^{2+} channels by α_2-adrenoceptors in three functional subclasses of rat sympathetic neurons. *J Neurophysiol,* **100,** 3055-63.

Li, D., Chen, B. M., Peng, J., Zhang, Y. S., Li, X. H., Yuan, Q., . . . Li, Y. J. (2009) Role of anandamide transporter in regulating calcitonin gene-related peptide production and blood pressure in hypertension. *J Hypertens,* **27,** 1224-32.

Li, T., Chen, Y., Gua, C. & Wu, B. (2018) Elevated oxidative stress and inflammation in hypothalamic paraventricular nucleus are associated with sympathetic excitation and hypertension in rats exposed to chronic intermittent hypoxia. *Front Physiol,* **9,** 840.

Liang, C., Rounds, N. K., Dong, E., Stevens, S. Y., Shite, J. & Qin, F. (2000) Alterations by norepinephrine of cardiac sympathetic nerve terminal function and myocardial beta-adrenergic receptor sensitivity in the ferret: normalization by antioxidant vitamins. *Circulation,* **102,** 96-103.

Liang, C. S., Fan, T. H., Sullebarger, J. T. & Sakamoto, S. (1989) Decreased adrenergic neuronal uptake activity in experimental right heart failure. A chamber-specific contributor to beta-adrenoceptor downregulation. *J Clin Invest,* **84,** 1267-75.

Liang, M. & Knox, F. G. (1999) Nitric oxide reduces the molecular activity of Na^+, K^+ ATPase in opossum kidney cells. *Kidney Int,* **56,** 627-34.

Lightman, S. L. & Iversen, L. L. (1969) The role of $uptake_2$ in the extraneuronal metabolism of catecholamines in the isolated rat heart. *Br J Pharmacol,* **37,** 638-49.

Lindmar, R. & Muscholl, E. (1964) Die wirkung von pharmaka auf die elimination von noradrenalin aus der perfusionsflüssigkeit und die noradrenalinaufnahme in das isolierte Herz. *Naunyn Schmiedebergs Arch Exp Pathol Pharmakol,* **247,** 469-92.

Liu, Y., Chen, J., Fontes, S. K., Bautista, E. N. & Cheng, Z. (2021) Physiological and pathological roles of protein kinase A in the heart. *Cardiovasc Res***,** [Online ahead of print].

Loder, M. K. & Melikian, H. E. (2003) The dopamine transporter constitutively internalizes and recycles in a protein kinase C-regulated manner in stably transfected PC12 cell lines. *J Biol Chem,* **278,** 22168-74.

Loewy, A. D. (1990) Central autonomic pathways *In:* Spyer, K. M. *Central Regulation of Autonomic Functions* Oxford: Oxford University Press. 88-103.

Löffelholz, K. & Muscholl, E. (1970) Inhibition by parasympathetic nerve stimulation of the release of the adrenergic transmitter. *Naunyn Schmiedebergs Arch Pharmakol,* **267,** 181-84.

Long, J. B. & Segal, S. S. (2009) Quantifying perivascular sympathetic innervation: regional differences in male C57BL/6 mice at 3 and 20 months. *J Neurosci Methods,* **184,** 124-28.

Loukas, M., Klaassen, Z., Merbs, W., Tubbs, R. S., Gielecki, J. & Zurada, A. (2010) A review of the thoracic splanchnic nerves and celiac ganglia. *Clin Anat,* **23,** 512-22.

Lucking, E. F., O'Halloran, K. D. & Jones, J. F. (2014) Increased cardiac output contributes to the development of chronic intermittent hypoxia-induced hypertension. *Exp Physiol,* **99,** 1312-24.

Ludwig, J., Grohmann, M. & Trendelenburg, U. (1986) Inhibition by K^+ of $uptake_2$ of ^3H-(±)-isoprenaline in the perfused rat heart. *Naunyn Schmiedebergs Arch Pharmacol,* **334,** 393-96.

Lundberg, J. M., Rudehill, A., Sollevi, A., Theodorsson-Norheim, E. & Hamberger, B. (1986) Frequency- and reserpine-dependent chemical coding of sympathetic transmission: differential release of noradrenaline and neuropeptide Y from pig spleen. *Neurosci Lett,* **63,** 96-100.

Luo, M., Hess, M. C., Fink, G. D., Olson, L. K., Rogers, J., Kreulen, D. L., . . . Galligan, J. J. (2003) Differential alterations in sympathetic neurotransmission in mesenteric arteries and veins in DOCA-salt hypertensive rats. *Auton Neurosci,* **104,** 47-57.

Macefield, V. G. & Wallin, B. G. (2018) Physiological and pathophysiological firing properties of single postganglionic sympathetic neurons in humans. *J Neurophysiol,* **119,** 944-56.

MacIntyre, I. M. & Webb, D. J. (2019) Renal denervation therapy for hypertension: still on trial. *Heart,* **105,** 1452-53.

Mackie, K. & Hille, B. (1992) Cannabinoids inhibit N-type calcium channels in neuroblastoma-glioma cells. *Proc Natl Acad Sci U S A,* **89,** 3825-9.

Maklad, A., Quinn, T. & Fritzsch, B. (2001) Intracranial distribution of the sympathetic system in mice: DiI tracing and immunocytochemical labeling. *Anat Rec,* **263,** 99-111.

Malinowska, B., Baranowska-Kuczko, M. & Schlicker, E. (2012) Triphasic blood pressure responses to cannabinoids: do we understand the mechanism? *Br J Pharmacol,* **165,** 2073-88.

Malinowska, B., Godlewski, G., Bucher, B. & Schlicker, E. (1997) Cannabinoid CB_1 receptor-mediated inhibition of the neurogenic vasopressor response in the pithed rat. *Naunyn Schmiedebergs Arch Pharmacol,* **356,** 197-202.

Malinowska, B., Piszcz, J., Koneczny, B., Hryniewicz, A. & Schlicker, E. (2001) Modulation of the cardiac autonomic transmission of pithed rats by presynaptic opioid OP_4 and cannabinoid CB_1 receptors. *Naunyn Schmiedebergs Arch Pharmakol,* **364,** 233-41.

Manabe, N., Foldes, F. F., Töröcsik, A., Nagashima, H., Goldiner, P. L. & Vizi, E. S. (1991) Presynaptic interaction between vagal and sympathetic innervation in the heart: modulation of acetylcholine and noradrenaline release. *J Auton Nerv Syst,* **32,** 233-42.

Mandela, P. & Ordway, G. A. (2006a) KCl stimulation increases norepinephrine transporter function in PC12 cells. *J Neurochem,* **98,** 1521-30.

Mandela, P. & Ordway, G. A. (2006b) The norepinephrine transporter and its regulation. *J Neurochem,* **97,** 310-33.

Mangoni, A. A., Mircoli, L., Giannattasio, C., Mancia, G. & Ferrari, A. U. (1997) Effect of sympathectomy on mechanical properties of common carotid and femoral arteries. *Hypertension,* **30,** 1085-88.

Manousiouthakis, E., Mendez, M., Garner, M. C., Exertier, P. & Makita, T. (2014) Venous endothelin guides sympathetic innervation of the developing mouse heart. *Nat Commun,* **5,** 3918.

Mansukhani, M. P., Kara, T., Caples, S. M. & Somers, V. K. (2014) Chemoreflexes, sleep apnea, and sympathetic dysregulation. *Curr Hypertens Rep,* **16,** 476.

Marijon, E., Le Heuzey, J. Y., Connolly, S., Yang, S., Pogue, J., Brueckmann, M., . . . Yusuf, S. (2013) Causes of death and influencing factors in patients with atrial fibrillation: a competing-risk analysis from the randomized evaluation of long-term anticoagulant therapy study. *Circulation,* **128,** 2192-201.

Marques, F. Z., Eikelis, N., Bayles, R. G., Lambert, E. A., Straznicky, N. E., Hering, D., . . . Lambert, G. W. (2017) A polymorphism in the norepinephrine transporter gene is associated with affective and cardiovascular disease through a microRNA mechanism. *Mol Psychiatry,* **22,** 134-41.

Marshall, J. M. (1982) The influence of the sympathetic nervous system on individual vessels of the microcirculation of skeletal muscle of the rat. *J Physiol,* **332,** 169-86.

Marshall, J. M. (2015) Interactions between local dilator and sympathetic vasoconstrictor influences in skeletal muscle in acute and chronic hypoxia. *Exp Physiol,* **100,** 1400-11.

Mason, J. N., Farmer, H., Tomlinson, I. D., Schwartz, J. W., Savchenko, V., DeFelice, L. J., . . . Blakely, R. D. (2005) Novel fluorescence-based approaches for the study of biogenic amine transporter localization, activity, and regulation. *J Neurosci Methods,* **143,** 3-25.

Matheson, P. J., Wilson, M. A. & Garrison, R. N. (2000) Regulation of intestinal blood flow. *J Surg Res,* **93,** 182-96.

Matthies, H. J. G., Han, Q., Shields, A., Wright, J., Moore, J. L., Winder, D. G., . . . Blakely, R. D. (2009) Subcellular localization of the antidepressant-sensitive norepinephrine transporter. *BMC Neuroscience,* **10,** 65.

Mechoulam, R., Hanuš, L. O., Pertwee, R. & Howlett, A. C. (2014) Early phytocannabinoid chemistry to endocannabinoids and beyond. *Nat Rev Neurosci,* **15,** 757-64.

Meiergerd, S. M., Patterson, T. A. & Schenk, J. O. (1993) D_2 receptors may modulate the function of the striatal transporter for dopamine: kinetic evidence from studies in vitro and in vivo. *J Neurochem,* **61,** 764-67.

Mekontso-Dessap, A., Brouri, F., Pascal, O., Lechat, P., Hanoun, N., Lanfumey, L., . . . Eddahibi, S. (2006) Deficiency of the 5-hydroxytryptamine transporter gene leads to cardiac fibrosis and valvulopathy in mice. *Circulation,* **113,** 81-89.

Mendizábal, V. E. & Adler-Graschinsky, E. (2007) Cannabinoids as therapeutic agents in cardiovascular disease: a tale of passions and illusions. *Br J Pharmacol,* **151,** 427-40.

Mendizábal, V. E., Orliac, M. L. & Adler-Graschinsky, E. (2001) Long-term inhibition of nitric oxide synthase potentiates effects of anandamide in the rat mesenteric bed. *Eur J Pharmacol,* **427,** 251-62.

Milligan, A. L., Szabo-Pardi, T. A. & Burton, M. D. (2020) Cannabinoid receptor type 1 and its role as an analgesic: an opioid alternative? *J Dual Diagn,* **16,** 106-19.

Miranda, S. M., Moscavitch, S. D., Pereira, S. B., de Azevedo, J. C., Messias, L. R., Rodrigues, R. C., . . . Mesquita, C. T. (2014) Heart failure patients with β_1-adrenoreceptor polymorphisms have augmented carvedilol response as detected by cardiac ^{123}-MIBG scintigraphy. *Int J Cardiol,* **177,** 111-13.

Mitchell, G. A. G. (1953) The innervation of the heart. *Br Heart J,* **15,** 159-71.

Mitsuma, T., Rhue, H., Hirooka, Y., Kayama, M., Wago, T., Takagi, J., . . . Sakai, J. (1998) Distribution of dopamine transporter in the rat: an immunohistochemical study. *Endocr Regul,* **32,** 71-75.

Moesgaard, B., Petersen, G., Mortensen, S. A. & Hansen, H. S. (2002) Substantial species differences in relation to formation and degradation of N-acyl-ethanolamine phospholipids in heart tissue: an enzyme activity study. *Comp Biochem Physiol B Biochem Mol Biol,* **131,** 475-82.

Mohan, R. M., Golding, S. & Paterson, D. J. (2001) Intermittent hypoxia modulates nNOS expression and heart rate response to sympathetic nerve stimulation. *Am J Physiol Heart Circ Physiol,* **281,** H132-8.

Molderings, G. J., Bönisch, H., Hammermann, R., Göthert, M. & Brüss, M. (2002) Noradrenaline release-inhibiting receptors on PC12 cells devoid of alpha$_2$ and CB_1 receptors: similarities to presynaptic imidazoline and edg receptors. *Neurochem Int,* **40,** 157-67.

Molderings, G. J., Likungu, J. & Göthert, M. (1999) Presynaptic cannabinoid and imidazoline receptors in the human heart and their potential relationship. *Naunyn Schmiedebergs Arch Pharmacol,* **360,** 157-64.

Mondal, P. P. (2014) Temporal resolution in fluorescence imaging. *Front Mol Biosci,* **1,** 11.

Montecucco, C. & Molgó, J. (2005) Botulinal neurotoxins: revival of an old killer. *COPHAR,* **5,** 274-79.

Montoya, A., Bruins, R., Katzman, M. A. & Blier, P. (2016) The noradrenergic paradox: implications in the management of depression and anxiety. *Neuropsychiatr Dis Treat,* **12,** 541-57.

Moraes, D. J., da Silva, M. P., Bonagamba, L. G., Mecawi, A. S., Zoccal, D. B., Antunes-Rodrigues, J., . . . Machado, B. H. (2013) Electrophysiological properties of rostral ventrolateral medulla presympathetic neurons modulated by the respiratory network in rats. *J Neurosci,* **33,** 19223-37.

Mukhopadhyay, P., Bátkai, S., Rajesh, M., Czifra, N., Harvey-White, J., Haskó, G., . . . Pacher, P. (2007) Pharmacological inhibition of CB_1 cannabinoid receptor protects against doxorubicin-induced cardiotoxicity. *J Am Coll Cardiol,* **50,** 528-36.

Mukhopadhyay, S. & Howlett, A. C. (2005) Chemically distinct ligands promote differential CB_1 cannabinoid receptor-G_i protein interactions. *Mol Pharmacol,* **67,** 2016-24.

Münch, G., Rosport, K., Bültmann, A., Baumgartner, C., Li, Z., Laacke, L. & Ungerer, M. (2005) Cardiac overexpression of the norepinephrine transporter uptake-1 results in marked improvement of heart failure. *Circ Res,* **97,** 928-36.

Myat, A., Redwood, S. R., Qureshi, A. C., Spertus, J. A. & Williams, B. (2012) Resistant hypertension. *BMJ,* **345,** e7473.

Nakajima, K., Matsunari, I. & Jacobson, A. F. (2018) I^{-123} metaiodobenzylguanidine innervation imaging as a tool for norepinephrine transporter research: A possible application for genetic analysis in heart failure. *J Nucl Cardiol,* **25,** 907-10.

Namura, I., Douillet, P., Sun, C. J., Pert, A., Cohen, R. M. & Chiueh, C. C. (1987) MPP^+ (1-methyl-4-phenylpyridine) is a neurotoxin to dopamine-, norepinephrine- and serotonin-containing neurons. *Eur J Pharmacol,* **136,** 31-37.

Narkiewicz, K. & Somers, V. K. (1997) The sympathetic nervous system and obstructive sleep apnea: implications for hypertension. *J Hypertens,* **15,** 1613-19.

Nedergaard, O. A. & Abrahamsen, J. (1990) Modulation of noradrenaline release by activation of presynaptic beta-adrenoceptors in the cardiovascular system. *Ann N Y Acad Sci,* **604,** 528-44.

Neri, M., Cerretani, D., Fiaschi, A. I., Laghi, P. F., Lazzerini, P. E., Maffione, A. B., . . . Fineschi, V. (2007) Correlation between cardiac oxidative stress and myocardial pathology due to acute and chronic norepinephrine administration in rats. *J Cell Mol Med,* **11,** 156-70.

Ng, G. A., Brack, K. E. & Coote, J. H. (2001) Effects of direct sympathetic and vagus nerve stimulation on the physiology of the whole heart – a novel model of isolated Langendorff perfused rabbit heart with intact dual autonomic innervation. *Exp Physiol,* **86,** 319-29.

NHS (2016) Clinical commissioning policy: renal denervation for resistant hypertension. National Health Service, UK: 16004/P. Available: https://www.england.nhs.uk/wp-content/uploads/2018/07/Renal-denervation-for-resistant-hypertension.pdf [Accessed 07/02/2021].

Ni, W., Thompson, J. M., Northcott, C. A., Lookingland, K. & Watts, S. W. (2004) The serotonin transporter is present and functional in peripheral arterial smooth muscle. *J Cardiovasc Pharmacol,* **43,** 770-81.

NICE (2018) National Institute for Health and Care Excellence: Chronic heart failure in adults: diagnosis and management. NICE [NG106]. Available: https://www.nice.org.uk/guidance/ng106/resources/chronic-heart-failure-in-adults-diagnosis-and-management-pdf-66141541311685 [Accessed 06/02/2021].

NICE (2019) National Institute for Health and Care Excellence: Hypertension in adults: diagnosis and management. NICE guideline [NG136]. Available: https://www.nice.org.uk/guidance/ng136/chapter/recommendations [Accessed 07/02/2021].

Nicholls, M. (2020) Dr Julius Axelrod. *Eur Heart J,* **41,** 3778-80.

Nicklas, W. J., Puszkin, S. & Berl, S. (1973) Effect of vinblastine and colchicine on uptake and release of putative transmitters by synaptosomes and on brain actomyosin-like protein. *J Neurochem,* **20,** 109-21.

Nicol, C. J. & Rae, R. M. (1972) Proceedings: Inhibition of accumulation of adrenaline and noradrenaline in arterial smooth muscle by steroids. *Br J Pharmacol,* **44,** 361-62.

Niederhoffer, N., Schmid, K. & Szabo, B. (2003) The peripheral sympathetic nervous system is the major target of cannabinoids in eliciting cardiovascular depression. *Naunyn Schmiedebergs Arch Pharmacol,* **367,** 434-43.

Niello, M., Gradisch, R., Loland, C. J., Stockner, T. & Sitte, H. H. (2020) Allosteric Modulation of Neurotransmitter Transporters as a Therapeutic Strategy. *Trends Pharmacol Sci,* **41,** 446-63.

Nilsson, H., Ljung, B., Sjöblom, N. & Wallin, B. G. (1985) The influence of the sympathetic impulse pattern on contractile responses of rat mesenteric arteries and veins. *Acta Physiol Scand,* **123,** 303-09.

Nishimaru, K., Tanaka, Y., Tanaka, H. & Shigenobu, K. (2000) Positive and negative inotropic effects of muscarinic receptor stimulation in mouse left atria. *Life Sci,* **66,** 607-15.

Novotny, M., Quaiserová-Mocko, V., Wehrwein, E. A., Kreulen, D. L. & Swain, G. M. (2007) Determination of endogenous norepinephrine levels in different chambers of the rat heart by capillary electrophoresis coupled with amperometric detection. *J Neurosci Methods,* **163,** 52-59.

Nozawa, T., Igawa, A., Yoshidan, N., Maeda, M., Inoue, M., Yamamura, Y., . . . Inoue, H. (1998) Dual-tracer assessment of coupling between cardiac sympathetic neuronal function and downregulation of β-receptors during development of hypertensive heart failure of rats. *Circulation,* **97,** 2359-67.

Numata, A., Miyauchi, Y., Ono, N., Fishbein, M. C., Mandel, W. J., Lin, S. F., . . . Karagueuzian, H. S. (2012) Spontaneous atrial fibrillation initiated by tyramine in canine atria with increased sympathetic nerve sprouting. *J Cardiovasc Electrophysiol,* **23,** 415-22.

O'Sullivan, S. E. (2015) Endocannabinoids and the cardiovascular system in health and disease. *Handb Exp Pharmacol,* **231,** 393-422.

O'Shea, C., Holmes, A. P., Yu, T. Y., Winter, J., Wells, S. P., Correia, J., . . . Pavlovic, D. (2019) ElectroMap: High-throughput open-source software for analysis and mapping of cardiac electrophysiology. *Sci Rep,* **9,** 1389.

Oakes, P. C., Fisahn, C., Iwanaga, J., DiLorenzo, D., Oskouian, R. J. & Tubbs, R. S. (2016) A history of the autonomic nervous system: part I: from Galen to Bichat. *Childs Nerv Syst,* **32,** 2303-08.

Oliveira, R. S., Alonso, S., Campos, F. O., Rocha, B. M., Fernandes, J. F., Kuehne, T. & dos Santos, R. W. (2018) Ectopic beats arise from micro-reentries near infarct regions in simulations of a patient-specific heart model. *Sci Rep,* **8,** 16392.

Omar, N. M. & Marshall, J. M. (2010) Age-related changes in the sympathetic innervation of cerebral vessels and in carotid vascular responses to norepinephrine in the rat: in vitro and in vivo studies. *J Appl Physiol (1985),* **109,** 314-22.

Oostendorp, J. & Kaumann, A. J. (2000) Pertussis toxin suppresses carbachol-evoked cardiodepression but does not modify cardiostimulation mediated through β_1- and putative β_4-adrenoceptors in mouse left atria: no evidence for β_2- and β_3-adrenoreceptor function. *Naunyn Schmiedebergs Arch Pharmacol,* **361,** 134-45.

Opthof, T. (2000) The normal range and determinants of the intrinsic heart rate in man. *Cardiovasc Res,* **45,** 173-76.

Oropeza, V. C., Mackie, K. & Van Bockstaele, E. J. (2007) Cannabinoid receptors are localized to noradrenergic axon terminals in the rat frontal cortex. *Brain Res,* **1127,** 36-44.

Orr, J. S., Dengo, L., Rivero, J. M. & Davy, K. P. (2009) Arterial destiffening with atorvastatin in overweight and obese middle-aged and older adults. *Hypertension,* **54,** 763-68.

Osborn, J. W., Fink, G. D. & Kuroki, M. T. (2011) Neural mechanisms of angiotensin II-salt hypertension: implications for therapies targeting neural control of the splanchnic circulation. *Curr Hypertens Rep,* **13,** 221-28.

Pacher, P., Bátkai, S. & Kunos, G. (2004) Haemodynamic profile and responsiveness to anandamide of $TRPV_1$ receptor knock-out mice. *J Physiol,* **558,** 647-57.

Pacher, P., Bátkai, S. & Kunos, G. (2005a) Blood pressure regulation by endocannabinoids and their receptors. *Neuropharmacology,* **48,** 1130-38.

Pacher, P., Bátkai, S. & Kunos, G. (2005b) Cardiovascular pharmacology of cannabinoids. *Handb Exp Pharmacol***,** 599-625.

Pacher, P., Bátkai, S., Osei-Hyiaman, D., Offertáler, L., Liu, J., Harvey-White, J., . . . Kunos, G. (2005c) Hemodynamic profile, responsiveness to anandamide, and baroreflex sensitivity of mice lacking fatty acid amide hydrolase. *Am J Physiol Heart Circ Physiol,* **289,** H533-41.

Pacher, P., Steffens, S., Haskó, G., Schindler, T. H. & Kunos, G. (2018) Cardiovascular effects of marijuana and synthetic cannabinoids: the good, the bad, and the ugly. *Nat Rev Cardiol,* **15,** 151-66.

Pacholczyk, T., Blakely, R. D. & Amara, S. G. (1991) Expression cloning of a cocaine-and antidepressant-sensitive human noradrenaline transporter. *Nature,* **350,** 350-54.

Paczkowski, F. A. & Bryan-Lluka, L. J. (2002) Amino acids involved in differences in the pharmacological profiles of the rat and human noradrenaline transporters. *Naunyn Schmiedebergs Arch Pharmacol,* **365,** 312-17.

Paczkowski, F. A., Bryan-Lluka, L. J., Porzgen, P., Bruss, M. & Bonisch, H. (1999) Comparison of the pharmacological properties of cloned rat, human, and bovine norepinephrine transporters. *J Pharmacol Exp Ther,* **290,** 761-67.

Pakdeechote, P., Dunn, W. R. & Ralevic, V. (2007) Cannabinoids inhibit noradrenergic and purinergic sympathetic cotransmission in the rat isolated mesenteric arterial bed. *British Journal of Pharmacology,* **152,** 725-33.

Palaić, D. & Panisset, J.-C. (1969) Effect of nerve stimulation and angiotensin on the accumulation of ^{3}H-norepinephrine and the endogenous norepinephrine level in guinea pig vas deferens. *Biochem Pharmacol,* **18,** 2693-700.

Palmer, M. (n.d.) *Propagation of uncertainty through mathematical operations* [Online]. Available: http://web.mit.edu/fluids-modules/www/exper_techniques/2.Propagation_of_Uncertaint.pdf [Accessed 28 Dec 2020].

Palomar, A. R., Larios, B. N., De Sanchez, V. C., Perez, L. M., Lopez Fde, L., Flores, G. & Gomez-Villalobos Mde, J. (2011) Expression and distribution of dopamine transporter in cardiac tissues of the guinea pig. *Neurochem Res,* **36,** 399-405.

Park, J., Galligan, J. J., Fink, G. D. & Swain, G. M. (2007) Differences in sympathetic neuroeffector transmission to rat mesenteric arteries and veins as probed by in vitro continuous amperometry and video imaging. *J Physiol,* **584,** 819-34.

Parker, L. K., Shanks, J. A., Kennard, J. A. & Brain, K. L. (2010) Dynamic monitoring of NET activity in mature murine sympathetic terminals using a fluorescent substrate. *Br J Pharmacol,* **159,** 797-807.

Paton, J. F., Boscan, P., Pickering, A. E. & Nalivaiko, E. (2005) The yin and yang of cardiac autonomic control: vago-sympathetic interactions revisited. *Brain Res Brain Res Rev,* **49,** 555-65.

Pavone, L. M., Spina, A., Muto, R. L., Santoro, D., Mastellone, V. & Avallone, L. (2008) Heart valve cardiomyocytes of mouse embryos express the serotonin transporter SERT. *Biochem Biophys Res Commun,* **377,** 419-22.

Pawley, J. B. (2006) Fundamental limits in confocal microscopy. *In:* Pawley, J. B. *Handbook of Biological Confocal Microscopy.* Boston, MA: Springer. 20-42.

Pędzińska-Betiuk, A., Weresa, J., Toczek, M., Baranowska-Kuczko, M., Kasacka, I., Harasim-Symbor, E. & Malinowska, B. (2017) Chronic inhibition of fatty acid amide hydrolase by URB597 produces

differential effects on cardiac performance in normotensive and hypertensive rats. *Br J Pharmacol,* **174,** 2114-29.

Pei, Y., Asif-Malik, A. & Canales, J. J. (2016) Trace amines and the trace amine-associated receptor 1: pharmacology, neurochemistry, and clinical implications. *Front Neurosci,* **10,** 148-48.

Peng, L., Liu, H., Ruan, H., Tepp, W. H., Stoothoff, W. H., Brown, R. H., . . . Dong, M. (2013) Cytotoxicity of botulinum neurotoxins reveals a direct role of syntaxin 1 and SNAP-25 in neuron survival. *Nat Commun,* **4,** 1472.

Pepper, G. S. & Lee, R. W. (1999) Sympathetic activation in heart failure and its treatment with β-blockade. *Arch Intern Med,* **159,** 225-34.

Pertwee, R. G. (2005) Pharmacological actions of cannabinoids. *In:* Pertwee, R. G. *Cannabinoids.* Berlin, Heidelberg: Springer Berlin Heidelberg. 1-51.

Pertwee, R. G., Howlett, A. C., Abood, M. E., Alexander, S. P., Di Marzo, V., Elphick, M. R., . . . Ross, R. A. (2010) International Union of Basic and Clinical Pharmacology. LXXIX. Cannabinoid receptors and their ligands: beyond CB_1 and CB_2. *Pharmacol Rev,* **62,** 588-631.

Pfitzer, T., Niederhoffer, N. & Szabo, B. (2005) Search for an endogenous cannabinoid-mediated effect in the sympathetic nervous system. *Naunyn Schmiedebergs Arch Pharmacol,* **371,** 9-17.

Plattner, H., Westphal, C. & Tiggemann, R. (1982) Cytoskeleton-secretory vesicle interactions during the docking of secretory vesicles at the cell membrane in Paramecium tetraurelia cells. *J Cell Biol,* **92,** 368-77.

Poddar, M. K. & Dewey, W. L. (1980) Effects of cannabinoids on catecholamine uptake and release in hypothalamic and striatal synaptosomes. *J Pharmacol Exp Ther,* **214,** 63-67.

Porat-Shliom, N., Milberg, O., Masedunskas, A. & Weigert, R. (2013) Multiple roles for the actin cytoskeleton during regulated exocytosis. *Cell Mol Life Sci,* **70,** 2099-121.

Prabhakar, N. H., Kumar, G. K. & Peng, Y. (2012) Sympatho-adrenal activation by chronic intermittent hypoxia. *J Appl Physiol,* **113,** 1304-10.

Prabhakar, N. R. & Semenza, G. L. (2016) Regulation of carotid body oxygen sensing by hypoxia-inducible factors. *Pflugers Arch - Eur J Physiol,* **468,** 71-75.

Qian, Y., Galli, A., Ramamoorthy, S., Risso, S., DeFelice, L. J. & Blakely, R. D. (1997) Protein kinase C activation regulates human serotonin transporters in HEK-293 cells via altered cell surface expression. *J Neurosci,* **17,** 45-57.

Qin, F., Rounds, N. K., Mao, W., Kawai, K. & Liang, C. S. (2001) Antioxidant vitamins prevent cardiomyocyte apoptosis produced by norepinephrine infusion in ferrets. *Cardiovasc Res,* **51,** 736-48.

Quick, M. W. (2002) Role of syntaxin 1A on serotonin transporter expression in developing thalamocortical neurons. *Int J Dev,* **20,** 219-24.

Racchi, H., Schliem, A. J., Donoso, M. V., Rahmer, A., Zúñiga, Á., Guzmán, S., . . . Huidobro-Toro, J. P. (1997) Neuropeptide Y Y_1 receptors are involved in the vasoconstriction caused by human sympathetic nerve stimulation. *Eur J Pharmacol,* **329,** 79-83.

Raffel, D. M. & Chen, W. (2004) Binding of [^{3}H]mazindol to cardiac norepinephrine transporters: kinetic and equilibrium studies. *Naunyn Schmiedebergs Arch Pharmacol,* **370,** 9-16.

Rajesh, M., Bátkai, S., Kechrid, M., Mukhopadhyay, P., Lee, W., Horváth, B., . . . Pacher, P. (2012) Cannabinoid 1 receptor promotes cardiac dysfunction, oxidative stress, inflammation, and fibrosis in diabetic cardiomyopathy. *Diabetes,* **61,** 716-27.

Ralevic, V. (2003) Cannabinoid modulation of peripheral autonomic and sensory neurotransmission. *Eur J Pharmacol,* **472,** 1-21.

Ralevic, V. & Kendall, D. A. (2002) Cannabinoids inhibit pre- and postjunctionally sympathetic neurotransmission in rat mesenteric arteries. *Eur J Pharmacol,* **444,** 171-81.

Ralevic, V. & Kendall, D. A. (2009) Cannabinoid modulation of perivascular sympathetic and sensory neurotransmission. *Curr Vasc Pharmacol,* **7,** 15-25.

Ram, C. V. S. (2019) Status of renal denervation therapy for hypertension. *Circulation,* **139,** 601-03.

Rand, M. J. & Whaler, B. C. (1965) Impairment of sympathetic transmission by botulinum toxin. *Nature,* **206,** 588-91.

Randall, D. C., Brown, D. R., McGuirt, A. S., Thompson, G. W., Armour, J. A. & Ardell, J. L. (2003) Interactions within the intrinsic cardiac nervous system contribute to chronotropic regulation. *Am J Physiol Regul Integr Comp Physiol,* **285,** R1066-75.

Randall, M. D., Harris, D., Kendall, D. A. & Ralevic, V. (2002) Cardiovascular effects of cannabinoids. *Pharmacol Ther,* **95,** 191-202.

Raum, W. J., Laks, M. M., Garner, D., Ikuhara, M. H. & Swerdloff, R. S. (1984) Norepinephrine increases beta-receptors and adenylate cyclase in canine myocardium. *Am J Physiol,* **246,** H31-36.

Ray, K. (2014) From fission to fusion: a perspective on the research that won the Nobel Prize in Physiology or Medicine, 2013. *J Biosci,* **39,** 3-12.

Rees, P. M. (1967) The distribution of biogenic amines in the carotid bifurcation region. *J Physiol,* **193,** 245-53.

Regehr, W. G., Carey, M. R. & Best, A. R. (2009) Activity-dependent regulation of synapses by retrograde messengers. *Neuron,* **63,** 154-70.

Reilly, J. P. & Diamant, A. M. (2011) Chapter 6: Model application to C-fibers and the heart. *In:* Reilly, J. P. & Diamant, A. M. *Electrostimulation: theroy, applications and computational model.* Artech House Publishers.

Reyes, B. A., Rosario, J. C., Piana, P. M. & Van Bockstaele, E. J. (2009) Cannabinoid modulation of cortical adrenergic receptors and transporters. *J Neurosci Res,* **87,** 3671-78.

Richards, J. R., Blohm, E., Toles, K. A., Jarman, A. F., Ely, D. F. & Elder, J. W. (2020) The association of cannabis use and cardiac dysrhythmias: a systematic review. *Clin Toxicol (Phila),* **58,** 861-69.

Ritter, J. M., Flower, R., Henderson, G., Loke, Y. K., MacEwan, D. & Rang, H. P. (2020) Chemical mediators and the autonomic nervous system. *Rang and Dale's Pharmacology.* 9th ed. United Kingdom: Elsevier Churchill Livingstone. 167-69.

Robinson, D. L., Venton, B. J., Heien, M. L. A. V. & Wightman, R. M. (2003) Detecting subsecond dopamine release with fast-scan cyclic voltammetry in vivo. *Clin Chem,* **49,** 1763-73.

Rodriguez, P. C., Pereira, D. B., Borgkvist, A., Wong, M. Y., Barnard, C., Sonders, M. S., . . . Sulzer, D. (2013) Fluorescent dopamine tracer resolves individual dopaminergic synapses and their activity in the brain. *Proc Natl Acad Sci U S A,* **110,** 870-75.

Rook, W., Johnson, C. D., Coney, A. M. & Marshall, J. M. (2014) Prenatal hypoxia leads to increased muscle sympathetic nerve activity, sympathetic hyperinnervation, premature blunting of neuropeptide Y signaling, and hypertension in adult life. *Hypertension,* **64,** 1321-27.

Roth, M., Obaidat, A. & Hagenbuch, B. (2012) OATPs, OATs and OCTs: the organic anion and cation transporters of the SLCO and SLC22A gene superfamilies. *Br J Pharmacol,* **165,** 1260-87.

Rowell, L. B. (1990) Importance of scintigraphic measurements of human splanchnic blood volume. *J Nucl Med,* **31,** 160-62.

Rudź, R., Schlicker, E., Baranowska, U., Marciniak, J., Karabowicz, P. & Malinowska, B. (2012) Acute myocardial infarction inhibits the neurogenic tachycardic and vasopressor response in rats via presynaptic cannabinoid type 1 receptor. *J Pharmacol Exp Ther,* **343,** 198-205.

Ruiz-Velasco, V. & Ikeda, S. R. (1998) Heterologous expression and coupling of G protein-gated inwardly rectifying K^+ channels in adult rat sympathetic neurons. *J Physiol,* **513,** 761-73.

Russ, H., Gliese, M., Sonna, J. & Schömig, E. (1992) The extraneuronal transport mechanism for noradrenaline ($uptake_2$) avidly transports 1-methyl-4-phenylpyridinium (MPP^+). *Naunyn Schmiedebergs Arch Pharmacol,* **346,** 158-65.

Rysevaite, K., Saburkina, I., Pauziene, N., Vaitkevicius, R., Noujaim, S. F., Jalife, J. & Pauza, D. H. (2011) Immunohistochemical characterization of the intrinsic cardiac neural plexus in whole-mount mouse heart preparations. *Heart Rhythm,* **8,** 731-38.

Sakurai-Yamashita, Y., Kataoka, Y., Fujiwara, M., Mine, K. & Ueki, S. (1989) Delta 9-tetrahydrocannabinol facilitates striatal dopaminergic transmission. *Pharmacol Biochem Behav,* **33,** 397-400.

Savchenko, V., Sung, U. & Blakely, R. D. (2003) Cell surface trafficking of the antidepressant-sensitive norepinephrine transporter revealed with an ectodomain antibody. *Mol Cell Neurosci,* **24,** 1131-50.

Šćepanović, D. (2011) *A model of sinoatrial node cell regulation by the autonomic nervous system.* PhD thesis, Massachusetts Institute of Technology.

Schlicker, E. & Feuerstein, T. (2017) Human presynaptic receptors. *Pharmacol Ther,* **172,** 1-21.

Schlicker, E., Redmer, A., Werner, A. & Kathmann, M. (2003) Lack of CB_1 receptors increases noradrenaline release in vas deferens without affecting atrial noradrenaline release or cortical acetylcholine release. *Br J Pharmacol,* **140,** 323-28.

Schroeder, C., Birkenfeld, A. L., Mayer, A. F., Tank, J., Diedrich, A., Luft, F. C. & Jordan, J. (2006) Norepinephrine transporter inhibition prevents tilt-induced pre-syncope. *J Am Coll Cardiol,* **48,** 516-22.

Schroeder, C. & Jordan, J. (2012) Norepinephrine transporter function and human cardiovascular disease. *Am J Physiol Heart Circ Physiol,* **303,** H1273-82.

Schroeter, S., Apparsundaram, S., Wiley, R. G., Miner, L. H., Sesack, S. R. & Blakely, R. D. (2000) Immunolocalization of the cocaine- and antidepressant-sensitive l-norepinephrine transporter. *J Comp Neurol,* **420,** 211-32.

Schultheiss, T., Flau, K., Kathmann, M., Göthert, M. & Schlicker, E. (2005) Cannabinoid CB_1 receptor-mediated inhibition of noradrenaline release in guinea-pig vessels, but not in rat and mouse aorta. *Naunyn Schmiedebergs Arch Pharmacol,* **372,** 139-46.

Schwartz, J. W., Blakely, R. D. & DeFelice, L. J. (2003) Binding and transport in norepinephrine transporters. Real-time, spatially resolved analysis in single cells using a fluorescent substrate. *J Biol Chem,* **278,** 9768-77.

Schwartz, J. W., Novarino, G., Piston, D. W. & DeFelice, L. J. (2005) Substrate binding stoichiometry and kinetics of the norepinephrine transporter. *J Biol Chem,* **280,** 19177-84.

Schwarz, P., Diem, R., Dun, N. J. & Förstermann, U. (1995) Endogenous and exogenous nitric oxide inhibits norepinephrine release from rat heart sympathetic nerves. *Circ Res,* **77,** 841-48.

Sekiguchi, H., Pavey, G. & Dean, B. (2019) Altered levels of dopamine transporter in the frontal pole and dorsal striatum in schizophrenia. *NPJ Schizophr,* **5,** 20.

Shahani, S. K., Lingamaneni, R. & Hemmings, H. C., Jr. (2002) General anesthetic actions on norepinephrine, dopamine, and gamma-aminobutyric acid transporters in stably transfected cells. *Anesth Analg,* **95,** 893-99.

Shanks, J., Mane, S., Ryan, R. & Paterson, D. J. (2013a) Ganglion-specific impairment of the norepinephrine transporter in the hypertensive rat. *Hypertension,* **61,** 187-93.

Shanks, J., Manou-Stathopoulou, S., Lu, C. J., Li, D., Paterson, D. J. & Herring, N. (2013b) Cardiac sympathetic dysfunction in the prehypertensive spontaneously hypertensive rat. *Am J Physiol Heart Circ Physiol,* **305,** H980-86.

Sheldon, R. S., Lei, L., Guzman, J. C., Kus, T., Ayala-Paredes, F. A., Angihan, J., . . . Raj, S. R. (2019) A proof of principle study of atomoxetine for the prevention of vasovagal syncope: the Prevention of Syncope Trial VI. *Europace,* **21,** 1733-41.

Shell, B., Faulk, K. & Cunningham, J. T. (2016) Neural control of blood pressure in chronic intermittent hypoxia. *Curr Hypertens Rep,* **18,** 19.

Shire, D., Calandra, B., Rinaldi-Carmona, M., Oustric, D., Pessègue, B., Bonnin-Cabanne, O., . . . Ferrara, P. (1996) Molecular cloning, expression and function of the murine CB_2 peripheral cannabinoid receptor. *Biochim Biophys Acta,* **1307,** 132-36.

Shirey-Rice, J. K., Klar, R., Fentress, H. M., Redmon, S. N., Sabb, T. R., Krueger, J. J., . . . Hahn, M. K. (2013) Norepinephrine transporter variant A457P knock-in mice display key features of human postural orthostatic tachycardia syndrome. *Dis Model Mech,* **6,** 1001-11.

Shivkumar, K. & Ardell, J. L. (2016) Cardiac autonomic control in health and disease. *J Physiol,* **594,** 3851-52.

Silva, A. Q. & Schreihofer, A. M. (2011) Altered sympathetic reflexes and vascular reactivity in rats after exposure to chronic intermittent hypoxia. *J Physiol,* **589,** 1463-76.

Singh, R. R. & Denton, K. M. (2018) Renal denervation. *Hypertension,* **72,** 528-36.

Snow, A. B., Khalyfa, A., Serpero, L. D., Capdevila, O. S., Kim, J., Buazza, M. O. & Gozal, D. (2009) Catecholamine alterations in pediatric obstructive sleep apnea: effect of obesity. *Pediatr Pulmonol,* **44,** 559-67.

Somers, V. K., Mark, A. L., Zavala, D. C. & Abboud, F. M. (1989) Contrasting effects of hypoxia and hypercapnia on ventilation and sympathetic activity in humans. *J Appl Physiol,* **67,** 2101-16.

Sorimachi, M., Oesch, F. & Thoenen, H. (1973) Effects of colchicine and cytochalasin B on the release of ^{3}H-norepinephrine from guinea-pig atria evoked by high potassium, nicotine and tyramine. *Naunyn Schmiedebergs Arch Pharmacol,* **276,** 1-12.

Starke, K. (2001) Presynaptic autoreceptors in the third decade: focus on α_2-adrenoceptors. *J Neurochem,* **78,** 685-93.

Stewart, S., MacIntyre, K., Hole, D. J., Capewell, S. & McMurray, J. J. (2001) More 'malignant' than cancer? Five-year survival following a first admission for heart failure. *Eur J Heart Fail,* **3,** 315-22.

Stjärne, L. (1989) Basic mechanisms and local modulation of nerve impulse-induced secretion of neurotransmitters from individual sympathetic nerve varicosities. *In:* Blaustein, M. P., Creutzfeldt, O., Grunicke, H., Habermann, E., Neurath, H., Numa, S., . . . Ullrich, K. J. *Reviews of Physiology, Biochemistry and Pharmacology.* Berlin, Heidelberg: Springer Berlin Heidelberg. **112,** 1-137.

Stjärne, L. (2000) Do sympathetic nerves release noradrenaline in "quanta"? *J Auton Nerv Syst,* **81,** 236-43.

Stjärne, L. (2001) Novel dual 'small' vesicle model of ATP- and noradrenaline-mediated sympathetic neuromuscular transmission. *Auton Neurosci,* **87,** 16-36.

Stjärne, L., Bao, J. X., Gonon, F. & Msghina, M. (1994) Nerve activity-dependent variations in clearance of released noradrenaline: Regulatory roles for sympathetic neuromuscular transmission in rat tail artery. *Neuroscience,* **60,** 1021-38.

Stjärne, L., Bao, J. X., Gonon, F., Msghina, M. & Stjärne, E. (1993) A nonstochastic string model of sympathetic neuromuscular transmission. *News Physiol Sci,* **8,** 253-60.

Stjärne, L. & Stjärne, E. (1995) Geometry, kinetics and plasticity of release and clearance of ATP and noradrenaline as sympathetic cotransmitters: roles for the neurogenic contraction. *Prog Neurobiol,* **47,** 45-94.

Struik, R. J. (2017) Stimulation and recording *In:* Horch, K. & Kipke, D. *Neuroprosthetics: Theory and Practise.* Second ed. Singapore World Scientific Co. 238.

Subramaniam, V. N., Menezes, A. R., DeSchutter, A. & Lavie, C. J. (2019) The cardiovascular effects of marijuana: are the potential adverse effects worth the high? *Mo Med,* **116,** 146-53.

Sugiura, T., Kodaka, T., Nakane, S., Kishimoto, S., Kondo, S. & Waku, K. (1998) Detection of an endogenous cannabimimetic molecule, 2-arachidonoylglycerol, and cannabinoid CB_1 receptor mRNA in human vascular cells: is 2-arachidonoylglycerol a possible vasomodulator? *Biochem Biophys Res Commun,* **243,** 838-43.

Sun, L., Yan, S., Wang, X., Zhao, S., Li, H., Wang, Y., . . . Li, Y. (2017) Metoprolol prevents chronic obstructive sleep apnea-induced atrial fibrillation by inhibiting structural, sympathetic nervous and metabolic remodeling of the atria. *Sci Rep,* **7,** 14941.

Sung, U., Apparsundaram, S., Galli, A., Kahlig, K. M., Savchenko, V., Schroeter, S., . . . Blakely, R. D. (2003) A regulated interaction of syntaxin 1A with the antidepressant-sensitive norepinephrine transporter establishes catecholamine clearance capacity. *J Neurosci,* **23,** 1697-709.

Sung, U., Binda, F., Savchenko, V., Owens, W. A. & Daws, L. C. (2017) Ca^{2+} dependent surface trafficking of norepinephrine transporters depends on threonine 30 and Ca^{2+} calmodulin kinases. *J Chem Neuroanat,* **83-84,** 19-35.

Svensson, E., Apergis-Schoute, J., Burnstock, G., Nusbaum, M. P., Parker, D. & Schiöth, H. B. (2019) General principles of neuronal co-transmission: insights from multiple model systems. *Front Neural Circuits,* **12**.

Szabo, B. & Schlicker, E. (2005) Effects of cannabinoids on neurotransmission. *In:* Pertwee, R. G. *Cannabinoids.* Berlin, Heidelberg: Springer Berlin Heidelberg. 327-65.

Takaki, F., Nakamuta, N., Kusakabe, T. & Yamamoto, Y. (2015) Sympathetic and sensory innervation of small intensely fluorescent (SIF) cells in rat superior cervical ganglion. *Cell Tissue Res,* **359,** 441-51.

Tas, P. W., Kress, H. G. & Koschel, K. (1987) Volatile anesthetics and n-alcohols inhibit the uptake of noradrenaline in pheochromocytoma cells. *Anaesthesist,* **36,** 340-44.

Thackeray, J. T., Beanlands, R. S. & Dasilva, J. N. (2007) Presence of specific ^{11}C-meta-Hydroxyephedrine retention in heart, lung, pancreas, and brown adipose tissue. *J Nucl Med,* **48,** 1733-40.

Thoa, N. B., Wooten, G. F., Axelrod, J. & Kopin, I. J. (1972) Inhibition of release of dopamine-β-hydroxylase and norepinephrine from sympathetic nerves by colchicine, vinblastine, or cytochalasin-B *Proc Natl Acad Sci U S A,* **69,** 520-22.

Thompson, E. L., Ray, C. J., Holmes, A. P., Pye, R. L., Wyatt, C. N., Coney, A. M. & Kumar, P. (2016) Adrenaline release evokes hyperpnoea and an increase in ventilatory CO_2 sensitivity during hypoglycaemia: a role for the carotid body. *J Physiol,* **594,** 4439-52.

Thomsen, M., Sorensen, G. & Dencker, D. (2018) Physiological roles of CNS muscarinic receptors gained from knockout mice. *Neuropharmacology,* **136,** 411-20.

Thorlacius, K., Zhoujun, C. & Bodelsson, M. (2003) Effects of sevoflurane on sympathetic neurotransmission in human omental arteries and veins. *Br J Anaesth,* **90,** 766-73.

Toczek, M. & Malinowska, B. (2018) Enhanced endocannabinoid tone as a potential target of pharmacotherapy. *Life Sci,* **204,** 20-45.

Toczek, M., Schlicker, E., Grzęda, E. & Malinowska, B. (2015) Enhanced function of inhibitory presynaptic cannabinoid CB_1 receptors on sympathetic nerves of DOCA–salt hypertensive rats. *Life Sci,* **138,** 78-85.

Toledo-Aral, J. J., Mendez-Ferrer, S., Pardal, R., Echevarria, M. & Lopez-Barneo, J. (2003) Trophic restoration of the nigrostriatal dopaminergic pathway in long-term carotid body-grafted parkinsonian rats. *J Neurosci,* **23,** 141-48.

Trendelenburg, A.-U., Gomeza, J., Klebroff, W., Zhou, H. & Wess, J. (2003a) Heterogeneity of presynaptic muscarinic receptors mediating inhibition of sympathetic transmitter release: a study with M_2- and M_4-receptor-deficient mice. *Br J Pharmacol,* **138,** 469-80.

Trendelenburg, A. U., Cox, S. L., Schelb, V., Klebroff, W., Khairallah, L. & Starke, K. (2000) Modulation of ^{3}H-noradrenaline release by presynaptic opioid, cannabinoid and bradykinin receptors and β-adrenoceptors in mouse tissues. *Br J Pharmacol,* **130,** 321-30.

Trendelenburg, A. U., Meyer, A., Wess, J. & Starke, K. (2005) Distinct mixtures of muscarinic receptor subtypes mediate inhibition of noradrenaline release in different mouse peripheral tissues, as studied with receptor knockout mice. *Br J Pharmacol,* **145,** 1153-59.

Trendelenburg, A. U., Philipp, M., Meyer, A., Klebroff, W., Hein, L. & Starke, K. (2003b) All three alpha$_2$-adrenoceptor types serve as autoreceptors in postganglionic sympathetic neurons. *Naunyn Schmiedebergs Arch Pharmacol,* **368,** 504-12.

Trendelenburg, U. (1987) The membrane potential of vascular smooth muscle appears to modulate uptake$_2$ of ^{3}H-isoprenaline. *Naunyn Schmiedebergs Arch Pharmacol,* **336,** 33-36.

Trendelenburg, U., Draskóczy, P. R. & Graefe, K. H. (1972) The influence of intraneuronal monoamine oxidase on neuronal net uptake of noradrenaline and on sensitivity to noradrenaline. *Adv Biochem Psychopharmacol,* **5,** 371-77.

Trendelenburg, U., Langeloh, A. & Bonisch, H. (1987) Mechanism of action of indirectly acting sympathomimetic amines. *Blood Vessels,* **24,** 261-70.

Twitchell, W., Brown, S. & Mackie, K. (1997) Cannabinoids inhibit N- and P/Q-type calcium channels in cultured rat hippocampal neurons. *J Neurophysiol,* **78,** 43-50.

Ungerer, M., Chlistalla, A. & Richardt, G. (1996) Upregulation of cardiac uptake$_1$ carrier in ischemic and nonischemic rat heart. *Circ Res,* **78,** 1037-43.

van Diepen, H., Schlicker, E. & Michel, M. C. (2008) Prejunctional and peripheral effects of the cannabinoid CB_1 receptor inverse agonist rimonabant (SR 141716). *Naunyn Schmiedebergs Arch Pharmakol,* **378,** 345-69.

Varga, K., Lake, K., Martin, B. R. & Kunos, G. (1995) Novel antagonist implicates the CB_1 cannabinoid receptor in the hypotensive action of anandamide. *Eur J Pharmacol,* **278,** 279-83.

Verna, A., Barets, A. & Salat, C. (1984) Distribution of sympathetic nerve endings within the rabbit carotid body: a histochemical and ultrastructural study. *J Neurocytol,* **13,** 849-65.

Vollert, C. T., Moree, W. J., Gregory, S., Bark, S. J. & Eriksen, J. L. (2015) Formaldehyde scavengers function as novel antigen retrieval agents. *Scientific Reports,* **5,** 17322.

Wagner, J. A., Járai, Z., Bátkai, S. & Kunos, G. (2001) Hemodynamic effects of cannabinoids: coronary and cerebral vasodilation mediated by cannabinoid CB_1 receptors. *Eur J Pharmacol,* **423,** 203-10.

Wang, K., Zhu, Z., Chi, R., Li, Q., Yang, Z., Jie, X., . . . Fan, B. (2019) The NADPH oxidase inhibitor apocynin improves cardiac sympathetic nerve terminal innervation and function in heart failure. *Exp Physiol,* **104,** 1638-49.

Wang, T., Li, G., Zhang, H., Zhang, Y. & Li, Q. (2017a) Overactivation of cannabinoid receptor type 1 in rostral ventrolateral medulla promotes cardiovascular responses in spontaneously hypertensive rats. *J Hypertens,* **35,** 538-45.

Wang, Y., Kaminski, N. E. & Wang, D. H. (2005) VR_1-mediated depressor effects during high-salt intake. *Hypertension,* **46,** 986-91.

Wang, Y., Lin, W. K., Crawford, W., Ni, H., Bolton, E. L., Khan, H., . . . Lei, M. (2017b) Optogenetic control of heart rhythm by selective stimulation of cardiomyocytes rerived from $Pnmt^+$ cells in murine heart. *Sci Rep,* **7,** 40687.

Wehrwein, E. A., Orer, H. S. & Barman, S. M. (2016) Overview of the anatomy, physiology, and pharmacology of the autonomic nervous system. *Compr Physiol,* **6,** 1239-78.

Wehrwein, E. A., Parker, L. M., Wright, A. A., Spitsbergen, J. M., Novotny, M., Babankova, D., . . . Kreulen, D. L. (2008) Cardiac norepinephrine transporter protein expression is inversely correlated to chamber norepinephrine content. *Am J Physiol Regul Integr Comp Physiol,* **295,** R857-63.

Whitaker, R. H. (2018) Anatomy of the heart. *Medicine,* **46,** 423-26.

Whitby, L. G., Axelrod, J. & Weil-Malherbe, H. (1961) The fate of H^3-norepinephrine in animals. *J Pharmacol Exp Ther,* **132,** 193-201.

Wichter, T., Matheja, P., Eckardt, L., Kies, P., Schafers, K., Schulze-Bahr, E., . . . Schafers, M. (2002) Cardiac autonomic dysfunction in Brugada syndrome. *Circulation,* **105,** 702-06.

Williams, B., Mancia, G., Spiering, W., Agabiti Rosei, E., Azizi, M., Burnier, M., . . . Desormais, I. (2018) 2018 ESC/ESH Guidelines for the management of arterial hypertension: The Task Force for the

management of arterial hypertension of the European Society of Cardiology (ESC) and the European Society of Hypertension (ESH); ESC Scientific Document Group. *Eur Heart J,* **39,** 3021-104.

Williams, D. J., Sidaway, P., Cunnane, T. C. & Brain, K. L. (2011) Mechanisms involved in nicotinic acetylcholine receptor-induced neurotransmitter release from sympathetic nerve terminals in the mouse vas deferens. *PLoS One,* **6,** e29209.

Williamson, K. L. & Broadley, K. J. (1989) Do both adrenaline and noradrenaline stimulate cardiac alpha-adrenoceptors to induce positive inotropy of rat atria? *Br J Pharmacol,* **98,** 597-611.

Wink, J., van Delft, R., Notenboom, R. G. E., Wouters, P. F., DeRuiter, M. C., Plevier, J. W. M. & Jongbloed, M. R. M. (2020) Human adult cardiac autonomic innervation: Controversies in anatomical knowledge and relevance for cardiac neuromodulation. *Auton Neurosci,* **227,** 102674.

Winter, J., Tanko, A. S., Brack, K. E., Coote, J. H. & Ng, G. A. (2012) Differential cardiac responses to unilateral sympathetic nerve stimulation in the isolated innervated rabbit heart. *Auton Neurosci,* **166,** 4-14.

Winter, J., Tipton, M. J. & Shattock, M. J. (2018) Autonomic conflict exacerbates long QT associated ventricular arrhythmias. *J Mol Cell Cardiol,* **116,** 145-54.

Wolfe, D. E., Potter, L. T., Richardson, K. C. & Axelrod, J. (1962) Localizing tritiated norepinephrine in sympathetic axons by electron microscopic autoradiography. *Science,* **138,** 440-42.

Wouters, E., Walraed, J., Banister, S. D. & Stove, C. P. (2019) Insights into biased signaling at cannabinoid receptors: synthetic cannabinoid receptor agonists. *Biochem Pharmacol,* **169,** 113623.

Wu, X., Jiang, H., Yu, L., Hu, X. & Liu, W. (2012) Desipramine pretreatment improves sympathetic remodeling and ventricular fibrillation threshold after myocardial ischemia. *J Biomed Biotechnol,* **2012,** 732909.

Yamaguchi, N., de Champlain, J. & Nadeau, R. (1975) Correlation between the response of the heart to sympathetic stimulation and the release of endogenous catecholamines into the coronary sinus of the dog. *Circ Res,* **36,** 662-68.

Yamamoto, H. & Kirpekar, S. M. (1972) Effects of nerve stimulation on the uptake of norepinephrine by the perfused spleen of the cat. *Eur J Pharmacol,* **17,** 25-33.

Yamashita, S. & Katsumata, O. (2017) Heat-induced antigen retrieval in immunohistochemistry: mechanisms and applications. *In:* Pellicciari, C. & Biggiogera, M. *Histochemistry of Single Molecules. Methods in Molecular Biology.* New York: Humana Press. **1560,** 147-61.

Yang, H. J., Gil, Y. C., Lee, W. J., Kim, T. J. & Lee, H. Y. (2008) Anatomy of thoracic splanchnic nerves for surgical resection. *Clin Anat,* **21,** 171-7.

Yang, Q., Sumner, A. D., Puhl, H. L. & Ruiz-Velasco, V. (2006) M_1 and M_2 muscarinic acetylcholine receptor subtypes mediate Ca^{2+} channel current inhibition in rat sympathetic stellate ganglion neurons. *J Neurophysiol,* **96,** 2479-87.

Yang, S. (1998) *The divine farmer's materia medica: a translation of the Shen Nong Ben Cao Jing*, Blue Poppy Enterprises Inc.

Yang, X., Zhang, L., Liu, H., Shao, Y. & Zhang, S. (2019) Cardiac sympathetic denervation suppresses atrial fibrillation and blood pressure in a chronic intermittent hypoxia rat model of obstructive sleep apnea. *J Am Heart Assoc,* **8,** e010254.

Yaranov, D., Smyrlis, A., Usatii, N., Butler, A., Petrini, J. R., Mendez, J. & Warshofsky, M. K. (2015) Effect of obstructive sleep apnea on frequency of stroke in patients with atrial fibrillation. *Am J Card,* **115,** 461-65.

Yokomizo, A., Takatori, S., Hashikawa-Hobara, N., Goda, M. & Kawasaki, H. (2015) Characterization of perivascular nerve distribution in rat mesenteric small arteries. *Biol Pharm Bull,* **38,** 1757-64.

Yokoyama, T., Lee, J. K., Miwa, K., Opthof, T., Tomoyama, S., Nakanishi, H., . . . Komuro, I. (2017) Quantification of sympathetic hyperinnervation and denervation after myocardial infarction by three-dimensional assessment of the cardiac sympathetic network in cleared transparent murine hearts. *PLoS One,* **12,** e0182072.

Yokoyama, T., Misuzu, Y. Y. & Yamamoto, Y. (2013) Immunohistochemical localization of tryptophan hydroxylase and serotonin transporter in the carotid body of the rat. *Histochem Cell Biol,* **140,** 147-55.

Yu, M., Bozek, J., Kagan, M., Guaraldi, M., Silva, P., Azure, M., . . . Robinson, S. P. (2013) Cardiac retention of PET neuronal imaging agent LMI1195 in different species: impact of norepinephrine uptake-1 and -2 transporters. *Nucl Med Biol,* **40,** 682-88.

Yu, T. Y. (2015) *Optical imaging of cardiac atrial activation and repolarisation in genetically altered models.* PhD thesis, University of Birmingham.

Zaglia, T. & Mongillo, M. (2017) Cardiac sympathetic innervation, from a different point of (re)view. *J Physiol,* **595,** 3919-30.

Zarzoso, M., Rysevaite, K., Milstein, M. L., Calvo, C. J., Kean, A. C., Atienza, F., . . . Noujaim, S. F. (2013) Nerves projecting from the intrinsic cardiac ganglia of the pulmonary veins modulate sinoatrial node pacemaker function. *Cardiovasc Res,* **99,** 566-75.

Zerbino, D. R., Achuthan, P., Akanni, W., Amode, M R., Barrell, D., Bhai, J., . . . Flicek, P. (2017) Ensembl 2018. *Nucleic Acids Res,* **46,** D754-61.

Zhao, J., Xu, W., Yun, F., Zhao, H., Li, W., Gong, Y., . . . Li, Y. (2014) Chronic obstructive sleep apnea causes atrial remodeling in canines: mechanisms and implications. *Basic Res Cardiol,* **109,** 427.

Zhong, X., Hilton, H. J., Gates, G. J., Jelic, S., Stern, Y., Bartels, M. N., . . . Basner, R. C. (2005) Increased sympathetic and decreased parasympathetic cardiovascular modulation in normal humans with acute sleep deprivation. *J Appl Physiol,* **98,** 2024-32.

Zhou, J. (2004) Norepinephrine transporter inhibitors and their therapeutic potential. *Drugs Future,* **29,** 1235-44.

Zimmermann, H. (1994) Signalling via ATP in the nervous system. *Trends Neurosci,* **17,** 420-26.

Zou, S. & Kumar, U. (2018) Cannabinoid receptors and the endocannabinoid system: signaling and function in the central nervous system. *Int J Mol Sci,* **19**.

Zugck, C., Lossnitzer, D., Backs, J., Kristen, A., Kinscherf, R. & Haass, M. (2003) Increased cardiac norepinephrine release in spontaneously hypertensive rats: role of presynaptic alpha-2_A adrenoceptors. *J Hypertens,* **21,** 1363-69.

Zukela, T., Zhou, Q., Wang, H., Zhou, X., Li, Y., Zhang, Y., . . . Tang, B. (2015) [Relationship between new-onset atrial fibrillation and sympathetic neural remodeling in a canine acute myocardial infarction model]. *Zhonghua Xin Xue Guan Bing Za Zhi,* **43,** 975-81.

Zwart, R., Verhaagh, S., Buitelaar, M., Popp-Snijders, C. & Barlow, D. P. (2001) Impaired activity of the extraneuronal monoamine transporter system known as uptake-$_2$ in Orct3/Slc22a3-deficient mice. *Mol Cell Biol,* **21,** 4188-96.

Zwartsen, A., Verboven, A. H. A., van Kleef, R., Wijnolts, F. M. J., Westerink, R. H. S. & Hondebrink, L. (2017) Measuring inhibition of monoamine reuptake transporters by new psychoactive substances (NPS) in real-time using a high-throughput, fluorescence-based assay. *Toxicol In Vitro,* **45,** 60-71.